

Investigating the magmatic drivers behind temporal variations in eruption frequency and style at Kelut volcano, Indonesia



Louise Goode, BSc (Hons.), MRes

Thesis presented for the Degree of Doctor of Philosophy

February 2018

Department of Earth and Planetary Sciences

Macquarie University

Cover photo of Kelut volcano edifice taken on the drive up to the summit.

“Tonight in presence of the firepit, with the glowing lava again gushing and pounding and shaking the seismographs, I am asked to tell you something of the scientific meaning of it” —Thomas A. Jaggar, Jr. (1945)

Abstract

Stratigraphic, petrological, mineralogical and geochemical records of volcanism are vital to understanding and forecasting the magmatic processes governing the cyclic effusive-explosive eruptive styles and patterns. Understanding the full range of eruptive behaviour at a volcano is fundamental in helping to reduce the disastrous impacts of eruptions to nearby vulnerable populations. Java (Indonesia) contains a large concentration of historically active and deadly volcanoes. However, few of these have well-constrained stratigraphic records that allow the variety of eruption styles and the eruption frequency to be estimated. Kelut volcano is one of the more deadly volcanoes in Indonesia, yet its geological record is poorly known. This thesis aims to improve our knowledge of Kelut, by examining detailed records of Kelut's pyroclastic deposits and geochemistry, including both the most recent eruption (2014) and a series of units emplaced over the last 1500 years.

The dynamics and chronology of individual eruptions of Kelut are complex. From AD ~560 to 1800's, glass shard compositions reveal that magmatic processes are the first-order control on eruptive behaviour. Mafic recharge events triggered the most explosive episodes. The system was maintained by variable rates and volumes of mafic magma influxes. In the early record, recharges were small or infrequent, and enough time between eruptions allowed homogenised high-Si magmas to erupt. More frequent eruptions took place from AD 1000 and variability of magmas was greater. From AD 1920 to 1990, eruptions tapped a continuously evolving magma system. The homogeneity of compositions from recent effusive-explosive rocks suggested that regular, small injections of gas-rich magma allowed for efficient mixing, buffering the system for some time. During this phase, other processes were of greater influence on eruptive styles. In some cases the presence of a conduit-capping lava dome inhibited gas release, eventually leading to overpressure and triggering a more explosive eruption, e.g., 2014. In the 2014 eruption, there is also potential evidence of mafic intrusion before eruption. This sudden intrusion left little trace, except in feldspar-rim compositions. Since 1920, explosive eruptions occurred every ~21 years at Kelut. If the alternate explosive/effusive cycle holds, the next eruption of Kelut is likely to be a period of lava dome effusion.

Author's declaration of originality

I, Louise Goode, declare that the material presented in this thesis is my own original research except where otherwise acknowledged, and that no part of this thesis has been submitted for a higher degree to any other university or institution.

A handwritten signature in black ink, appearing to read 'L. Goode', written in a cursive style.

Louise Goode

21/09/2018

Date

Department of Earth and Planetary Sciences

Macquarie University

North Ryde, Australia

Acknowledgements

This thesis is dedicated to the memories of three people without whom I wouldn't be here. To my Father, Vincent Goode, you are always my inspiration and motivation, and I will always follow in your footsteps. To my dearest late friend and partner in crime Lara Crook, I also dedicate this thesis. Without her encouragement to 'go get those volcanoes' and make the move to Australia, I would not have had the courage to take on this PhD. Your inspirational strength and resilience throughout your illness provided me with a constant daily reminder that I can do it and reach my goals. To Grandad, you also originally sparked my love for science, and continued to keep that spark ignited throughout my career. I struggled many times to keep going throughout this PhD, but my Grandad told me I wasn't to quit and to keep going. Without him I wouldn't have finished and be where I am today.

Thank you to my supervisors Heather Handley and Shane Cronin. Without your guidance, time, patience, insights and enthusiasm this thesis would not have been possible.

I would also like to thank Simon Turner, Chris Firth, Lucy McGee and Michael Turner for your input and supportive conversations.

Thanks to Anna Hicks who recommended and encouraged me to apply for this PhD in the first place!

Thanks to Dermadi Madi and Reza Firmansyah for their assistance in the field. Thanks to the research staff (past and present) in the Macquarie Geoanalytical labs, including but not limited to Norm Pearson, Nigel Wilson, David Adams, Tim Murphy, Sarah Gain and Peter Wieland. I also extend thanks to Robert Rapp at the Australian National University, Ian Schipper at the University of Victoria, Wellington, and Fiona Petchey and Alan Hogg at the Radiocarbon Dating Laboratory, University of Waikato. Many thanks also to Steve Craven in the Mineral Processing Unit at Macquarie University. All of your guidance and expertise was critical in producing the quality data that is the fundamental core to this thesis.

I would like to extend a great thanks to the amazing MRes and PhD cohort at Macquarie University for the endless moral support, through providing discussions and advice over many coffees, lunches, and drinks at the bar. Particular thanks goes to Cait Stuart and Sarah Gain for all the cheese and wine, and Beñat Oliveira, Bruno Colas, Nicole McGowan, Paul Harvey, Hadrien Henry, Rosa

Didonna and Emma Singh, I cherish your friendships. Special thanks to Cait for helping me so much at the end; reading drafts, formatting and cheering me on! Cheers to Meg Stuart for providing meals for me! To my friends across the pond and beyond, particularly Fiona Gardner, Lucy Speed, Yara Shennan-Farpón, Lizzie Minchener, Amy Morris, Matt Goldspink, Steve Spittle, my fellow ‘hazards girls’, and the Stroud High girls, thank you for always keeping in touch and being there despite the time difference!

Thanks to my medical specialists, without whom I wouldn’t have been able to manage my endometriosis and finish this PhD.

I am extremely lucky to have an incredibly supportive family, so thank you so much to my Mum, Sister Nat, Granny, Grandad and Uncle Bruce, especially since the time during my studies has been extremely difficult for our family. I don’t know where I would be without all of your constant support, endless love, and care packages full of percy pigs. You guys, as always, have been a huge source of strength.

Last but certainly not least I would like to thank my partner Jon. You have been my literal rock and I cannot express how grateful I am to you for taking such good care of me, and I am especially thankful for your unwavering support.

Thank you to my examiners Valentin Troll, Richard Brown and Rebecca Carey for their encouraging comments that made this thesis a stronger piece of work.

L. Goode was funded by an International Macquarie University Research Excellence Scholarship (iMQRES) (2012196) associated with an Australian Research Council Future Fellowship awarded to H. Handley (FT120100440).

Table of Contents

Chapter One: Introduction and Motivation	1
1.1: General Introduction	1
1.2: Tephrochronology	1
1.3: Petrological, mineralogical and geochemical constraints on magma plumbing systems	3
1.4: Effusive-explosive transitions	3
1.5: Tectonic and geological setting of Java	4
1.6: Overview of Kelut	5
1.7: Aim and objectives	8
1.8: Outline of the Thesis	9
1.9: Published Parts	9
1.10: Author Contributions	10
1.11: References	10
 Chapter Two: Insights into eruption dynamics from the 2014 pyroclastic deposits of Kelut volcano, Java, Indonesia, and implications for future hazards	 17
2.1: Abstract	19
2.2: Introduction	20
2.2.1: Geological setting	22
2.2.2: The pre-2014 eruptive history of Kelut	23
2.2.2.1: The 1990 Eruption	23
2.2.2.2: The 2007-2008 eruption	24
2.2.3: The February 2014 eruption	25
2.2.3.1: Pre-eruption observations	25
2.2.3.2: Syn- and post-eruption observations	25
2.3: Strategy and Methodology	26
2.4: Results	29
2.4.1: Field observations	29
2.4.2: Stratigraphy, grain size and componentry of the 2014 pyroclastic deposits	32

2.4.2.1: Onset-phase pyroclastic units	33
2.4.2.2: Plinian-phase PDC units	35
2.4.2.3: Climactic plinian tephra fall	37
2.5: Discussion	38
2.5.1: Correlating the stratigraphy to the eruption chronology and dynamics	38
2.5.1.1: Stage 1: Eruption initiation and dome destruction	38
2.5.1.2: Stage 2: Plinian column formation and marginal column collapses	41
2.5.1.3: Stage 3: Climactic phase of the plinian event and tephra fallout	43
2.6: Eruption patterns and hazard implications	45
2.6.1: Pre-1900's	45
2.6.2: Recent activity – 1901 onwards	46
2.6.3: Hazard monitoring and implications	46
2.6.4: Hazard analysis framework	47
2.7: Conclusions	48
2.8: Acknowledgements	49
2.9: References	49

Chapter Three: Eruption frequency, style and composition variations at Kelut volcano, Indonesia, based on 1500 years of tephra records

3.1: Abstract	59
3.2: Introduction	60
3.3: Methodology	63
3.4: Results	67
3.4.1: Stratigraphy	67
3.4.2: Clast/pumice morphology	72
3.4.3: Glass geochemistry	72
3.5: Discussion	75
3.5.1: Eruptive behaviour and magmatic processes	75
3.5.1.1: Activity from ~AD 500 to 850	79
3.5.1.2: Activity from ~AD 1000 to 1400's	79
3.5.1.3: Activity from ~AD 1500 to early 1900's	80
3.5.1.4: Activity after 1901 to 2014	80

3.5.2: Eruptive frequency	81
3.5.3: Hazard scenarios	82
3.5.4: Completeness of the geological record	82
3.6: Conclusions	83
3.7: Acknowledgements	85
3.8: References	85

Chapter Four: The pre-eruptive magma storage system of the 1990 and 2014 Plinian, and 2007-2008 effusive dome-forming eruptions at Kelut volcano, Indonesia: insights into cyclic transitions in eruptive style

4.1: Abstract	93
4.2: Introduction	95
4.2.1: Geological and tectonic setting	97
4.2.2: Eruptive and geologic history	98
4.3: Methodology and analytical techniques	99
4.4: Results	102
4.4.1: Petrography and Mineralogy	102
4.4.2: General petrography of the 2014, 1990 and 2007-2008 samples	102
4.4.2.1: Plagioclase	106
4.4.2.2: Clinopyroxene and orthopyroxene	109
4.4.2.3: Titanomagnetite and amphibole	109
4.4.3: Mineralogy of the 2014, 1990 and 2007-2008 samples	110
4.4.3.1: Plagioclase	110
4.4.3.2: Clinopyroxene	113
4.4.3.3: Orthopyroxene	116
4.4.3.4: Titanomagnetites and amphibole	119
4.4.4: Summary of the main petrographic features	119
4.4.5: Major and trace element geochemistry	120
4.5: Discussion	124
4.5.1: Determination of pre-eruptive magma storage conditions	124
4.5.1.1: Amphibole pre-eruptive pressure, temperature and water estimates	124
4.5.1.2: Pyroxene pre-eruptive pressure and temperature estimates	124

4.5.1.3: Plagioclase-melt pre-eruptive pressure and temperature estimates	127
4.5.2: Depth of magma crystallisation and storage beneath Kelut	128
4.5.3: Discrete mafic influxes resulting in magma mixing and convection	130
4.5.4: Efficient mixing, and thermal and chemical buffering of magma	132
4.5.5: Silicic magma at shallowest chamber regions	133
4.5.6: Petrogenetic summary and model for Kelut magmas	135
4.5.7: Regional and longer-term geochemical comparison	138
4.5.8: Regional and global eruptive patterns	139
4.6: Conclusions	140
4.7: Acknowledgements	141
4.8: References	141

Chapter Five: Conclusions and Future Work **151**

5.1: Improving the understanding of eruption dynamics from deposits of single explosive eruptions at Kelut	151
5.1.1: The 2014 eruption of Kelut	151
5.1.2: Other older large explosive eruptions of Kelut	152
5.2: Variation in Kelut's eruptive behaviour and magmatic processes from a series of eruptions	153
5.2.1: Pre-eruptive influences on the magma system; large recharge versus small influxes of magma and eruption triggers	153
5.3: A deeper understanding of pre-eruptive magma storage regions	155
5.3.1: Pre-eruptive processes providing insights into the magmatic system	155
5.3.2: Degassing conditions between effusive and explosive eruptions	155
5.4: Possibility of tectonic triggered eruptions	
5.5: Eruptive frequency at Kelut	156
5.5.1: The current state of the magmatic system at Kelut	156
5.6: Implications for hazard analysis	157
5.7: Summary and broader implications of this work	158
5.8: Future directions and research suggestions	159
5.9: References	160

Appendix A	167
Electronic Appendices Contents	172

List of Tables

Chapter 2: Insights into eruption dynamics from the 2014 pyroclastic deposits of Kelut volcano, Java, Indonesia, and implications for future hazards

Table 1: Eruptive history of Kelut	21
Table 2: Lithological classifications used in componentry analysis	28
Table 3: Deposit type with location, sample number, eruptive stage and unit code	32

Chapter 3: Eruption frequency, style and composition variations at Kelut volcano, Indonesia, based on 1500 years of tephra records

Table 1: Eruptive history of Kelut	62
Table 2: Deposit type with location, sample number, lithofacies code, and eruption dates from charcoal	64-65
Table 3: Major element glass shard analysis	75
Table 4: Summary table of descriptions of units and interpretation of eruption style	76-77

Chapter 4: The pre-eruptive magma storage system of the 1990 and 2014 Plinian, and 2007-2008 effusive dome-forming eruptions at Kelut volcano, Indonesia: insights into cyclic transitions in eruptive style

Table 1: Mineral modes and types of textures for groundmass and minerals for each sample	103
Table 2: Textural descriptions and classification of plagioclase	105
Table 3: Textural descriptions and classification of clinopyroxene	107
Table 4: Textural descriptions and classification of orthopyroxene	108
Table 5: Representative plagioclase analyses	109
Table 6: Representative clinopyroxene analyses	115
Table 7: Representative orthopyroxene analyses	117
Table 8: Representative titanomagnetite analyses	119
Table 9: Representative amphibole analyses	119
Table 10: Major and trace elements for all samples	121

Electronic Appendices

Supplementary Table 1: Componentry and grain size distribution for the 2014 pyroclastic deposits.

Supplementary Table 1: Major elemental analyses of glass shards by EMP.

Supplementary Table 1: Petrography description of all thin sections

Supplementary Table 2: EMP analyses of plagioclase, clinopyroxene, orthopyroxene, titanomagnetite and amphibole for Kelut samples.

List of Figures

Chapter 1: Introduction and Motivation

Figure 1: Tectonic and geological setting of the Sunda arc and Java, Indonesia	2
Figure 2: Topographic map of Kelut volcano	6
Figure 3: Explosive and effusive eruption schematics at Kelut	7

Chapter 2: Insights into eruption dynamics from the 2014 pyroclastic deposits of Kelut volcano, Java, Indonesia, and implications for future hazards

Figure 1: Topographic map of Kelut volcano with sampling locations	20
Figure 2: Satellite imagery of Kelut pre- and post-2014 eruption	23
Figure 3: Photos from the field of 2014 pyroclastic deposits	27
Figure 4: Stratigraphic sections of 2014 pyroclastic deposits	30
Figure 5: Generalised stratigraphic section and componentry of the 2014 pyroclastic deposits	31
Figure 6: Photos of 2014 pyroclastic deposits	34
Figure 7: Componentry of deposits	34
Figure 8: Proportion of lithic clasts in deposits	35
Figure 9: Grain size distribution and componentry of tephra fall deposits	37
Figure 10: 2014 eruption schematic	39

Chapter 3: Eruption frequency, style and composition variations at Kelut volcano, Indonesia, based on 1500 years of tephra records

Figure 1: Topographic map of Kelut volcano with sampling locations	60
Figure 2: Photos from the field of stratigraphic sections	66
Figure 3: Correlations across stratigraphic sections	68
Figure 4: Composite stratigraphic section with geochemical variations	70
Figure 5: Back scatter electron images of glass shards	71
Figure 6: Harker plots of glass shard major elements	73
Figure 7: Plots of average Harker plots of glass shard major elements with group numbers	74
Figure 8: Main eruptive scenarios overtime with interpretation of magmatic processes	78

Chapter 4: The pre-eruptive magma storage system of the 1990 and 2014 Plinian, and 2007-2008 effusive dome-forming eruptions at Kelut volcano, Indonesia: insights into cyclic transitions in eruptive style

Figure 1: DEM of Kelut, map of tectonic setting of the Sunda arc and Java	96
Figure 2: Variation in geochemistry, temperature, and pressure estimates with stratigraphy	100
Figure 3: Photomicrographs of glomerocryst and groundmass textures	104
Figure 4: Ternary classification of plagioclase, clinopyroxene and orthopyroxene	110
Figure 5: Frequency histograms of Anorthite in plagioclase	111
Figure 6: Abundance of zoning patterns in plagioclase	112
Figure 7: Variations in Anorthite and Iron from core to rim of 2014 plagioclase	113
Figure 8: Variations in Anorthite and Iron from core to rim of 1990 and 2007-2008 plagioclase	114
Figure 9: Frequency histograms of Mg# in clinopyroxenes	115
Figure 10: Frequency histograms of Mg# in orthopyroxenes	116
Figure 11: End member variation plots of clinopyroxenes and orthopyroxenes	118
Figure 12: Harker plots of whole rock major element analyses	122
Figure 13: Chondrite and N-MORB normalised rare earth element plots	123
Figure 14: Trace element whole rock data plots	123
Figure 15: Test for equilibrium in for clinopyroxene-melt thermobarometry	125
Figure 16: Pressure temperature estimates	126
Figure 17: Frequency histograms of depths of clinopyroxene crystallisation and storage	129
Figure 18: Petrogenetic model of Kelut volcano	134
Figure 19: Total alkali silica of Javan volcanoes	138

Conclusions and Future Work

Figure 1: Summarising flow chart of main magmatic and eruptive scenarios	154
--	-----

Appendix A:

Supplementary Figure 1: Stratigraphy and deposit descriptions for Section 1	168
Supplementary Figure 2: Stratigraphy and deposit descriptions for Section 2	169
Supplementary Figure 3: Stratigraphy and deposit descriptions for Section 3	170
Supplementary Figure 4: Stratigraphy and deposit descriptions for Section 4	171

1. Introduction and Motivation

1.1. General Introduction

Java in Indonesia contains the largest number of historically active volcanoes, many of which have erupted with devastating impacts (e.g., Merapi, Bromo-Tengger, Semeru and Kelut; Fig. 1; Van Gerven and Pichler, 1995; Andreastuti et al., 2000; Thouret et al., 2007; Solikhin et al., 2012; Global Volcanism Program, GVP, 2015). Yet the volcanoes of Java are largely understudied against those in other subduction zone settings such as the Cascades, Antilles, Kamchatka-Kuriles, and Japan. There are few well-constrained, stratigraphic studies of Indonesian volcanoes (e.g., Andreastuti et al., 2000; Gertisser and Keller, 2003) and only 0.4% of known eruptions across Indonesia have been dated (other than by historical techniques; GVP, 2015). It is therefore vital that investigations into the stratigraphic records of volcanism in this region are undertaken to assess eruptive mechanisms, chronology, dynamics, and patterns over time. Geochemical analysis of erupted rocks permits insight into the inner working of volcanoes at depth, to establish the mechanisms and processes that control eruption behaviour and magnitudes (e.g., Dahren et al., 2012; Troll et al., 2013). Therefore, developing well-constrained, combined investigations of geochemistry and volcanology of Javan volcanoes can provide short-term forecasts based on the recognition of eruptive patterns (e.g., Turner et al., 2008; Damaschke et al., 2017; Torres-Orozco, 2017), and are crucial in helping to reduce the disastrous impacts of volcanic eruptions.

1.2. Tephrochronology

Determining the stratigraphy, lithology, size and distribution of volcanic deposits provides a record of the eruption chronology, and gives insight into the dynamics of eruptions, such as the style, size, volume, duration and extent of eruptions. Conducting stratigraphical investigations to understand eruption dynamics is particularly important when studying the mechanisms of emplacement of pyroclastic deposits from known large explosive eruptions (e.g., Bourdier et al., 1997; Carey et al., 2007; Pardo et al., 2008, 2012; Turner et al., 2011; Cronin et al., 2013). Stratovolcanoes often display eruptions with variable magnitudes and styles, often with long and complex eruptive episodes (e.g., Cioni et al., 2003; Turner et al., 2008; Damaschke et al., 2017; Torres-Orozco, 2017). Geochronological techniques such as tephrochronology can be used to evaluate and reconstruct the dynamics of these episodes from a stratigraphic framework. Tephrochronology involves combining a detailed characterisation of pyroclastic deposits in the field (such as individual bed thickness, lithology, and grain size), with radiocarbon dating and the geochemical composition of glass shards sampled throughout the stratigraphic sequence. When integrated with dating of the stratigraphic units, a longer-term chronological framework for previously uncharacterised volcanic events can be obtained (e.g., Lowe, 2011; Turner et al., 2009; Damaschke et al., 2017). The geochemical signature of glass shards within the deposits

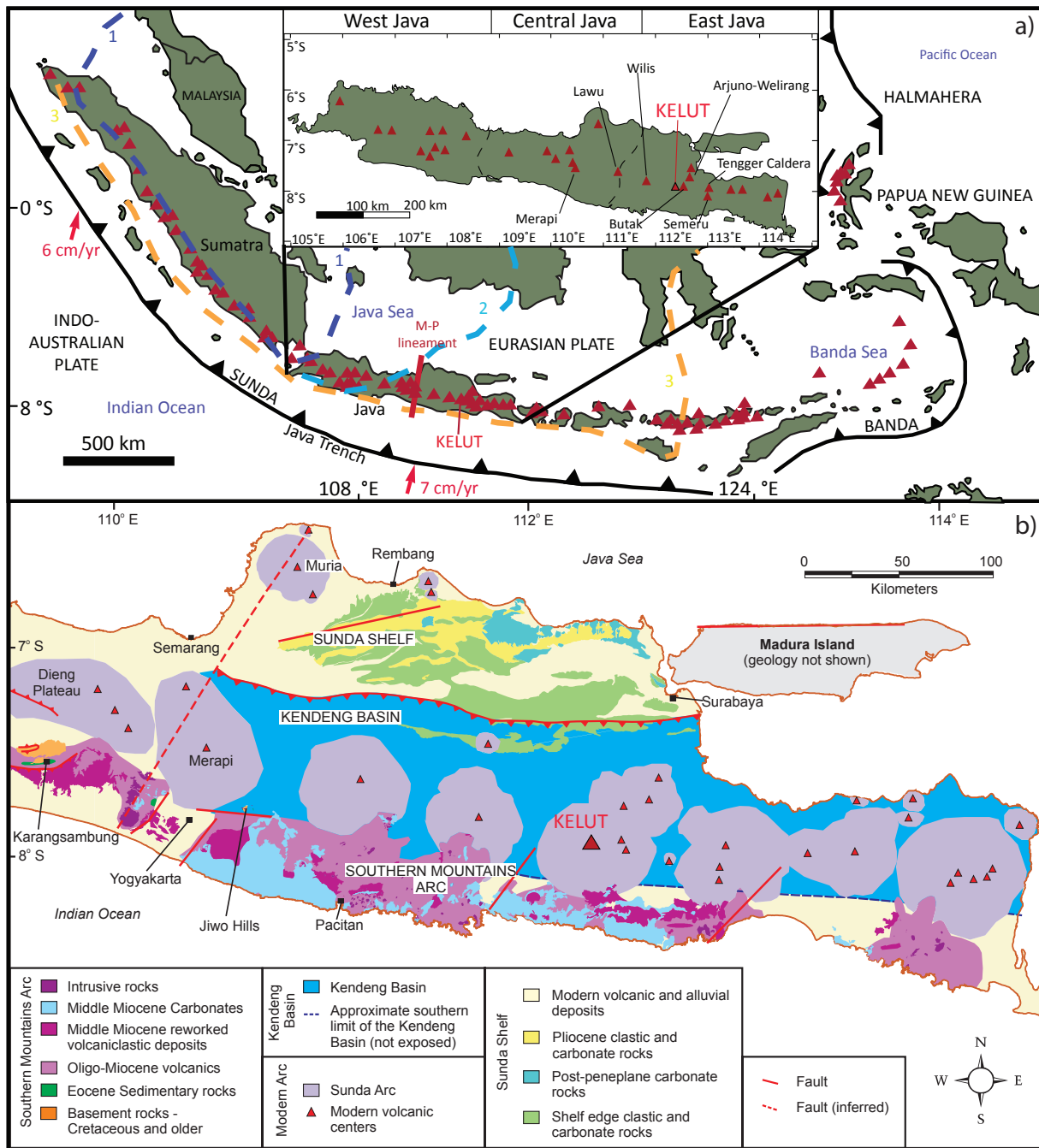


Figure 1: Tectonic setting of the Sunda arc and Java modified from Handley et al. (2014). Dashed lines show the limits for the growth of Sundaland. 1: represents the pre-Cretaceous Sundaland, 2: limit for material added to the pre-Cretaceous Sundaland in the Early Cretaceous, 3: the Eastern limit of material added in the mid-Cretaceous. Inset: red dashed line across Java shows the location of the Muria-Progo lineament on the Java inset map. Black dashed lines show the divisions of West, Central and East Java. Location of Kelut volcano shown in East Java.

give insight into volcanic and magmatic processes (Lowe, 2011), such as magma recharge, which is thought to be an important eruption trigger (e.g., Sparks et al., 1977; Tepley et al., 2000), and elucidate the relationship between eruptive cycles and magma composition (e.g., Turner et al., 2008; Torres-Orozco, 2017). A tephrochronological approach is crucial in determining a record of explosive volcanism, recurrence rates and frequency of eruptions (e.g., Andreastuti et al., 2000; Gertisser and Keller, 2003), and can allow for a framework of eruptive and magmatic evolution of

a volcano to be built (Larsen, 1981; Newhall et al., 2000; Shane, 2000; Gertisser and Keller, 2003; Larsen & Eiríksson, 2007; Lowe, 2011). This assessment is essential to better mitigate against the devastating effects that eruptions pose to society.

1.3. Petrological, mineralogical and geochemical constraints on magma plumbing systems

Petrological and mineralogical investigations of volcanic rocks are fundamental to understanding the conditions in the magma plumbing system that the rock forms out of, and is essential for predicting the behaviour of volcanoes. The chemistry of the minerals can be utilised to provide insights into magmatic processes occurring at depth, such as magma mixing, influx or recharge, assimilation, differentiation, and fractional crystallisation (e.g., Sparks et al., 1977; Davidson and Tepley, 1997; Tepley et al., 2000; Couch et al., 2001; Annen et al., 2006; Humphreys et al., 2006; Chadwick et al., 2007; Handley et al., 2008, 2010; Dahren et al., 2012; Troll et al., 2013). When mineral chemistry is combined with whole-rock geochemical data, they can be utilised to determine the pre-eruptive pressure and temperature conditions controlling crystallisation of magma, and can identify levels of magma storage regions (e.g., Devine et al., 1998; Putirka, 2008; Dahren et al., 2012; Jeffery et al., 2013). Geochemistry can also provide further constraints on magma dynamics such as ascent rate, flux, rate of magma supply, and the degree of open- and closed-system degassing, and fragmentation processes and conditions (e.g., Sparks et al., 1977; Woods and Koyaguchi, 1994; Cashman and Blundy, 2000; Ripepe et al., 2005; Adams et al., 2006; Edmonds and Herd, 2007; Castro and Gardner, 2008; Preece et al., 2016). These act as magmatic drivers that influence the style, magnitude, extent and duration of eruptions, particularly those originating from different eruptive styles at the same volcano.

1.4. Effusive-explosive transitions

Transitions from explosive to effusive behaviour during eruptions are common at many volcanoes worldwide such as Shiveluch, Kamchatka, Soufriere Hills, Montserrat, and Colima, Mexico (e.g., Druitt et al., 2002; Varley and Taran, 2003; Humphreys et al., 2006; Platz et al., 2007; Lavallée et al., 2012), and regionally to Java (e.g., Merapi; Costa et al., 2013; Preece et al., 2014, 2016). Textural and petrological analysis of products of explosive and effusive activity can determine the pre- and syn-eruptive crystallisation processes, to analyse driving forces behind the eruptive variants. Triggers of explosive volcanism can include increases in magma flux, volatile content of magmas, magma ascent rates, and inhibited gas loss (e.g., Eichelberger, and Westrich, 1981; Cashman and Blundy, 2000; Edmonds and Herd, 2007; Lavallée et al., 2012; Costa et al., 2013; Preece et al., 2016). In addition, the potential for explosive volcanism depends on how rapidly magma ascends in the chamber and conduit. This is a function of the pressure and temperature conditions of the magma storage regions, the properties of magma, such as composition, viscosity, and crystallinity, and the rate of magma flux (e.g., Woods and Koyaguchi, 1994; Massol and Jaupart,

1999; Scandone et al., 2007; Rutherford, 2008). Therefore, a complex interplay of magmatic processes within the plumbing system governs the style and recurrence of eruptions at volcanoes. Combining the information obtained from these petrological and geochemical investigations with volcanological studies are vital to understanding the full range of eruptive behaviour that a volcano is capable of producing.

1.5. Tectonic and geological setting of Java

The Sunda arc is part of the Indonesian subduction zone system that extends over 3000 km from the Andaman Islands in the north-west, through Sumatra and Java to Flores in the Banda Sea in the east (Fig. 1). It is formed by the subduction of the Indo-Australian plate beneath the Eurasian plate at a rate of 6-7 cm yr⁻¹ (Le Pichon, 1968; DeMets et al., 1990; Tregoning et al., 1994). The age of the subducting oceanic crust beneath the Java sector of the Sunda arc increases eastwards from ~80 to 130 Ma (Syracuse and Abers, 2006). The basement of the Sunda arc is thought to consist of a series of Gondwanan lithospheric fragments that were accreted to the pre-Cretaceous Sundaland margin in the Cretaceous (e.g., Hall, 2002, 2011). A Gondwanan continental fragment is proposed to lie underneath East Java in the Southern Mountains, and extend to western Sulawesi (Smyth et al., 2005, 2008). The majority of exposed rocks in Java comprise Cenozoic sedimentary sequences and volcanic arc rocks (van Bemmelen, 1949; Hamilton, 1979; Clements et al., 2009). However, Cretaceous accretionary-collisional complexes are exposed in West Java and Central Java (Wakita et al., 1994; Smyth et al., 2005, 2008).

Java can be split into three regions, West, Central and East Java, based on major structural and geological features. A significant structural divide is inferred between Merapi volcano (Central Java) and Kelut volcano (East Java), striking approximately NE-SW across the island at around 110.5 °E (Fig. 1). This lineament was described by Chotin et al. (1984) and Hoffmann-Rothe et al. (2001) as the strike-slip Central Java Fault, and by Smyth et al. (2005, 2007) as the Progo-Muria lineament. The lineament is suggested to represent the eastern limit of accreted Cretaceous terranes and sutures (Hoffmann-Rothe et al., 2001), and western limit of Archean-aged zircons in the southern mountains (Smyth et al., 2007). There is also a significant change in volcano geochemistry, volcanic activity and volcano morphology at this location (Handley, 2006).

Recent isotopic studies of Javanese volcanic rocks have revealed that there is heterogeneity in the composition of the subducted source input component involved in volcanic rock petrogenesis along the island, which reflects the composition of sediment entering the Java Trench. It is suggested that the amount of sedimentary crustal material incorporated in the subducting slab varies from West to East Java, with negligible amounts incorporated in Eastern Java (e.g., Plank and Langmuir, 1998; Handley et al., 2014). In addition, there is a greater influence of shallow level assimilation of crustal material in West and Central Java compared to East Java (Tuner and Foden, 2001; Handley et al., 2008, 2010, 2011; Chadwick et al., 2007; Troll et al., 2013).

The development of the modern, active Sunda arc occurred during the Quaternary (Pacey et al., 2013). The arc holds 78% of Indonesia's volcanoes (GVP, 2015) and active volcanism runs parallel to, and north of the Java trench along Java. Hough Transform analysis of volcano location indicates that their distribution is controlled by stress regimes in the arc lithosphere (Pacey et al., 2013). The volcanoes in Eastern Java are built on marine strata, conglomerates, and sandstone sediments, with small plutonic exposures (Smyth et al., 2008; Clements et al., 2009; Fig. 1b) In the area between Merapi and Kelut volcanoes (~215 km), only solfataric activity is reported for the main stratovolcanoes of Lawu and Wilis (Wheller et al., 1987). Kelut volcano marks the eastern continuity of recent volcanic activity along Java.

1.6. Overview of Kelut

Kelut, or Kelud (Indonesian name) volcano overlies 8-11 km of reworked volcanoclastic crustal sediments, and deeper metamorphosed ophiolitic material (Smyth et al., 2005, 2008). Kelut (Fig. 2) comprises two craters, of which the eastern crater is currently dormant, and the western crater is currently active. The volcano is shaped by 10 craters from previous explosive eruptions, the remains of several older lava domes, and parasitic cones (Bourdier et al., 1997; Jeffery et al., 2013), associated with the clockwise construction of the volcanic edifice from ~ 238 Ka to <40 Ka (Wirakusumah, 1991).

Kelut volcano is one of the most active and hazardous volcanic complexes in Indonesia, and is renowned for its often-unpredictable eruptive styles. Historical records show that Kelut has a long, frequent eruptive history with changes in eruptive style. There are 34 recorded eruptions since AD 1000. Eruptions are typically phreatic and phreatomagmatic due to the presence of the crater lake (Fig. 2), which leads to deadly and destructive syn-eruptive lahars (Bourdier et al., 1997, 1997a; Jeffery et al., 2013; GVP, 2014). The historic eruptive record is dominated by eruptions of volcanic explosivity index (VEI) 3 to 4. These eruptions are typically of short-duration and violent, such as the 1990 eruption (Bourdier et al., 1997; Siebert et al., 2011; GVP, 2014). The largest VEI 5 eruption occurred in 1585, with ~10,000 fatalities. Since 1920, the eruptive record is dominated by periods of lava-dome effusion (e.g., 1920, 2007-2008), followed by explosive VEI 4 eruptions that destroy the dome and widen the crater area (Fig. 3; e.g., 1990, 2014; Hadikusumo, 1974; GVP, 2014, Bourdier et al., 1997; Jeffery et al., 2013).

Deposits from the volcano comprise pyroclastic density current (PDC) deposits, tephra falls, lahar and debris avalanche deposits. The current crater opens to the south-west, therefore, the edifice and surrounds are most affected by channelised PDCs and lahars in this direction. Material is channelised towards the nearby cities of Kediri and Blitar (Fig. 2). Syn- and post-eruptive (rain derived) lahars pose the greatest volcanic hazards at proximal (≤ 5 km distance from the crater) and distal locations (≥ 5 km distance from the crater) (Suryo and Clarke, 1985; Bourdier et al., 1997b; De Bélizal et al., 2012; Andreastuti, in press). Since 1919, tunnels have been built in the side of main crater in order to reduce the volume of the lake and recurrence of lahars (Zen and

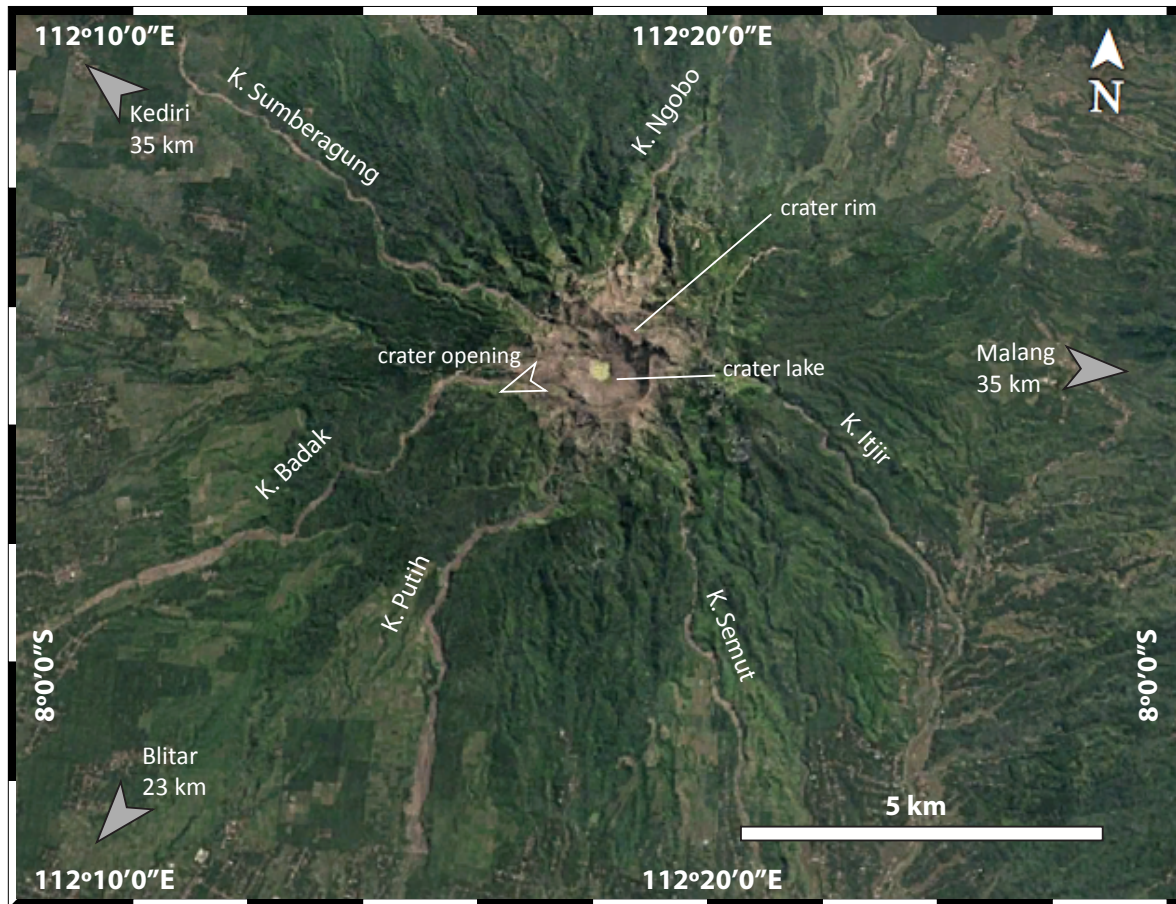


Figure 2: Topographic map of Kelut, with morphological features of the volcano outlined. Marked with arrows are the direction of the opening of the crater (to the south-west), and distance from the vent to the largest nearby population centres of Malang, Kediri and Blitar. Channelisation of lahars and pyroclastic density currents are down the main river valleys, which are marked.

Hadikusumo, 1965; Bernard and Mazot, 2004). Tephra falls are commonly dispersed south-west in the prevailing wind direction, however accumulate radially proximal to the volcano ($\leq 5\text{km}$). Fine tephra fall disperses across Java, often affecting flight paths and even leading to closures of airports. The official hazard maps by the Centre for Volcanology and Geologic Hazard Mitigation (CVGHM) include these hazards as a threat to proximal and distal areas (Mulyana et al., 2004; Primulyana et al., 2014).

The products of the most recent explosive 1990 and effusive 2007-2008 eruptions have been studied in detail (e.g., Bourdier et al., 1997, 1997a; Hidayati et al., 2009; Jeffery et al., 2013). Bourdier et al. (1997) presented observations from the stratigraphy of the 1990 explosive eruption deposits in order to identify eruptive processes. The 1990 eruption produced scoria-flow, pumice-flow and tephra falls from two eruptive phases; a pre-plinian and plinian phase. Bernard and Mazot (2004) evaluated the evolution and re-equilibration of the volcanic crater lake after the 1990 eruption, and identified that two hydrothermal systems feed the lake. Hidayati et al. (2009) looked at the seismic precursors for the 2007-2008 emergence of a lava dome, and stated that seismic activity began 3 months prior to the eruption. Jeffery et al. (2013) studied the petrology

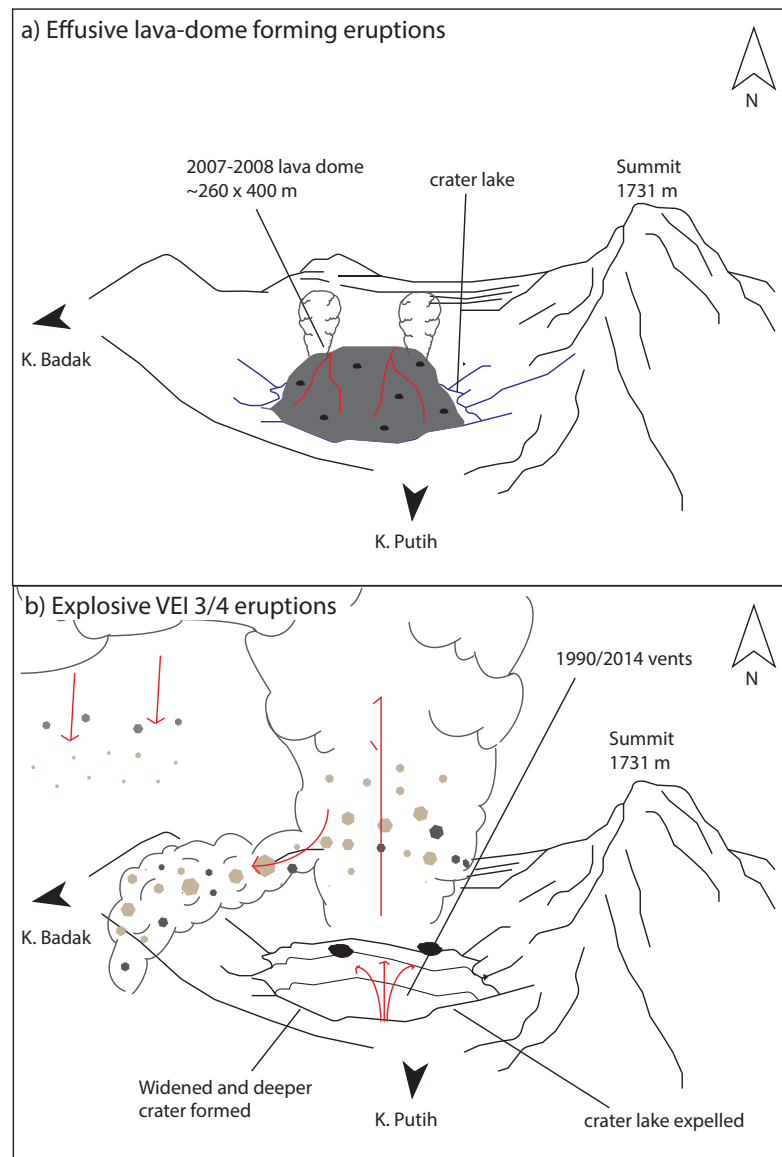


Figure 3: Schematic of effusive-explosive eruptions at Kelut crater modified from Bernard and Mazot (2004). Crater opens to the south-west. a) Emergence of a lava dome, in this case the 2007-2008 lava dome, through the crater-lake accompanied by plumes of steam. b) Explosive eruption at the same vent, such as the 1990 and 2014 eruptions. No crater lake is present and the crater is widened and deepened. Pyroclastic deposits are directed down the K. (meaning river valley) Putih and Badak.

and mineralogy of the 2007-2008 lava dome in order to determine pre-eruptive magmatic processes, and build an understanding of the complex, multi-level plumbing system below Kelut. They proposed that magma mixing was a major pre-eruptive process, with shallow level crustal assimilation also playing a role. The authors noted a wide range in crystal textures and suggested that crystallisation occurs at two main depths. The most recent explosive (VEI 4) eruption of Kelut occurred in February 2014, when investigations comprising this thesis first began. Comparisons of the petrology and geochemistry of this eruption with the VEI 4 1990 eruption, and the effusive 2007-2008 eruption to determine drivers behind the transitions in eruptive behaviour are yet to be undertaken at Kelut. In addition, other than the historical records reported by the Global Volcanism

Program (2014), and the information presented in mentioned studies, little is known about the longer-term volcanological and geochemical history of the volcano.

Kelut volcano therefore remains poorly understood and drastically understudied. A complete and robust record of eruptive activity, and a framework for magmatic evolution does not exist for Kelut. Since it has a long eruptive history, recent activity, and variations in eruptive styles it is an ideal volcano to study in order to determine its eruptive and magmatic evolution over time. Such records are essential in order to understand the types, magnitude and frequency of possible eruptive phenomena, particularly in the context of understanding cyclic transitions in effusive-explosive eruptive behaviour. Indonesia has the largest population living in close proximity to volcanoes, more so than any other region in the World. More than 68 million Indonesians live within 30 km of a Holocene volcano (Brown et al., 2015), and this results in a high number of eruptions that produce fatalities and damage to human infrastructure. Kelut has a number of small and large population centres within ≤ 35 km of the volcano, such as Blitar, Kediri and Malang (Fig. 2), each with populations of $\sim 130,000$ to $\sim 820,000$ people (UNdata, 2010). To mitigate against the devastating effects that the large eruptions impinge on society, this thesis aims to build a robust record of magmatic drivers behind temporal variations in eruption frequency and style at Kelut. The assessment of information presented in this thesis is vital to aiding in the forecasting of eruptive styles and identifying potential hazards, so that fatalities can be avoided. This is crucial to the region, since many Indonesians are adversely affected by damage to livelihoods, casualties and even fatalities (e.g., Andreastuti et al., in press). Further to this, forecasting and monitoring of the volcano is vital in order to determine when large-scale evacuations may take place in order to reduce vulnerability to Indonesian populations.

1.7. Aim and objectives

The main aim of the thesis is to build a stratigraphically well-constrained record of the volcanological and geochemical evolution of Kelut volcano, Indonesia, to increase our understanding of its eruptive behaviour and frequency.

The objectives of this study are to:

1. Improve the understanding of eruption dynamics of intermediate composition explosive eruptions from deposition records at Kelut;
2. Build long-term detailed and combined records of volcanology, geochronology and geochemistry in order to understand how Kelut's eruptive behaviour has varied over time;
3. Use petrography and mineralogy to gain insight into the magma plumbing system dynamics, storage regions and pre-eruptive magmatic processes that influence the style and magnitude of eruptions; and

4. Establish the pattern and frequency of eruptive activity over time at Kelut, particularly the recurrence of large eruptions, and determine how this aids in eruption forecasting and identifying potential hazards.

1.8. Outline of the Thesis

This thesis comprises five related chapters. This includes an introductory chapter (this chapter), three main data chapters (chapters 2, 3 and 4), and a final synthesis and concluding chapter that links all the data presented in this thesis. Chapters are arranged logically, whereby a well-constrained stratigraphic study is first needed to give context to any in depth geochemical, petrological, and mineralogical studies.

Chapter 2 presents observational accounts of the stratigraphy and componentry of the pyroclastic deposits of the most recent 2014 eruption of Kelut. This new information is combined with geophysical and eyewitness reports in order to build a chronology of the eruption, and determine eruption dynamics.

Chapter 3 presents a stratigraphically well-constrained, long-term volcanological and geochemical study of Kelut, with insights into the magma plumbing system over time and how this has governed eruptive frequency and eruptive styles.

Chapter 4 presents a petrogenetic study of the 2014 eruptive deposits in order to determine Kelut's recent magma storage levels and plumbing system dynamics. 2014 eruptive deposits are directly compared to new data for the 1990 and 2007-2008 eruptions to elucidate if changes in eruptive style are linked to pre-eruptive magmatic processes.

Chapters are written according to the manuscript preparation requirements as set forward by each journal, resulting in length and style differences between chapters. Each chapter includes an introduction and discussion that is relevant to that specific study.

1.9. Published Parts

Chapter 2: Insights into eruption dynamics from the 2014 pyroclastic deposits of Kelut volcano, Java, Indonesia, and implications for future hazards. This chapter has been submitted to the Journal of Volcanology and Geothermal Research, Special Volume on Kelud and Sinabung Volcanoes in November 2016. This article was accepted after revisions in January 2017 and is now available in press online (doi: <https://doi.org/10.1016/j.jvolgeores.2018.02.005>).

Chapter 3: Eruption frequency, style and composition variations at Kelut volcano, Indonesia, based on 1500 years of tephra records. This manuscript was submitted to Bulletin of Volcanology in February 2018 and is under review.

Chapter 4: The pre-eruptive magma storage system of the 1990 and 2014 Plinian, and 2007-2008 effusive dome-forming eruption at Kelut volcano, Indonesia: insights into cyclic transitions in eruptive style. To be submitted to Contributions to Mineralogy and Petrology.

1.10. Author contributions

Fieldwork was planned by the author and supervisory team, with the assistance of Mirzam Abdurachman (MA) around January 2014 to take place in late March to April 2014. All samples were collected in the field by Shane Cronin (SC) and the author, with the assistance of local counterparts in the field.

Chapter 2: The volcano erupted on the 13 February 2014, so it was an ideal opportunity to collect fresh samples in order to assess the 2014 eruption. Therefore, the original idea for this manuscript was developed by the author, Heather Handley (HH), and SC during and after fieldwork. The author is responsible for 100% of data collection. Data analysis and interpretation were undertaken by the author under the supervision of HH and SC. Contributions to the writing of the manuscript are by the author (80%), with edits provided by HH (10%) and SC (10%).

Chapter 3: The original idea for this manuscript was developed by the author, HH, and SC during and after fieldwork. The author is responsible for 95% of data collection (bar radiocarbon dating of charcoal). Data analysis and interpretation were undertaken by the author under the supervision of HH and SC. Contributions to the writing of the manuscript are by the author (80%), with edits provided by HH (10%) and SC (10%).

Chapter 4: The original idea for this manuscript was developed by the author, HH, SC, and Simon Turner (ST) after fieldwork. One sample was collected on a previous excursion by SC. The author is responsible for 95% of data collection (trace elements were obtained with the assistance of Peter Wieland). Data analysis and interpretation were undertaken by the author under the supervision of HH, ST and Chris Firth (CF). Contributions to the writing of the manuscript are by the author (80%), with edits provided by HH (10%), CF (6%), and ST (4%).

1.11. References

- Adams, N.K., Houghton, B.F., Fagents, S.A., and Hildreth, W. (2006). The transition from explosive to effusive eruptive regime: The example of the 1912 Novarupta eruption, Alaska. *GSA Bulletin*. 118. 620-634.
- Andreastuti, S.D., Alloway, B.V., and Smith, I.E.M. (2000). A detailed tephrostratigraphic framework at Merapi Volcano, Central Java, Indonesia: implications for eruption predictions and hazard assessment. *Journal of Volcanology and Geothermal Research*. 100. 51-67.
- Andreastuti, S., Paripuno, E.K., Gunawan, H., Budianto, A., Syahbana, D., and Pallister, J. (in press). Character of community response to volcanic crises at Sinabung and Kelud volcanoes. *Journal of Volcanology and Geothermal Research*. DOI: <https://doi.org/10.1016/j.jvolgeores.2017.01.022>
- Annen, C., Blundy, J.D., and Sparks, R.S.J. (2006). The genesis of intermediate and silicic magmas in deep crustal hot zones. *Journal of Petrology*. 47. 505-539.
- Bernard, A., and Mazot, A. (2004). Geochemical evolution of the young crater lake of Kelud volcano in Indonesia. In: Wanty, R.B., and Seal II, R.B. (2004) eds. *Water-rock interaction, (WRI-11)*. London: Taylor and Francis group plc. 87- 90.

- Bourdier, J-L., Pratomio, I., Thouret, J-C., Boudon, G., and Vincent, P.M. (1997). Observations, stratigraphy and the eruptive processes of the 1990 eruption of Kelut volcano, Indonesia. *Journal of Volcanology and Geothermal Research*. 79. 181-203.
- Bourdier, J-L., Thouret, J-C., Pratomio, I., Vincent, P.M., and Boudon, G. (1997a). Volcanic hazards at Kelut volcano (Java island, Indonesia): lessons learned from the 1990 eruption. *Geomaterials*. 324. 961-968.
- Brown, S.K., Auken, M.R., and Sparks, R.S.J. (2015). Chapter 4 – Populations around Holocene volcanoes and development of Population Exposure Index. In: Loughlin, S.C., Sparks, R.S.J., Brown, S.K., Jenkins, S.F., and Vye-Brown, C. (eds). *Global Volcanic Hazards and Risk*. Cambridge University Press. 223-232.
- Carey, R.J., Houghton, B.F., Sable, J.E., Wilson, C.J.N. (2007). Contrasting grain size and componentry in complex proximal deposits of the 1886 Tarawera basaltic Plinian eruption. *Bulletin of Volcanology*. 69. 903-926.
- Cashman, K., and Blundy, J. (2000). Degassing and crystallisation of ascending andesite and dacite. *Philosophical Transactions of the Royal Society*. 358.
- Castro, J.M., Gardner, J.E. (2008). Did magma ascent rate control the explosive-effusive transition at the Inyo volcanic chain, California? *Geology*. 36. 279-282.
- Chadwick, J.P., Troll, V.R., Ginibre, C., Morgan, D., Gertisser, R., Waight, T.E., & Davidson, J.P. (2007). Carbonate assimilation at Merapi Volcano, Java, Indonesia: insights from crystal isotope stratigraphy. *Journal of Petrology*. 48. 1793-1812.
- Chotin, P., Rasplus, L., Rampnoux, J.P., and Suminta Nur. Hasim. (1984). Major strike slip fault zone and associated sedimentation in the central part of Java Island (Indonesia). *Bulletin de la Societe Geologique de France*. 6. 1259-1268.
- Clements, B., Hall, R., Smyth, H.R., & Cottam, M.A. (2009). Thrusting of a volcanic arc: a new structural model for Java. *Petrological Geoscience*. 15. 159-174.
- Costa, F., Andreastuti, S., Bouvet de Maisonneuve, C., and Pallister, J.S. (2013). Petrological insights into the storage conditions, and magmatic processes that yielded the centennial 2010 Merapi explosive eruption. *Journal of Volcanology and Geothermal Research*. 261. 209-235.
- Couch, S., Sparks, R.S.J., and Carroll, M.R. (2001). Mineral disequilibrium in lavas explained by convective self-mixing in open magma chambers. *Nature*. 411. 1037-1039.
- Cronin, S.J., Lube, G., Dayudi, D.S., Sumarti, S., Subrandiyo, S., Surono. (2013). Insights into the October-November 2010 Gunung Merapi eruption (Central Java, Indonesia) from the stratigraphy, volume and characteristics of its pyroclastic deposits. *Journal of Volcanology and Geothermal Research*. 261. 244-259.
- Dahren, B., Troll, V.R., Andersson, U.B., Chadwick, J.P., Gardner, M.F., Jaxybulatov, K., and Koulakov, I. (2012). Magma plumbing beneath Anak Krakatau volcano, Indonesia: evidence for multiple magma storage regions. *Contributions to Mineralogy and Petrology*. 163. 631-651.
- Damaschke, M., Cronin, S.J.C., Holt, K.A., Bebbington, M.S., and Hogg, A.G. (2017). A 30,000 year high-precision eruption history for the andesitic Mt. Taranaki, North Island, New Zealand. *Quaternary Research*. 87. 1-23.
- Davidson, J.P., and Tepley, F.J. (1997). Recharge in volcanic systems: evidence from isotopic profiles of phenocrysts. *Science*. 275. 826-829.

Chapter One

- De B lizar, E., Lavigne, F., Gaillard, J.C., Grancher, D., Pratomy, I., and Komorowski, J.C. (2012). The 2007 eruption of Kelut volcano (East Java, Indonesia): Phenomenology, crisis management and social response. *Geomorphology*. 136. 165-175.
- DeMets, C., Gordon, R.G., Argus, D.F., and Stein, S. (1990). Current plate motions. *Journal of International Geophysics*. 101. 425-478.
- Devine, J.D., Murphy, M.D., Rutherford, M.J., Barclay, J., Sparks, R.S.J., Carroll, M.R., Young, S.R., and Gardner, J.E. (1998). Petrologic evidence for pre-eruptive pressure-temperature conditions, and recent reheating of andesitic magma erupting at the Soufriere Hills volcano, Montserrat, W.I. *Geophysical Research Letters*. 25. 3669-3672.
- Druitt, T.H., and Kokelaar, B.P. eds., (2002). The eruption of Soufriere Hills volcano, Montserrat, from 1995 to 1999. *Geological Society of London*.
- Edmonds, M., and Herd, R.A. (2007). A volcanic degassing event at the explosive-effusive transition. *Geophysical Research Letters*. 34.
- Eichelberger, J.C., and Westrich, H.R. (1981). Magmatic volatiles in explosive rhyolitic eruptions. *Geophysical Research Letters*. 8. 757-760.
- Gertisser, R., and Keller, J. (2003). Temporal variation in magma composition at Merapi Volcano (Central Java, Indonesia): magmatic cycles during the past 2000 years of explosive activity. *Journal of Volcanology and Geothermal Research*. 123. 1-23.
- Global Volcanism Program (GVP). (2014). Eruptive History. In: Kelut Eruption Page. *Smithsonian Institution*. Accessed March 2015. Available: <http://www.volcano.si.edu/volcano.cfm?vn=263280>
- Global Volcanism Program (GVP) (2015). *Smithsonian Institution. The Indonesia Region*. Accessed March 2016. Available: <http://www.volcano.si.edu/region.cfm?rn=6>
- Hadikusumo, D. (1974). The rise and drop of Mt. Kelut crater bottom after paroxysmal eruptions. *Tectonophysics*. 23. 341-347.
- Hall, R. (2002). Cenozoic geological and plate tectonic evolution of SE Asia and the SW Pacific: computer-based reconstructions, model and animations. *Journal of Asian Earth Science*. 20. 353-431.
- Hall, R. (2011). Australia-SE Asia collision: plate tectonics and crustal flow. In: Hall, R., Cottam, M.A., & Wilson, M.E.J. (eds): The SE Asian gateway: history and tectonics of Australia-Asia collision. *Geological Society of London Special Publication*. 75 – 109.
- Hamilton, W. (1979). Tectonics of the Indonesian Region. *US Geological Survey Professional Paper*. 1078.1-50
- Handley, H.K., Macpherson, C.G., Davidson, J.P., Berlo, K., and Lowry, D. (2007). Constraining fluid and sediment contributions of subduction-related magmatism in Indonesia: Ijen Volcanic Complex, Indonesia. *Journal of Petrology*. 48. 1155-1183.
- Handley, H.K., Davidson, J.P., Macpherson, C.G., & Stimac, J.A. (2008). Untangling differentiation in arc lavas: constraints from unusual minor and trace element variations at Salak Volcano, Indonesia. *Chemical Geology*. 255. 360-376.

- Handley, H.K., Macpherson, C.G., & Davidson, J.P. (2010). Geochemical and Sr-O isotopic constraints on magmatic differentiation at Gede Volcanic Complex, West Java, Indonesia. *Contributions to Mineralogy and Petrology*. 159. 885-908.
- Handley, H.K., Turner, S., Macpherson, C.G., Gertisser, R., & Davidson, J.P. (2011). Hf-Nd isotope and trace element constraints on subduction inputs at island arcs: Limitations of Hf anomalies as sediment input indicators. *Earth and Planetary Science Letters*. 304. 212-223.
- Handley, H.K., Blichert-Toft, J., Gertisser, R., Macpherson, C.G., Turner, S.P., Zaennudin, A., and Abdurrachman, M. (2014). Insights from Pb and O isotopes into along-arc variations in subduction inputs and crustal assimilation for volcanic rocks in Java, Sunda arc, Indonesia. *Geochimica et Cosmochimica Acta*. 139. 205-226.
- Hidayati, S. H., Basuki, A., Kristianto, and Mulyana, I., (2009). Emergence of lava dome from the crater lake of Kelud volcano, East Java. *Jurnal Geologi Indonesia*. 4. 229-238.
- Hoffman-Rothe, A., Ritter, O., and Haak, V. (2001). Magnetotelluric and geomagnetic modelling reveals zones of very high electrical conductivity in the upper crust of Central Java. *Physics of the Earth and Planetary Interiors*. 124. 131-151.
- Humphreys, M.C.S., Blundy, J., and Sparks, R.S.J. (2006). Magma evolution and open-system processes at Shiveluch volcano: insights from phenocryst zoning. *Journal of Petrology*. 47. 2303-2334.
- Jeffery, A.J., Gertisser, R., Troll, V.R., Jolis, E.M., Dahren, B., Harris, C., Tindle, A.G., Preece, K., O'Driscoll, B., Humaida, H., and Chadwick, J.P. (2013). The pre-eruptive magma plumbing system of the 2007-2008 dome-forming eruption of Kelut volcano, East Java, Indonesia. *Contributions to Mineralogy and Petrology*. 166. 275-308.
- Larsen, G. (1981). Tephrochronology by Microprobe Glass Analysis. In: Self, S., Sparks, R.S.J. (eds). *Tephra Studies. NATO Advanced Study Institutes Series (Series C – Mathematical and Physical Sciences)*, 75. Springer, Dordrecht. 95-102.
- Larsen, G., and Eiriksson, J. (2007). Late Quaternary terrestrial tephrochronology of Iceland – frequency of explosive eruptions, type and volume of tephra deposits. *Journal of Quaternary Science*. 23. 109-120.
- Lavallée, Y., Varley, N.R., Alatorre-Ibarguengoitia, M.A., Hess, K.U., Kueppers, U., Mueller, S., Richard, D., Scheu, B., Spieler, O., Dingwell, D.B. (2012). Magmatic architecture of dome-building eruptions at Volcan de Colima, Mexico. *Bulletin of Volcanology*. 74. 249-260.
- Le Pichon, X. (1968). Seafloor spreading and continental drift. *Geophysical Research Letters*. 73. 3661-3697.
- Lowe, D.J (2011). Tephrochronology and its application: a review. *Quaternary Geochronology*. 6: 107-153.
- Massol, H., and Jaupart, C. (1999). The generation of gas overpressure in volcanic eruptions. *Earth and Planetary Science Letters*. 166. 57-60
- Mulyana, A.R., Nasution, A., Martono, A., Sumpena, A.D., Purwoto, and Santoso, M.S. (2004). Peta Kawasan Rawan Bencana Gunungapi Kelud, Propinsi Jawa Timur (Volcanic hazards map of Kelud volcano, East Java Province), Pusat Vulkanologi dan Mitigasi Bencana Geologi, Badan Geologi, Departemen Energi dan Sumber Daya Mineral. Scale 1:100,000, 1 plate.

Chapter One

- Newhall, C.G., Bronto, S., Alloway, B., Banks, N.G., Bahar, I., del Marmol, M.A., Hadisantono, R.D., Holcomb, R.T., McGeehin, J., Miksic, J.N., Rubin, M., Sayudi, S.D., Sukhyar, R., Andreastuti, S., Tilling, R.I., Torley, R., Trimble, D., and Wirakusumah, A.D. (2000). 10,000 years of explosive eruptions of Merapi Volcano, Central Java: archaeological and modern implications. *Journal of Volcanology and Geothermal Research*. 100. 9-50.
- Pacey, A., Macpherson, C.G., & McCaffrey, K.J.W. (2013). Linear volcanic segments in the central Sunda Arc, Indonesia, identified using Hough Transform analysis: Implications for arc lithosphere control upon volcano distribution. *Earth and Planetary Science Letters*. <http://dx.doi.org/10.1016/j.epsl.2013.02.040>
- Pardo, N., Cronin, S.J., Palmer, A., Procter, J., Smith, I. (2012). Andesitic Plinian eruptions at Mt. Ruapehu: quantifying the uppermost limits of eruptive parameters. *Bulletin of Volcanology*. 74. 1161-1185.
- Pardo, N., Avellán, D.R., Macías, J.A., Scolamacchia, T., and Rodríguez, D. (2008). The ~1245 yr BP Asososca Maar: New advances on recent volcanic stratigraphy of Managua (Nicaragua) and hazard implications. *Journal of Volcanology and Geothermal Research*. 176. 493-512.
- Plank, T., & Langmuir, C.H. (1998). The chemical composition of subducting sediment and its consequences for the crust and mantle. *Chemical Geology*. 145. 325-394.
- Platz, T., Cronin, S.J., Cashman, K.V., Stewart, R.B., and Smith, I.E.M. (2007). Transition from effusive to explosive phases in andesite eruptions – A case study from the AD 1655 eruption of Taranaki, New Zealand. *Journal of Volcanology and Geothermal Research*. 161. 15-34.
- Preece, K., Gertisser, R., Barclay, J., Berlo, K., Herd, R.A., Edinburgh Ion Microprobe Facility. (2014). Pre- and syn-eruptive degassing and crystallisation processes of the 2010 and 2006 eruptions of Merapi volcano, Indonesia. *Contributions to Mineralogy and Petrology*. 168. 1-25.
- Preece, K., Gertisser, R., Barclay, J., Charbonnier, S.J., Komorowski, J-C., and Herd, R.A. (2016). Transitions between explosive and effusive phases during the cataclysmic 2010 eruption of Merapi volcano, Java, Indonesia. *Bulletin of Volcanology*. 78. 54.
- Primulyana, S., Hariwaseso, A., Zaenuddin, A., Budianto, A. (2014). Peta Kawasan Rawan Bencana Gunungapi Kelud, Propinsi Jawa Timur (Volcanic hazards map of Kelud volcano, East Java Province), Pusat Vulkanologi dan Mitigasi Bencana Geologi, Badan Geologi, Kementerian Energi dan Sumber Daya Mineral. Scale 1:100,000, 1 plate.
- Putirka, K.D. (2008). Thermometers and barometers for volcanic systems. *Reviews in Mineralogy & Geochemistry*. 69. 61-120.
- Ripepe, M., Marchetti, E., Olivieri, G., Harris, A., Dehn, J., Burton, M., Caltabiano, T., and Salerno, G. (2005). Effusive to explosive transition during the 2003 eruption of Stromboli volcano. *Geology*. 33. 341-344.
- Rutherford, M.J. (2008). Magma ascent rates. In: Putirka, K.D., Tepley, F.J. (eds). Mineral, inclusions and volcanic processes. *Reviews in Mineralogy and Geochemistry*. 69. 241-271.
- Scandone, R., Cashman, K.V., Malone, S.D. (2007). Magma supply, magma ascent and style of volcanic eruptions. *Earth and Planetary Science Letters*. 253. 513-529.
- Shane, P. (2000). Tephrochronology: a New Zealand case study. *Earth Science Reviews*. 49. 223-259.

- Siebert, L., Simkin, T., and Kimberly, P. (2011). *Volcanoes of the World*. 3rd Ed. University of California Press: Los Angeles. 83-102.
- Smyth, H., Hall, R., Hamilton, J., & Kinny P. (2005). East Java: Cenozoic basins, volcanoes and ancient basement. In: 30th Annual Convention of the Indonesian Petroleum Association. Jakarta, Indonesia: *Indonesian Petroleum Association*. 251-266.
- Smyth, H.R., Hall, R., & Nichols, G.J. (2008). Cenozoic volcanic arc history of East Java, Indonesia: The stratigraphic record of eruptions on an active continental margin. *The Geological Society of America, special paper*. 436. 199-221
- Solikhin, A., Thouret, J-C., Gupta, A., Harris, A.J.L., and Liew, S.C. (2012). Geology, tectonics, and the 2002-2003 eruption of the Semeru volcano, Indonesia: Interpreted from high-spatial resolution satellite imagery. *Geomorphology*. 138. 364-379.
- Sparks, R.S.J., Sigurdsson, H., and Wilson, L. (1977). Magma mixing: a mechanism for triggering acid explosive eruptions. *Nature*. 267. 315-318.
- Suryo, I., and Clarke, M.C.G. (1985). The occurrence and mitigation of volcanic hazards in Indonesia as exemplified at the Mount Merapi, Mount Kelut, and Mount Galunggung volcanoes. *Quarterly Journal of Engineering Geology*. 18. 79-98.
- Syracuse, E.M., & Abers, G.A. (2006). Global compilation of variations in slab depth beneath arc volcanoes and implications. *Geochemistry, geophysics and Geosystems*. 7. Doi: <http://dx.doi.org/10.1029/2005GC0010045>.
- Tegoning, R., Brunner, F.K., Bock, Y., Puntodewo, S.S.O., MaCaffrey, R., Genrich, J.F., Calais, E., Rais, J., and Subarya, C. (1994). First geodetic measurement of convergence across the Java Trench. *Geophysical Research Letters*. 21. 2135-2138.
- Tepley, F.J., Davidson, J.P., Tilling, R.I., and Arth, J.G. (2000). Magma mixing, recharge and eruption histories recorded in plagioclase phenocrysts from El Chichón volcano, Mexico. *Journal of Petrology*. 41. 1397-1411.
- Thouret, J-C., Lavigne, F., Suwa, H., Sukatja, B., and Surono. (2007). Volcanic hazards at Mount Semeru, East Java (Indonesia), with emphasis on lahars. *Bulletin of Volcanology*. 70. 221-244.
- Torres-Orozco, R., Cronin, S.J., Pardo, N., and Palmer, A.S. (2017a). New insights into Holocene eruption episodes from deposit sequences at Mt. Taranaki (Egmont), New Zealand. *Bulletin of Volcanology*. 79:3.
- Troll, V.R., Deegan, F.M., Jolis, E.M., Harris, C., Chadwick, J.P., Gertisser, R., Schwarzkopf, L.M., Borisova, A.Y., Bindeman, I.N., Sumarti, S., & Preece, K. (2013). Magmatic differentiation processes at Merapi Volcano: inclusion petrology and oxygen isotopes. *Journal of Volcanology and Geothermal Research*. 261. 38-49.
- Turner, S., & Foden, J. (2001). U, Th and Ra disequilibria, Sr, Nd and Pb isotope and trace element variations in Sunda arc lavas: predominance of a subducted sediment component. *Contributions to Mineralogy and Petrology*. 142. 43 – 57.
- Turner, M.B., Cronin, S.J., and Smith, I.E.M. (2008) Eruption episodes and magma recharge events in andesitic systems, Mt Taranaki, New Zealand. *Journal of Volcanology and Geothermal Research*. 177. 1063-1076.

- Turner, M.B., Cronin, S.J., Bebbington, M.S., Smith, I.E.M., and Stewart, R.B. (2009). Integrating records of explosive and effusive activity from proximal and distal sequences: Mt. Taranaki, New Zealand. *Quaternary International*. 246. 364-373.
- UNdata (2010). *City population, Demographic Statistics*. United Nations Statistics Division. Updated 27/05/2017. Accessed January 2018.
- Varley, N.R., and Taran, Y.A. (2003). Degassing processes of Popocatepetl and Volcán de Colima, Mexico. In: Oppenheimer, C., Pyle, D.M and Barclay, J. (eds) Volcanic degassing. *Geological Society, London*. 263-280.
- Van Bemmelen, R.W. (1949). *The Geology of Indonesia and Adjacent Archipelago*. Government Printing Office: The Hague. 1-150.
- Van Gerven, M., and Pichler, H. (1995). Some aspects of the volcanology and geochemistry of the Tengger Caldera, Java, Indonesia: eruption of a K-rich tholeiitic series. *Journal of Southeast Asian Earth Sciences*. 11. 125-133.
- Wakita, K., Munsari, and Widoyoko, B. (1994). Cretaceous radiolarian from the Luk Ulo melange complex in the Karangsambung area, Central Java, Indonesia. *Journal of Southeast Asian Earth Sciences*. 9. 29-43.
- Woods, A.W., and Koyaguchi, T. (1994). Transitions between explosive and effusive eruptions of silicic magmas. *Nature*. 370. 641-644.
- Wheller, G.E., Varne, R., Foden, J.D., & Abbott, M.J. (1987). Geochemistry of quaternary volcanism in the Sunda-Banda arc, Indonesia, and three-component genesis of island-arc basaltic magmas. *Journal of Volcanology and Geothermal Research*. 32. 137-160.
- Whitford, D.J. (1975). Strontium isotope studies of the volcanic rocks of the Sunda Arc, Indonesia, and their petrogenetic implications. *Geochimica et Cosmochimica Acta*. 39. 1287-1302.
- Zen, M.T., and Hadikusumo, D. (1965). The future danger of Mt. Kelut (Eastern Java – Indonesia). *Bulletin Volcanologique*. 28. 275-282.

2. Insights into eruption dynamics from the 2014 pyroclastic deposits of Kelut volcano, Java, Indonesia, and implications for future hazards

Louise R. Goode¹, Heather K. Handley¹, Shane J. Cronin², Mirzam Abdurrachman³

¹Department of Earth and Planetary Sciences, Macquarie University, Sydney, NSW 2109, Australia.

²School of Environment, University of Auckland, Private Bag 92019, Auckland 1142, New Zealand.

³Department of Geological Engineering, Bandung Institute of Technology, Bandung 40132, Indonesia.

2.1 Abstract

On 13 to 14 February 2014 a ~4 hour long, VEI 4 eruption occurred at Kelut volcano (Java, Indonesia). Pyroclastic density currents (PDCs) and extensive ash fall led to 7 fatalities and disruption to flights across the Asia-Pacific region. New sedimentological descriptions of the pyroclastic deposits from the 2014 eruption were compared with eyewitness and satellite reports to elucidate temporal variations in eruptive dynamics. The stratigraphy of the deposits is presented in 3 stages, associated with two eruptions that occurred approximately ~15-30 minutes apart. Stage 1 PDC deposits originate from the smaller onset eruption. The PDC deposits from stage 2, and tephra fall deposits from stage 3 originate from the second, plinian eruption. During the onset eruption (stage 1), low energy PDCs were produced that ran out to <2.6 km. Basal layers show characteristics of deposits similar to ash-cloud surges that carried dominantly fine ash and crystal fragments. These are capped by deposits typical of high-particle concentrated pyroclastic flows. All stage 1 deposits have high contents of dense lithic fragments (up to 44% by vol.), sourced from the 2007-2008 lava dome and conduit walls, indicating that the eruption onset was driven by an explosive release of gas-overpressure below the vent-capping dome. Increases in the magma flux and transition to a more constant eruption led to a growing eruption column during the ~2-hour long stage 2 plinian eruption. Pumice rich (>70% by vol.) PDC deposits ran out to 4.7 km from the vent. The deposits reflect an increased output of fresh fragmented magma, and some conduit widening evidenced by dense lithic fragments. Vent instabilities and incorporation of dense material into basal margins of the plume led to the marginal collapse and formation of these PDCs. Stage 3 occurred in the final hour at the peak of the plinian eruption, around 01:00 to 02:00, and produced reversely graded lapilli fall deposits with ≤ 90 vol.% pumice from a 26 km-high plume. This indicates that there was a sustained flux of juvenile magma to the now open vent system, and expansion and fragmentation of the gas-rich magma was at its most efficient. Our study of the eruptive sequence of Kelut provides some constraints on predicted patterns for future explosive activity, critical for further hazard assessment of the volcano. Since 1901 Kelut has erupted on intervals of 1 to 23 years, and the 2014 event characterises a typical ‘explosive’ style of eruption that alternates regularly with effusive dome-formation and collapse events. The pattern depends on the dynamics of magma renewal to the system, the rate of magma ascent, and degassing conditions in the shallow magma reservoir and upper conduit. If this pattern holds, and the next eruption occurs within the next two decades, a return of prolonged dome growth could be anticipated.

Keywords: Kelud, Lava dome, pyroclastic flow, pyroclastic surge, pyroclastic density current, plinian, tephra fall

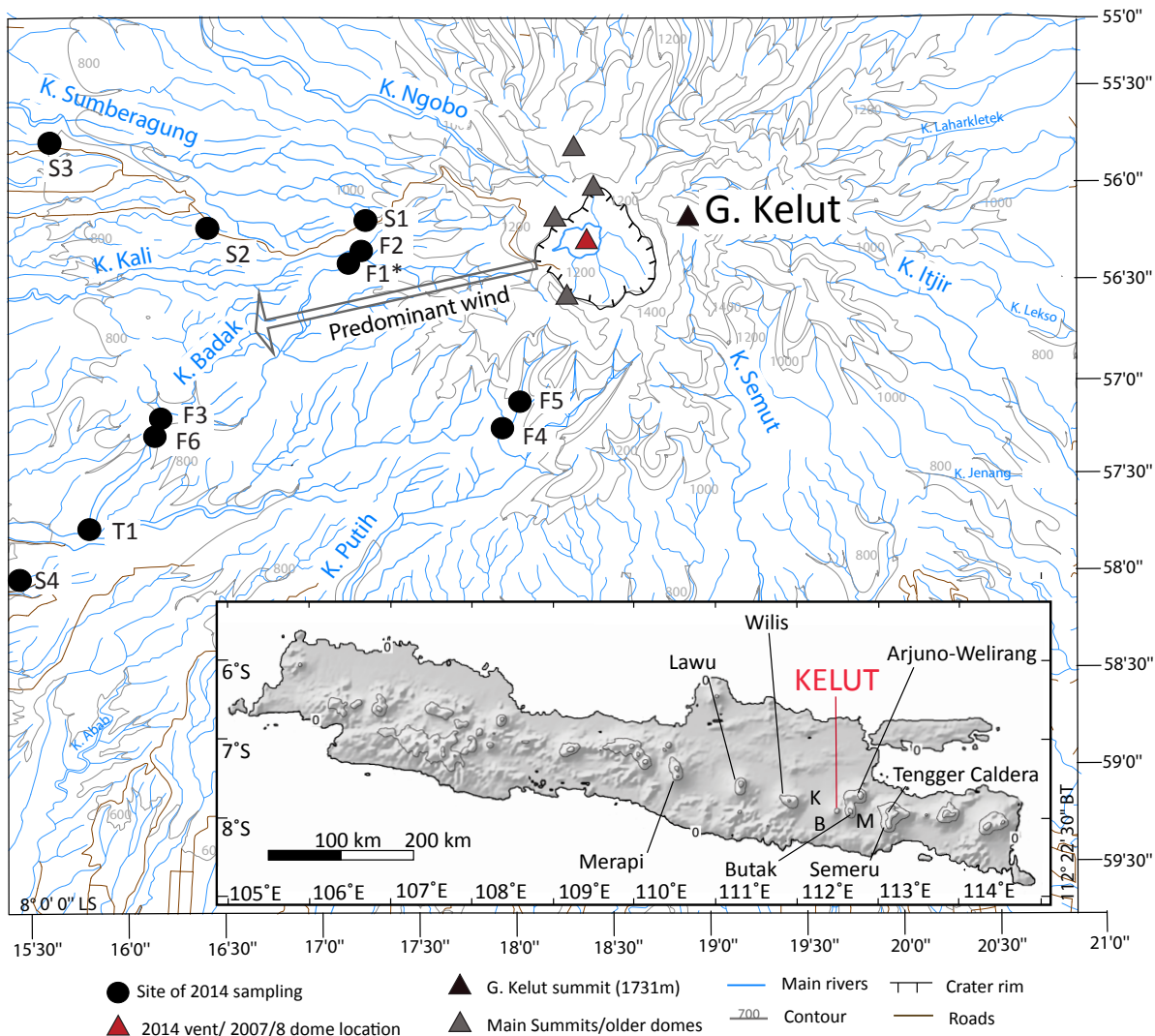


Figure 1: Topographic map of Kelut volcano showing the location of sampling sites (Modified from BDI, 2013). The main crater rim opens to the south-west of the edifice. Contours are in 200 m intervals. Grey arrow shows the prevailing wind direction reported in Kristiansen et al. (2015). Sampling sites S1-S4 and T1 are fall samples. S1-S4 denote sites where PDC deposits are absent and the fall deposits rest on a thin layer of soil above the 1990 deposits. Sites F1*-F6 are samples found in a 2014 stratigraphic sequence of a PDC deposit (note F1* denotes two PDC deposits observed at one location), with some tephra falls mantling the tops of the PDCs. Inset shows a DEM of Java, with the location of Kelut volcano marked. Letters on inserted map show the locations of K – Kediri, B – Blitar and M – Malang around Kelut volcano.

2.2 Introduction

Kelut volcano in East Java is renowned for its unpredictable, often destructive and hazardous explosive eruptions, and the production of deadly syn- and post-eruptive lahars (Bourdier et al., 1997; Bourdier et al., 1997a; De Bélizal et al., 2012; Jeffery et al., 2013; GVP, 2014). Due to the frequent presence of a crater lake and densely populated surrounds (Fig. 1), Kelut is considered one of Indonesia's most deadly volcanoes (Bourdier et al., 1997; Siebert et al., 2011; Jeffery et al., 2013). To address the lahar hazard a sophisticated tunnel drainage system for the lake in started construction in 1919 and was rebuilt following its destruction by subsequent eruptions (Zen and Hadikusumo, 1965).

Table 1: Known eruptive history of Kelut volcano, with details of individual eruptions

Eruption Year	Eruption	VEI	Volume (km ³)	Deposits/Hazards	Composition	Reference
1000	P-exp; exp	3	?	Lh, Tf	?	1, 2, 3
1311	P-exp; exp	3	?	Lh	?	1, 3
1334	P-exp; exp	3	?	Lh, Tf	?	1, 2, 3
1376	P-exp; exp; D	3	?	?	?	1
1385	P-exp; exp	3	?	Lh	?	1
1395	P-exp; exp	3	?	?	?	1
1411	P-exp; exp	3	?	?	?	1
1451	P-exp; exp	3	?	?	?	1
1462	P-exp; exp	3	?	?	?	1
1481	P-exp; exp	3	?	?	?	1
1548	P-exp; exp	3	?	Lh	?	1
1586	P-exp; exp	5	0.4	Lh	?	1, 2, 3, 8
1641	P-exp; exp	4	0.22	?	?	1, 8
1716	P-exp; exp	2	?	?	?	1, 3
1752	P-exp; exp	2	?	?	?	1, 2
1771	P-exp; exp	2	?	Tf	?	1, 2, 3
1776	P-exp; exp	2	?	?	?	1
1785	P-exp; exp	2	?	?	?	1
1811	P-exp; exp	2	?	Tf	?	1, 3
1825	P-exp; exp	2	?	Lh	?	1, 3
1826	P-exp; exp	4	0.22	Pf, Tf, Lh	?	1, 2, 3, 8
1835	P-exp; exp	2	?	Lh	?	1, 3
1848	P-exp; exp	3	?	Lh	?	1, 3
1851	P-exp; exp	2	?	Lh	?	1
1864	P-exp; exp	2	?	Lh	?	1, 5 (and references within)
1901	P-exp; exp	3	0.2	Pf, Tf, Lh	?	1, 3, 5 (and references within), 8, 9
1919	P-exp; exp	4	0.1	Tf, Lh, Pf	?	1, 3, 5 (and references within), 8, 9
1920	P-exp; exp; D	2	?	No substantial deposits	?	1, 3
1951	P-exp; exp; D-d	4	0.1	Tf, Pf, Lh	?	1, 3, 5 (and references within), 8
1966	P-exp; exp	4	0.09	Tf, Lh, Pf	?	3, 5, 8, 9
1967	D	1	?	No substantial deposits	?	3
1967	?	1	?	No substantial deposits	?	8
1990	P-exp; exp (plinian); D-d	4	0.13	Tf, Pf, Ps, Lh	Basaltic andesite	2, 3, 5, 7, 8
2007-2008	D	2	0.035	Some dome remnants	Basaltic andesite	3, 4, 5 (and references within), 6, 7, 8
2014	P-exp; exp (plinian); D-d	4	0.1	Tf, Pf, Ps, Lh	Basaltic andesite	8, 9, 10

Code for eruptions: P-exp: initial phreatomagmatic eruption; exp: explosive eruption at central crater; D: dome extrusion; D-d: destruction of dome

Code for deposits: Tf: tephra fall; Pf: pyroclastic flow; Lh: lahar; Ps: pyroclastic surge.

Volumes reported as bulk deposit volume. All Volcanic Explosivity Indices (VEI's) from GVP (2014a).

References: 1: Zen and Hadikusumo, 1965; 2: Pratomo, 1992; 3: Bourdier et al., 1997; 4: GVP, 2008; 5: De Belizal et al., 2012; 6: GVP, 2012; 7: Jeffery et al., 2013; 8: GVP, 2014; 9: VSI, 2014; 10: Kristiansen et al., 2015

Historic eruptions have varied in magnitude with Volcanic Explosivity Index (VEI) ranging from 2 to 5 (Table 1). Since 1919, eruptions of Kelut have shown a cyclic pattern of alternating VEI 4 explosive eruptions (destroying lava domes) and periods of lava dome effusion (Table 1; Zen and Hadikusumo, 1965; Pratomio, 1992; Bourdier et al., 1997; De Bélizal et al., 2012; GVP, 2012; 2014; Jeffery et al., 2013; VSI, 2014). Similar alternating patterns are common regionally and globally at dome-forming arc volcanoes such as Merapi, Indonesia (Newhall et al., 2000; Andreastuti et al., 2000; Gertisser et al., 2012; Cronin et al., 2013; Preece et al., 2014), Colima, Mexico (Robin et al., 1991; Arámbula-Mendoza et al., 2011; Lavallée et al., 2012), Montserrat, Lesser Antilles (Druitt and Kokelaar, 2002; Edmonds and Herd, 2007) and Shiveluch, Kamchatka (Gorshov and Dubik, 1970; Dirksen et al., 2006; Zharinov and Demyanchuk, 2013). Previous research on volcanic activity and deposits at Kelut has concentrated on the explosive 1990 and effusive 2007-2008 eruptions (Bourdier et al., 1997; Bourdier et al., 1997a; Thouret et al. 1998; Hidayati et al., 2009; De Bélizal et al., 2012; Jeffery et al., 2013). After the 1990 (VEI 4) plinian eruption (described by Bourdier et al., 1997) there was a 17-year quiescence, followed by a dome-extrusion episode in 2007-2008. The growing dome gradually displaced most of the crater lake, without producing lahars (Hidayati et al., 2009; Jeffery et al., 2013). On 13 February 2014, another VEI 4 plinian eruption occurred, destroying the 2007-2008 dome (GVP, 2014, 2014a, 2014b), with two eruptive pulses occurring over approximately 4.5 hours (GVP, 2014; Kristiansen et al., 2015)

In order to understand the eruption dynamics and mechanisms of emplacement of pyroclastic deposits during large explosive eruptions at volcanoes like those of Kelut in 1990 and 2014, it is necessary to combine detailed descriptions of the volcanic deposits (stratigraphy, lithology, size and distribution) with geophysical and eyewitness accounts (e.g., Bourdier et al., 1997; Carey et al., 2007; Pardo et al., 2008, 2012; Turner et al., 2011; Cronin et al., 2013). Here we present a summary of the observational accounts, field sedimentological data, and componentry and grain size analysis of the 2014 pyroclastic deposits to reconstruct the eruption chronology, and provide insight into the eruption dynamics. The significant features of the 2014 eruption are described in the context of the overall pattern of apparent cyclic behaviour at the volcano, which will assist in forecasting future eruption styles and hazards.

2.2.1 Geological setting

Volcanism on Java is attributed to the Sunda arc subduction system, formed by the northward subduction of the Indo-Australian plate beneath the Eurasian plate at $\sim 6\text{--}7\text{ cm/yr}^{-1}$ (Van Bemmelen, 1949; Hamilton, 1979; Hall, 2002; 2011). Although it appears to have the general form of a stratovolcano, Kelut is best described as a dome-complex. It has a complex morphology and summit profile, with several peaks composed of large lava domes, hosting numerous craters, and steep valleys (Fig. 1; Wirakusumah, 1991; GVP, 2014b). The main edifice was constructed by the growth of three lava domes and multiple viscous and large andesitic lava flows. Explosive eruptions have produced craters to the east, south, and west of the summit area. The eastern crater

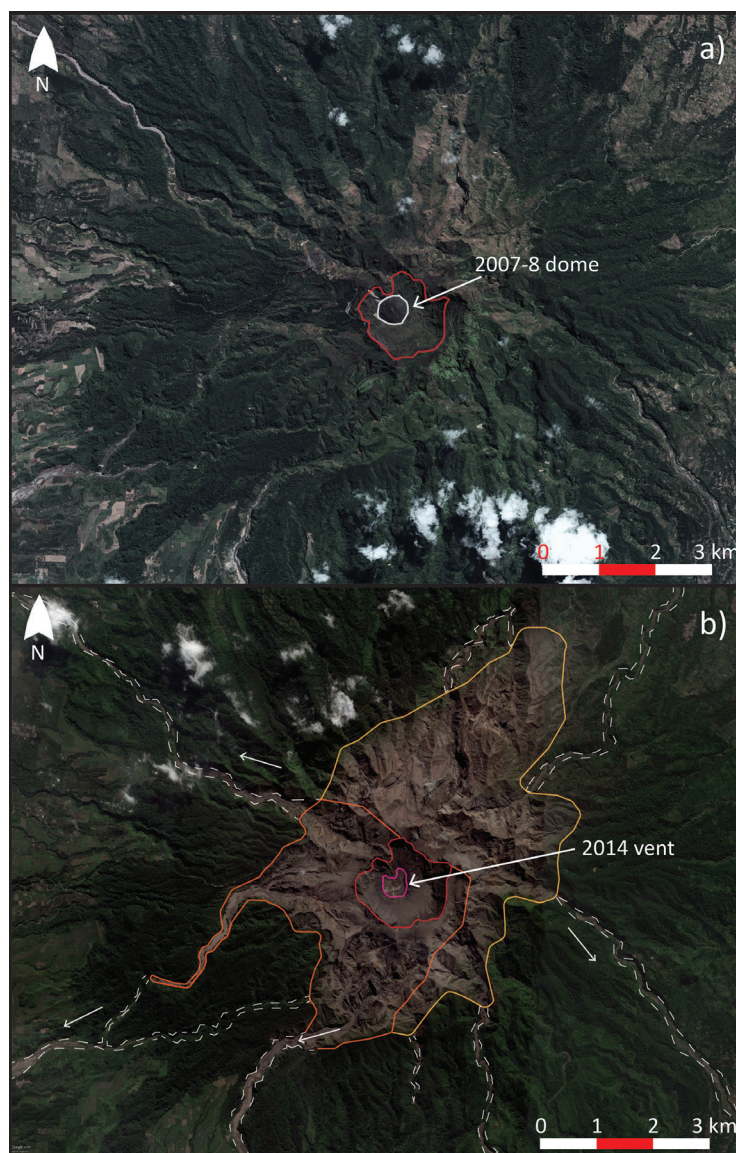


Figure 2: Satellite imagery showing Kelut volcano and peripheral areas surrounding the crater before (a) and after (b) the February 2014 eruption. a) Captured on the 23/08/2012, showing the 2007-2008 dome still occupying the summit crater lake. b) Captured on the 19/05/2014 after the 2014 eruption, showing the destruction of the 2007-2008 dome and creation of the new crater and the 2014 vent location. Red lines show the crater area of Kelut in both a) and b). White dashed line in a) shows the outline of the 2007-2008 lava dome. Pink line in b) shows the location of the 2014 eruption vent. Orange line in b) shows the extent of overbank and valley-confined PDCs in the K. Putih and K. Badak from this study (including ash blanketing the peripheral proximal crater area). Yellow line shows the extent of pyroclastic deposits in the proximal area north and north-east of the vent, not sampled in this study. White dashed lines and arrows show the deposition of further extensive valley-confined PDCs, and/or post-eruptive secondary lahars down the surrounding river valleys. Acquired using Google Earth Pro (2015), Copyright DigitalGlobe inc. (2015).

area is dormant as there has been a clockwise migration of the active vent location (Wirakusumah, 1991; Humaida et al., 2011; De Bélizal et al., 2012; Jeffery et al., 2013). Current activity occurs within a horseshoe-shaped scar that opens to the west (Fig. 2). The crater contains a 1 km-wide lake that has often affected the style of eruptions and produced voluminous lahars (e.g. the 1586 eruption) (Pratomo, 1992; Bourdier et al., 1997; De Bélizal et al., 2012). The volcanoes flanks comprise bedded pyroclastic density current (PDC) deposits, tephra fall deposits, with lahar sequences forming several large radial laharic fans (Bourdier et al., 1997; Thouret et al., 1998).

2.2.2 The pre-2014 eruptive history of Kelut

Kelut has been periodically active since AD 1000 with 34 recorded eruptions (Table 1). Most recorded episodes were short-lived, violent, typically subplinian to plinian eruptions (VEI 3 to 4). Six eruptions of this style have occurred since 1901 also forming destructive syn- and post-eruption lahars related to the summit crater lake (Bourdier et al., 1997; Siebert et al., 2011; GVP, 2014a). The largest and most deadly recorded eruption of 1586 (VEI 5), and its associated lahars, caused ~10,000 casualties (Zen and Hadikusumo, 1965; Bourdier et al., 1997; van Bergen et al., 2000). Pyroclastic deposits were mainly andesitic in composition, with the more recent eruptions producing basaltic-andesites (Bourdier et al., 1997; Jeffery et al., 2013). The 1919, 1951, 1966 and 1990 eruptions produced similar extensive tephra fall and PDC deposits and syn- and post-eruptive lahars (Bourdier et al., 1997; Siebert et al., 2011).

2.2.2.1 The 1990 Eruption

The VEI 4 1990 eruption occurred after 24 years of dormancy at 11:41 local time, 10 February 1990, and although it was short lived it caused 32 fatalities. The eruption completely removed a growing embryonic lava dome and the crater lake, excavating a new 400 m × 500 m-wide crater (GVP, 1990; Bourdier et al., 1997). The eruption produced a total of 0.13 km³ of basaltic andesite volcanic rocks, including extensive pumice- and scoria-rich PDC deposits reaching 5 km south and west of the crater. Widespread fallout comprised 0.10 km³ of the total deposit volume (GVP, 1990a; Bourdier et al., 1997). The first phase of the eruption was a phreatomagmatic explosion, followed by seven discrete eruptions and associated ‘wet ash’ fallout. The eruptive products became progressively darker in colour throughout the eruption, although no compositional variation was noted. At 12:35 a major eruption produced a sustained, plinian eruption column that was dispersed by wind to the south-west. A further pulse of activity occurred around 15:10 to 19:30, and was accompanied by ash and accretionary lapilli fallout from a 12 km-high plinian plume. The eruption decreased in intensity throughout the night, ceasing on 12 February (Bourdier et al., 1997). Bourdier et al. (1997) noted that on the 7 April 1990, a small, embryonic lava dome was growing in the summit crater in muddy water, measuring a few tens of metres in height. The new dome was compositionally and petrographically similar to the material erupted in February and was subsequently covered as the lake re-formed (Pratomo, 1992; Bourdier et al., 1997).

2.2.2.2 The 2007-2008 eruption

Starting in November 2007 and continuing over a seven-month period to 2008, a lava dome was extruded in the crater, which almost completely displaced the crater lake (Fig. 2a) (GVP, 2008; Hidayati et al., 2009; Jeffery et al., 2013). Plumes of steam rose 2 km from phreatic activity, although there was no explosive magmatic activity associated with this eruption (GVP, 2008). The dome grew rapidly until December 2007, when seismic activity and growth rate decreased, and growth ceased around May 2008 (Hidayati et al., 2009; De Bélizal et al., 2012; Jeffery et al., 2013). At this stage it was ~260 m in height with a basal width of ~400 m, totalling 3.5×10^7 m³ in volume

(Siebert et al., 2011; Jeffery et al., 2013). Jeffery et al. (2013) concluded from petrological studies that the eruption was preceded by a complex interplay of magma mixing, crustal assimilation and decompression-driven resorption of the crystal cargo. The dominantly basaltic-andesite dome rocks contained zoned, and texturally varied plagioclase, orthopyroxene, clinopyroxene, Ti-magnetite and minor apatite (Jeffery et al., 2013). The dome was closely monitored in fear of renewed sudden explosive activity (GVP, 2012; De B  lizar et al., 2012). However, only small white plumes rose from the dome after 2008, up until it was completely destroyed in the February 2014 eruption (Fig. 2b).

2.2.3 The February 2014 eruption

The most recent explosive eruption of Kelut occurred on 13 February 2014, which ejected the remaining water of the crater lake and completely excavated the 2007-2008 dome (GVP, 2014; Fig. 2). The general nature and extent of the deposits are similar to those of the February 1990 eruption.

2.2.3.1 Pre-eruption observations

The Indonesian Centre for Volcanology and Geological Hazard Mitigation (CVGHM; known locally as Pusat Vulkanologi dan Mitigasi Bencana Geologi, PVMBG) described seismic events at Kelut from mid-January onwards (GVP, 2014). Prior to the eruption, volcanic earthquakes occurred between 2 and 8 km deep, with 14 seismic events recorded in the first week of January, rising up to 693 the week before the eruption. Tiltmeter data showed inflation of the dome at one station. The remaining crater-lake water warmed by 5.5  C from September to 2 February 2014. At 21:15 local time on 13 February 2014, the Indonesian National Board for Disaster Management (Badan Nasional Penanggulangan Bencana, BNPB) raised the alert level to the highest level (4) meaning, ‘Awat’ or danger/warning, with eruption expected within 24 hours (see De B  lizar et al. (2012) and Andreastuti et al. (2018) for a description of alert levels). A 10 km-radius exclusion zone was set up, leading to the evacuation of ~166,000 people (Andreastuti et al., 2018).

2.2.3.2 Syn- and post-eruption observations

The BNPB reported that the first eruption occurred at ~22:50 local time on 13 February 2014, followed by the second, main plinian phase starting ~23:30, lasting 4-4.5 hours in total (GVP, 2014). The 2007-2008 dome was destroyed during this time, and a new 400 m-diameter crater excavated (Fig. 2b). Satellite imagery (CALIPSO) taken at ~01:12 local time showed that the eruption plume reached ~18-19 km in altitude. Imaged hourly by MTSAT-2 IR after 23:32 local time, the plume rapidly expanded, with parts of the plume rising to a maximum altitude of 26 km. A series of photographs from a local eyewitness (Putra, 2014) in Blitar taken from around 00:38 to 01:00 local time on 14 February 2014, show the eruption gradually increasing in intensity, with an initial dark-grey plume that became progressively paler in colour. The plume dispersed primarily west of the volcano, out over the Indian Ocean, with pale-brown coloured ash falling as

far as 240 km from the volcano to the north-east, north-west, south-west and west (GVP, 2014; Kristiansen et al., 2015; Fig. 1). The ash disrupted 40 flights from airports across Indonesia, including Yogyakarta (~215 km west), Surabaya (~91 km north) and around the Asia-Pacific area (GVP, 2014; Kristiansen et al., 2015). Satellite imagery from the International Charter Space and Major Disasters (2014) shows extensive PDC deposits, which destroyed forested areas proximal to the crater, and were directed down the Kali (meaning river, abbreviated to K.) Sumberagung, K. Badak and K. Putih valleys, reaching approximately 4 km from the crater (GVP, 2014; Fig. 2). Grey-to-black plumes accompany successive eruptions, reaching 400-600 m in height above the crater on 14 February, with further 3 km-high, grey-white steam-rich plumes observed on 15 February 2014. On 18 February, heavy rainfall generated lahars that reached Kediri (35 km west north-west), Blitar (20 km south-west), and Malang (35 km east; Fig. 1 insert), which flooded houses and destroyed arable land and several bridges (Dibyosaputro et al., 2015). Seven fatalities were reported in Malang due to the collapse of roofs from accumulated ash fall deposits (GVP, 2014). On 18 and 19 February 2014, the alert level for Kelut was lowered to 2, and the exclusion zone was reduced to a 5 km radius (GVP, 2014). Eruptions further declined until 20 February, with steam plumes reaching only 1 km altitude.

2.3 Strategy and methodology

Fieldwork and sample collection took place in April 2014. Access to the summit crater was prohibited at the time, thus samples were collected near to, and within, river valleys to the west, south and south-west of the summit (GVP, 2014; Fig. 1). Samples from different stages of the 2014 eruption, including fall and PDC deposits were collected from eleven different localities (Fig. 1). At each locality sedimentological data was collected: individual bed thickness, deposit grain size (using the classification scheme of White and Houghton, 2006), bedding and sedimentary structures, sorting and contact relationships, and the presence of fumarolic activity, charcoal and breadcrust bombs was noted (Fig. 3). Evidence of deposit reworking and damage to vegetation and building structures was also noted. Observational accounts of the 2014 eruption chronology were directly compared to the stratigraphy of the 2014 pyroclastic deposits observed in the field.

Grain size distributions (GSDs) were obtained of 20 samples from the 2014 pyroclastic deposits by sieving at 1ϕ intervals from <63 mm (-6ϕ) to <32 μ m (5ϕ). The componentry of 18 samples were determined by counting (where possible) up to 500 grains in each grain size fraction selected, where for most samples the <8 mm (-3ϕ) to 500 μ m (0ϕ) fractions were used. However, for the finer ash fall deposits the 1 mm (0ϕ) to 125 μ m (3ϕ) fractions were used for componentry analysis. The lithological classes used in componentry analysis are listed in Table 2, and comprise: pumice (light grey (juvenile), dark brown/grey and oxidised), scoria, crystals (single free and aggregates) and lithics (dark dense, light dense, dense oxidised (all of magmatic origin), and brown/ accidental country rock (of non-magmatic origin)). Six samples from sections F1 and F2 (PDCs) were split into ash matrix (samples K40 and K37), pumice lapilli clasts (samples K41 and K38), and lithic

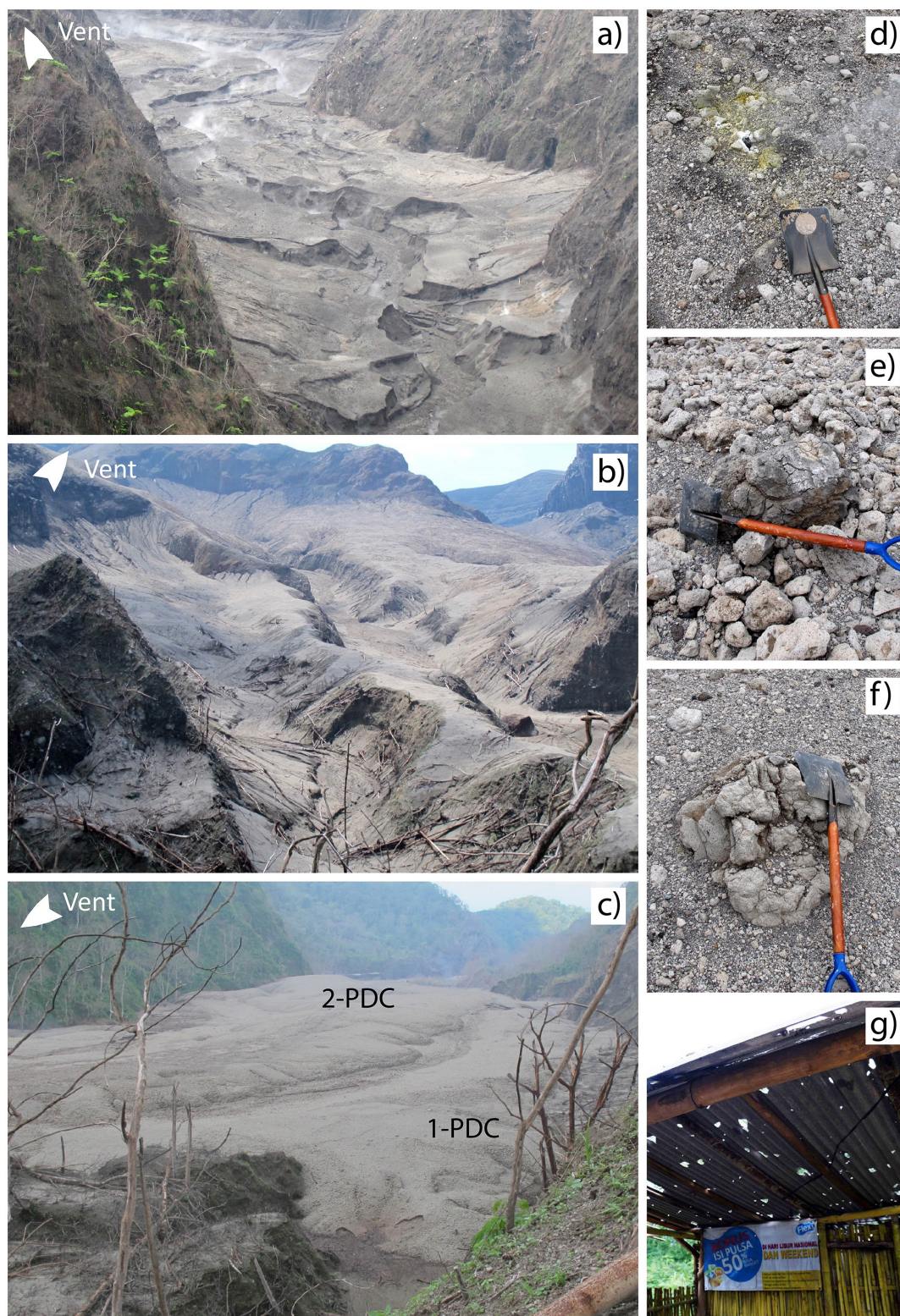



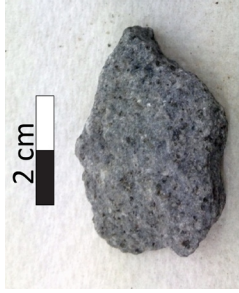



Figure 3: Photos of the 2014 volcanic deposits. a) Steaming PDC deposits near the vent in the K. Putih, infilling the valley, and possibly incised by post-eruption rainfall or lahars reworking material. b) Overbanking PDC and ash fall deposits down the K. Badak valley, sheeting topographic highs, and showing tree destruction and flattening. c) Two PDCs (1-PDC and 2-PDC) at F1 in the K. Badak. d) Fumaroles on top of the pyroclastic flow deposit (2-PDC) at location F1. e) Breadcrust bomb on top of the pyroclastic flow deposit (1-PDC) at site F1. f) Fragmented pumice block on top of the pumice-rich pyroclastic flow deposit (1-PDC) at site F1. g) Ballistic/tephra fall damage on the roof of a hut along the main access road to the vent. See text for further discussion. Photographs taken between the 02/04/2014 and 05/04/2014.

Table 2: Lithology classifications used in componentry analysis, including description of sub-classifications

Clast Type		Pumice		Scoria	Lithics	
Sub class		Grey/light brown Oxidised/alterd	Darker grey/brown Oxidised/alterd		Dense light grey Oxidised/alterd Accidental/brown (country rock)	Dense darker grey/black Oxidised/alterd Accidental/brown (country rock)
Photo						
Colour		Light grey or light brown	Dark yellowish brown	Dark grey/black	Light grey	Dark grey/black
Texture		Vitric, porous/foamy vesicular	Vitric, porous/foamy vesicular	Highly vesicular	Porphyritic	Porphyritic
Shape		Elongated – subspherical	Elongated – subspherical	Subspherical	Elongated – blocky	Elongated – blocky
Rounding		Subangular – subrounded	Angular – subrounded	Subrounded	Subangular	Subangular – subrounded
Vesicle shape and size		Common centimetric elongated vesicles. Milimetric vesicles finely sub-spherical to spherical.	Common centimetric elongated vesicles. Milimetric vesicles finely sub-spherical to spherical.	Common millimetric, elongated and highly distorted, with smaller angular vesicles	Rare – milimetric	Rare – milimetric
Groundmass		Vitric	Vitric, often oxidised/alterd	Vitric	Microcrysts of plagioclase and pyroxene	Microcrysts of plagioclase and pyroxene
Phenocrysts		Milimetric euhedral – subhedral plagioclase, clinopyroxene and orthopyroxene	Milimetric euhedral – subhedral plagioclase, clinopyroxene and orthopyroxene	Milimetric rare fragmented/anhydral clinopyroxene and orthopyroxene, rare plagioclase	Euhedral – subhedral milimetric dominantly plagioclase, with lesser clinopyroxene and orthopyroxene.	Euhedral – subhedral milimetric phenocrysts of dominantly clinopyroxene and orthopyroxene, lesser plagioclase.
Description		Vesicles can display directional distortion, or flow-foliation, and can be colour banded. Often centimetric crystal ‘clots’ appear in large vesicle holes in the bomb-shaped clasts. Very vitric with frothy texture. Only definitive juvenile clasts.	Differ to grey pumice clasts as often more altered, and less vitric. Clasts often show flow-stretched vesicles and colour banding. Some clasts are tuff like aggregation of clasts, which are less porous. Often centimetric crystal ‘clots’ appear in large vesicle holes in the bomb-shaped clasts similar to lighter grey clasts.	More mafic/basaltic vesicular clasts relative to pumice clasts. Also less crystalline overall, and contain predominantly less plagioclase than pumice clasts. Vesicles are also predominantly smaller.	Dense, crystal-rich lava clasts. Similar to 2007-2008 dome lava (Jeffery et al., 2013). Varying in size and occurrence in deposits. Glomerocrysts common. Less vesicular than pumice clasts.	Lava clasts. Some are often more weathered possibly older. Others appear very fresh. Rounding depends on clast size. Glomerocrysts common. Less vesicular than pumice clasts.

lapilli clasts (samples K42 and K39) in the field and so each of these were counted separately. The full grain-size and componentry results are given in Appendix Table 1. The term deposit is used to refer to the general depositional accumulations of ash or tephra from an eruption. The term unit refers to the individual tephra layers that can be attributed to each separate eruption, or from different eruptive phases/pulses within one eruption (where specified – see contact relationships on Fig. 4); of which is each unit has individual facies determined by their architectural description (e.g., grading, bedding). Note that individual unit may have two different facies descriptions within it.

2.4 Results

2.4.1 Field observations

Evaluation of damage in proximal areas (<5 km from the vent) concentrated mostly on the impacts to vegetation associated with valley-ponded, or overbank PDCs on the south-west flanks of the volcano (Fig. 1). It is clear from satellite imagery that all of the forest within this radius around the vent was destroyed (Fig. 2b, outlined by the yellow and orange lines). Pyroclastic deposits cover most of this proximal destruction area, up to and including ~4 km north of the vent, ~3 km south, ~2 km west, and ~1.6 km east of the vent (Fig. 2b). Valley-confined and –infilling PDCs were distributed down the west and south-west flanks of the volcano, and are thickest in the K. Putih (at location F4; Fig. 3a) and K. Badak river valleys (location F1 to F6). Along both river valley margins near locations F5, F4, F1 and F2 (all within 2.6 km from the vent) all vegetation has been completely removed, with trees felled in the downstream direction of the flow (south or south-west), or completely uprooted (Fig. 3b), with burnt vegetation. Many of the PDC deposits were still hot when sampled, with local weak fumarolic activity (PDC sequences at location F1; Fig. 3c-d). The PDC deposits in valley floors showed well-developed marginal levees concentrating coarse clasts (up to 0.5 m in diameter) with little matrix material (Fig. 3c-f). A further ~2 km from the vent in the K. Badak valley, the valley-ponded, blocky, pumice-rich PDCs are also found with large fragments of burnt branches. Here, laterally continuous overbanking facies (associated with the valley-floor PDC sections at F1) are observed at F3 and F6, in areas where trees have been singed and snapped. Fall deposits, including elutriated co-PDC ash was best preserved mantling gentle slopes and interfluves (Fig. 3b). Fine ash from surges surmounts ~85 m high ridges in both the K. Badak and K. Putih valleys, and blankets all of the banks and tops of interfluves and levees in the proximal and medial areas, with multi-directional felled and snapped trees (Fig. 2b, also within orange line; Fig. 3b). Additionally, ballistic bombs falling within ~2 km of the vent along the main access road have caused ~10 cm holes in roofed structures (near S1; Fig. 1; Fig. 3g). It can be observed on satellite imagery that further possible PDCs and large, post-eruptive lahars have inundated medial to distal areas of the K. Putih (further than F4 and F5), K. Semut, K. Itjir, K. Sumberagung, and K. Kali valleys, ≥ 8 km from the vent (Fig. 1, 2b).

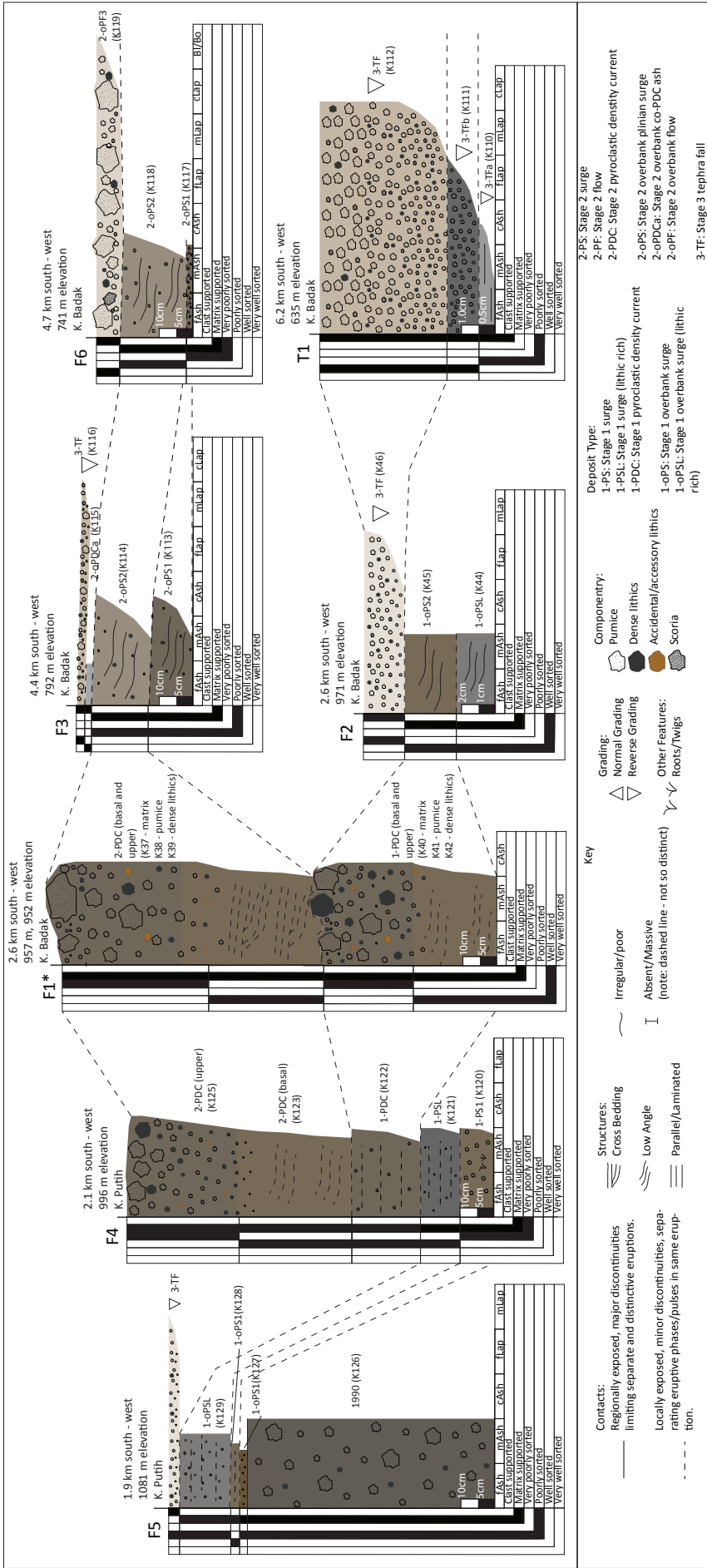


Figure 4: Simplified stratigraphic sections of the 2014 Kelut eruption pyroclastic deposits. Locations refer to those given in Figure 1 and unit names and sample numbers are listed in Table 3 (note F1* denotes two PDC sections described at the same location). Fall samples found at S1-S4 are not included as stratigraphic sections, as the samples were not found above a 2014 PDC deposit. The river valley locations, elevations, distance and direction from the vent for each section are also indicated. See key for explanation of features. Note that the scale differs on each stratigraphic section. Blacked out boxes on the left of each sequence denote the sorting (very well to very poorly) and whether the sample is clast- or matrix-supported. Grain size scale is: fAsh: fine ash, 63-250 μm ; mAsh: medium ash, 250-500 μm ; cAsh: coarse ash, 500 μm – 2mm; fLap: fine lapilli, 2-4 mm; mLap: medium lapilli, 4-16 mm; cLap: coarse lapilli, 16-64 mm; Bl/Bo: block/bomb; >64 mm.

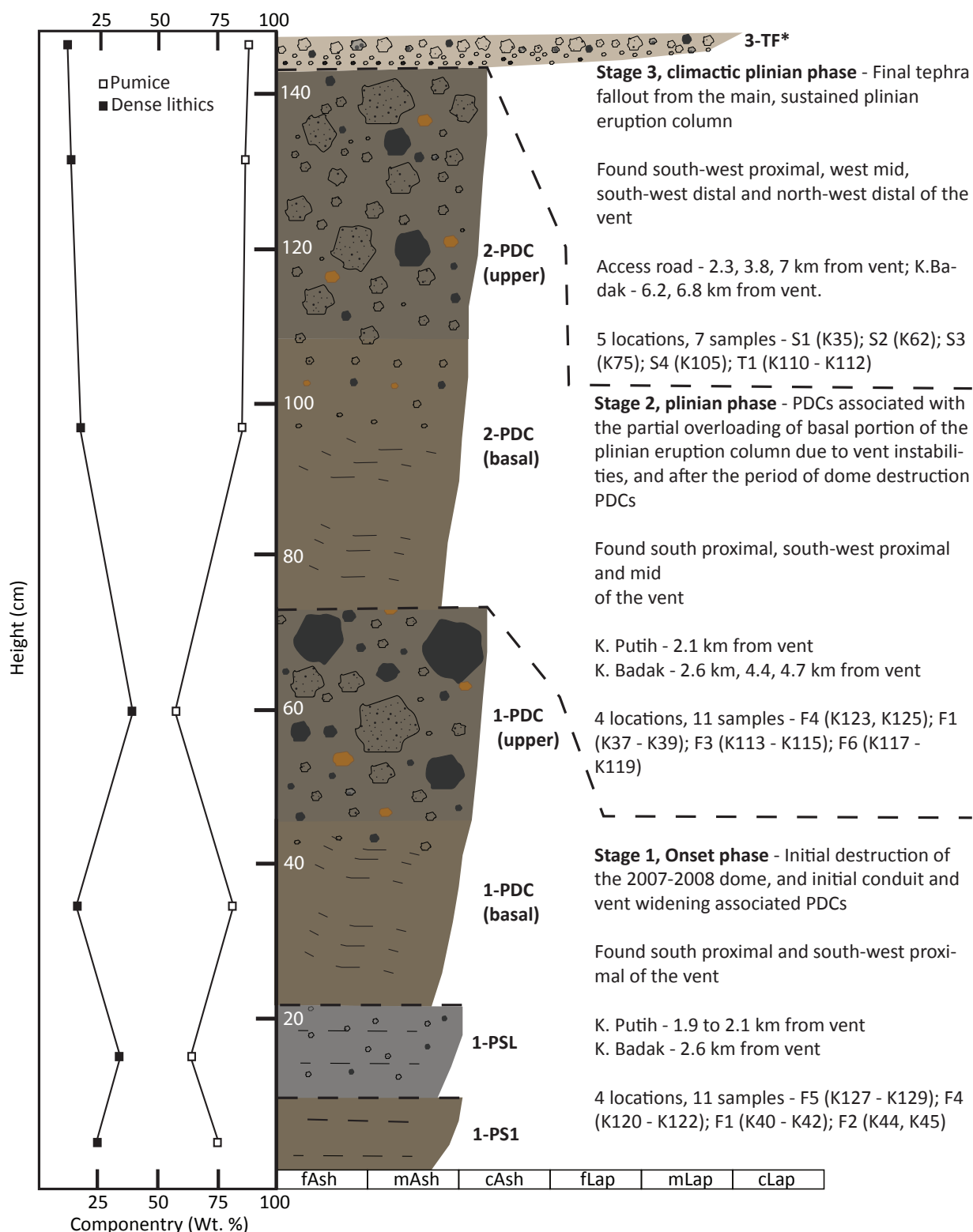


Figure 5: Generalised stratigraphic section of pyroclastic deposits for the Kelut 2014 eruption, including details on deposit location, number of sections and samples analysed from each eruptive stage. See text for further details of the units and associated facies variations. Weight percentage of dense lava dome-like lithics (minus the brown, country rock lithics; black squares), and pumice (white squares) within the deposits (normalised to 100) are shown with variation in height in the stratigraphic sequence. Grain size data are taken from the 0.5 to 1.0 mm class from representative samples of that unit; 1-PS1 data from sample K120; 1-PSL data from sample K121; 1-PDC basal facies data from sample K122; 1-PDC upper facies data from sample K40; 2-PDC basal facies data from sample K123; 2-PDC upper facies data from sample K37; 3-TF from sample K112 (see Appendix Table 1 for GSD and componentry results). Black arrows indicate a gradational PDC cross section.

Table 3: Deposit type listed with location, sample number, associated eruptive stage, and deposit unit code

Location	Latitude (°S), Longitude (°E)	Phenomena	Sample number	Stage/phase	Deposit/Sample Type	Unit code
F5	7°57'13.29", 112°17'42.82"	Unconfined overbank dilute PDC that detached from the main parent/channelised block rich PDCs. 85 m up in elevation from parent flow in valley floor.	K127	1/onset	Overbank PDC - surge	1-oPS1
			K128	1/onset	Overbank PDC - surge	1-oPS1
			K129	1/onset	Overbank PDC - surge (lithic rich)	1-oPSL
F4	7°57'19.20", 112°17'47.80"	PDC lobes at valley margins from channelised concentrated, block-rich PDCs from multiple eruptive stages, 2 m up from valley floor.	K120	1/onset	PDC - surge	1-PS1
			K121	1/onset	PDC - surge (lithic rich)	1-PSL
			K122	1/onset	PDC	1-PDC
			K123	2/plinian	PDC - surge	2-PDC
F1*	7°56'21.38", 112°16'45.25"	Channelised high-energy block-rich PDCs (bipartite) from dome explosions	K125	2/plinian	PDC - flow	2-PDC
			K40	1/onset	PDC - matrix	
			K41	1/onset	PDC - pumice	1-PDC
			K42	1/onset	PDC - light and dark dense lithics	
F2	7°56'18.64", 112°16'47.95"	Unconfined overbank dilute PDC that detached from the main parent/channelised block rich PDCs. 20 m up in elevation from parent flow in valley floor.	K44	1/onset	Overbank PDC - surge (lithic rich)	1-oPSL
			K45	1/onset	Overbank PDC - surge	1-oPS2
			K46	3/climactic plinian	Tephra fall	3-TF
F1*	7°56'22.67", 112°16'50.02"	Channelised high-energy block-rich PDCs (bipartite) from vent and mass ejection rate instabilities	K37	2/plinian	PDC - matrix	2-PDC
			K38	2/plinian	PDC - pumice	2-PDC
					PDC - light and dark dense lithics	2-PDC
			K39	2/plinian	lithics	2-PDC
F3	7°57'12.48", 112°15'58.57"	Laterally continuous (up to 4.7 km from vent) overbank PDC lobes from channelised concentrated block-rich PDCs	K113	2/plinian	Overbank PDC - surge	2-oPS1
			K114	2/plinian	Overbank PDC - surge	2-oPS2
			K115	2/plinian	Overbank co-pdc ash	2-oPDCa
			K116	3/climactic plinian	Tephra fall	3-TF
F6	7°57'12.48", 112°15'58.57"	Laterally continuous (up to 4.7 km from vent) overbank PDC lobes from channelised concentrated block-rich PDCs	K117	2/plinian	Overbank PDC - surge	2-oPS1
			K118	2/plinian	Overbank PDC - surge	2-oPS2
			K119	2/plinian	Overbank PDC - flow	2-oPF3
			K110	3/climactic plinian	Tephra fall	3-TFa
T1	7°57'53.10", 112°15'19.32"	Reversely graded tephra fall	K111	3/climactic plinian	Tephra fall	3-TFb
			K112	3/climactic plinian	Tephra fall	3-TF
S1	7°56'09.65", 112°16'57.92"		K35	3/climactic plinian	Tephra fall	3-TF
S2	7°56'10.33", 112°16'9.52"		K62	3/climactic plinian	Tephra fall	3-TF
S3	7°55'36.28", 112°14'30.18"	Reversely graded tephra fall	K75	3/climactic plinian	Tephra fall	3-TF
S4	7°58'11.15", 112°15'3.08"		K105	3/climactic plinian	Tephra fall	3-TF

Deposit types refer to locations in Fig. 1 (F1* denotes two PDC deposits in one location). Sample numbers are shown with stratigraphic units in Fig. 4, with associated eruption phase and stage or chronological timing and subsequent unit code (see Figs. 5 and 10). Unit codes are abbreviated as the following according to eruptive phase and deposit type: 1-PS1: Stage 1 pyroclastic surge unit; 1-oPS1: unit with overbank facies of 1-PS1; 1-PSL: interbedded Stage 1, lithic rich pyroclastic surge unit; 1-oPSL: unit with overbank facies from 1-PSL; 1-PS2: the second, larger Stage 1 basal surge unit; 1-oPS2: overbank facies of 1-PS2; 1-PDC: Stage 1 main bipartite pyroclastic density current (a is the basal facies, and b the upper facies); 2-PDC: Stage 2 main bipartite pyroclastic density current (a is the basal facies, and b the upper facies); 2-oPS1 and 2-oPS2: overbank unit of 2-PDC with surge like facies, numbered successively; 2-oPF3: overbank unit of 2-PDC with coarse flow facies; 2-oPDCa: co-PDC ash fall; 3-TF: Stage 3 final tephra fall; 3-TFa and 3-TFb: lower units of the 3-TF tephra fall.

2.4.2 Stratigraphy, grain size and componentry of the 2014 pyroclastic deposits

The 2014 stratigraphic sections (Fig. 4) examined in the proximal area (at F1-F6 and T1; Fig. 2) include two valley-floor PDC section (at F1); one valley-margin PDC section (F4); four overbank PDC section (at F2, F3, F5 and F6); and a full section of the 2014 ash fall deposits (at T1). The stratigraphic sections of all 2014 pyroclastic deposits are shown in Fig. 4, and are used to construct an overall composite stratigraphic section for the 2014 eruption, which is shown in Fig. 5. The stratigraphy of the pyroclastic deposits will be presented in relation to the 13 February 2014 eruption chronology. Stage 1 deposits originate from the first eruption, named the onset phase; Stage 2 deposits are from the earlier phase of second, more intense plinian phase; and finally stage 3 deposits are from the climactic phase of the second, plinian eruption. Table 2 presents a description of the lithological components, and Table 3 gives an integrated list of the deposit types, with their unit codes linked to eruptive stage and chronology.

2.4.2.1 Onset-phase pyroclastic units

The onset-phase PDC units (see Table 3, starting with 1- unit code) and associated overbank units are only found proximally, in the K. Putih valley, 1.9 and 2.1 km from the vent (sections at F5 and F4), and the K. Badak valley, 2.6 km from the vent (lower PDC section at F1) (Figs. 1, 2b and 4). The first 2014 unit lies directly on top of a thin layer of soil separating it from the 1990 PDC deposits below (Fig. 4). There are 3 main vertical PDC units associated with this stage of the eruption, which are defined by vertical facies variations: 1-PS1 is a fine-grained deposit with friable lapilli; 1-PSL is a horizontally bedded ash deposit, rich in lithic lapilli; and 1-PDC unit with bipartite facies, with a basal facies consist of low-angle laminated medium ash, and a coarse, massive and blocky, lithic-rich, upper deposit with little matrix material (Figs. 4, 5 and 6a, b). These valley fill units thicken downstream from 0.45 to 0.60 m within a short 0.5 km distance.

Two discrete onset-phase PDC units are found in the K. Putih valley (1-PS1 and 1-PSL). The first depositional unit 1-PS1 is only observed in the K. Putih valley at two locations (sections at F4 and F5), and not found beyond 2.1 km from the vent (Fig. 4). Unit 1-PS1 (5-15 cm-thick) is poorly sorted and consists of mostly finely horizontally-laminated, crystal-rich medium ash (Appendix Table 1), with fine lapilli-sized clasts of mostly juvenile grey to light pale brown coloured, highly vitric, friable and sub-angular pumice, with some denser lithic clasts (Fig. 4). The unit also contains rare root fragments.

The second depositional unit 1-PSL directly overlies 1-PS1 at localities F4 and F5 and is a 10–15 cm-thick, distinctive, discretely horizontally laminated, very poorly sorted lapilli tuff with a pale grey, fine, crystal-rich to medium-sized ash (125–250 μm) matrix, containing dispersed lapilli up to 4 mm in size (Appendix Table 1). The coarse particles consist of lithics of dense, pale grey porphyritic lava (53%), as well as pumice fragments (47%). This unit is generally darker in colour due to a higher proportion of lithic lapilli clasts (Fig. 5), and contains a higher proportion of larger medium-lapilli sized clasts than 1-PS1 (Appendix Table 1). Both 1-PSL and 1-PS1 are not present downstream in the onset-phase PDC section at location F1 in the K. Badak valley.

The third depositional unit, 1-PDC, is above the 1-PS1 and 1-PSL unit, and is a thicker onset-phase PDC unit, found at F4 and F1 (Fig. 4). This unit is 0.2-0.25 m thick (Fig. 6a) and comprises medium-coarse brown ash with discrete horizontal laminations and sporadic fine-pumice lapilli at F4 (Fig. 4). The matrix of this layer is dominantly 125–250 μm , rich in crystal fragments (35%), with some fine vesicular pumice (54%), and slightly less fine lithics (11%). Upward, this unit also contains less dense dome-like lithics when compared to lithic rich unit 1-PSL (Fig. 5). The 1-PDC unit facies laterally transitions to gently low-angled, discrete laminations of a similar medium-coarse ash layer at F1 (1-PDC). This basal facies of the 1-PDC unit of medium-ash varies vertically into an upper, more massive and blocky facies at F1 (Figs. 4, 5 and 6a). This upper facies shows a gradually increasing concentration of reversely graded lapilli to large block fragments, supported in a medium to coarse-ash matrix (250–500 μm fraction; Fig. 7). The juvenile, sub-angular, light grey pumice blocks (sample K41) are 12-75 cm in diameter, and contain large euhedral phenocrysts

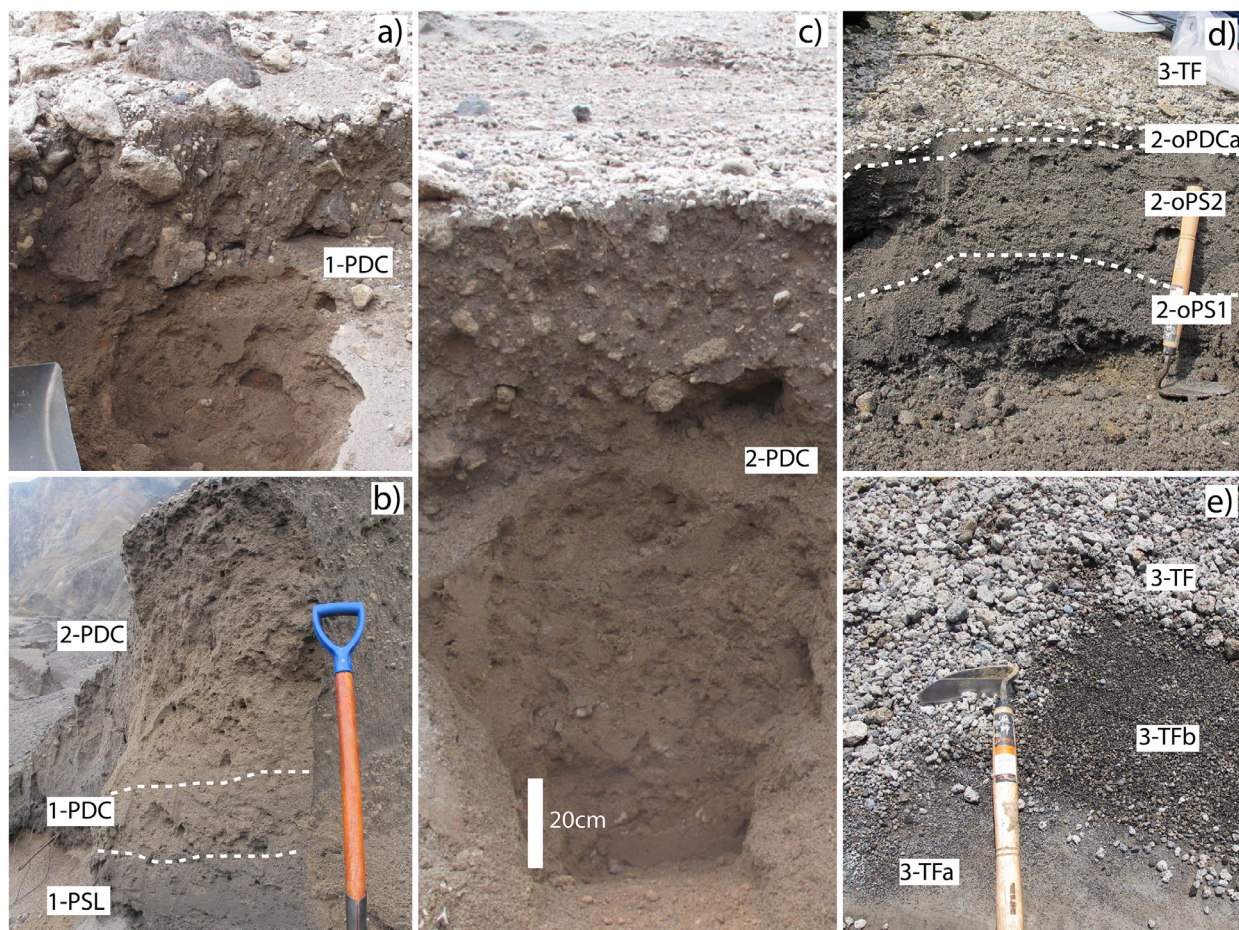


Figure 6: Photos of 2014 pyroclastic deposits. a) The lower PDC deposit at F1 (1-PDC). b) Multiple PDC deposits at location F4 in the K. Putih. c) The upper PDC deposit at F1 (2-PDC) d) Overbank PDC deposit at F3, further downstream (4.4 km from the vent) down the K. Badak. e) The 2014 tephra fall deposit at T1, showing 3-TF units, with units 3-TFa and 3-TFb. Photographs taken between the 02/04/2014 and 05/04/2014.

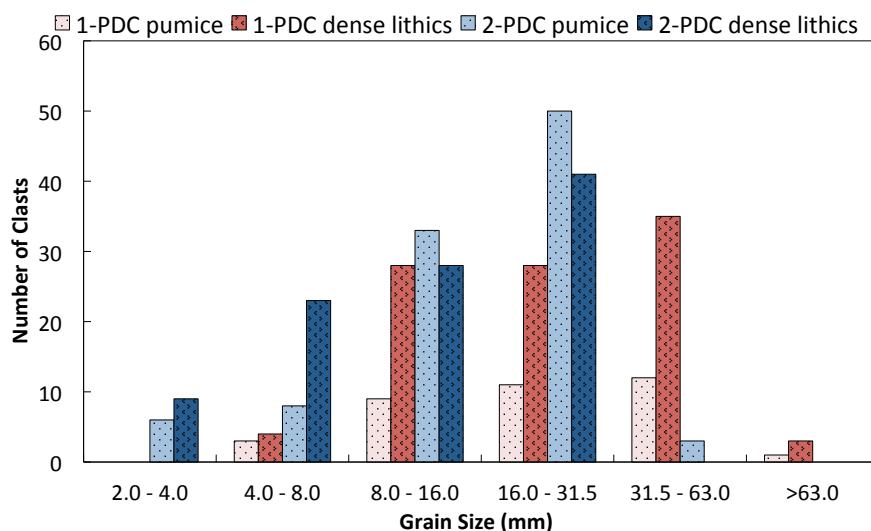


Figure 7: Number of pumice and dense lithic clasts per size class from the PDC deposits at location F1 (in the upper facies from 1-PDC and 2-PDC respectively); pumice and dense lithic clasts from lapilli to block/bomb sized clasts (2 - >63 mm) were counted for each section. Note that lithics and pumice have been sampled separately. The lower PDC section at F1 (1-PDC) has pumice clasts (sample K41) and dense lithic clasts (sample K42) are represented by red bars. The second PDC at F1 (2-PDC) has pumice clasts (K38) and dense lithic clasts (sample K39) are represented by blue bars (see key).

Supplementary table provided in Electronic Appendix A

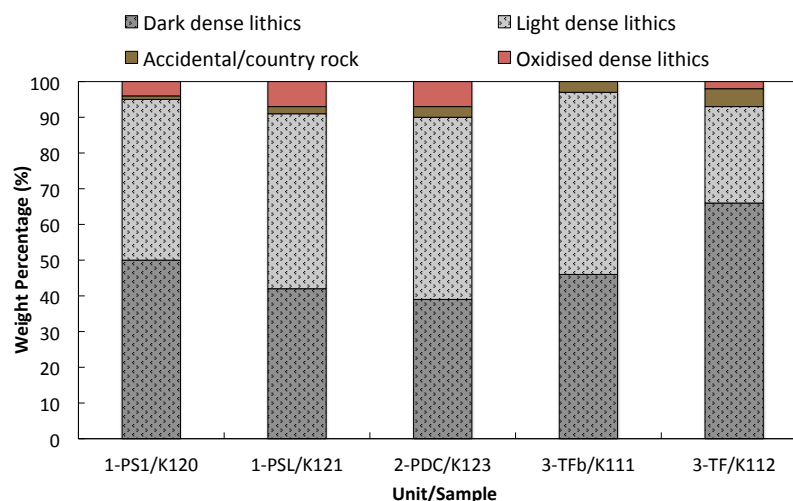


Figure 8: Plot of total proportions of varying lithic clasts (for 1 – 2 mm size fraction) per unit, with sample name labelled. Amounts of the following lithologies are shown (weight percentage): Dark, dense lithic lava clasts; light, dense lithic lava clasts; brown accidental lithics/country rock; and oxidised dense older, weathered lithic clasts.

of pyroxene and plagioclase (1–7 mm in length), and other pumice clasts are oxidised. The dense lithics present include fresh porphyritic basalts (dark grey in colour), with occasionally fragmented and pale grey fresh lava lapilli and bombs up to 35–65 cm in diameter (sample K42) (Fig. 7), rich in plagioclase phenocrysts. These account for 90–95% of the lithic population, with the other 5–10% of the lithics across all onset phase PDC units comprising oxidised dense lava clasts and brown accidental (or country rock), highly altered lithics (Fig. 8). Comparatively, for the same grain size fraction, the ash matrix in this upper facies contains more lithics than any other deposited unit in this stage (Fig. 5).

The flow front of the 1-PDC is found 400 m downstream of the section at F1 (~3 km from the vent) in the K. Badak valley. The flow front, like the levees alongside the valley, is dominantly composed of coarse blocks of pumice and lithics, with little or no matrix.

The valley-unconfined overbank units at F5 and F2 (Fig. 4) are located 85 m and 20 m respectively up in elevation from the valley floor, on ridges adjacent to the main valley, detached from the parent PDCs and associated units (at F4 and F1 respectively). At F5, the units are found above a layer of soil covering the 1990 PDC deposits, and include 1-oPS1, 1-oPSL and 1-oPS2. These units have more finer-grained facies than the basal 1-PDC facies, with clear, low-angle laminations of ash. These overbank units consist of dominantly crystal rich (66%), fine-medium ash (125–250 μm), with some rare fine and friable pumice and lithic lapilli (see Appendix Table 1). This represents the final depositional units from the onset stage of the eruption.

2.4.2.2 Plinian-phase PDC units

The plinian-phase PDC units and associated overbank units (see Table 3, starting with 2- unit code) are observed up to 2.1 km from the vent in the K. Putih valley (section at F4), and 2.6 to 4.7 km down the K. Badak valley (upper section at F1, and sections at F3 and F6; Figs. 1, 2b and 4). There

is one main vertical PDC deposit succession associated with this stage of the eruption, and it is defined by vertical facies variations: 2-PDC is a unit with bipartite facies (similar to 1-PDC), with a basal low angle laminated medium ash, and a coarse, massive and blocky, pumice-rich upper facies with little matrix material (Figs. 4, 5 and 6a, b). Proximally, the basal facies of 2-PDC have discrete low-angle cross-bedding, but are laterally continuous and overbanking at greater distance from the vent, with clearer low-angle to horizontal laminations (at F3, F6; 2-oPS1, 2-oPS2) (Fig. 4). Disimilar to the onset-phase units, the 2-PDC units become thinner with distance from source, from 0.8 m thick in the K. Putih (F4) and proximal K. Badak locations (F1), to 0.3 m thick at F3 and F6 (Figs. 1 and 4).

The 2-PDC units occur above the onset-phase PDC units at location F4 and F1 (Figs. 1, 4, 5, 6b). The plinian phase PDC at locality F1 (Fig. 6c) lies directly on top of the onset phase PDC deposit (Fig. 3c), and is distinguishable from 1-PDC due to the larger volume of the deposit (Figs. 6a, 6c), that is also more pumice-rich and contains less block-sized clasts (Fig. 7). The lower-most climactic stage PDC unit at F4 is 40 cm thick (K123), with low-angle cross bedding of the fine-medium ash matrix (125-500 μm), and represents the basal facies of the climactic PDC unit. The unit consist of mostly juvenile, pale to dark grey-brown pumice clasts, with dense lithics and crystals (Appendix Table 1; Fig. 5). The fine lapilli (4–8 mm) in this basal facies comprise 71% pumice and 29% lithics. In both sections at F4 and F1, this finer-grained facies coarsens upwards into a very poorly sorted, massive deposit with a matrix of medium ash, with randomly dispersed fine lapilli to block-sized clasts (Figs. 4, 5, 6c). In general, the climactic PDC units contain greater pumice contents than the onset-phase units (Fig. 5). The coarser grained clasts within the upper facies of 2-PDC unit are very poorly-sorted lapilli and blocks from 3.5-13.5 cm in diameter of dense light grey, vitric juvenile pumice, and darker brownish-grey oxidised pumice (sample K38), and dense grey to black lava (sample K39) lithics 14-20 cm in diameter (Figs. 6c and 7). This unit contains less oxidised pumice (by ~5-6%) than the onset phase PDC units. Lithic lapilli and blocks within this unit are dominantly lightly coloured, dense lava clasts. There is also a higher percentage of oxidised dense lithics and brown accidental lithics than that recorded in the upper 1-PDC unit (Fig. 8). The flow front of 2-PDC is on top of the flow front from 1-PDC at the same location (both 3 km from the vent), and comprises a matrix-poor levee of blocks of pale grey or greyish-brown pumice.

The laterally continuous associated overbank units from 2-PDC include 2-oPS1, 2-oPS2, 2-oPF3 and 2-oPDCa are observed at localities F3 and F6 (Figs. 1, 4, and 5) and show similar facies and componentry to the 2-PDC unit at F1, but are better sorted. At F3, the beds are 10-15 cm-thick, consisting of grey to greenish-grey, medium ash showing low-angle laminations (Fig. 6d). The lowermost units (2-oPS1) have a matrix of medium to coarse ash, with 2.0-4.0 mm pumice fine lapilli (74%), and minor lithic lapilli (26%). The 2-oPS2 unit is directly above 2-oPS1, and is very similar in componentry, but has a finer ash matrix (125-250 μm) (Appendix Table 1). Above 2-oPS2 at F3, there is a thin layer of crystal-rich fine ash (2-oPDCa), which shows a gradation upwards

to pale grey, pumice- and crystal-rich, fine ash (63-125 μm) with low-angle laminations (Fig. 6d). The section at location F6 (elevation 741 m, Fig. 4) is 200 m downstream of F3 (792 m) and shows further lateral continuation of the overbank flow units and facies. The 2-oPS1 unit at F3 thins to ~2 cm at F6, and is dominated by coarse ash. The 2-oPS2 unit is 5 cm thicker at F6 than at F3. Pumice blocks up to ~20 cm in diameter and minor dense, fine lithic lapilli cap the section F6 (2-oPF3). All the climactic-phase PDC units are characterised by higher pumice to lithic contents (Fig. 5). Pumice contents within the deposits of the overall eruption increase from 62-70% at stage 1, to 85% at stage 2 (Fig. 5).

2.4.2.3 Climactic plinian tephra fall

There is one main deposit associated from this stage of the eruption; the final plinian tephra fall unit, 3-TF, is found at sites S1-S4, F2, F3, F5 and T1 (Figs. 1 and 4; Table 3; Appendix Table 1). All the deposits are sampled under the broad dispersal axis of the plume (Fig. 1). Where PDC deposits are absent (at S1-S4), the fall deposits rest on a thin layer of soil, forming on top of the 1990 pyroclastic deposits, and found along the main access road parallel to K. Sumberagung (Figs. 1 and 4). The 3-TF unit varies in thickness from ~0.5-5 cm thick. At 2.3 km south-west (S1), and 3.8 km west of the vent (S2) the 3-TF unit is 5 cm thick, thinning to 3 cm at 6.2-6.8 km south-west (T1 and S4), and 7 km north-west of the vent (S3). Unit 3-TF is ~3 cm thick and found directly on top of the overbank PDC units at F2, F3 and F5 (Figs. 4; 6d). Modal pumice lapilli are 8-16 mm in size in proximal sites, with the mode decreasing to 2-4 mm over a distance of 4.3 km from the vent.

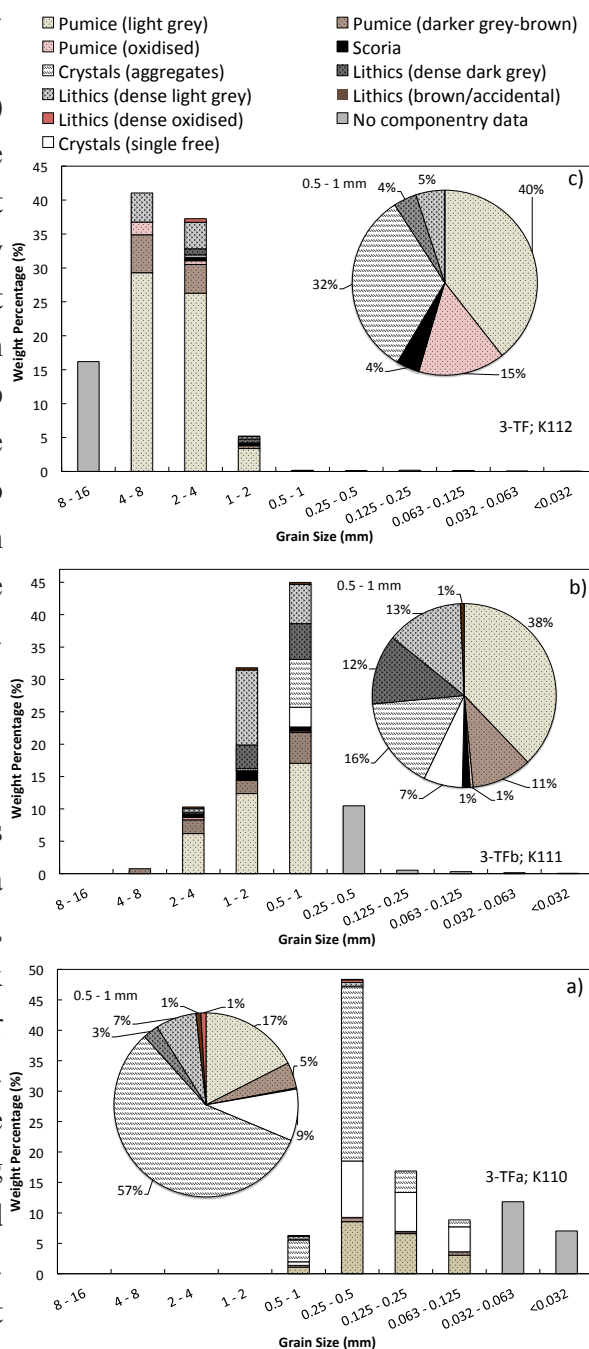


Figure 9: Grain size distribution and componentry of the tephra fall deposit at T1 (see Fig. 4), showing a) 3-TFa; sample K110 b) 3-TFb; sample K111 c) 3-TF; sample K112. The componentry for the 0.5 to 1 mm grain size class is displayed in pie charts for each unit. See key for lithology, and see Table 2 for a description of each componentry classifications.

At all locations where sampled (S1–S4, F2, F3, F5 and T1) unit 3-TF is the uppermost 2014 pyroclastic deposit, and is comprised predominantly of reversely graded, moderately-sorted, grey or pale greyish brown, vesicular (and tube-vesicular), angular to sub-rounded, pumice lapilli (4–16 mm in diameter). The clasts are highly vitric and crystal-rich, with 1–5 mm euhedral-subhedral pyroxene and plagioclase phenocrysts (Table 2). These angular, grey-light brown, vitric pumice clasts represent the only definitive juvenile clast identified, similar to the blocky pumice clasts in 1-PDC and 2-PDC.

The tephra fall deposit at site T1 (Figs. 6e and 9) comprises 3 layers: lower units 3-TFa and 3-TFb, and the main fall deposit 3-TF (Fig. 4). The lowermost 3-TFa (sample K110), and 3-TFb (sample K111) units are only observed at this location, approximately 6.2 km south-west of the vent. Unit 3-TFa is a pale grey, 0.5 cm-thick, well-sorted medium ash (250–500 μ m) deposit that is weakly-stratified and reversely graded. Angular crystal aggregates dominates (of mostly clinopyroxene and orthopyroxene and lesser plagioclase feldspar) the ash-sized particles, with some pumice and minor lithics (Fig. 9a). This unit grades up to 3-TFb above (Fig. 9b). 3-TFb is a reversely-graded, 1–2 cm-thick, coarse ash to fine lapilli (0.5–>2 mm) deposit, rich in dense and poorly-vesicular lithic clasts of mostly light and dark dense lithics (Fig. 8), with lesser pale greyish-brown, juvenile pumice lapilli. This grades upwards into the uppermost fall unit, 3-TF (sample K112). This unit is similar to the tephra fall deposits observed at all other locations examined (and mentioned above at S1–S4) (Figs. 1, 4 and 6e). It consists of $\leq 90\%$ fine to medium lapilli-sized (4–8 mm) grey and oxidised pumice, with minor lithic lapilli. The lithic lapilli clasts include grey to black fresh lava (93%), with the remainder of the lithic clasts including weathered and oxidised brown, accidental country rock fragments (7%) (Fig. 8). Similar to the PDC units, the fall units from 3-TFa to 3-TF (at T1) becomes more pumice-rich upward (from 66 to 87% for the same grain size class), with a corresponding drop in the content of dense lithics. Stratigraphically, the tephra fall deposits from this stage also show some of the highest pumice contents compared to deposits from the first and second stages of the eruption (Fig. 5)

2.5 Discussion

2.5.1 Correlating the stratigraphy to the eruption chronology and dynamics

The 2014 deposit characteristics detailed above are compared with eyewitness accounts and satellite reports of the eruption, in order to estimate the timing of eruptive events and place constraints on the mechanisms, processes and dynamics leading to the origin, formation and emplacement of the PDC and tephra fall deposits.

2.5.1.1 Stage 1: Eruption initiation and dome destruction

The earliest reported start time of the onset phase of the 13 February 2014 eruption is at 22:32 local time (Kristiansen et al., 2015), lasting approximately 15 to 30 minutes (Fig. 10). This period

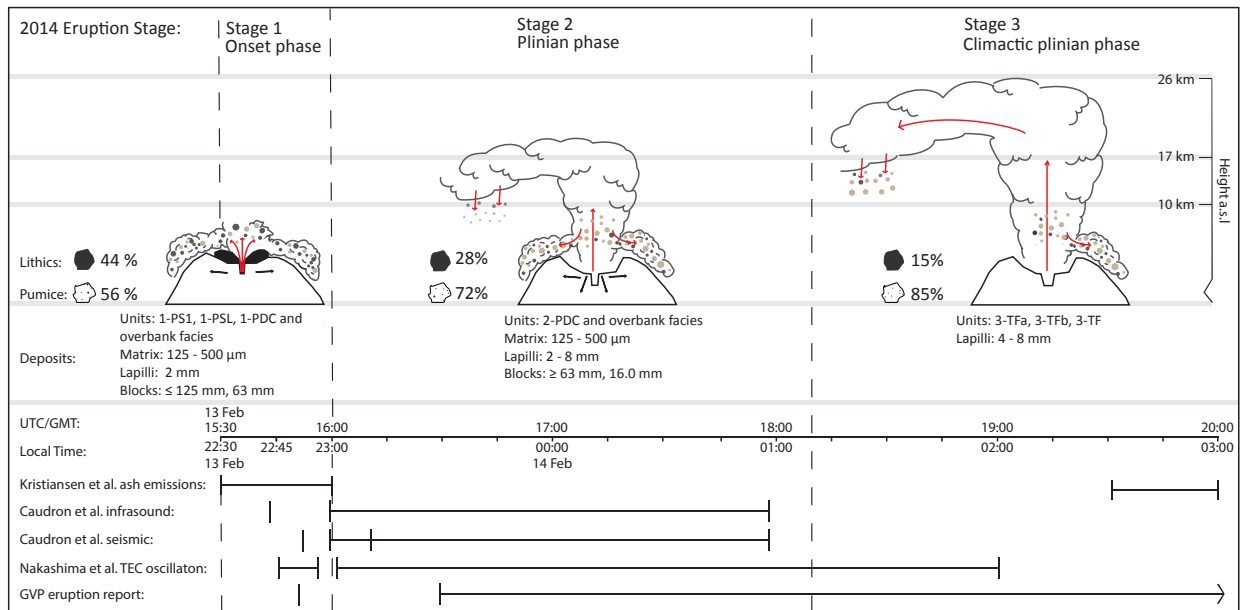


Figure 10: Schematic diagram of dynamics occurring during stages 1 to 3 of the eruption with start times and eruption duration (in UTC and local time) for each phase as documented in geophysical and observational reports (GVP, 2014; Caudron et al., 2014; Kristiansen et al., 2015; Nakashima et al., 2016). Filled polyhedrons indicate dense lithic content (percentage, minus accidental/brown lithics), white speckled polyhedrons indicate pumice content (percentage) after normalisation (see Table 2). The componentry data is taken from the 2 – 4 mm grain size fraction of representative samples for each stage; Stage 1 taken from sample K120; Stage 2 taken from sample K123; Stage 3 taken from sample K112. In stages 1 and 2, modal grain sizes for the matrix ash, lapilli and blocks for PDC units are shown. In stage 3, modal lapilli grain size is shown for the air fall units only. Red arrows indicate dispersal of pyroclastic material. Black arrows indicate conduit and vent widening during the eruption. Maximum height of the eruption column (26 km) taken from GVP (2014) and Kristiansen et al. (2015) at 01:10 to 01:13 local time. See the discussion section for a detailed description of the eruption chronology. References listed are (GVP, 2014; Caudron et al., 2015; Kristiansen et al., 2015; Nakashima et al., 2016).

included five short, impulsive infrasound signals at the International Monitoring System (IMS) at the International Data Centre (IDC) (Hidayat 2014; Caudron et al., 2015). Nakashima et al. (2016) detected acoustic waves from the eruption in the ionosphere, observed as changes in the Total Electron Content (TEC) using data from the Global Navigation Satellite System (GNSS) receivers. The first wave was recorded at ~22:46 local time and was associated with an explosion (Nakashima et al., 2016). This seismic signal was taken as the eruption start time by Maeno et al. (2017), however earlier infrasound signals suggest this eruption may have started ~14 minutes earlier (~22:32). Further seismic signals were recorded at 22:51 local time (M_s of ~2.3; Caudron et al., 2015) (Fig. 10).

The pyroclastic deposits associated with the onset phase include PDC units (1-PS1, 1-PSL and 1-PDC) and the overbanking units with laterally continuous facies (Fig. 4). The first deposited 1-PS1 and 1-PSL units have surge facies characteristics of low-particle density PDCs, similar to ash-cloud surge units, carrying dominantly fine ash and crystal fragments (up to 47%) in the upper depositing part of the cloud. This is similar to the laminated, fine-grained and poorly-sorted surge deposits observed by Lube et al. (2014) at Mt. Tongariro, and Cronin et al. (2013) at Merapi. The poor sorting and gentle low-angle laminations of these deposits are consistent with low-level

turbulence in the parental surge (e.g., Branney and Kokelaar, 2002; Sulpizio et al., 2016). Units 1-PS1 and 1-PSL stop at 2.1 km from the vent, although thin deposits of these units may have been eroded farther away. Similar pre-plinian surge deposits, that are fines-rich, 10-20 cm thick in valleys, and 1-5 cm thick on adjacent ridges, were observed from the 1990 eruption, but travelled up to 5 km from the vent (Bourdier et al., 1997). Maeno et al. (2017) present four major depositional units from the 2014 eruption attributed to three eruptive stages. They identify dilute high-energy PDCs associated with the pre-plinian, partial destruction of the existing lava dome (Unit A) in the first stage of the eruption, beginning around 22:45 local time, similar to this study. These deposits and units were found to the north-east of the vent in proximal ridge-top sections, and are described as originating from a small lateral blast, similar to that of the 2010 Merapi dome-destroying eruption. It could be possible that units 1-PS1 and 1-PSL are related to an upper and more distal facies of this lateral blast, due to the similar occurrence of juvenile and non-juvenile clasts. However, since the deposits described in this study were found south-west of the vent, it may be likely that Maeno et al. (2017) are recording an earlier blast based on near-vent stratigraphy that was only exposed on ridge-tops.

The 1-PDC valley infill unit (at F1) and valley margin (at F4) facies show typical characteristics for deposits from highly-particle concentrated PDC or pyroclastic flows, with a fine-grained basal portion grading up into a more poorly sorted massive deposit and overall coarse-tail reverse grading. There is a higher proportion of dense, lithic clasts and vesicular pumice (including blocks) in the upper 1-PDC facies than in the lower 1-PDC facies (Fig. 5). The lower, basal facies of the 1-PDC unit is likely emplaced by traction from the base of a current, whilst the upper, massive part is likely emplaced *en masse* as the overriding flow came to rest, similar to the mechanism explained by Sparks et al. (1973) responsible for the inverse grading of larger clasts in ignimbrites. The presence of oxidised pumice clasts in upper most layer of the PDC deposit could suggest temperature variation within the flow (Fink, 1987). The onset phase units (apart from the lower facies from unit 1-PDC and unit 1-PS1) include high contents of dense light grey and dark grey lithic fragments (lapilli to block sized), similar to the 2007-2008 lava dome, which was likely destroyed during this phase (Table 2; Figs. 5, 7, and 8). Calder et al. (2000) interpret similar lithic-rich deposits from Lascar, Chile, as being produced by a highly concentrated granular flow. Other dense lava and brown country rock lithics are commonly altered and weathered (Fig. 8), and were probably derived from fragmentation of older vent wall rock. Vent clearing and blockage along with low mass-ejection rates, meant that the onset phase PDCs were of low energy and runout (≤ 2.6 km from the vent) (Fig. 10; e.g., Carey et al., 2007; Wallace et al., 2013). The higher abundance of dense lava and also brown country rock lithics in the stage 1 deposits and units may suggest that initial, partial vent and conduit widening occurred during this time, which initially lowered explosive fragmentation, and may be responsible for the greater pumice clast size observed when compared to later deposits (Smith and Kokelaar, 2013).

The overbank PDC deposits and units are similar in componentry, but finer-grained than the initial 1-PSL and 1-PS2 units, and derive from the spill out and detachment of higher (up to 20 and 85 m in elevation from the valley floor), more turbulent and pumice-rich, and less concentrated parts of the density currents to the adjacent valley tops and banks, similar to the Merapi overbank deposits as described by Lube et al. (2011) and Cronin et al. (2013). It is likely that due to transport time such overbanking units may have been deposited at a later stage, however, the parent current and plume was generated during this stage. The absence of co-PDC fine ash at the top of the PDC deposit likely reflects there being only a brief interval ($\sim <30$ minutes) before further PDCs were formed in stage 2.

Jeffery et al. (2013) suggested that pre-eruptive processes in the 2007-2008 lava dome effusion involved fractional crystallisation, along with magma mixing and mafic magma recharge at shallow-levels. The Jeffery et al. (2013) model for magmatic processes was based on binary bulk mixing models, and mineral textures and zoning patterns in the 2007-2008 dome lavas. Therefore, Caudron et al. (2015) hypothesised that the first 2014 eruption episode was similar to that in 2007-2008, and could have been induced by mixing of replenishing magma into an existing shallow reservoir, causing gas-overpressure, and destabilising the conduit capping dome (e.g., Girona et al., 2015). Similar eruptions have occurred in 1919 and 1990 at Kelut, after a small explosion displaced the crater-lake, and unroofed a capped shallow magma in the conduit (Bourdier et al., 1997; Caudron et al., 2015). A weak seismic signal ($M_s = \sim 2.3$) likely indicated the vent-opening explosion (Caudron et al., 2015). There was no evidence for large-scale magma-water interaction in the onset-phase deposits, despite the common white clouds observed. Accretionary lapilli, blocky shards or wet-fine ash emplacement structures were not observed, unlike that of the phreatomagmatic phase of the 1990 eruption (Bourdier et al., 1997; Porreca et al., 2006).

2.5.1.2 Stage 2: Plinian column formation and marginal column collapses

The earliest reported start time for stage 2 is at 22:58 local time (Caudron et al., 2015), with the latest start time reported at 23:30 local time (GVP, 2014) (Fig. 10). Variations in reported start and end times for this eruption, and stage 1, are shown in Figure 10. The IDC detected 14 global infrasound signals associated with a separate, larger event, ~ 15 minutes after the onset phase (Hidayat, 2014; Caudron et al., 2015). Furthermore, a sustained seismic signal was recorded from 22:58, overlapping with the arrival times of the infrasound signals (Caudron et al., 2015). The GNSS also detected a large acoustic wave in the ionosphere at $\sim 23:01$ (Nakashima et al., 2016) and a further brief seismic event was recorded at 23:11 (M_s of ~ 4.7 ; Caudron et al., 2015). Satellite imagery showed the plinian ash cloud clearly from 00:30 (GVP, 2014). The stage 2 pyroclastic density current generation and subsequent deposition likely began around 22:58 local time and continued until around 01:00 local time, when ionosphere data suggested that the plume reached its maximum height at 26 km (Figs. 5 and 10).

The first stage 2 PDC units are deposited directly on top of stage 1 deposits (where present; Fig. 4). The upper part of the 2-PDC unit shows a more massive structure, with a poorly sorted concentration of more block-sized clasts than in the cross-stratified, medium-ash facies that define the basal part of the 2-PDC deposit. The deposit is similar to the onset phase PDC deposit at F1 with coarse-tail grading. Similar to 1-PDC, the lower, basal facies is likely emplaced by traction from the base of a current, whilst the upper, massive part is likely emplaced *en masse* as the overriding flow came to rest (e.g. Sparks et al., 1973). Such PDCs and similar pumice-rich deposits were observed at Lascar, Chile (Calder et al., 2000). A large block-rich flow front and similar marginal levees occur in 2-PDC at 3 km from the vent, and at 4.7 km from the vent (deposit 2-oPF3). These reflect deflection and concentration of segregated large, often low density clasts towards the flow margins and levees due to the internal velocity gradients in dense-granular flows (e.g., Calder et al., 2000; Lube et al., 2007; Sulpizio et al., 2007; Cronin et al., 2013). At F1 the stage 2 deposits and units (2-PDC) are thicker, but less coarse than the stage 1 deposits and units (1-PDC). The differences in the sizes of blocky clasts in the units between these stages could possibly be linked different fragmentation conditions in both eruptions (McBirney and Murase, 1970).

In the stage 2 PDC deposits and units, pumice contents in ash and lapilli-sized clasts are ~25% higher than in most earlier units (Fig. 5). The continued presence of rare, fine, dark and pale grey dense lava lithic clasts, along with fragments of country rock and oxidised dense material within these deposits suggests on-going conduit erosion and vent widening (Figs. 8 and 10), such as that inferred at Tarawera, (Carey et al., 2007), and at Monte dei Porri (Sulpizio et al., 2016). Vent widening is confirmed by satellite imagery of the vent region after the eruption (Fig. 2b; GVP, 2014), which shows a deep vent crater, similar to that following other intense eruptions from Kelut (e.g. 1951, Hadikusumo, 1974; 1990, Bourdier et al., 1997). Such instabilities in the vent can cause changes in mass ejection rates. Due to the increased vent radius, the incorporation of additional blocky material into the lower portions of the building plume may have generated an increase in the lateral extent of the jet region at the start of this second eruption. This can limit the ability of pyroclastic material mixing with the atmosphere. It is therefore possible that the incorporation of conduit wall rock, an increase in the proportion of blocky pumice clasts, and vent widening may have contributed to collapse or overloading of this eruptive column at the beginning of the plinian eruption (e.g., Cioni et al., 2004) (Fig. 10). Similar valley infilling, coarse-grained pumice rich flows reaching 3 km from the crater were also formed during the beginning of the plinian phase of the 1990 eruption at Kelut (Bourdier et al., 1997).

Photographic accounts of the eruption from 00:38 to 01:00 local time on 14 February, taken by an eyewitness in Blitar (Putra, 2014), show a tall eruption column, that progressively becomes paler in colour as the eruption progresses. Voluminous and extensive PDCs are visible from 00:45 onwards to the west and south-west of Blitar. The longer runout of stage 2 PDCs likely reflects a more-sustained feeding and boiling over of material. Higher pumice content might also have played a role, as found by Calder et al. (1999) for a sequence of pumice- or lithic-rich PDCs

at Montserrat, where pumice-rich PDCs were more mobile due to the segregation of denser lithic clasts proximal to the vent. This may account for observing more pumice-rich, less blocky PDCs at greater runout distances (Figs. 4 and 5). These deposits are similar to the pumiceous lobate deposits (Unit C) described by Maeno et al. (2017), containing abundant pumice and lava blocks up to 20 cm in diameter. These deposits are interpreted similarly to our stage 2 deposits, unit 2-PDC, generated by the collapse of the plinian eruption column. However, the deposits described by Maeno et al. (2017) are attributed to the third stage of the eruption, not the second as in this study. The laterally- continuous, fining and better preserved bedding, pumice-rich overbank PDC lobes found 4.7 km from the vent in the K. Badak (Fig. 4), originated from the channelized block-rich PDC units of which were found ~2 km further up in the valley (at F1). The thin, capping 2-oPDCa co-PDC fall unit is rich in crystals (>60%), representing fines that were elutriated from the parent pyroclastic flows (e.g., Branney and Kokelaar, 2002; Edmonds et al., 2006; Cronin et al., 2013). Maeno et al. (2017) also describe grey, thinner, poorly-sorted ash-rich layers on ridge tops that are similar to these thin units. They are interpreted similarly as accompanying dilute portions of the current that have travelled over ridges, or also as co-PDC ash (Unit D). The localised fall unit (2-oPDCa) records the cessation of a semi-continuous series of PDCs. It is possible that further PDCs were generated during this time, but travelled farther from the vent (Fig. 2b) and therefore, were deposited later on during the course of the eruption. Such was the case in the 1990 eruption, where several series of ash and pumice lapilli falls were intercalated within pumice surge and flow deposits, as well as scoria-rich flow deposits, with initial evidence of phreatomagmatism (Bourdier et al., 1997). Intercalations of fall and PDC deposits are not a common feature of the 2014 deposits, although co-PDC falls indicate a brief pause between each of the 2014 eruption stages.

2.5.1.3 Stage 3: Climactic phase of the plinian event and tephra fallout

The final stage of the 13-14 February 2014 eruption involved the production of the tallest plinian eruption and umbrella cloud. Associated with this stage is the injection of tephra into the stratosphere, imaged from 00:30 (GVP, 2014). The main part of the pumice rich lapilli fall (3-TF unit; Figs. 4 and 6e) was deposited once the plume reached its maximum altitude (26 km above sea level), at ~01:12 local time on 14 February (seen by CALIPSO satellite with the CALIPOP lidar instrument; GVP, 2014) (Fig. 10). Tephra fall started during the earlier stage 2, but it is not found as an obvious layer within PDC and co-PDC ash sequences described above. Nakashima et al. (2016) estimate the duration of this climactic phase at 1 hour. Dare et al. (2016) estimated that the tephra plume was depositing between 23:00 to 03:00 local time, with Kristiansen et al. (2015) reporting a strong MTSAT ash mass loading west of the coast of Java at 02:32. A plane travelling from Perth to Jakarta encountered the dispersed plume off the coast of Java, west of Kelut, at around 04:50 (GVP, 2014; Kristiansen et al., 2015). Further ash detected was reported distally west of Kelut at 09:32 on 14 February 2014 (GVP, 2014). The final stage of the 13-14 February 2014 eruption therefore likely ended around 02:00 to 03:00 local time, with small phreatic explosive events occurring until 20 February, 2014.

The 2014 tephra fall deposit, unit 3-TF, is described in proximal locations from 1.9 to 6.8 km south-west of the vent, and ~7 km to the north-west (Figs. 1 and 4). In these locations, the fall deposits are 5–8 cm thick, fining with distance from source from coarse to fine lapilli. The broad lateral uniformity in thickness and clast size of the proximal fall deposit suggests that it sedimented from the umbrella cloud region of a strong, rapidly expanding plume, driven by a high and sustained mass flux (Walker, 1981; Cioni et al., 2000; Bonadonna and Philips, 2003). A strong south-westerly wind deposited several millimetres of very fine pale brownish-grey ash over the city of Yogyakarta, ~215 km west of the volcano (GVP, 2014; Kristiansen et al., 2015). Fine ash is missing from the proximal climactic fall deposits and associated units, but sedimentation of fine ash 6.2 km south-west of the vent (3-TFa) may have resulted from its aggregation due to atmospheric moisture (Bonadonna and Philips, 2003; Brown et al., 2012) during the earlier stages of the plinian phase, similar to that seen at Redoubt volcano, Alaska (Wallace et al., 2013), although accretionary lapilli were not observed. Maeno et al. (2017) are also in agreement that most of the tephra fall deposits were dispersed westward of the volcano. They describe a similar pumice-rich deposit (Unit B) to 3-TF, with similar grading, a small amount of fresh and altered lithic material, and a clast size that decreases with distance from the vent. Unit B from Maeno et al. (2018) is found overlying the ground surface to the west and south-west, similar to this study. It was also found directly overlying Unit A (pre-plinian PDCs) only in areas north-east of the volcano, not observed in this study. Maeno et al. (2017) attribute these deposits to the second eruptive stage. Stage 2 (reported around 12:31–01:01 local time) and 3 (reported around 01:00–01:30 local time) are reversed in their interpretation of the eruptive events compared to those presented in this study, based on their observation that no pumice-rich PDC deposits were found underneath the plinian fall deposits.

The main 3-TF climactic units have a modal grain size of 4–8 mm (fine lapilli), and reversely grade from coarse ash (500 μm) to coarse lapilli (<64 mm). They are dominated by pumice (85–91%), with rare dense lava and country rock lithic lapilli (Figs. 8 and 9). Increasing pumice content is common within a deposit from a sustained eruptive blast with great intensity (Walker, 1981), and similar pumice rich fall deposits are observed at Nevado de Toluca (Arce et al., 2003). The abundance of oxidised pumices increases from 3-TFb to 3-TF (Fig. 9), which could reflect temperature changes or increases during the later part of the eruption (Tait et al., 1998). The reverse grading reflects the progressive increase in the intensity and mass flux of the plinian eruption (e.g., Walker, 1971, 1981; Carey & Sigurdsson, 1989). A similar plinian pumice-rich tephra fall unit was observed from the 1990 eruption, but was strongly normally graded (Bourdier et al., 1997). Bourdier et al. (1997) also document 4 separate units of ash fall, probably as a result of 7 discrete, short-lived explosions when compared to the two main explosions in the 2014 eruption. The dominance of fine to medium lapilli at varying distances from the vent suggest that the eruption was also sustained for a few hours, allowing large clasts to reach the upper, turbulent portions of the plume (Fig. 10) (e.g., Mount St. Helens, 1980; Bursik et al., 1992; Paulick and Franz, 1997; Cioni et al., 2000; Bonadonna and Philips, 2003). Caudron et al. (2015) estimated

the intensity of the eruption, at ~10.8 to 11.0, with magnitude (M) of 4.3 to 4.5 (following Pyle, 2000). The high pumice content of the fall units shows that during this final stage the conduit was open and stable (Fig. 10; e.g. Arce et al., 2003). Elongated vesicles, up to 20 mm-long, show rapid bubble growth, coalescence and shear occurred as magma travelled up through and exited the conduit during continuing magma fragmentation (e.g., Klug and Cashman, 1996; Paulick and Franz, 1997; Klug et al., 2002). The greater abundance of juvenile pumice pyroclasts (Fig. 5), and decrease in clast size from large blocks to fine lapilli (Fig. 10) over the course of the eruption (from stage 1 to Stage 3), suggest it is possible that increased fresh magma flux and gas expansion drove further fragmentation, and may have contributed to this later more energetic eruption (Klug et al., 2002; Melnik et al., 2005; Voight et al., 2006; Wallace et al., 2013; Caudron et al., 2015; Girona et al., 2015).

The few lithics present in the climactic plinian tephra fall unit show a slightly higher percentage of brown country rock or accidental lithics reflecting the earlier loss of the 2007-2008 dome and conduit material during widening and deepening of the vent (Figs. 8 and 10). The freshest lithics of this phase are darker grey and dense, but slightly more porous than those of earlier units, which may represent the excavation of shallow degassed magma from the reservoir (e.g. Cioni et al., 2000). As the eruption mass flux decreased towards the end of the eruption, it is possible that marginal instabilities may have generated subsequent column collapse pumice-rich PDCs (not observed in this study).

2.6 Eruption patterns and hazard implications

2.6.1 Pre-1900's

Little is known about the pre-1901 eruptive activity of Kelut. Historic accounts of the eruptions lack significant detail on the style of the eruptions. However, an estimation of VEIs has been made by the Global Volcanism Program, and based on reports in Indonesian and Dutch. Since AD 1000, Kelut's explosive eruptions have often reached VEIs of 3 to 4 (Table 1; Zen and Hadikusumo, 1965; Pratomo, 1992; Bourdier et al., 1997; De Bélizal et al., 2012; GVP, 2014). In this time frame, 25 eruptions were recorded (every ~24 years), and at least one also produced a dome (AD 1376). The shortest interval between eruptions was 1 year (1825 to 1826, 1919 to 1920 and 1966 to 1967). Explosive volcanism (VEI 3) continued through to 1586, when the largest recorded eruption for Kelut occurred, following a 38-year period of quiescence (VEI 5; Pratomo, 1992; GVP, 2014). The largest repose, 75 years, occurred after this cataclysmic event, and was followed by a VEI 4 event in 1641. After this was a 185-year long period consisting of seven VEI 2 eruptions, which could mark longer periods of lava effusion. In 1826, a VEI 4 eruption occurred, followed by 4 eruptions of VEI 3-2 for the next 75 years. The most significant volcanic hazard during this period was syn- and post-eruptive lahars (Bourdier et al., 1997; De Bélizal et al., 2012; Jeffery et al., 2013).

2.6.2 Recent activity – 1901 onwards

More detail is known about the more recent activity of Kelut, with an average 15-year interval between events (and a range of 1-23 years; Table 1) (Zen and Hadikusumo, 1965; Pratomo, 1992; Bourdier et al., 1997; De Bélizal et al., 2012; GVP, 2014). There appears to be a repeating pattern of lava dome effusion and short-lived explosive eruptions. For example, in 1966, a VEI 4 eruption occurred, followed by dome effusion in 1967. The 1967 dome remained for 23 years, before being completely destroyed in the 1990 plinian eruption (Bourdier et al., 1997; GVP, 2014). A post-1990 dome grew and the latest dome extrusion took place in 2007-2008 (Jeffery et al., 2013).

2.6.3 Hazard monitoring and implications

Monitoring the temperature and chemistry of the crater-lake has been a useful forecasting tool at Kelut (Suryo and Clarke, 1985; Bernard and Mazot, 2004). Degassing from hot springs and subaqueous fumaroles has caused a rise in temperature from an ambient 19°C to as much as 31-50°C (Bernard and Mazot, 2004). In 1990, the temperature rose to 41°C, 3 months before the eruption (GVP, 1990; Vandemeulebrouck et al., 2000). Between 1993 and 2003 the temperature of the crater-lake cycled and occasionally spiked to 50°C, with gas bubbling occurring in 1996 and 2003 (Bernard and Mazot, 2004). Prior to the 2007 dome effusion, the lake temperature rose over four months to 50°C the day before the eruption (GVP, 2008). Also, a threefold increase in the carbon dioxide flux into the lake was measured by an echo sounding survey ~4 months prior to the 2007 eruption (Caudron et al., 2012). Increased CO₂ flux indicates activation of the deep magmatic system beneath Kelut, similar to that observed at other volcanic crater lakes (e.g., El Chichón, Mexico; Jácome Paz et al., 2015). Caudron et al. (2012) noted discontinuous vertical trains of bubbles or “puffing” from July to August 2007 in normally quiet regions of the crater-lake, while the main CO₂ upwelling and temperature anomalies, were located directly above the narrow magmatic conduit, suggesting the renewal of magmatic activity at depth (Caudron et al., 2012). Caudron et al. (2012) estimated that ~30% of the CO₂ entering the Kelut crater-lake is gaseous, whilst the bulk is dissolved within water. Passive, continuous degassing likely led to the effusion-dominated 2007-2008 eruption episode.

Prior to the 2014 eruption, the number of deep volcanic earthquakes increased and the crater-lake temperature rose by 5.5°C from September 2013 to February 2014 (GVP, 2014). The lake contained ~2.1 million m³ of water pre-2007 (Bernard & Mazot, 2004). Jeffery et al. (2013) estimated the 2007 dome almost completely displaced the lake, leaving a small crescentic lake forming from rainfall runoff collecting around the dome margins. The detection of such heightened activity would be difficult if there is not a crater lake present over the area of emissions to measure the changes in water temperature.

2.6.4 Hazard analysis framework

The primary hazard to life for proximal and distal populations around Kelut is from large and extensive lahars (Hadikusumo, 1974; Suryo and Clarke, 1985; Bourdier et al., 1997a; De Bélizal et al., 2012). In AD 1586 and 1919 extensive syn- and post-eruptive lahars caused up to ~10,000 casualties. The largest syn-eruptive lahars occurred when the crater lake was at its greatest volume (Hadikusumo, 1974). The lahars led to the construction of a system of drainage tunnels that started in 1919 with further efforts in 1923 and 1954, to control the lake level and reduce the impact of lahars (Zen and Hadikusumo, 1965; Bernard and Mazot, 2004).

While no syn-eruptive, hot primary crater-lake derived lahars were formed during the 13-14 February 2014 eruption, five days after it secondary rain-derived lahars were generated when rain remobilised pyroclastic material in several river channels (GVP, 2014; Dibyosaputro et al., 2015). The resulting lahars filled dams and irrigation systems with debris, damaged bridges and roads, and inundated much farmland (Dibyosaputro et al., 2015). Secondary, rain-derived lahars are a persistent hazard at Kelut, while primary syn-eruptive lahars depend on the status of the lake at the time of the eruption. Several generations of hazard maps have been produced for this area (e.g., Suryo and Clarke, 1985; Mulyana et al., 2004; De Bélizal et al., 2012), identifying major risk catchments to the north-west, west, and south-west of the volcano. The official hazard maps by the Centre for Volcanology and Geologic Hazard Mitigation (Mulyana et al., 2004; Primulyana et al., 2014; Andreastuti et al., 2018) are comprehensive, and include hazards in both proximal and distal areas. The Primulyana et al. (2014) map was also updated on the basis of the effects of the 2014 eruption.

The generally cyclic nature of eruption styles between explosive to effusive variants since the 1900's, suggests that the next eruption of Kelut could be a long period of dome growth or repose, lasting anywhere from 7 to 31 years. The eruption will depend on the rate of ascent of the magma, due to degassing conditions of the magma in the upper conduit (Gardner et al., 1996; Klug et al., 2002), and on the occurrence of an interval of magmatic recharge. Alternations between dome-building and explosive eruptions occur at many other similar volcanoes (e.g. Merapi, Indonesia and Colima, Mexico) although the pattern at Kelut appears to be remarkably regular in recent times. There have, however, also been semi-continuous periods of smaller eruptions with sporadically timed larger events (VEI 3 to 5). Generally the very largest eruptions (e.g. 1586) are followed by the longest repose periods (in this case 75 years).

It should also be recognised that the Kelut edifice includes many older domes, centred away from the currently active crater. Although these are not well dated, shifts in the eruption site and lateral dome extrusions must also be included in hazard analysis.

2.7 Conclusions

The 2014 Kelut eruption was sudden in onset and relatively brief in comparison to other plinian eruptions. Despite this, it was highly explosive and in its climactic phase produced a stable eruption column with a well-formed and dispersed umbrella region. Three stages of the 2014 eruption have been identified.

The onset eruption of stage 1 lasted for only ~15-30 minutes and produced PDCs that were rich in dense lava lithics, reflecting the progressive destruction of the 2007-2008 lava dome, upper conduit and vent walls (Figs. 5 and 10). Gas overpressure drove this eruption, induced by a possible replenishment of magma into a shallow magma reservoir, destabilising the conduit-capping 2007-2008 dome. We hypothesize that this caused a top-down decompression wave, leading to rapid expansion and rise of gas-rich magma (Klug et al., 2002; Caudron et al., 2015), and has also been proposed at other Javanese volcanoes such as Merapi (Voight et al., 2006; Girona et al., 2015). There was no evidence for phreatomagmatism during this onset phase, likely because the crater lake and underlying aquifers were a small fraction of their pre-2007 sizes. Increases in the magma flux and transition to a more constant eruption led to a growing eruption column during the 2-hour-long stage 2 plinian eruption. Our data indicate that continued magma fragmentation, along with further vent wall and conduit widening led to overloading of unstable, basal column margins. The incorporation prevented buoyant rise and atmospheric mixing of blocky pyroclasts, and thus generated longer runout PDCs, with higher pumice contents and decreasing dome and conduit fragments (Fig. 10). The final climactic plinian phase produced a plinian column up to 26 km in altitude, with a well-developed umbrella region. The deposits from this stage contain reversely graded, medium-ash to coarse-lapilli, juvenile pumice rich ($\geq 90\%$) tephra falls. Widespread proximal and distal fall likely emplaced during the one-hour (to 02:00 local time) climax of the plinian eruption, in the third and final stage (stage 3), although it is possible that fine ash may have fallen proximally from 23:00 local time. These deposits reflect an eruption progressively becoming more energetic with time, with increased mass flux and gas expansion of fresh magma, and continued fragmentation sustaining the plinian eruption.

Although the 2014 eruption was similar in duration, volume and general style to the 1990 event, the 2014 eruption shows a simpler overall stratigraphic succession. Many of the 2014 PDC deposits were emplaced *en masse*. Therefore, intercalations of contemporaneous fall and PDC deposits common in 1990 deposits were not a feature of the 2014 deposits, although co-PDC fall deposits indicate a brief pause between each of the 2014 eruption stages.

The nature of post-1900's Kelut eruptions shows a general cycle between explosive and effusive variants, probably depending on the renewal of magma, rate of magma ascent, and magma degassing conditions in the shallow magma reservoir and upper conduit. This suggests that the next eruption, if it occurs within the next 20 years, may be a long (up to decadal) period of dome growth.

In order to understand the dynamics and processes responsible for the cyclic nature of eruptions, and accurately pinpoint triggers for more intense episodes at Kelut, petrological, mineralogical and geochemical analyses of pyroclastic deposits from the 1990 and 2014 explosive eruptions are needed, which can then be compared to the 2007-2008 dome. A better insight into the past eruptive activity of Kelut (pre-1990) is also needed to understand the relationship between magma intrusion cycles and eruption patterns.

2.8 Acknowledgements

Reza Firmansyah and Dermadi Madi from Bandung Institute of Technology are acknowledged for their assistance during fieldwork. Lucy McGee is thanked for many supportive conversations. We would also like to thank the two anonymous reviewers for their thought provoking comments that improved the manuscript. The Guest Editor Wendy McClausland is also thanked for handling the manuscript. L. Goode is funded by an International Macquarie University Research Excellence Scholarship (iMQRES) (2012196) associated with an Australian Research Council Future Fellowship awarded to H. Handley (FT120100440). S. Cronin is funded by the New Zealand Natural Hazard Research Platform “Quantifying exposure to volcanic hazards” project.

2.9 References

- Andreastuti, S.D., Alloway, B.V., and Smith, I.E.M. (2000). A detailed tephrostratigraphic framework at Merapi Volcano, Central Java, Indonesia: implications for eruption predictions and hazard assessment. *Journal of Volcanology and Geothermal Research*. 100. 51-67.
- Andreastuti, S., Paripurno, E.T., Gunawan, H., Budianto, A., Syahbana, D., and Pallister, J. (2018). Character of community response to volcanic crises at Sinabung and Kelud volcanoes, *Journal of Volcanology and Geothermal Research*. <http://dx.doi.org/10.1016/j.jvolgeores.2017.01.022>.
- Andreastuti, S., Widiwijayanti, C., Heriwaseso, A., and Budianto, A. (2018). Revision of hazard map considered from eruptive style and impact: the case of Kelud volcano. *Journal of Volcanology and Geothermal Research*.
- Arámbula-Mendoza, R., Lesage, R., Valdés-González, C., Varley, N.R., Reyes-Dávila, G., and Navarro, C. (2011). Seismic activity that accompanied the effusive and explosive eruptions during the 2004-2005 period at Volcán de Colima, Mexico. *Journal of Volcanology and Geothermal Research*. 205. 30-46.
- Arce, J.L., Macias, J.L., Vazquez-Selem, L. (2003). The 10.5 km plinian eruption of Nevado de Toluca volcano, Mexico: stratigraphy and hazard implications. *Geological Society of America Bulletin*. 115. 230-248.
- Badan Informasi Geospasial (BDI) (2013). Bakosurtanal (In Indonesian). Topographical map of Kelut volcano.
- Bernard, A., and Mazot, A. (2004). Geochemical evolution of the young crater lake of Kelud volcano in Indonesia. In: Wanty, R.B., and Seal II, R.B. (2004) eds. *Water-rock interaction, (WRI-11)*. London: Taylor and Francis group plc. 87- 90.
- Bonadonna, C., and Philips, J. (2003). Sedimentation from strong volcanic plumes. *Journal of Geophysical Research*. 108. 1-28

Chapter Two

- Bourdier, J.-L., Pratomio, I., Thouret, J.-C., Boudon, G., and Vincent, P.M. (1997). Observations, stratigraphy and the eruptive processes of the 1990 eruption of Kelut volcano, Indonesia. *Journal of Volcanology and Geothermal Research*. 79. 181-203.
- Bourdier, J.-L., Thouret, J.-C., Pratomio, I., Vincent, P.M., and Boudon, G. (1997a). Volcanic hazards at Kelut volcano (Java island, Indonesia): lessons learned from the 1990 eruption. *Geomaterials*. 324. 961-968.
- Branney, M.J., and Kokelaar, P. (2002). Pyroclastic density currents and the sedimentation of ignimbrites. *Geological Society, London, Memoirs*. 27.
- Brown, R.J., Bonadonna, C., and Durant, A.J. (2012). A review of volcanic ash aggregation. *Physics and Chemistry of the Earth*. 45-46. 65-78.
- Bursik, M.I., Sparks, R.S.J., Gilbert, J.S., and Carey, S.N. (1992). Sedimentation of tephra by volcanic plumes, I, theory and its comparison with a study of the Fogo A plinian deposit, Sao Miguel (Azores). *Bulletin of Volcanology*. 54. 329-344.
- Calder, E.S., Cole, P.D., Dade, W.B., Druitt, T.H., Hoblitt, R.P., Huppert, H.E., Richie, L., Sparks, R.S.J., and Young, S.R. (1999). Mobility of pyroclastic flows and surges at the Soufriere Hills Volcano, Montserrat. *Geophysical Research Letters*. 26. 537-540.
- Calder, E.S., Sparks, R.S.J., and Gardeweg, M.C. (2000). Erosion, transport and segregation of pumice and lithic clasts in pyroclastic flows inferred from ignimbrite at Lascar Volcano, Chile. *Journal of Volcanology and Geothermal Research*. 104. 201-235.
- Carey, S.N., and Sigurdsson, H. (1989). The intensity of plinian eruptions. *Bulletin of Volcanology*. 51. 28-40.
- Carey, R.J., Houghton, B.F., Sable, J.E., Wilson, C.J.N. (2007). Contrasting grain size and componentry in complex proximal deposits of the 1886 Tarawera basaltic Plinian eruption. *Bulletin of Volcanology*. 69. 903-926.
- Caudron, C., Mazot, A., and Bernard, A. (2012). Carbon dioxide dynamics in Kelud volcanic lake. *Journal of Geophysical Research*. 117. 1-11.
- Caudron, C., Taisne, B., Garces, M., Alexis, L.P., and Mialle, P. (2015). On the use of remote infrasound and seismic stations to constrain the eruptive sequence and intensity for the 2014 Kelud eruption. *Geophysical Research Letters*. 6614-6621.
- Cioni, R., Marianelli, P., Santacroce, R., and Sbrana, A. (2000). *Plinian and Subplinian Eruptions*. In: Encyclopedia of Volcanoes. Eds. Sigurdsson, H., Houghton, B., Rymer, H., McNutt, S., and Stix, J. Academic Press. p477 – 494.
- Cioni, R., Gurioli, L., Lanza, R., and Zanella, E (2004). Temperatures of A.D. 79 pyroclastic density currents deposits (Vesuvius, Italy): *Journal of Geophysical Research*. 109.
- Cronin, S.J., Lube, G., Dayudi, D.S., Sumarti, S., Subrandiyo, S., Surono. (2013). Insights into the October-November 2010 Gunung Merapi eruption (Central Java, Indonesia) from the stratigraphy, volume and characteristics of its pyroclastic deposits. *Journal of Volcanology and Geothermal Research*. 261. 244-259.
- Dare, R.A., Smith, D.H., and Naughton, M.J. (2016). Ensemble prediction of the dispersion of volcanic ash from the 13 February 2014 eruption of Kelut, Indonesia. *Journal of Applied Meteorology and Climatology*. 55. 61-80.
- Dempsey, S.R. (2013). Geochemistry of volcanic rocks from the Sunda Arc. PhD Thesis, Durham University, UK. http://etheses.dur.ac.uk/6948/1/ScottDempsey_Thesis.pdf

- De B lizar, E., Lavigne, F., Gaillard, J.C., Grancher, D., Pratomo, I., and Komorowski, J.C. (2012). The 2007 eruption of Kelut volcano (East Java, Indonesia): Phenomenology, crisis management and social response. *Geomorphology*. 136. 165-175.
- Dibiyosaputro, S., Dipayana, G.A., Nugraha, H., Pratiwi, K., and Valeda, H.P. (2015). Lahar at Kali Konto after the 2014 eruption of Kelud volcano, East Java: Impacts and risk. *Forum Geografi*. 29. 59-72.
- Dirksen, O., Humphreys, M.C.S., Pletchov, P., Melnik, O., Demyanchuk, Y., Sparks, R.S.J., and Mahony, S. (2006). The 2001-2004 dome-forming eruption of Shiveluch volcano, Kamchatka: Observation, petrological investigation and numerical modelling. 155. 201-226.
- Druitt, T.H., and Kokelaar, B.P. eds., (2002). The eruption of Soufriere Hills volcano, Montserrat, from 1995 to 1999. *Geological Society of London*.
- Edmonds, M., and Herd, R.A. (2007). A volcanic degassing event at the explosive-effusive transition. *Geophysical Research Letters*. 34.
- Edmonds, M., Herd, R.A., and Strutt, M.H. (2006). Tephra deposits associated with a large lava dome collapse, Soufriere Hills Volcano, Montserrat, 12-15 July 2003. *Journal of Volcanology and Geothermal Research*. 153. 313-330.
- Fink, J.H. (1987). The emplacement of silicic domes and lava flows. *Geological Society of America*. 212. 37.
- Folk, R.L., and Ward, W.C. (1957). Brazos river bar: a study in the significance of grain size parameters. *Journal of Sedimentary Petrology*. 27. 3-26.
- Gardner, J.E., Thomas, R.M.E., Jaupart, C., and Tait, S. (1996). Fragmentation of magma during plinian volcanic eruptions. *Bulletin of Volcanology*. 58. 144-162.
- Gertisser, R., and Keller, J. (2003). Temporal variations in magma composition at Merapi Volcano (Central Java, Indonesia): magmatic cycles during the past 2000 years of explosive activity. *Journal of Volcanology and Geothermal Research*. 123. 1-23.
- Gertisser, R., Charbonnier, S.J., Keller, J., Quidelleur, X. (2012). The geological evolution of Merapi volcano, Central Java, Indonesia. *Bulletin of Volcanology*. 74. 1213-1233.
- Girona, T., Costa, F., and Schubert, G. (2015). Degassing during quiescence as a trigger of magma ascent and volcanic eruptions. *Scientific Reports*. 5. 18212.
- Global Volcanism Program (GVP) (1990). Report on Kelut (Indonesia). In: McClelland, L. (ed.), *Bulletin of the Global Volcanism Network*, 15:1. Smithsonian Institution. Available: <http://dx.doi.org/10.5479/si.GVP.BGVN199001-263280>.
- Global Volcanism Program (GVP) (1990a). Report on Kelut (Indonesia). In: McClelland, L. (ed.), *Bulletin of the Global Volcanism Network*, 15:9. Smithsonian Institution. Available: <http://dx.doi.org/10.5479/si.GVP.BGVN199009-263280>.
- Global Volcanism Program (GVP) (2008). Report on Kelut (Indonesia). In: Wunderman, R. (ed.), *Bulletin of the Global Volcanism Network*, 33:3. Smithsonian Institution. Available: <http://dx.doi.org/10.5479/si.GVP.BGVN200803-263280>.
- Global Volcanism Program (GVP) (2012). Report on Kelut (Indonesia). In: Wunderman, R. (ed.), *Bulletin of the Global Volcanism Network*, 37:3. Smithsonian Institution. Available: <http://dx.doi.org/10.5479/si.GVP.BGVN201203-263280>

Chapter Two

- Global Volcanism Program (GVP). (2014). Report on Kelut (Indonesia). In: Wunderman, R. (ed.), Bulletin of the Global Volcanism Network, 39:2. Smithsonian Institution. Available: <http://dx.doi.org/10.5479/si.GVP.BGVN201402-263280>.
- Global Volcanism Program (GVP). (2014a). Eruptive History. In: Kelut Eruption Page. Smithsonian Institution. Accessed March 2015. Available: <http://www.volcano.si.edu/volcano.cfm?vn=263280>
- Global Volcanism Program (GVP) (2014b). Smithsonian Institution, Kelut Eruption Page. Accessed March 2015. Available: <http://www.volcano.si.edu/volcano.cfm?vn=263280>.
- Global Volcanism Program (GVP) (2015). Smithsonian Institution. The Indonesia Region. Accessed March 2014. Available: <http://www.volcano.si.edu/region.cfm?rn=6>
- Google Earth Pro 7.1.1.1580 (2015) Kelut and surrounding areas. 7°56'55.11"S, 112°18'30.00"E, elevation 1335m, eye alt 16.26km. World View, DigitalGlobe Inc., 2015. Viewed 23/08/2015.
- Gorshkov, G.S., and Dubik, Y.M. (1970). Gigantic directed blast at Shiveluch volcano (Kamchatka). *Bulletin Volcanologique*. 34. 261-288.
- Hadikusumo, D. (1974). The rise and drop of Mt. Kelut crater bottom after paroxysmal eruptions. *Tectonophysics*. 23. 341-347.
- Hall, R. (2002). Cenozoic geological and plate tectonic evolution of SE Asia and the SW Pacific: computer-based reconstructions, model and animations. *Journal of Asian Earth Science*. 20. 353-431.
- Hall, R. (2011). Australia-SE Asia collision: plate tectonics and crustal flow. In: Hall, R., Cottam, M.A., and Wilson, M.E.J. (eds): The SE Asian gateway: history and tectonics of Australia-Asia collision. *Geological Society of London Special Publication*. 75 – 109.
- Hamilton, W. (1979). Tectonics of the Indonesian Region. *US Geological Survey Professional Paper*. 1078.1-50
- Hidayati, S. H., Basuki, A., Kristianto, and Mulyana, I., (2009). Emergence of lava dome from the crater lake of Kelud volcano, East Java. *Jurnal Geologi Indonesia*. 4. 229-238.
- Hidayat, M. (2014). Infrasound monitoring in Indonesia, paper presented at Infrasound Technology Workshop, 2014, Vienna, Austria, October.
- Humaida, H., Brotopuspito, K.S., Pranowo, H.D., and dan Narsito. (2011). Modelling of magma density and viscosity changes and their influences towards the characteristic of Kelud Volcano Eruption (In Indonesian). *Jurnal Geologi Indonesia*. 6. 227-237.
- Jácome Paz, M.P, Taran, Y., Inguaggiato, S., and Collard, N. (2015). CO₂ flux and chemistry of El Chichón crater lake (Mexico) in the period of 2013-2015: Evidence for enhanced volcano activity. *Geophysical Research Letters*. 127-134.
- Jeffery, A.J., Gertisser, R., Troll, V.R., Jolis, E.M., Dahren, B., Harris, C., Tindle, A.G., Preece, K., O'Driscoll, B., Humaida, H., and Chadwick, J.P. (2013). The pre-eruptive magma plumbing system of the 2007-2008 dome-forming eruption of Kelut volcano, East Java, Indonesia. *Contributions to Mineralogy and Petrology*. 166. 275-308.
- Klug, C. and Cashman, K.V. (1996). Permeability development in vesiculating magmas: implications for fragmentation. *Bulletin of Volcanology*. 58. 87-100.

- Klug, C., Cashman, K.V., and Bacon, C.R. (2002). Structure and physical characteristics of pumice from the climactic eruption of Mount Mazama (Crater Lake), Oregon. *Bulletin of Volcanology*. 64. 486-501.
- Kristiansen, N.I., Prata, A.J., Stohl, A., and Carn, S.A. (2015). Stratospheric volcanic ash emissions from the 13 February 2014 Kelut eruption. *Geophysical Research Letters*. 42, 588-596.
- Lavallée, Y., Varley, N.R., Alatorre-Ibarguengoitia, M.A., Hess, K.U., Kueppers, U., Mueller, S., Richard, D., Scheu, B., Spieler, O., Dingwell, D.B. (2012). Magmatic architecture of dome-building eruptions at Volcan de Colima, Mexico. *Bulletin of Volcanology*. 74. 249-260.
- Lube, G., Cronin, S.J., Platz, T., Freundt, A., Procter, J.N., Henderson, C., and Sheridan, M.F. (2007). Flow and deposition of pyroclastic granular flows: A type example from the 1975 Ngauruhoe eruption, New Zealand. *Journal of Volcanology and Geothermal Research*. 161. 165-186.
- Lube, G., Cronin, S.J., Thouret, J.-C., Surono (2011). Kinematic characteristics of pyroclastic density currents at Merapi and controls on their avulsion from natural and engineered channels. *Geological Society of America Bulletin*. 123. 1127-1140.
- Lube, G., Breard, E.C.P., Cronin, S.J., Procter, J.N., Brenna, M., Moebis, A., Pardo, N., Stewart, R.B., Jolly, A., Fournier, N. (2014). Dynamics of surges generated by hydrothermal blasts during the 6 August 2012 Te Maari eruption, Mt. Tongariro, New Zealand. *Journal of Volcanology and Geothermal Research*. 286. 348-366.
- Maeno, F., Nakada, S., Yoshimoto, M., Shimano, T., Hokanishi, N., Zaennudin, A., and Iguchi, M. (2017). A sequence of a plinian eruption preceded by dome destruction at Kelud volcano, Indonesia, on February 13, 2014, revealed from tephra fallout and pyroclastic density current deposits. *Journal of Volcanology and Geothermal Research*. <http://dx.doi.org/10.1016/j.jvolgeores.2017.03.002>
- McBirney, A.R., and Murase, T. (1970). Factors governing the formation of pyroclastic rocks. *Bulletin of Volcanology*. 34. 372-384.
- Melnik, O., Barmin, A.A., and Sparks, R.S.J. (2005). Dynamics of magma flow inside volcanic conduits with bubble overpressure buildup and gas loss through permeable magma. *Journal of Volcanology and Geothermal Research*. 143. 53-68.
- Mulyana, A.R., Nasution, A., Martono, A., Sumpena, A.D., Purwoto, and Santoso, M.S. (2004). Peta Kawasan Rawan Bencana Gunungapi Kelud, Propinsi Jawa Timur (Volcanic hazards map of Kelud volcano, East Java Province), Pusat Vulkanologi dan Mitigasi Bencana Geologi, Badan Geologi, Departemen Energi dan Sumber Daya Mineral. Scale 1:100,000, 1 plate.
- Nakashima, Y., Heki, Takeo, A., Cahyadi, M.N., Aditiya, A., and Yoshizawa, K (2016). Atmospheric resonant oscillations by the 2014 eruption of the Kelud volcano, Indonesia, observed with the ionospheric total electron contents and seismic signals. *Earth and Planetary Science Letters*. 434. 112-116.
- Newhall, C.G., Bronto, S., Alloway, B., Banks, N.G., Bahar, I., del Marmol, M.A., Hadisantono, R.D., Holcomb, R.T., McGeehin, J., Miksic, J.N., Rubin, M., Sayudi, S.D., Sukhyar, R., Andreastuti, S., Tilling, R.I., Torley, R., Trimble, D., and Wirakusumah, A.D. (2000). 10,000 years of explosive eruptions of Merapi Volcano, Central Java: archaeological and modern implications. *Journal of Volcanology and Geothermal Research*. 100. 9-50.
- Pardo, N., Avellan, D.R., Macias, J.L., Scolamacchia, T., Rodriguez, D. (2008). The ~ 1245 yr BP Asososca maar: New advances on recent volcanic stratigraphy of Managua (Nicaragua) and hazard implications. *Journal of Volcanology and Geothermal Research*. 176. 493-512.

Chapter Two

- Pardo, N., Cronin, S.J., Palmer, A.S., and Nemeth, K. (2012). Reconstructing the largest explosive eruptions of Mt. Ruapehu, New Zealand: lithostratigraphic tools to understand subplinian-plinian eruptions at andesitic volcanoes. *Bulletin of Volcanology*. 74. 617-640.
- Paulick, H., and Franz, G. (1997). The colour of pumice: case study on a trachytic fall deposit, Meidob volcanic field, Sudan. *Bulletin of Volcanology*. 59. 171-185.
- Porreca, M., Giordano, G., Mattei, M., and Musacchio, P. (2006). Evidence of two Holocene phreatomagmatic eruptions at Stromboli volcano (Aeolian Islands) from paleomagnetic data. *Geophysical Research Letters*. 33. 1-6.
- Pratomo, I. (1992). Etude de l'éruption de 1990 du volcan Kelut (Java- Est Indonesie): son apport a l'interpretation de l'activite historique du volcan. Unpublished PhD Thesis, Blaise Pascal Clermont-Ferrand II.
- Preece, K., Gertisser, R., Barclay, J., Berlo, K., Herd, R.A., Edinburgh Ion Microprobe Facility. (2014). Pre- and syn-eruptive degassing and crystallisation processes of the 2010 and 2006 eruptions of Merapi volcano, Indonesia. *Contributions to Mineralogy and Petrology*. 168. 1-25.
- Primulyana, S., Hariwaseso, A., Zaenuddin, A., Budianto, A. (2014). Peta Kawasan Rawan Bencana Gunungapi Kelud, Propinsi Jawa Timur (Volcanic hazards map of Kelud volcano, East Java Province), Pusat Vulkanologi dan Mitigasi Bencana Geologi, Badan Geologi, Kementerian Energi dan Sumber Daya Mineral. Scale 1:100,000, 1 plate.
- Putra, H.P. (2014). Erupsi G. Kelud Blitar In: *Erupsi Kelud M*. <https://www.flickr.com/photos/117472423@N05/12515534124/in/photostream/> . HTP Studio digital art photography. Accessed 04/2015.
- Pyle, D. (2000). Sizes of volcanic eruptions. In: *Encyclopedia of Volcanoes*, vol. 1. Edited by Sigurdsson, H. Academic Press, San Diego, California. 263-269.
- Robin, C., Camus, G., Gourgaud, A. (1991). Eruptive and magmatic cycles at Fuego de Colima volcano (Mexico). *Journal of Volcanology and Geothermal Research*. 45. 209-225.
- Siebert, L., Simkin, T., and Kimberly, P. (2011). *Volcanoes of the World*. 3rd Ed. University of California Press: Los Angeles. 83-102.
- Smith, N.J., and Kokelaar, B.P. (2013). Proximal record of the 273 ka Poris caldera-forming eruption, Las Canadas, Tenerife. *Bulletin of Volcanology*. 75. 768-789.
- Sparks, R.S.J., Self, S., and Walker, G.P.L. (1973). Products of ignimbrite eruptions. *Geology*. 1. 115-118.
- Sparks, R.S.J., Bursik, M.I., Carey, S.N., Gilbert, J.S., Glaze, S., Sigurdsson, H., and Woods, A.W. (1977). *Volcanic plumes*. John Wiley: New York.
- Sulpizio, R., Mele, D., Dellino, P., and La Volpe, L. (2007). Deposits and physical properties of the pyroclastic density currents during complex Subplinian eruptions: the AD 472 (Pollena) eruption of Somma-Vesuvius, Italy. *Sedimentology*. 54. 607-635.
- Sulpizio, R., Dellino, P., Doronzo, D.M., and Sarocchi, D. (2014). Pyroclastic density currents: state of the art and perspectives – a review. *Journal of Volcanology and Geothermal Research*. 283. 36-65.
- Sulpizio, R., Lucchi, F., Forni, F., Massaro, S., and Tranne, C. (2016). Unravelling the effusive-explosive transitions and the construction of a volcanic cone from geological data: The example of Monte dei Porri, Salina Island (Italy). *Journal of Volcanology and Geothermal Research*. <http://dx.doi.org/10.1016/j.jvolgeores.2016.06.024>

- Suryo, I., and Clarke, M.C.G. (1985). The occurrence and mitigation of volcanic hazards in Indonesia as exemplified at the Mount Merapi, Mount Kelut, and Mount Galunggung volcanoes. *Quarterly Journal of Engineering Geology*. 18. 79-98.
- Tait, S., Thomas, R., Gardner, J., and Jaupart, C. (2014). Constraints on cooling rates and permeabilities of pumice in an explosive eruption jet from colour and magnetic mineralogy. *Journal of Volcanology and Geothermal Research*. 86. 79-91.
- Thouret, J.-C., Abdurachman, K.E., Bourdier, J.-L., and Bronto, S. (1998). Origin, characteristics, and behaviour of lahars following the 1990 eruption of Kelud volcano, eastern Java (Indonesia). *Bulletin of Volcanology*. 59. 460-480.
- Turner, M.B., Cronin, S.J., Bebbington, M.S., Smith, I.E.M., Stewart, R.B. (2011). Integrating records of explosive and effusive activity from proximal and distal sequences: Mt. Taranaki, New Zealand. *Quaternary International*. 246. 364-373.
- Van Bemmelen, R.W. (1949). *The Geology of Indonesia and Adjacent Archipelago*. Government Printing Office: The Hague. 1-150.
- Van Bergen, M.J., Bernard, A., Sumarti, S., Sriwana, T., and Sitorus, K. (2000). Crater lakes of Java: Dieng, Kelud, Ijen. Excursion Guidebook – *International Association of Volcanology and Chemistry of the Earth's Interior (IAVCEI)*, General Assembly. Bali, 2000. 42
- Vandemeulebrouck, J., Sabroux, J.C., Halbwachs, M., Surono, Poussielgue, N., Grangeon, J., and Tabbagh, J. (2000). Hydroacoustic noise precursors of the 1990 eruption of Kelut volcano, Indonesia. *Journal of Volcanology and Geothermal Research*. 97. 443-456.
- Voight, B., Linde, A.T., Sacks, I.S., Mattioli, G.S., Sparks, R.S.J., Elsworth, D., Hidayat, D., Malin, P.E., Shalev, E., Widiwijayanti, C., Young, S.R., Bass, V., Clarke, A., Dunkely, P., Johnston, W., McWhorter, N., Neuberg, J., and Williams, P. (2006). Unprecedented pressure increase in deep magma reservoir triggered by lava-dome collapse. *Geophysical Research Letters*. 33. 1-4.
- VSI, CVGHM (Volcanological Survey of Indonesia, Center for Volcanology and Geological Hazard Mitigation) (2014). G. Kelud, Jawa Timur: Sejarah Letusan (Historical Eruptions). *Data Dasar Gunungapi (Volcano Data)*. Badan Geologi (In Indonesian). <http://www.vsi.esdm.go.id/index.php/gunungapi/data-dasar-gunungapi/538-g-kelud>
- Walker, G.P.L. (1971). Grainsize characteristics of pyroclastic deposits. *Journal of Geology*. 79. 696-714.
- Walker, G.P.L. (1981). Plinian eruptions and their products. *Bulletin of Volcanology*. 44. 221-240.
- Wallace, K.L., Schaefer, J.R., and Coombs, M.L. (2013). Character, mass, distribution, and origin of tephra-fall deposits from the 2009 eruption of Redoubt volcano, Alaska – Highlighting the significance of particle Bonda. *Journal of Volcanology and Geothermal Research*. 259. 145-169.
- White, J.D.L. and Houghton, B.F. (2006). Primary volcanoclastic rocks. *Geology*. 34. 677-680.
- Wirakusumah, A.D. (1991). Some studies of the volcanology, petrology and structure of Mt. Kelut, East Java, Indonesia. PhD Thesis, Victoria University, Wellington.
- Zen, M.T., and Hadikusumo, D. (1965). The future danger of Mt. Kelut (Eastern Java – Indonesia). *Bulletin Volcanologique*. 28. 275-282.

Zharinov, N.A., and Demyanchuk, Y.V. (2013). Large explosive eruptions of Shiveluch volcano, Kamchatka resulting in partial destruction of the extrusive dome (February 28, 2005 and October 27, 2010). *Journal of Volcanology and Seismology*. 7. 131-144.

3. Eruption frequency, style and composition variations at Kelut volcano, Indonesia, based on 1500 years of tephra records

Louise R. Goode¹, Heather K. Handley¹, Shane J. Cronin², Mirzam Abdurrachman³

¹Department of Earth and Planetary Sciences, Macquarie University, Sydney, NSW 2109, Australia.

²School of Environment, University of Auckland, Private Bag 92019, Auckland 1142, New Zealand.

³Department of Geological Engineering, Bandung Institute of Technology, Bandung 40132, Indonesia.

3.1 Abstract

Well-constrained, long pyroclastic records of volcanoes when integrated with geochemical studies are a useful tool to understand the time-variability of volcanic systems, and reliably forecast eruptive behaviours. This study concentrates on the variation of volcanic activity at Kelut volcano, Indonesia, over the last ~1500 years. A total of 25 eruptive events are recorded from tephra sequences west and south west of the volcano. New radiocarbon dates of charcoal preserved in deposits shows activity from ~AD 560 to 2014. Variations in major elemental analyses of glass shards from each eruptive event indicate that a wide range of magmatic processes govern the eruptive frequency and style at Kelut volcano. The earliest eruptions (~AD 560 to 1000) have some of the coarsest and thickest lapilli fall deposits from sub-plinian to plinian eruptions, and the most evolved glass compositions (~72 wt.% SiO₂). The apparently high-explosivity of these eruptions corresponds with a low eruptive frequency (~88 years) during this period, allowing magmatic evolution. AD 1000 to 1919 marked a change in deposit character, and thus eruptive style and more frequent eruptions (~35 years). Each eruption comprises complex sets of events that produce PDCs and tephra falls. The post- AD 1000 eruptions were mainly dome- collapse followed by -growth periods, with frequent phreatic/phreatomagmatic explosions, and vulcanian eruptions. Large variations in compositions (~64-71 wt.% SiO₂) from ~AD 1000 to 1726 indicate sudden mafic magma influxes, interrupting magmatic differentiation, by mixing to a varying extent with resident magma in the system. Distinct mafic recharge events based on decreasing silica compositions of glass shards (to ~64 wt.% SiO₂), appear to have triggered some of the largest eruptions at Kelut, such as 1586. Eruptions post- AD 1726 to the most recent eruption in 2014 are regularly tapping a continuously evolving magma system (from 66-70 wt.% SiO₂). Despite no major chemical changes of the magma, eruption style varied from 1920 onwards between alternating periods of lava-dome effusion, and explosive plinian eruptions, with 1 eruption every ~12 years, but plinian eruption occurring every ~21 years. This variation therefore likely reflects pressurisation conditions in the magma chamber, and thus the rate of ascent of magma. Our results show how volcanic eruption variability (in frequency, size and style) can be related to mafic recharge cycles, feeding rates and upper conduit conditions.

Key words: Kelud, Kelut, glass geochemistry, stratigraphy, pyroclastic, stratigraphic records, effusive, explosive, cyclic

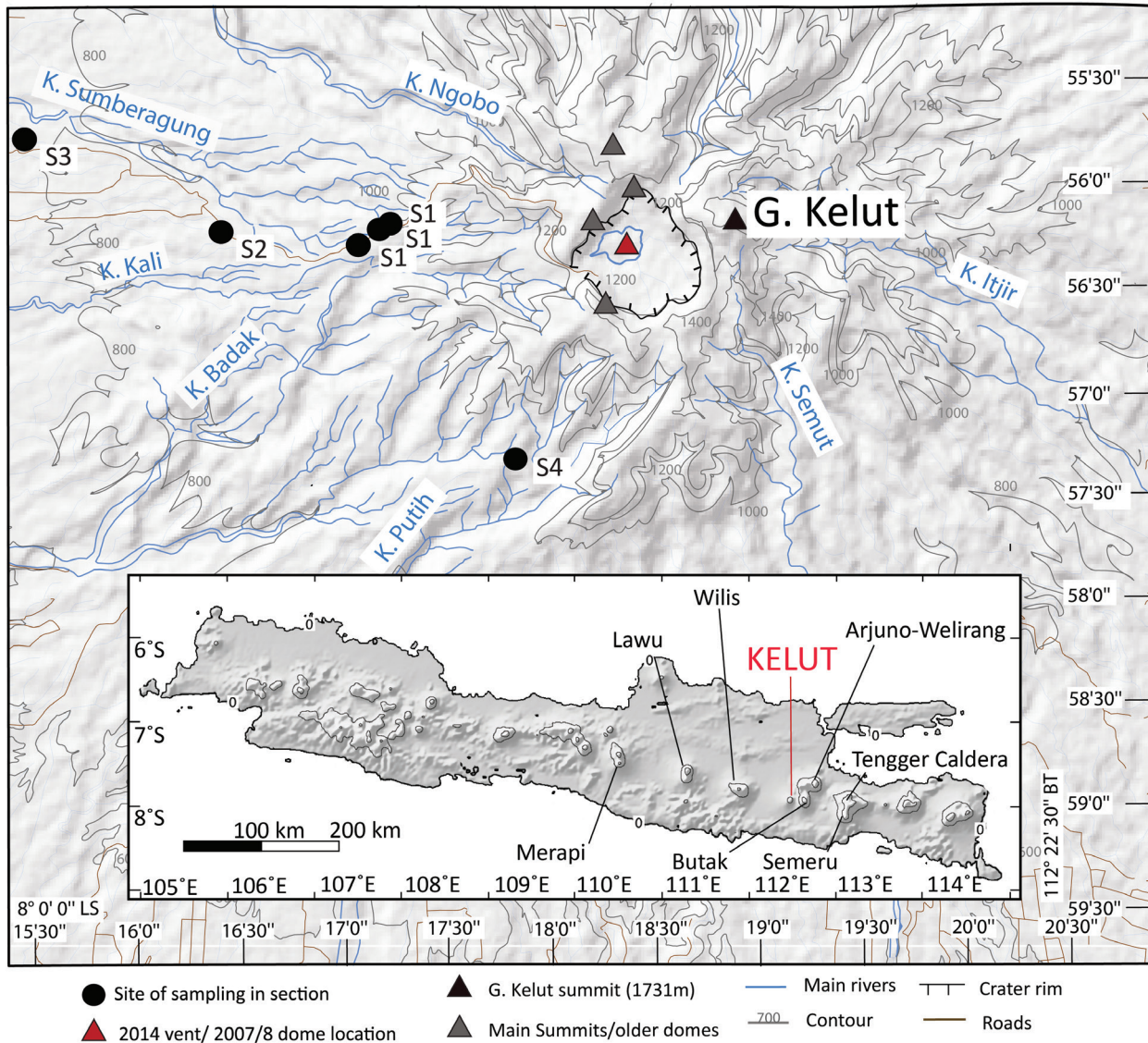


Figure 1: Topographic map of Kelut volcano, showing the location of sampling sites (black circles) according to stratigraphic section number listed Table 1. Grey contours are in 200 m intervals, main roads shown in brown, and main rivers in blue. Inset map and DEM of Java shows the location of all volcanoes in the region (Modified from BDI, 2013 and Chapter 2).

3.2 Introduction

Investigations into long and complete sequences of tephra deposits are the most robust basis for understanding time-varying eruption behaviour and probabilistic event forecasting at re-awakening stratovolcanoes (Turner et al., 2008). Many intermediate composition stratovolcanoes are characterised by apparently cyclic eruption episodes, with alternating plinian explosion and dome-effusion eruptions, such as Merapi, Indonesia, (e.g., Andreastuti et al., 2000; Newhall et al., 2000), Mt. Pelée, Martinique (e.g., Roobol and Smith, 1976; Westercamp and Traineau, 1983), Soufriere Hills, Montserrat (e.g., Sparks and Young, 2002; Smith et al., 2007), Popocatepetl (e.g., Siebe and Macías, 2006; Gómez-Vazquez et al., 2016) and Colima, Mexico (e.g., González et al.,

2002; Luhr et al., 2010). Long records of pyroclastic volcanism on Java, Indonesia, are largely understudied or have not been produced when compared to other regions such as New Zealand (e.g., Mount Taranaki, Turner et al., 2008, 2009; Damaschke et al., 2017; Torres-Orozco et al., 2017a, b; Mount Ruapheu, Pardo et al., 2012; Mount Tonagiro, Pardo et al., 2014), the Antilles (e.g., Soufriere Hills, Montserrat, Smith et al., 2007; Cassidy et al., 2014), the Cascades (e.g., Mount St. Helens, Clynne et al., 2008; Mount Rainier, Donoghue et al., 2006), the Kamchatka-Kurile and Aleutians (Prueher & Rea, 2001), Japan (Machida, 1999), and the Mexican Volcanic Belt (e.g., Colima, Arce et al., 2003; Luhr et al., 2010). One exception is the deadly Merapi volcano on Java (e.g., Andreastuti et al., 2000, Newhall et al., 2000; Gertisser & Keller, 2003). Despite studies on single eruptions, there are no tephrastratigraphy studies on the nearby Kelut volcano, which has also caused many fatalities.

Kelut is a dome-complex stratovolcano in East Java, Indonesia (Fig. 1). The first historically recorded eruption occurred in AD 1000 and was followed by a series of 34 eruptions of mostly VEI (Volcanic Explosivity Index) 3 to 4, subplinian to plinian eruptions (Table 1; Zen and Hadikusumo, 1965; Pratomo, 1992; De Bélizal et al., 2012; GVP, 2014b). Details on individual eruptions from AD 1000 to 1967 (listed in Table 1) are based on historical observational reports from direct eyewitness accounts of the eruptions, and so the estimations of each VEI given are based on these accounts (Pratomo, 1992 and references within; De Bélizal et al., 2012 and references within). Eyewitness accounts during this period are likely the most reliable source of information due to the lack of volcano monitoring equipment at the time. The VEI of the 1990, 2007-2008 and 2014 eruptions are based on the measured bulk deposit volumes from each eruption (GVP, 2014b).

The largest VEI 5 eruption took place in 1586. Before this date, all 11 eruptions were estimated at VEI 3 (see Table 1 and references within). Following 1586, another two large VEI 4 eruption occurred in 1641 and 1826, along with 10 VEI 2 and 3 eruptions. In recent times (post-1919) there was a periodic repeated pattern of lava dome-forming eruptions (VEI 2), alternating with explosive VEI 4 plinian eruptions (Zen and Hadikusumo, 1965; Pratomo, 1992; De Bélizal et al., 2012; GVP, 2014b). At the onset of most eruption (both plinian and dome forming) episodes phreatomagmatic or phreatic events occurred, likely due to the common presence of Kelut's crater lake. The most recent and best-studied eruptions in 1990, 2007-2008 and 2014 follow this pattern (Table 1; Chapter 2, Bourdier et al., 1997; GVP, 2008; Jeffery et al., 2013; GVP, 2014). The 1990 and 2014 eruptions were very similar in eruptive style (both VEI 4), destroying a pre-existing lava-dome, and producing localised pyroclastic density currents (PDC) and pumice rich tephra fall deposits (Chapter 2; Bourdier et al., 1997). The 2014 eruption completely excavated the 3.5×10^7 m³ in volume 2007-2008 lava dome, and widened the crater area (Jeffery et al., 2013; GVP, 2014). There is little detail known on the eruptive style, composition and scale of older eruptions at Kelut, limiting the comprehensiveness of hazard assessments.

Constructing detailed records of volcanic activity combined with geochronology and geochemistry can provide insights into the processes that prime and trigger eruptions. They can

Table 1: Known eruptive history of Kelut volcano, with details of individual eruptions

Eruption Year	Eruption	VEI	Volume (km ³)	Deposits/Hazards	Fatalities	Composition	Reference
1000	P-exp; exp	3		Lh, Tf			1, 2 (and references within), 3
1311	P-exp; exp	3		Lh	Reported		1, 3
1334	P-exp; exp	3		Lh, Tf			1, 2 (and references within), 3
1376	P-exp; exp; D	3					1
1385	P-exp; exp	3		Lh	Reported		1
1395	P-exp; exp	3					1
1411	P-exp; exp	3					1
1451	P-exp; exp	3					1
1462	P-exp; exp	3					1
1481	P-exp; exp	3					1
1548	P-exp; exp	3		Lh			1
1586	P-exp; exp	5	0.4	Lh	~ 10,000		1, 2 (and references within), 3, 8
1641	P-exp; exp	4	0.22		reported		1, 8
1716	P-exp; exp	2			Reported		1, 3
1752	P-exp; exp	2					1, 2 (and references within)
1771	P-exp; exp	2		Tf			1, 2 (and references within), 3
1776	P-exp; exp	2					1
1785	P-exp; exp	2					1
1811	P-exp; exp	2		Tf			1, 3
1825	P-exp; exp	2		Lh			1, 3
1826	P-exp; exp	4	0.22	PDC, Tf, Lh	Reported		1, 2 (and references within), 3, 8
1835	P-exp; exp	2		Lh			1, 3
1848	P-exp; exp	3		Lh	Reported		1, 3
1851	P-exp; exp	2		Lh			1
1864	P-exp; exp	2		Lh			1, 2 (and references within), 5 (and references within)
1901	P-exp; exp	3	0.2	PDC, Tf, Lh	Reported		1, 2 (and references within), 3, 5 (and references within), 8, 9
1919	P-exp; exp	4	0.1	Tf, Lh, PDC	5110		1, 2 (and references within), 3, 5 (and references within), 8, 9
1920	P-exp; exp; D	2		No substantial deposits			1, 3
1951	P-exp; exp; D-d	4	0.1	Tf, PDC, Lh	7		1, 2 (and references within), 3, 5 (and references within), 8
1966	P-exp; exp	4	0.09	Tf, Lh, PDC	211		2 (and references within), 3, 5 (and references within), 8, 9
1967	D	1		No substantial deposits			3
1967	?	1		No substantial deposits			8
1990	P-exp; exp (plinian); D-d	4	0.13	Tf, PDC, Lh	32	Basaltic andesite	2 (and references within), 3, 5 (and references within), 7, 8
2007-2008	D	2	0.035	Some dome remnants		Basaltic andesite	3, 4, 5 (and references within), 6, 7, 8
2014	P-exp; exp (plinian); D-d	4	0.1	Tf, PDC, Lh	7	Basaltic andesite	8, 9, 10

Code for eruptions: P-exp: initial phreatomagmatic eruption; exp: explosive eruption at central crater; D: dome extrusion; D-d: destruction of dome

Code for deposits: Tf: tephra fall; PDC: pyroclastic density current; Lh: lahar.

All Volcanic Explosivity Indices (VEI's) from GVP (2014a).

References: 1: Zen and Hadikusumo, 1965; 2: Pratomo, 1992; 3: Bourdier et al., 1997; 4: GVP, 2008; 5: De B  lizar et al., 2012; 6: GVP, 2012; 7: Jeffery et al., 2013; 8: GVP, 2014b; 9: VSI, 2014; 10: Kristiansen et al., 2015

Eruptions highlighted in grey are those of VEI 4 or greater.

also help to understand broader magma system properties that influence the style, magnitude and duration of eruptions, such as the viscosity and gas content of the magmas. Such studies are reported here in order to help improve our understanding of the variety and scale of Kelut's earlier volcanism. This assessment is vital to better mitigate against the devastating effects that large eruptions pose to society. Here we integrate historical evidence with new radiocarbon dating and examination of tephra sections, to present new evidence of the variety and rates of volcanism at Kelut, and the possible magma-system drivers behind it. This study provides the first long-term view into the geochemical and volcanological evolution of Kelut volcano from ~AD 560 until present.

3.3 Methodology

To investigate the eruptive history of Kelut, stratigraphic sections were examined alongside roads and river valleys, mainly on the volcanic flanks west (downwind) of the vent area. The stratigraphic sections were logged in the field (see Fig. 1 for localities), where detail was noted on sedimentary bedding structures, contact relationships, bed thickness, deposit grain size and sorting, along with contacts and evidence for weathering/time breaks. A total of 120 tephra samples were collected across four stratigraphic sections (Table 2), with 37 samples sub-selected for geochemical analysis (highlighted in Table 2) and charcoal for radiocarbon dating. Geochemical samples were selected where possible to analyse one sample/unit from each tephra package. Tephra package here refers to a single unit or layer, or multiple units or layers across a time period (series of layers), separated by distinctive evidence of time breaks indicated by weathered horizons or soil/paleosols units (see Fig. 2). Unit or layer refers to the individual tephra layers within a given tephra package, and their facies is determined by the architectural description of each unit or layer (see Table 4, and Appendix A Supplementary Figs. 1 to 4). Correlation of units across different locations were based on their facies architecture and stratigraphy, hand-over-hand mapping, and geochemical signatures. Distinctive features of tephras enabled some to be used as marker layers e.g., those containing accretionary lapilli, or distinctive pumice or lithic clast types. Where no charcoal was found, the relative timing of events was related to dated horizons and correlated to the historic records of volcanism.

Samples were cleaned in de-ionised (DI) water, dried and dry-sieved. The 125 – 250 μm grain size fraction for each sample was separated and prepared for grain mounts according to the methods of Lowe (2011) to retrieve glass shards, then injected with epoxy resin and polished to ensure flat surfaces for Electron Microprobe analyses (EMPA). Major element concentrations of glass shards were analysed using a JEOL JXA-8230 SuperProbe Electron Probe Microanalyser at the University of Victoria, Wellington, New Zealand. Analyses were run with a beam voltage of 15 Kv and beam current of 8 nA using a defocused beam of 5 – 10 μm size to minimise alkali loss (larger beam sizes could not be used due to microlite density and thin bubble walls). Count times of all elements apart from Na were 30 s on-peak and 15 s off-peak. Na was run at 5 s on-peak and 5

Table 2: Deposit type listed with location, sample number, lithofacies code and charcoal or known eruption dates.

Section	Tephra Package Number	Sample/ unit number	Latitude (°S), Longitude (°E)	Distance from vent (km)	Direction from vent	Sample type	Radiocarbon Age (BP)	Calibrated Age (AD)
1	TP1	K1	7° 56' 18.12", 112° 16' 38.15"	2.97	W	Charcoal	1008 ± 20	1012 ± 10
1	TP1	K2	7° 56' 18.12", 112° 16' 38.15"	2.97	W	PDC		
1	TP1	K3	7° 56' 18.12", 112° 16' 38.15"	2.97	W	PDC		
1	TP2	K4	7° 56' 18.12", 112° 16' 38.15"	2.97	W	Tephra Fall		
1	TP2	K5	7° 56' 18.12", 112° 16' 38.15"	2.97	W	PDC		
1	TP2	K6	7° 56' 18.12", 112° 16' 38.15"	2.97	W	PDC		
1	TP3	K7	7° 56' 18.12", 112° 16' 38.15"	2.97	W	Tephra Fall		
1	TP4	K8	7° 56' 18.12", 112° 16' 38.15"	2.97	W	Tephra Fall		
1	TP4	K9	7° 56' 18.12", 112° 16' 38.15"	2.97	W	PDC		
1	TP5	K10	7° 56' 8.74", 112° 16' 59.38"	2.38	W	Tephra Fall		
1	TP5	K11	7° 56' 8.74", 112° 16' 59.38"	2.38	W	Tephra Fall		
1	TP6	K12	7° 56' 8.74", 112° 16' 59.38"	2.38	W	Tephra Fall		
1	TP7	K13	7° 56' 8.74", 112° 16' 59.38"	2.38	W	Charcoal	185 ± 20	1799 ± 126
1	TP7	K14	7° 56' 8.74", 112° 16' 59.38"	2.38	W	Tephra Fall		
1	TP7	K15	7° 56' 8.74", 112° 16' 59.38"	2.38	W	Charcoal	228 ± 20	1719 ± 69
1	TP7	K16	7° 56' 8.74", 112° 16' 59.38"	2.38	W	PDC		
1	TP7	K17	7° 56' 8.74", 112° 16' 59.38"	2.38	W	PDC		
1	TP7	K18	7° 56' 8.74", 112° 16' 59.38"	2.38	W	PDC		
1	TP7	K19	7° 56' 8.74", 112° 16' 59.38"	2.38	W	Charcoal	223 ± 20	1720 ± 68
1	TP7	K20	7° 56' 8.74", 112° 16' 59.38"	2.38	W	PDC		
1	TP7	K21	7° 56' 8.74", 112° 16' 59.38"	2.38	W	PDC		
1	TP7	K22	7° 56' 8.74", 112° 16' 59.38"	2.38	W	Charcoal	210 ± 20	1726 ± 67
1	TP8	K23	7° 56' 8.74", 112° 16' 59.38"	2.38	W	PDC		
1	TP8	K24	7° 56' 8.74", 112° 16' 59.38"	2.38	W	PDC		
1	TP9	K25	7° 56' 9.46", 112° 16' 57.85"	2.33	W	Tephra Fall		
1	TP10	K26	7° 56' 9.46", 112° 16' 57.85"	2.33	W	PDC		
1	TP10	K27	7° 56' 9.46", 112° 16' 57.85"	2.33	W	PDC		
1	TP11	K28	7° 56' 9.46", 112° 16' 57.85"	2.33	W	Tephra Fall		
1	TP11	K29	7° 56' 9.46", 112° 16' 57.85"	2.33	W	PDC		
1	TP11	K30	7° 56' 9.46", 112° 16' 57.85"	2.33	W	PDC		
1	TP12	K31	7° 56' 9.65", 112° 16' 57.92"	2.33	W	PDC		1990
1	TP12	K32	7° 56' 9.65", 112° 16' 57.92"	2.33	W	PDC		1990
1	TP12	K33	7° 56' 9.65", 112° 16' 57.92"	2.33	W	PDC		1990
1	TP12	K34	7° 56' 9.65", 112° 16' 57.92"	2.33	W	Tephra Fall		1990
1	TP13	K35	7° 56' 9.65", 112° 16' 57.92"	2.33	W	Tephra Fall		2014
2	TP11	K47	7° 56' 10.33", 112° 16' 9.52"	3.82	W	PDC		
2	TP12	K48	7° 56' 10.33", 112° 16' 9.52"	3.82	W	PDC		
2	TP13	K49	7° 56' 10.33", 112° 16' 9.52"	3.82	W	Tephra Fall		
2	TP14	K50	7° 56' 10.33", 112° 16' 9.52"	3.82	W	PDC		
2	TP14	K51	7° 56' 10.33", 112° 16' 9.52"	3.82	W	Tephra Fall		
2	TP14	K52	7° 56' 10.33", 112° 16' 9.52"	3.82	W	Tephra Fall		
2	TP15	K53	7° 56' 10.33", 112° 16' 9.52"	3.82	W	PDC		
2	TP15	K54	7° 56' 10.33", 112° 16' 9.52"	3.82	W	Tephra Fall		
2	TP15	K55	7° 56' 10.33", 112° 16' 9.52"	3.82	W	PDC		
2	TP16	K56	7° 56' 10.33", 112° 16' 9.52"	3.82	W	PDC		
2	TP16	K57	7° 56' 10.33", 112° 16' 9.52"	3.82	W	PDC		
2	TP17	K58	7° 56' 10.33", 112° 16' 9.52"	3.82	W	Tephra Fall		1990
2	TP17	K59	7° 56' 10.33", 112° 16' 9.52"	3.82	W	Tephra Fall		1990
2	TP18	K62	7° 56' 10.33", 112° 16' 9.52"	3.82	W	Tephra Fall		2014
2	TP10	K63	7° 56' 10.33", 112° 16' 9.52"	3.82	W	Tephra Fall		
2	TP10	K64	7° 56' 10.33", 112° 16' 9.52"	3.82	W	Tephra Fall		
2	TP10	K65	7° 56' 10.33", 112° 16' 9.52"	3.82	W	Tephra Fall		
2	TP9	K66	7° 56' 10.33", 112° 16' 9.52"	3.82	W	Tephra Fall		
2	TP8	K67	7° 56' 10.33", 112° 16' 9.52"	3.82	W	PDC		
2	TP7	K68	7° 56' 10.33", 112° 16' 9.52"	3.82	W	PDC		
2	TP6	K69	7° 56' 10.33", 112° 16' 9.52"	3.82	W	PDC		
2	TP5	K70	7° 56' 10.33", 112° 16' 9.52"	3.82	W	PDC		
2	TP4	K71	7° 56' 10.33", 112° 16' 9.52"	3.82	W	PDC		
2	TP3	K72	7° 56' 10.33", 112° 16' 9.52"	3.82	W	PDC		
2	TP2	K73	7° 56' 10.33", 112° 16' 9.52"	3.82	W	PDC		
2	TP1	K74	7° 56' 10.33", 112° 16' 9.52"	3.82	W	PDC		

Dates of charcoal in **red** are those with a large error (over 100 years). Samples highlighted in grey are those sub-selected for EMPA of glass shards.

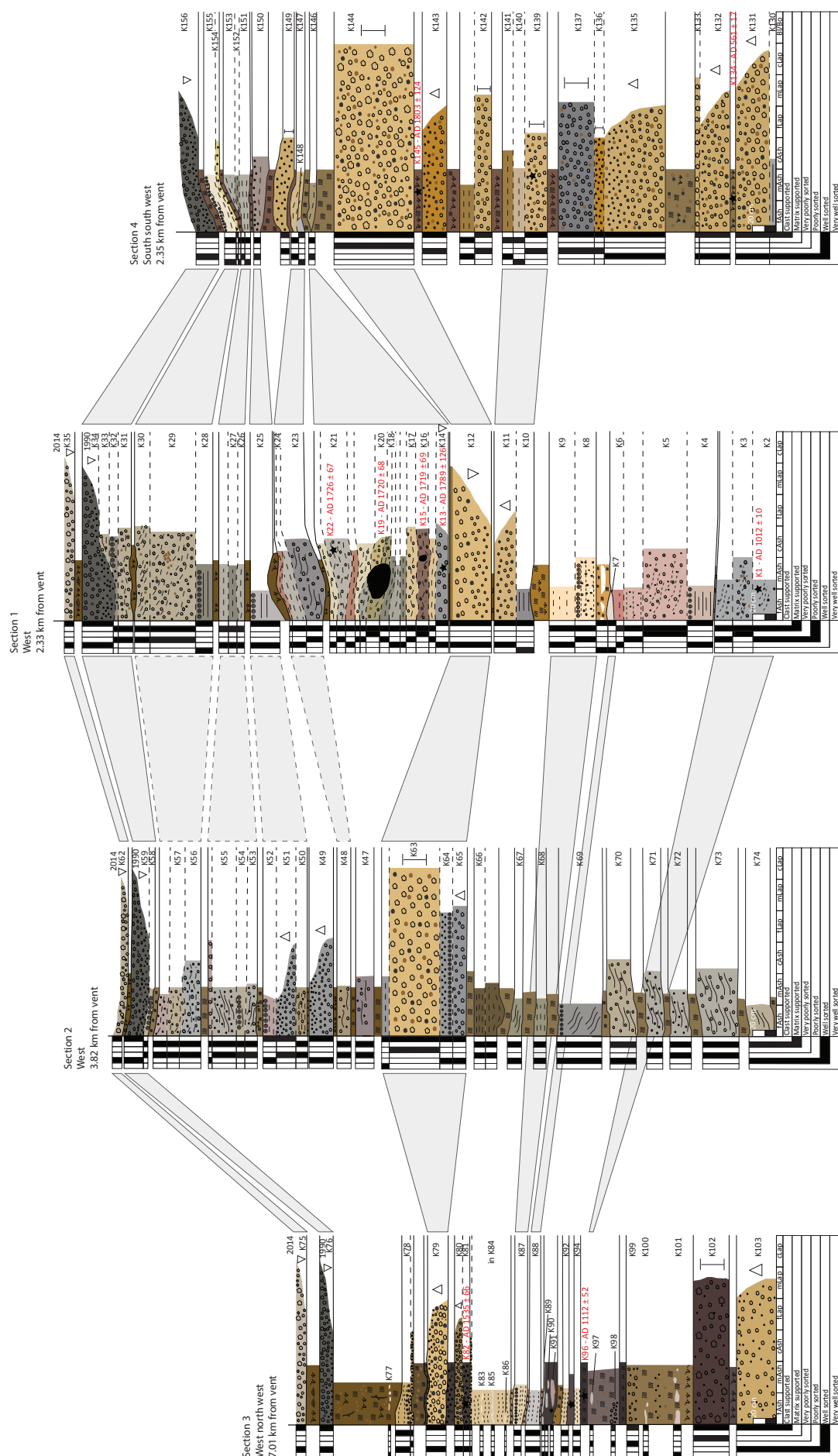
Table 2 continued

Section	Tephra Package Number	Sample/ unit number	Latitude (°S), Longitude (°E)	Distance from vent (km)	Direction from vent	Sample type	Radiocarbon Age (BP)	Calibrated Age (AD)
3	TP19	K75	7° 55' 36.28" , 112° 14' 30.18"	7.01	WNW	Tephra Fall		2014
3	TP18	K76	7° 55' 36.28" , 112° 14' 30.18"	7.01	WNW	Tephra Fall		1990
3	TP17	K77	7° 55' 36.28" , 112° 14' 30.18"	7.01	WNW	Tephra Fall		
3	TP16	K78	7° 55' 36.28" , 112° 14' 30.18"	7.01	WNW	PDC		
3	TP15	K79	7° 55' 36.28" , 112° 14' 30.18"	7.01	WNW	Tephra Fall		
3	TP14	K80	7° 55' 36.28" , 112° 14' 30.18"	7.01	WNW	Tephra Fall		
3	TP14	K81	7° 55' 36.28" , 112° 14' 30.18"	7.01	WNW	Tephra Fall		
3	TP14	K82	7° 55' 36.28" , 112° 14' 30.18"	7.01	WNW	Charcoal	369 ± 23	1535 ± 66
3	TP13	K83	7° 55' 36.28" , 112° 14' 30.18"	7.01	WNW	Tephra Fall		
3	TP13	K84	7° 55' 36.28" , 112° 14' 30.18"	7.01	WNW	PDC		
3	TP13	K85	7° 55' 36.28" , 112° 14' 30.18"	7.01	WNW	Tephra Fall		
3	TP13	K86	7° 55' 36.28" , 112° 14' 30.18"	7.01	WNW	Tephra Fall		
3	TP12	K87	7° 55' 36.28" , 112° 14' 30.18"	7.01	WNW	PDC		
3	TP11	K88	7° 55' 36.28" , 112° 14' 30.18"	7.01	WNW	Tephra Fall		
3	TP10	K89	7° 55' 36.28" , 112° 14' 30.18"	7.01	WNW	Tephra Fall		
3	TP10	K90	7° 55' 36.28" , 112° 14' 30.18"	7.01	WNW	Tephra Fall		
3	TP10	K91	7° 55' 36.28" , 112° 14' 30.18"	7.01	WNW	Tephra Fall		
3	TP9	K92	7° 55' 36.28" , 112° 14' 30.18"	7.01	WNW	PDC		
3	TP10	K93	7° 55' 36.28" , 112° 14' 30.18"	7.01	WNW	Charcoal		
3	TP8	K94	7° 55' 36.28" , 112° 14' 30.18"	7.01	WNW	PDC		
3	TP8	K95	7° 55' 36.28" , 112° 14' 30.18"	7.01	WNW	Charcoal		
3	TP7	K96	7° 55' 36.28" , 112° 14' 30.18"	7.01	WNW	Charcoal	898 ± 22	1112 ± 52
3	TP7	K97	7° 55' 36.28" , 112° 14' 30.18"	7.01	WNW	Tephra Fall		
3	TP6	K98	7° 55' 36.28" , 112° 14' 30.18"	7.01	WNW	Tephra Fall		
3	TP5	K99	7° 55' 36.28" , 112° 14' 30.18"	7.01	WNW	Tephra Fall		
3	TP4	K100	7° 55' 36.28" , 112° 14' 30.18"	7.01	WNW	Tephra Fall		
3	TP3	K101	7° 55' 36.28" , 112° 14' 30.18"	7.01	WNW	Tephra Fall		
3	TP2	K102	7° 55' 36.28" , 112° 14' 30.18"	7.01	WNW	Tephra Fall		
3	TP1	K103	7° 55' 36.28" , 112° 14' 30.18"	7.01	WNW	Tephra Fall		
3	TP1	K104	7° 55' 36.28" , 112° 14' 30.18"	7.01	WNW	Charcoal		
4	TP1	K130	7° 57' 22.08" , 112° 17' 34.62"	2.35	SSW	Tephra Fall		
4	TP1	K131	7° 57' 22.08" , 112° 17' 34.62"	2.35	SSW	Tephra Fall		
4	TP2	K132	7° 57' 22.08" , 112° 17' 34.62"	2.35	SSW	Tephra Fall		
4	TP2	K133	7° 57' 22.08" , 112° 17' 34.62"	2.35	SSW	Tephra Fall		
4	TP2	K134	7° 57' 22.08" , 112° 17' 34.62"	2.35	SSW	Charcoal	1510 ± 10	561 ± 17
4	TP3	K135	7° 57' 22.08" , 112° 17' 34.62"	2.35	SSW	Tephra Fall		
4	TP3	K136	7° 57' 22.08" , 112° 17' 34.62"	2.35	SSW	Tephra Fall		
4	TP3	K137	7° 57' 22.08" , 112° 17' 34.62"	2.35	SSW	Tephra Fall		
4	TP4	K138	7° 57' 22.08" , 112° 17' 34.62"	2.35	SSW	Charcoal		
4	TP4	K139	7° 57' 22.08" , 112° 17' 34.62"	2.35	SSW	Tephra Fall		
4	TP4	K140	7° 57' 22.08" , 112° 17' 34.62"	2.35	SSW	PDC		
4	TP4	K141	7° 57' 22.08" , 112° 17' 34.62"	2.35	SSW	PDC		
4	TP5	K142	7° 57' 22.08" , 112° 17' 34.62"	2.35	SSW	Tephra Fall		
4	TP6	K143	7° 57' 22.08" , 112° 17' 34.62"	2.35	SSW	Tephra Fall		
4	TP7	K144	7° 57' 22.08" , 112° 17' 34.62"	2.35	SSW	Tephra Fall		
4	TP7	K145	7° 57' 22.08" , 112° 17' 34.62"	2.35	SSW	Charcoal	174 ± 20	1803 ± 124
4	TP8	K146	7° 57' 22.08" , 112° 17' 34.62"	2.35	SSW	PDC		
4	TP9	K147	7° 57' 22.08" , 112° 17' 34.62"	2.35	SSW	PDC		
4	TP9	K148	7° 57' 22.08" , 112° 17' 34.62"	2.35	SSW	Tephra Fall		
4	TP10	K149	7° 57' 22.08" , 112° 17' 34.62"	2.35	SSW	PDC		
4	TP11	K150	7° 57' 22.08" , 112° 17' 34.62"	2.35	SSW	PDC		
4	TP12	K151	7° 57' 22.08" , 112° 17' 34.62"	2.35	SSW	PDC		
4	TP12	K152	7° 57' 22.08" , 112° 17' 34.62"	2.35	SSW	PDC		
4	TP12	K153	7° 57' 22.08" , 112° 17' 34.62"	2.35	SSW	PDC		
4	TP13	K154	7° 57' 22.08" , 112° 17' 34.62"	2.35	SSW	PDC		
4	TP13	K155	7° 57' 22.08" , 112° 17' 34.62"	2.35	SSW	PDC		
4	TP14	K156	7° 57' 22.08" , 112° 17' 34.62"	2.35	SSW	Tephra Fall		1990

Dates of charcoal in red are those with a large error (over 100 years). Samples highlighted in grey are those sub-selected for EMPA of glass shards.

s off-peak, with a pre-defined peak position to negate the effects of drift. Analyses were calibrated to internal mineral standards, with rhyolite and basalt glass standards run after every group of 25 analyses.

Organic material was sent to the Waikato Radiocarbon Dating Laboratory (WRDL) at the University of Waikato, New Zealand, where samples were cleaned and chemically pre-treated. Of 13 charcoal samples sent, 4 were abandoned due to too little material to obtain an accurate



KEY

Contacts:

- Regionally exposed, major discontinuities limiting separate and distinctive eruptions
- Locally exposed, minor discontinuities, separating eruptive phases/pulses in same eruption

Structures/Depositional features:

- Low Angle
- Prismatic/laminated
- Irregular/poor
- Absent/Massive (note: dashed line - not so distinct)

K1 - sample code

Red/charcoal age of charcoal

Grading:

- Normal Grading
- Reverse Grading

Other Features:

- Accretionary Lapilli
- Charcoal
- Charred log
- Roots/Twigs
- Leaf
- Loamy Paleosol

Componentry:

- Pumice
- Lithics
- Non juvenile/accidental lithics
- Scoria

Figure 2 (opposite): Correlations across stratigraphic sections from Kelut volcano, with the direction and distance of the sections from the vent indicated. Colours of units represent true colour as seen in the field. Sections are arranged with increasing distance from the vent, the volcano lies between sections 1 and 4. Locations refer to those on Figure 1. Correlations are shown by grey filled boxes with solid outlines. Grey boxes with dashed outlines are estimated correlations. Blacked out boxes on the left of each section denote the sorting (very well to very poorly), and whether the sample is clast- or matrix-supported. Grain size scale is: fAsh: fine ash, 63–250 μm ; mAsh: medium ash, 250–500 μm ; cAsh: coarse ash, 500 μm – 2 mm; fLap: fine lapilli, 2–4 mm; mLap: medium lapilli, 4–16 mm; cLap: coarse lapilli, 16–64 mm; Bl/Bo: block/bomb, >64 mm. Refer to Key for more details.

date. The Carbon-13 stable isotope value was measured using an Accelerator Mass Spectrometer (AMS) using appropriate charcoal modern, background and continuity standards, then corrected and reported as a conventional age (BP), with an error of 1 standard deviation. Uncertainties on the reported conventional age are included in Table 2, and are based on the counting and normalisation of primary standards and statistics, the background measurements, and scatter on repeated runs on the sample (WRDL, 2017). Conventional ages were then recalculated to calendar age (AD) using the CalPal Online Radiocarbon Calibration software by the University of Cologne, Germany (Table 2).

3.4 Results

3.4.1 Stratigraphy

The overall stratigraphy of correlated volcanic deposits and dated charcoal is presented in Figure 2 and Table 2, with key field photos in Figure 3. Detailed diagrams with section descriptions are presented in Supplementary Materials Appendix A (Supplementary Figs. 1–4).

The most well preserved stratigraphic sections were found to the west and south-west of the vent alongside river valleys (see localities in Fig. 1). Tephra layers were thinner and more strongly weathered east of the vent. Section 1 is proximal to the vent alongside a road cutting parallel to the river “Kali” Sumberagung (Fig. 2; Fig. 3a–c). This is a section of the best preserved, series of discrete units of multiple (without paleosols between) poorly sorted, lithic- and pumice-rich lapilli rich matrix-supported deposits (e.g., K16 – K21; Fig. 3b), with few well sorted pumice-rich, clast-supported lapilli deposits (e.g. K12; Supplementary Fig. 1). Radiocarbon dates on charcoal within the tephra units indicate this section spans from AD 1012 ± 10 to 2014. The base of section 2 (Fig. 2, 3d; Supplementary Fig. 2) (below K66) is made up of a series of weathered, well-laminated, poorly sorted, matrix-supported, fine- to coarse-ash units, separated by ash-rich paleosols (Fig. 3d). The upper part of section 2 comprises a series of clast-supported, coarse-ash to coarse-lapilli layers, alternating with poorly sorted, matrix-supported units with scoria, pumice and lithic lapilli. These layers are readily correlated across to other sections due to distinct features such as accretionary lapilli, and dominance of pumice or scoria (Figs. 2 and 3e–f). Section 3 is the farthest from the source, and comprises discontinuous ash lenses and layers intercalated by weathered ash-rich paleosols (Fig. 3g). This site contains a few key identifiable scoria and pumice lapilli clast-supported layers, (e.g., K103, K102, K79; Fig. 3h) and some poorly laminated, fine-grained matrix-supported units (e.g. K94; Fig. 3j). At section 3, radiocarbon ages indicate oldest

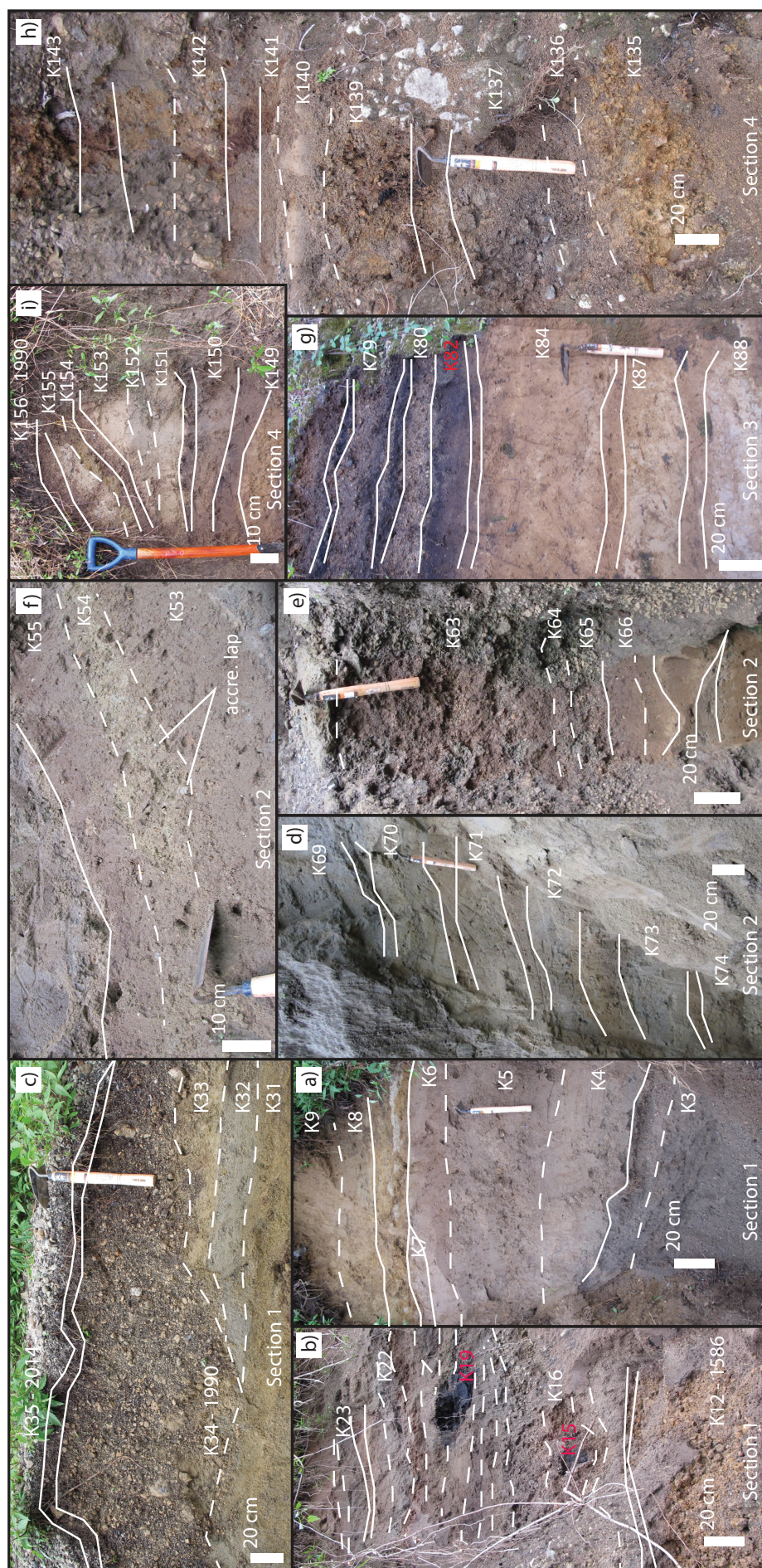


Figure 3: Photos from the field of stratigraphic deposits. Taken in April 2014. a) Oldest, lower deposits from section 1. b) 1586 and 1700s eruption series of deposits from section 1. c) Top 1990 and 2014 eruptive deposits from section 1. d) Lower most deposits from section 2. e) 1586 massive tephra with units below from Section 2. f) Upper deposits from section 2 showing accretionary lapilli. g) Part of the most well preserved parts of section 3, including several charcoal stained soils. h) Section 4 tephra deposits from the south. i) Upper, thin deposits from section 4.

Supplementary figures provided in Appendix A, and table in Electronic Appendix B

units are $>AD\ 1112 \pm 52$ (Supplementary Fig. 3). Section 4 is the most proximal site, alongside the upper Kali Putih (Fig. 1), and is dominated by large, massive clast-supported, pumice-rich, fine-lapilli to block clast sized layers (e.g., K131, K135, K144; Fig. 2), separated by distinct weathered ash horizons. This section shows deposits dating from $AD\ 561 \pm 17$ to 1990 (Supplementary Fig. 4). This pre-dates the historic knowledge of activity at Kelut ($AD\ 1000$; Table 1).

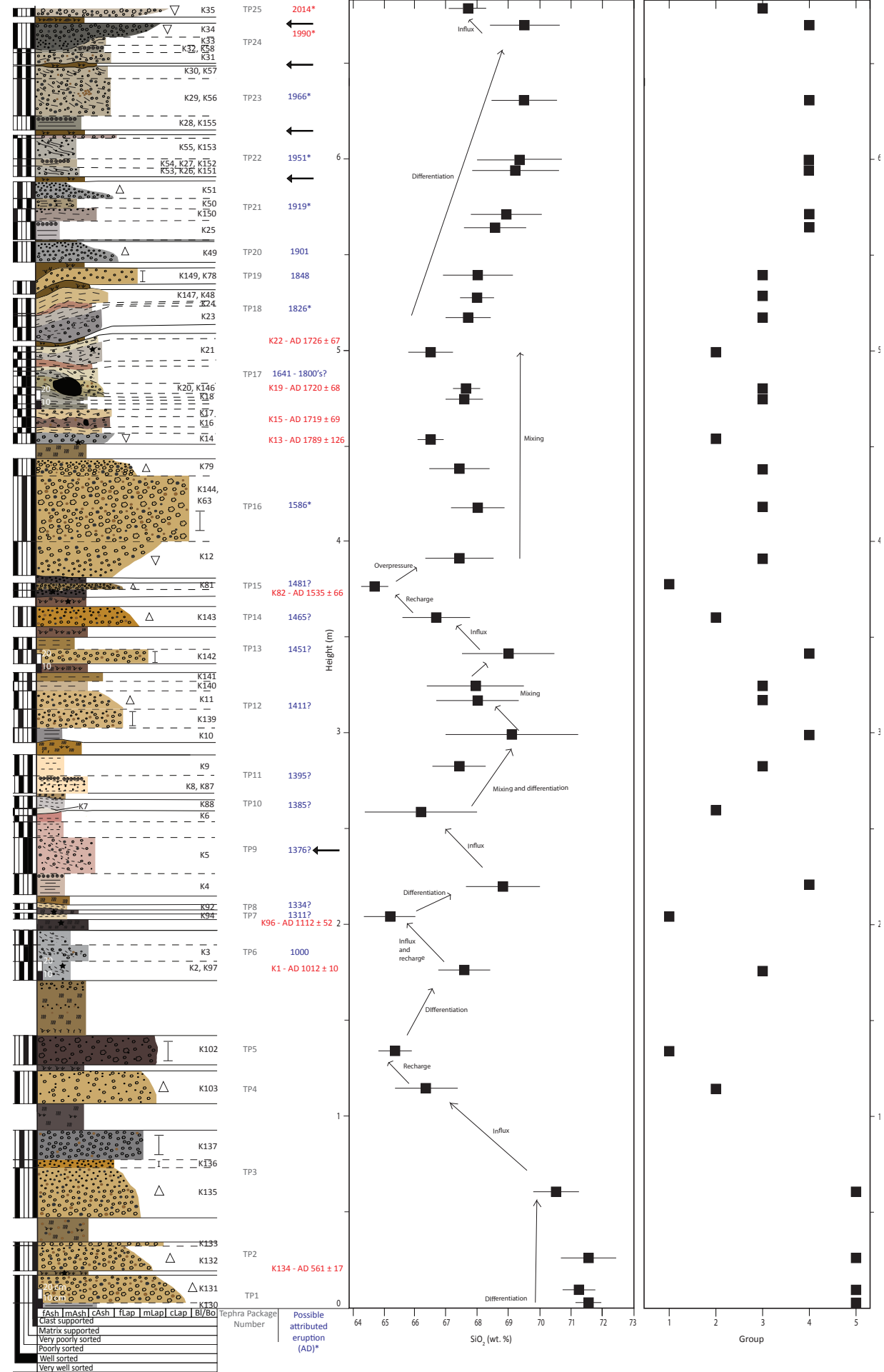
Spatial correlations of units/layers across the four sections were possible using distinctive marker layer features and radiocarbon dates (Fig. 2). From these, a composite master section was developed (Fig. 4). This composite section includes 25 tephra packages. The oldest tephra package (TP1, ~26 cm thick), consists of 2 layers normally graded, predominantly clast-supported pumice- and lithic coarse-lapilli. Charcoal in the <5 cm ashy paleosol between TP1 and TP2 was dated at $AD\ 561 \pm 10$. TP2 also consists of 2 layers, including a 25 cm-thick normally graded, clast-supported, medium- to fine-lapilli, and is capped by a 5 cm pumice-rich, coarse-lapilli layer. A thick weathered ash paleosol (22 cm) indicates a long hiatus in eruptions before TP3 was deposited. TP3 consists of three graded or massive, clast-supported pumice lapilli units, totalling ~75 cm thick. Another significant time break is indicated by a 28 cm paleosol to TP4. TP4 and TP5 (only observed in section 4) are soil separated, single layers of weathered, clast-supported, pumice-rich lapilli separated by soil.

Upwards, the next tephra packages have different characteristics. A thick, (60 cm) weathered ash passes up to a six packages (TP6-11) of matrix-supported lapilli rich layers of varying thickness. The tephra packages are separated by thin ash paleosols, which indicate brief periods of hiatus. Charcoal within the oldest package, TP6, was dated at $AD\ 1012 \pm 10$. The layers in TP6 to TP11 are dominantly matrix-supported dominantly pumice and scoria rich lapilli units in sections 1-2 (e.g., K3, K9), passing to thinner units in the more distal section 3 (Figs. 2 and 4). The thickest tephra package, TP9, comprises a ~58 cm fine- to coarse-ash matrix-supported layers with scoria and pumice lapilli, underlain by an ash deposit rich in accretionary lapilli. The TP6 to TP11 deposits record 6 eruptions between ~ $AD\ 1000$ -1395 (Table 1).

A further transition in deposit character occurs with the next units. TP12 includes a pumice-rich lapilli layer, overlain by two discretely-bedded, ash matrix-supported lapilli layers. TP13 shows a similar sequence as TP12, while TP14 is a more weathered layer of normally graded, clast-supported, pumice and lithic lapilli layer. Charcoal between TP14 and the fine lapilli bed of TP15 is dated at $AD\ 1535 \pm 66$. The TP12 to TP15 packages comprises four separate events separated by soils (Table 1, Fig. 4). Of the 11 VEI 3 eruptive events in written records between $AD\ 1000$ to 1548 (GVP, 2014b; Table 1), all but one are recorded in the deposits in TP6 to 15 (Table 1).

The TP16 package is the most distinctive of the entire section described here, it has 3 layers of yellow-brown, graded or massive, clast-supported pumice lapilli units that are 20 to 60 cm-thick. This deposit is likely attributed to the largest historic eruption recorded at Kelut in 1586,

Chapter Three



Supplementary figures provided in Appendix A,
and table in Electronic Appendix B

Figure 4 (opposite): Composite stratigraphic section determined from correlations made of main events across all sections, determined in Figure 2. Plots show groups determined from Harker plots of glass chemistry (Fig. 6) for each sample, and average SiO_2 (wt %) with standard deviation error bars, both plotted against height in the stratigraphic column (m) to show evolution of glass shard chemistry with time from Figure 7 and Table 3. Deposit codes with interpretation are listed in Table 4. Arrows next to the stratigraphic section indicate when dome-growth has been recorded in the historic records. Possible attributed eruptions with a * by them are coded to mean eruptions of VEI 4 and above. The context of influx, recharge and overpressure are discussed in the text.

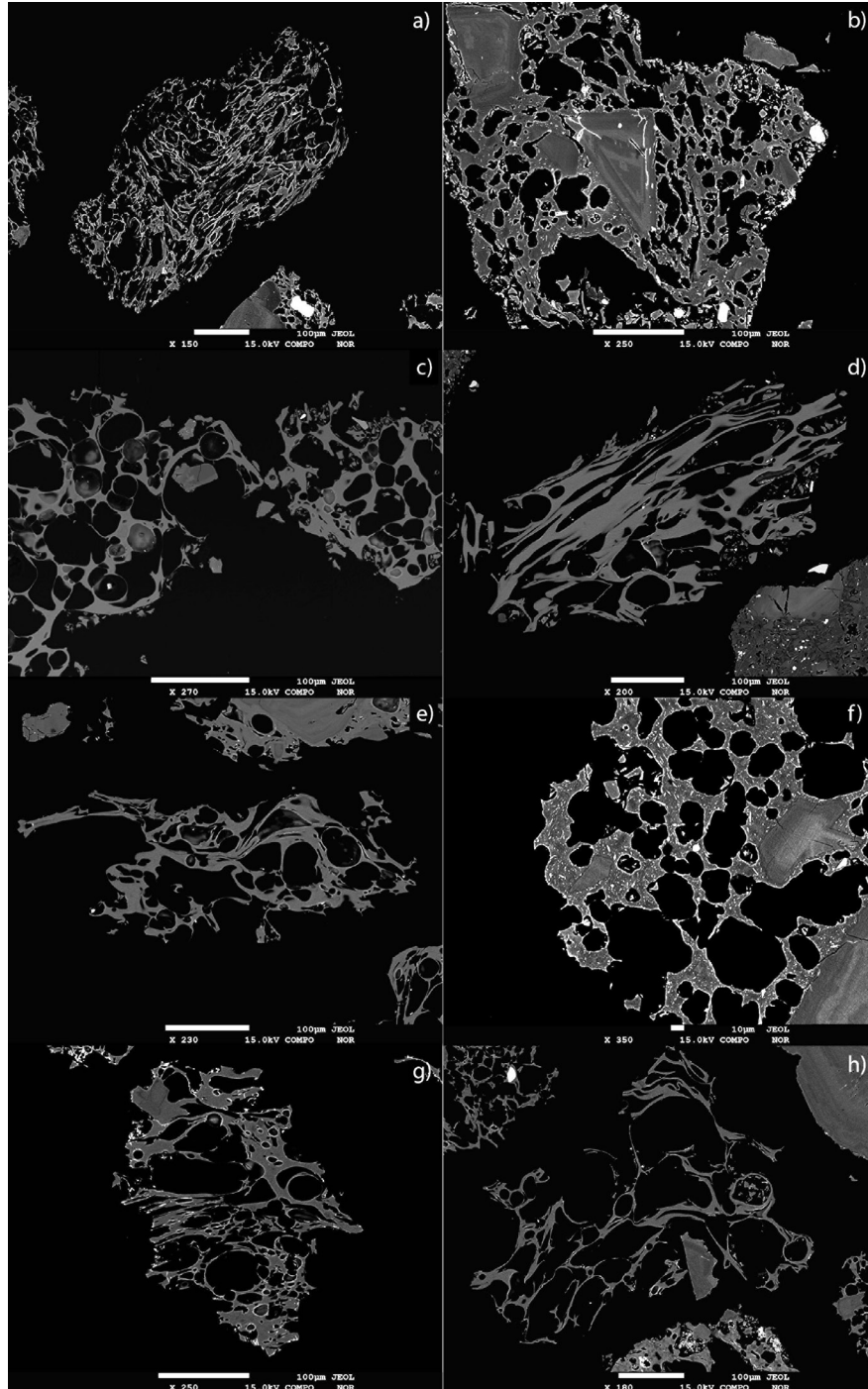


Figure 5: Back-scatter electron (BSE) images of glass shards taken on the EMPA at the University of Victoria, at 15.0kV, see each figure for scale (μm). a) A pumice glass shard with distorted vesicles from K131, ~AD 560 eruption. b) Groundmass glass rich in microlites from sample K152, ~1951 eruption. c) Spherically vesicular, angular clasts from K4 ~1300's eruption. d) Glass shard with elongated and spherical vesicles from sample K144, ~1586 eruption. e) Wipsey, vesicular glass shard with thin bubble walls from K20, ~1700 eruption. f) Very microlite rich groundmass glass and some large plagioclase phenocrysts from sample K34, 1990 eruption. g) Vesicular glass shard from K135 ~AD 700 eruption. h) Wispy vesicular glass shard from K102, ~AD 800 eruption.

which is supported by the radiocarbon ages of charcoal within the unit (Fig. 4; Table 2).

The next set of tephra packages (TP17-21) occur above a ~20 cm-thick weathered, fine ash-rich paleosol (Fig. 4). Charcoal samples within the ~1.2 m series of multiple fine- to coarse-ash matrix-supported units (TP17), were dated at AD 1719 \pm 69 to 1726 \pm 67. TP18 is similar but comprises thinner series of discretely bedded, matrix-supported layers, while TP19 and TP20 stand out as individual clast-supported normally graded or massive pumice and scoria-rich lapilli layers. TP20 possibly correlates to the VEI 4 1826 eruption. Above this, TP21 comprises 4 layers; starting with a well-sorted lapilli bed containing accretionary lapilli, followed by two discretely horizontally bedded, matrix-supported layers, overlain by a normally graded fine-ash to coarse lapilli layer (Fig. 3f). The TP21 complex deposit series indicates a range of different eruptive stages that is consistent with eruptions recorded in either 1901 or 1919 (Table 1).

The next tephra package above, TP22, is distinctive in containing abundant accretionary lapilli within low-angle cross-bedded, matrix-supported layers (Fig. 4). TP23 is similar with a ~55 cm thick package of ash layers containing accretionary lapilli, capped by a pumice-rich matrix-supported unit. These deposits likely correlate with the 1951 or the VEI 4 1966 eruption (GVP, 2014b). The VEI 4 1990 event is represented by the TP24 package of four layers, including a basal lapilli rich matrix-supported unit, ash with accretionary lapilli, capped by <30 cm reversely graded, pumice- lapilli. Above a thin soil, pumice -lapilli deposits from the most recent VEI 4 2014 eruption occur (Fig. 3c).

3.4.2 Clast/pumice morphology

All tephra fall deposits across all tephra packages show a wide range of clast textures (Fig. 5a, b, d and f), including: highly vesicular pumice with thin, stretched bubble walls (e.g. K131; Fig. 5a); moderate vesicularity pumice with isolated spherical vesicles (e.g., K144, K135, K102; Fig. 5d, e, g and h); dense, low-vesicularity glass with blocky and angular forms, rich in phenocrysts of plagioclase and clinopyroxene (and a microlite-rich groundmass (e.g., K131, K135, K34, K35; Fig. 5b, f and h). Zoned plagioclase and clinopyroxene phenocrysts were also present (Fig. 5b, d, e, f, h; K152, K144, K34, K102). Ash particles from matrix-supported deposits have a similar range in morphology. Glassy ash particles (e.g., K4, K25, K28) are predominantly angular and vesicular with distinct vesicle wall textures. Many ash particles have adhering dust of very fine ash in vesicle hollows (Fig. 5c). Ash particles associated with lapilli from matrix-supported deposits include lithic fragments and glass showing angular, broken shapes, but also showing particles with very thin $\leq 5 \mu\text{m}$ bubble walls, and elongated vesicles (e.g., K20, K21, K155; Fig. 5e).

3.4.3 Glass geochemistry

Major element compositions of glass shards from the Kelut tephra deposits (Fig. 6, Table 3; along with Supplementary Table 1) show a range of 63.8 (K81) to 72.7 (K135) wt.% SiO_2 . The most variable SiO_2 compositions occur in samples K10 and K152, with standard deviations of 2.03

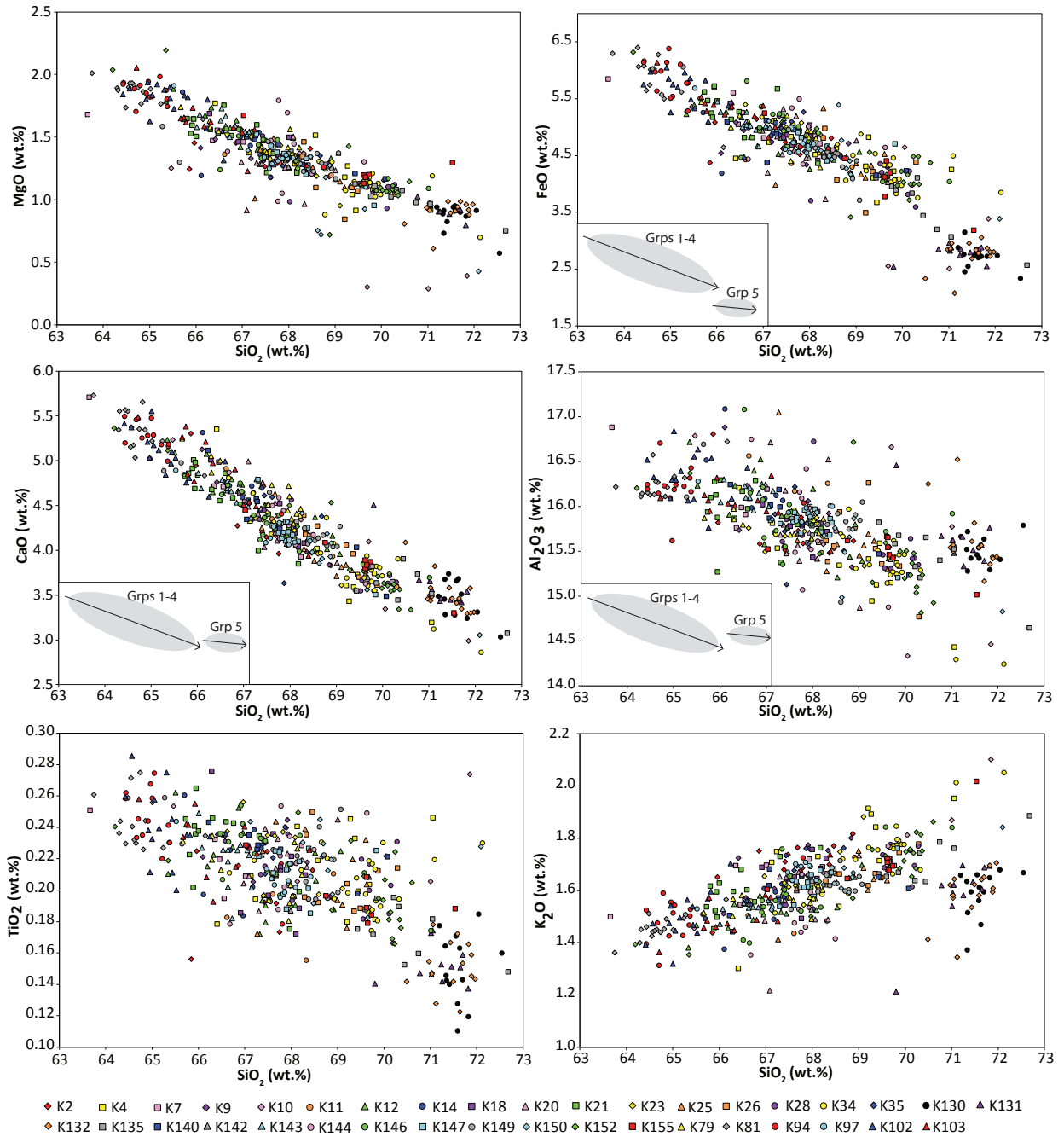


Figure 6: Harker plots of CaO, FeO, MgO, Al_2O_3 , K_2O and total alkali against SiO_2 wt% for sub-selected samples listed in Table 2. Inset on selected plots shows illustrative vectors of proposed magmatic trends (not to scale), for an explanation of Grp – Groups, see Figure 7 and text.

and of 1.78 wt.% respectively. The least variable compositions are in K130 and K81 (standard deviation of <0.53 wt.%). The elements CaO, FeO and MgO show strong negative correlations with SiO_2 , while Al_2O_3 varies very little, and there is a slight positive correlation for K_2O (Figs. 6 and 7).

Using average glass compositions for each unit, five compositional groups are seen (Fig. 7), most distinctly with FeO, MgO and CaO concentrations. Group 1 is the least evolved (64.5–65.4 wt.% SiO_2), while group 5 is the most felsic (70.1–72.5 wt.% SiO_2). The closest-spaced groups are 3 and 4 with some minor overlap (Fig. 7). When examining the chemical groupings over

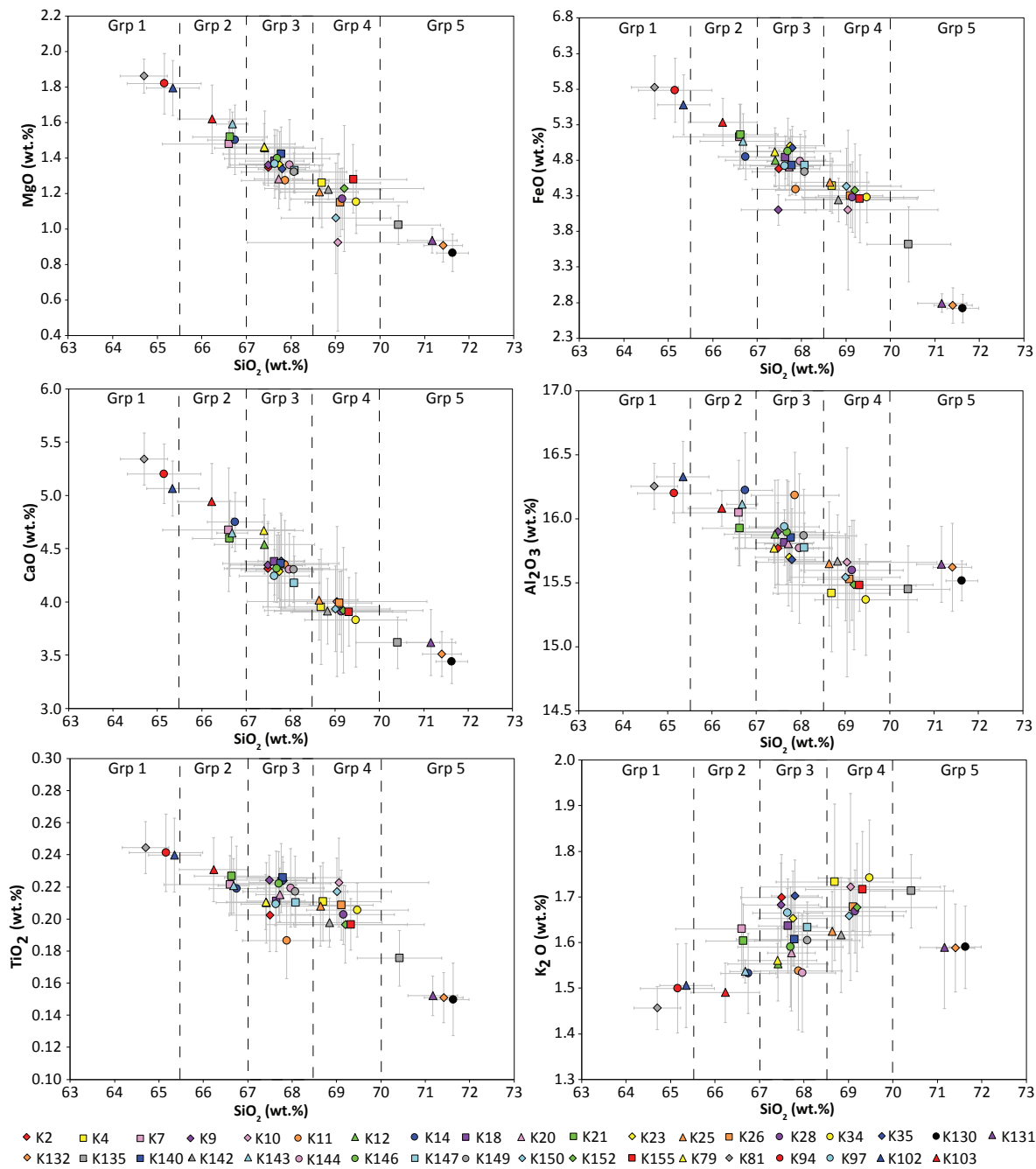


Figure 7: Plots of average CaO, FeO, MgO, Al₂O₃, K₂O and total alkali against SiO₂ wt%, with standard deviation from the mean displayed as grey error bars. Groups (Grp in short) boundaries are shown with dashed vertical lines based on SiO₂ compositions. Group 1 SiO₂ ranges from 64.5 to 65.4 wt% and includes 3 samples (K81, K94, K102). Group 2 has an average SiO₂ range of 65.5 to 67.0 wt% and includes 5 samples (K103, K7, K14, K21 and K143). Group 3 has an average SiO₂ range of 67.1 to 68.5 wt% and includes 16 samples, the most populous group yet (K2, K9, K11, K12, K18, K20, K23, K35, K79, K97, K140, K144, K145, K146 and K147). Group 4 has an average SiO₂ range of 68.6 to 70.0 wt% and includes 10 samples (K4, K10, K25, K26, K28, K34, K142, K150, K152 and K155). The final group SiO₂ compositions range from 70.1 to 72.5 wt% and includes 4 samples (K130, K131, K132 and K135).

time, clear variations are seen, where the eruptives vary irregularly between more felsic or mafic compositions (Figs. 4, 7). TP1 and TP2 show the most evolved compositions (K130, K131 and K132; group 5; Fig. 7). The large TP3 (K135) deposit is slightly less evolved, transitional between groups 4 and 5, but is still in group 5. Above, TP4 (K103) has a very different composition (group

Table 3: Average major element glass shard analysis from EMP. All results are in Weight Percentage Oxide (wt%).

Section 1	Tephra Package #*	CaO	TiO ₂	Na ₂ O	MgO	P ₂ O ₅	SiO ₂	Al ₂ O ₃	K ₂ O	MnO	FeO	Cl	SO ₃	Total
K2	6	4.31	0.20	4.11	1.35	0.11	67.49	15.77	1.70	0.14	4.68	0.15	0.02	100
K4	9	3.95	0.21	3.94	1.26	0.08	68.69	15.42	1.73	0.14	4.44	0.16	0.01	100
K7	10	4.67	0.22	3.82	1.48	0.11	66.61	16.05	1.63	0.14	5.13	0.15	0.02	100
K9	11	4.34	0.22	3.99	1.36	0.10	67.49	15.90	1.68	0.12	4.67	0.15	0.01	100
K10	12	4.00	0.22	3.92	0.93	0.12	69.05	15.66	1.72	0.14	4.10	0.15	0.02	100
K11	12	4.35	0.19	3.86	1.27	0.10	67.87	16.19	1.54	0.13	4.39	0.12	0.02	100
K12	16	4.54	0.21	3.76	1.46	0.09	67.42	15.88	1.55	0.16	4.80	0.14	0.02	100
K14	17	4.75	0.22	3.79	1.50	0.11	66.75	16.22	1.53	0.16	4.85	0.14	0.01	100
K18	17	4.38	0.21	3.75	1.38	0.10	67.64	15.81	1.64	0.11	4.84	0.15	0.02	100
K20	17	4.35	0.22	3.97	1.28	0.10	67.73	15.80	1.58	0.14	4.72	0.14	0.02	100
K21	17	4.59	0.23	3.91	1.52	0.14	66.63	15.93	1.60	0.16	5.16	0.14	0.02	100
K23	18	4.29	0.23	3.61	1.36	0.14	67.75	15.70	1.65	0.14	5.00	0.16	0.01	100
K25	21	4.02	0.21	3.80	1.21	0.10	68.64	15.65	1.62	0.14	4.49	0.14	0.02	100
K26	22	3.99	0.21	3.71	1.15	0.07	69.10	15.53	1.68	0.13	4.30	0.15	0.01	100
K28	23	3.91	0.20	3.69	1.17	0.05	69.15	15.60	1.67	0.14	4.28	0.16	0.01	100
K34	24	3.83	0.21	3.62	1.15	0.05	69.47	15.37	1.74	0.15	4.28	0.16	0.01	100
K35	25	4.38	0.22	3.63	1.34	0.00	67.80	15.67	1.70	0.14	4.98	0.14	0.02	100
Section 4														
K130	1	3.44	0.15	3.84	0.87	0.01	71.63	15.52	1.59	0.13	2.72	0.14	0.00	100
K131	1	3.62	0.15	3.83	0.93	0.00	71.16	15.64	1.59	0.14	2.79	0.16	0.01	100
K132	2	3.51	0.15	3.81	0.91	0.00	71.41	15.62	1.59	0.11	2.76	0.15	0.01	100
K135	3	3.62	0.18	3.70	1.02	0.02	70.42	15.45	1.71	0.13	3.62	0.17	0.01	100
K140	12	4.36	0.23	3.64	1.42	0.11	67.78	15.85	1.61	0.15	4.73	0.15	0.02	100
K142	13	3.91	0.20	3.95	1.22	0.06	68.84	15.67	1.62	0.19	4.24	0.13	0.00	100
K143	14	4.65	0.22	3.73	1.59	0.13	66.68	16.11	1.54	0.16	5.07	0.14	0.01	100
K144	16	4.30	0.22	3.68	1.36	0.12	67.97	15.77	1.53	0.14	4.79	0.14	0.00	100
K146	17	4.31	0.22	3.57	1.40	0.11	67.69	15.90	1.59	0.15	4.92	0.16	0.01	100
K147	18	4.18	0.21	3.68	1.33	0.09	68.08	15.77	1.63	0.16	4.73	0.15	0.02	100
K149	20	4.30	0.22	3.61	1.32	0.09	68.07	15.87	1.60	0.13	4.64	0.16	0.02	100
K150	21	3.93	0.22	3.80	1.06	0.09	69.01	15.54	1.66	0.14	4.43	0.14	0.01	100
K152	22	3.92	0.20	3.56	1.23	0.08	69.20	15.48	1.68	0.16	4.38	0.14	0.01	100
K155	23	3.89	0.20	3.51	1.27	0.06	69.43	15.46	1.72	0.15	4.19	0.14	0.02	100
Section 3														
K79	16	4.67	0.21	3.60	1.46	0.10	67.40	15.77	1.56	0.17	4.92	0.15	0.01	100
K81	15	5.34	0.24	3.83	1.86	0.17	64.70	16.26	1.46	0.16	5.83	0.15	0.05	100
K94	7	5.20	0.24	3.67	1.82	0.14	65.16	16.20	1.50	0.17	5.78	0.14	0.01	100
K97	8	4.24	0.21	3.85	1.37	0.09	67.63	15.94	1.66	0.15	4.72	0.16	0.02	100
K102	5	5.06	0.24	3.73	1.79	0.13	65.35	16.33	1.51	0.17	5.58	0.13	0.01	100
K103	4	4.86	0.23	3.66	1.59	0.12	66.41	16.03	1.51	0.16	5.28	0.16	0.02	100

*Tephra package # refers to those in the Composite stratigraphic section (Fig. 4)

2), while TP5 is even more mafic with a group 1 affinity. There was a long hiatus in activity before TP6 was erupted (K2, K3) with an intermediate composition (group 3). Between \sim AD 1000 to \sim 1535 \pm 66 (TP6 to TP15), large variations in composition occur (Fig. 4), including a rise in SiO₂ content from TP7 (to TP13 (K142), a drop by 2 wt.% SiO₂ to TP14 (K143) and TP15 (K81), before rising again to the large TP16 (AD 1586) deposit (Table 3; Figs. 4, 6 and 7). Above this during a close-spaced series of tephras K14 to K19, variations of only \sim 2 wt.% SiO₂ occur. Following this, TP19 to TP24 (AD 1848-1990) show little variation in glass chemistry, varying by \sim 0.8 wt.% SiO₂. The most recent 2014 eruption had 1.7 wt.% lower SiO₂ concentration than the 1990 event (Figs. 4, 6 and 7).

3.5 Discussion

3.5.1 Eruptive behaviour and magmatic processes

An interpretation of emplacement mechanism is based on deposit character, including matrix vs clast-support, degree of sorting, bedding, grading, and lithology (e.g., pumice, dense lapilli (magmatic origin), accidental/non-magmatic lapilli). This information was combined with the historical eruptive records to interpret eruptive style (included in Table 4), and temporal compositional variations over time (Figs. 4, 6, and 7). This has been used to further interpret changes in the physical conditions governing the generation and evolution of magma batches (Fig. 8).

Chapter Three

Table 4: Summary table including descriptions of units and facies, and subsequent interpretation of eruption style with each tephra package and eruption date or time period. Continued overleaf

Time Period (AD)*	Tephra Package #	Unit Numbers	Average SiO ₂ (wt. %)	Description of unit facies	Interpretation of eruption style	Eruptive Frequency
560	TP1	K130	71.6	6 cm of grey, horizontally laminated, clast-supported, coarse-ash	Initial tephra fall at the beginning of an eruption [1]	1 every 88 years
		K131	71.2	20 cm of clast-supported, normally graded, yellow-brown coarse- to medium-lapilli, with dominantly pumice and some lithic clasts	Tephra fall from second episode of a plinian eruption with sudden onset that wanes over time [2, 3]	
600	TP2	K132	71.4	25 cm of clast-supported, normally graded, yellow-brown, fine- to medium-lapilli. Dominantly pumice with some lithic lapilli clasts	Tephra fall from a plinian eruption with sudden explosive onset that wanes over time [2, 3]	1 every 88 years
		K133		5 cm of clast-supported, coarse, weathered coarse-pumice lapilli	Coarse tephra fall from the last episode, ending the eruption [2, 3]	
700	TP3	K135	70.4	40 cm of clast-supported, coarse, normally-graded pumice rich medium- to fine-lapilli, with some lithic lapilli clasts	Tephra fall from a plinian eruption with sudden explosive onset [3]	1 every 88 years
		K136		10 cm mid unit of clast-supported, massive and friable, brown-orange fine- pumice lapilli with some lithics	Continuous tephra fall from the same plinian eruption [3]	
		K137		25 cm of clast-supported, massive, poorly sorted, medium- dominantly pumice, with lithic and scoria lapilli	Tephra fall from the final episode of the eruption that gains intensity from the previous episode, and is continued for some time [2, 3]	
800	TP4	K103	66.4	38 cm of clast-supported, normally graded, yellow-brown, medium- to fine-pumice lapilli	Tephra fall from a plinian eruption with sudden explosive onset that wanes over time [2, 3]	1 every 88 years
850	TP5	K102	65.4	35 cm of massive, clast-supported, brown-red, medium- pumice lapilli with some lithic clasts	Tephra fall from a plinian eruption that continues for some time [2, 3]	1 every 88 years
1000	TP6	K2, K97	67.6	20 cm of matrix-supported, poorly sorted, discrete low angle laminations of grey medium-ash, with poorly distributed pumice, scoria, and dense lapilli	PDC likely originated from single eruption of an explosive blast and destruction of a dome. PDC with a granular-fluid based lower-flow boundary, with discrete stratification and sporadic lapilli [4, 7]	1 every 35 years
		K3		18 cm of matrix-supported, poorly sorted, discrete low angle laminations of grey coarse-ash, with poorly distributed pumice, scoria, and dense lithic lapilli		
1311	TP7	K94	65.2	9 cm of matrix-supported, well sorted, yellow, poorly horizontally laminated, medium-ash, with no lapilli sized clasts	Single PDC that has travelled far from the vent (7 km) leaving a thin, erodable deposit, fineing from the source. Possibly from a dilute, overbank current where suspension dominates [4, 7]	1 every 35 years
1334	TP8	K92		9 cm of matrix-supported, well sorted, yellow, poorly horizontally laminated, medium-ash, with no lapilli sized clasts	Single PDC that has travelled far from the vent (7 km) leaving a thin, erodable deposit, fineing from the source. Possibly from a dilute, overbank current where suspension dominates [4, 7]	1 every 35 years
1376	TP9	K4	68.7	12-20 cm of pink-grey, clast-supported, well laminated, fine-ash with some accretionary lapilli	Initial tephra fall at the beginning of an eruption, presence of accretionary lapilli suggest a phreatomagmatic eruption took place, likely due to the presence of a crater lake [1]	1 every 35 years
		K5		28 cm of matrix-supported, poorly sorted, pink-red, coarse-ash with discretely low-angle laminations, and sporadic dense lithic, and some pumice lapilli	PDC may have developed from a large, unsteady, collapsing surtseyan type eruption column, influenced by the presence of a crater lake that destroyed an emerging lava dome. PDC with a granular-fluid based lower-flow boundary, with discrete stratification and sporadic lapilli [4, 5]. Presence of red ash suggests high-temperature PDC that rapidly chilled [6]	
		K6		10 cm top unit of red, well sorted, matrix-supported, discretely horizontally laminated medium-ash with no lapilli sized clasts		
1385	TP10	K7, K88	66.6	15-20 cm of matrix-supported, well sorted, light grey, medium-ash, with discrete horizontal laminations and lack of lapilli clasts	Single PDC that has travelled far from the vent (7 km) leaving a thin, erodable deposit, fineing from the source. Possibly from a dilute, overbank current where suspension dominates [4, 7]	1 every 35 years
1395	TP11	K8, K87	67.5	15 cm of matrix-supported, poorly sorted, coarse-ash, that is discretely horizontally laminated, with sporadic pumice and lithic lapilli, and accretionary lapilli towards the top of the unit	PDC may have developed from a large, unsteady, collapsing surtseyan type eruption column, influenced by the presence of a crater lake. PDC with a granular-fluid based lower-flow boundary, with discrete stratification and sporadic lapilli and some accretionary lapilli [4, 5]	1 every 35 years
		K9		20 cm of matrix-supported, medium-ash with discrete horizontal laminations and no lapilli sized clasts		
1411	TP12	K10	69.1	8 cm of dark grey, clast-supported, horizontally laminated, fine-ash with no lapilli sized clasts	Initial tephra fall at the beginning of an eruption [1]	1 every 35 years
		K139		16 cm of clast-supported, massive, yellow, fine pumice lapilli with some lithic clasts	Tephra fall from a continued sub-plinian eruption [2, 3]	
		K11	67.9	16 cm of clast-supported, normally graded, yellow, medium- to fine- dominantly pumice lapilli with some scoria and lithic clasts	Tephra fall from a sub-plinian eruption that is waning over time [2, 3]	
		K140	67.8	12 cm of matrix-supported, well sorted, light brown, discretely horizontally laminated coarse-ash with no lapilli sized clasts	Single PDC possibly from a dilute, fineing from source, fluid overbanking current [4, 7]	
		K141		10 cm of matrix-supported, well sorted, brown, discretely horizontally laminated coarse-ash with no lapilli sized clasts	Single PDC possibly from a dilute, fineing from source, fluid overbanking current [4, 7]	
1451	TP13	K142	68.8	15 cm of clast-supported, massive, yellow-brown, dominantly fine pumice lapilli, with some lithic clasts	Tephra fall from a sub-plinian, continued eruption [2, 3]	1 every 35 years
1462	TP14	K143	66.7	20 cm of clast-supported, normally graded, orange-yellow medium- to fine-lapilli consiting of pumice, and lesser lithic clasts	Tephra fall from a sub-plinian eruption that is waning over time [2, 3]	1 every 35 years
1481	TP15	K81	64.7	10 cm of clast-supported, normally graded, yellow-brown, dominantly pumice medium- to fine-lapilli with some lithic and scoria clasts	Tephra fall from a sub-plinian eruption that is waning over time, likely this deposit was not in the direction of the main dispersal axis of the eruption plume [2, 3]	1 every 35 years

Supplementary figures provided in Appendix A, and table in Electronic Appendix B

Table 4 continued:

Time Period (AD)*	Tephra Package #	Unit Numbers	Average SiO ₂ (wt. %)	Description of unit facies	Interpretation of eruption style	Eruptive Frequency
1586	TP16	K12	67.4	35 cm of clast-supported, reversely graded, yellow-brown coarse-ash to coarse-lapilli. Dominantly pumice with little scoria and lithic lapilli	Tephra fall from an eruption that gained intensity, and rised to a large eruption column over time [2, 3]	1 every 35 years
		K144, K63	68.0	60 cm of massive, clast-supported, poorly sorted, yellow-brown coarse lapilli. Dominantly pumice lapilli, but a large mixture of different lithic clasts with some scoria	Continuous tephra fall from the same large eruption column that continued with the same intensity for some time (climax of the eruption) [2, 3]	
		K79	67.4	16-20 cm of clast-supported, normally graded, yellow-brown medium- to fine- pumice lapilli	Continued tephra fall from the same large eruption that is gradually waning in intensity [3]	
1641 - 1800	TP17	K14	66.8	10 cm of clast-supported, grey, reversely graded, fine- scoria and pumice rich lapilli	Small tephra fall from an eruption that is gaining intensity with time [2, 3]	1 every 35 years
		K16		50-75 cm complex series of matrix-supported, coarse- and medium-ash units, discretely laminated, some with sporadic pumice and lithic lapilli. Some units are eroded and discontinuous.	A series of repeated, alternating PDCs with layers of fine- to medium- ash with lapilli are likely from a period of continous, multiple vulcanian type eruptions. Discontinuous, eroded units from PDCs of low-energy and run out [4, 5]	
		K17				
		K18	67.6	Above K20 is a red, 5 cm coarse-ash matrix-supported unit. Above this is another irregular matrix-supported, coarse-ash, discretely laminated unit		
		K20, K146	67.7			
K21	66.6					
1826	TP18	K23	66.8	16-20 cm of grey matrix-supported, poorly sorted coarse-ash, discrete low angle laminations, with some scoria and pumice lapilli, that is of irregular thickness	PDCs likely originated from a collapse of a plinian eruption column. PDC with a granular-fluid based lower-flow boundary, with discrete stratification and sporadic lapilli [4, 5]	1 every 35 years
		K24	68.6	5-10 cm of light-grey, matrix-supported, well sorted coarse-ash, with discrete low angle laminations and no lapilli clasts		
		K147, K48	68.1	10 cm of matrix-supported, yellow-brown, well sorted medium-ash, with discrete low angle laminations		
1848	TP19	K149, K78	68.1	12 cm of clast-supported, yellow-brown, normally graded or massive medium- to fine-lapilli, dominantly pumice with some lithic clasts	Tephra fall from a sub-plinian eruption, here recording either it waning with time, or the climax, most intense part of the eruption [2, 3]	1 every 35 years
1901	TP20	K49		28 cm of clast-supported, grey, normally graded, medium- to fine-pumice and scoria lapilli, with some lithic clasts	Tephra fall from a sub-plinian eruption that is waning over time [2, 3]	1 every 35 years
1919	TP21	K25	68.6	25 cm of clast-supported, grey, medium-ash that is horizontally laminated, with accretionary lapilli	Initial tephra fall at the beginning of an eruption, presence of accretionary lapilli suggest a phreatomagmatic eruption took place, likely due to the presence of a crater lake [1]	1 every 35 years
		K150	69.0	5-12 cm of irregular, grey-red, matrix-supported, coarse-ash with fine horizontal laminations and very few sporadic pumice lapilli	PDC likely originated from a collapse of an initial surtseyan eruption column. PDC with a granular-fluid based lower-flow boundary, with discrete stratification and sporadic lapilli [4, 5]	
		K50		8 cm of brown-yellow, matrix-supported, medium-ash that is discretely horizontally laminated, with some pumice and lithic lapilli.		
		K51		16 cm of clast-supported, normally graded, grey, fine- lapilli to coarse-ash, with dominantly scoria and pumice clasts	Tephra fall from a second episode, the main plinian eruption with sudden explosive onset that wanes over time [2, 3]	
1951	TP22	K53, K26, K151	69.1	11 cm of matrix-supported, grey-green, medium or fine-ash depending on unit. Low angled laminations with some sporadic pumice and lithic lapilli	PDC that likely originated from a collapse of an initial phreatomagmatic eruption column followed by the collapse of a plinian eruption column from the second explosive episode. PDCs with a granular-fluid based lower-flow boundary, with discrete stratification and sporadic lapilli [4, 5]	1 every 12 years
		K54, K27, K152	69.2	9 cm of matrix-supported, yellow-green, medium-ash, finely horizontally laminated, sometimes with accretionary lapilli		
		K55, K153		20 cm of matrix-supported, light grey, medium-ash, with low angle laminations and some sporadic pumice and lithic lapilli		
1966	TP23	K28, K155	69.3	15 cm of matrix-supported, grey-green, horizontally laminated medium-ash with some accretionary lapilli	Initial tephra fall at the beginning of an eruption, presence of accretionary lapilli suggest a phreatomagmatic eruption took place, likely due to the presence of a crater lake [1]	1 every 12 years
		K29, K56		30 cm of matrix-supported, poorly sorted, yellow-grey, coarse-ash with discrete low angle laminations, and dominantly sporadic pumice lapilli, and some different lithic lapilli and scoria	PDC likely originated from a collapse of a plinian eruption column. PDCs with a granular-fluid based lower-flow boundary, with discrete stratification and sporadic lapilli [4, 5]	
		K30, K57		10 cm of matrix-supported, poorly sorted, yellow-grey, coarse-ash with discrete low angle laminations and sporadic pumice lapilli		
1990	TP24	K31		8 cm of matrix-supported, poorly sorted, yellow-grey, coarse-ash with discrete low angle laminations and sporadic pumice lapilli	PDC that likely originated from a collapse of an initial phreatomagmatic eruption [1] column followed by the collapse of a plinian eruption column from the second explosive episode. PDCs with a granular-fluid based lower-flow boundary, with discrete stratification and sporadic lapilli [4, 5]	1 every 12 years
		K32, K58		5 cm of clast-supported, grey-green, irregular medium-ash unit with some accretionary lapilli		
		K33		5 cm irregular unit of matrix-supported, yellow-grey coarse ash with few pumice lapilli		
		K34	69.5	25-30 cm of clast-supported, reversely graded, dark grey, fine- to medium-lapilli with dominantly pumice and scoria, with some lithic clasts	Tephra fall from a plinian eruption that gained intensity, and rised to a large eruption column over time [2, 3]	
2014	TP25	K35	67.8	5-8 cm of clast-supported, reversely graded, light yellow-grey fine- to medium- pumice lapilli, with some scoria and lithic clasts	Tephra fall from a plinian eruption that gained intensity, and rised to a large eruption column over time [2, 3]	1 every 12 years

*Asterisk donates roughly from an eruption in this time period unless explicitly known and stated in the text and on Fig. 4. Eruptive frequency averages rounded up to the nearest whole number.

Interpretation of eruption style has been combined with the historic information given in Table 1. For an interpretation of eruption style with magma system processes see Fig. 8

Numerals [1] refer to references: [1] Bonadonna and Philips, 2003; [2] Cioni et al., 2000; [3] Walker, 1981; [4] Branney and Kokelaar, 2002; [5] Sulpizio et al., 2016; [6] Fink, 1987; [7] Lube et al., 2004

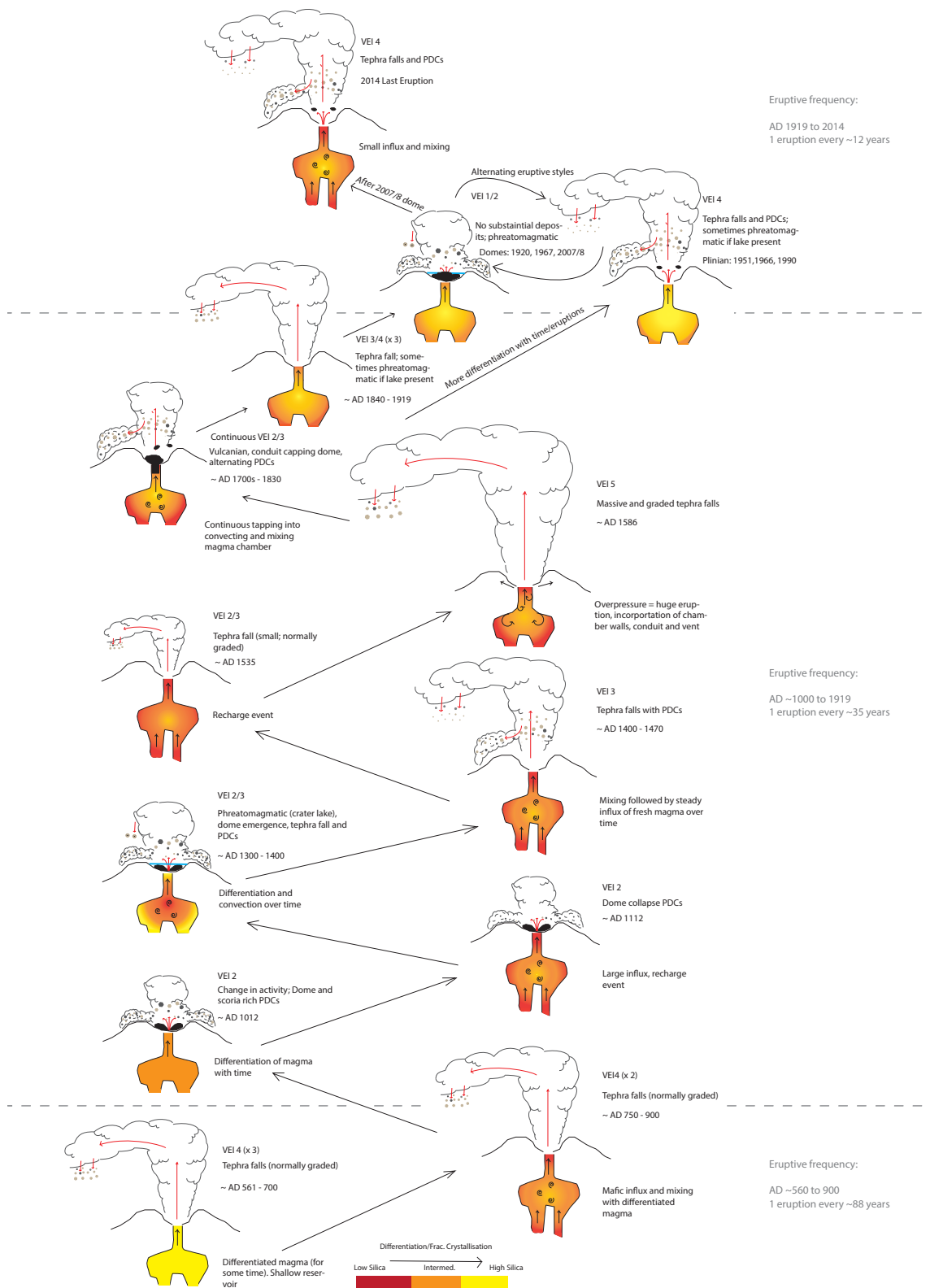


Figure 8: Main eruptive scenarios over time based on the interpretation of eruptive styles and magmatic processes based on the composite stratigraphic section and changes in SiO_2 over time (Fig. 4 and Table 4). Yellow indicates a more silicic magma, and red a less silicic magma. Those with radially graded coloured magma chambers show i.e. the influence of fresh influx or total recharge of mafic magma to a differentiated magma, or the magma differentiating with time without a mafic input influencing the chemistry of the magma. Text surrounding each graphic indicates the VEI of the eruption/s, and how many eruptions occurred, followed a summary of details on the deposits or eruptive style (please see Table 4 for full interpretation), when the eruption occurred, and finally magma chamber processes occurring. Dotted grey lines indicate separating time intervals defined by different eruption frequencies, which are listed in grey text to the right of the graphics.

Supplementary figures provided in Appendix A, and table in Electronic Appendix B

3.5.1.1 Activity from ~AD 500 to 850

Kelut's activity from ~AD 561 \pm 17 to ~700 consisted of three VEI 4 eruptions, represented in the sections studied here by tephra fall deposits. The deposit grain size and thickness (≥ 25 cm), with respect to distance from source, are consistent with moderately high and sustained sub-plinian eruption columns (Walker, 1981; Cioni et al., 2000), at least on the order of magnitude of those observed in 1990 and 2014 (Bourdier et al., 1997; Maeno et al., 2017). This period erupted the most evolved glass chemistries with little temporal variation. This may indicate the successive tapping of a large mid-crustal reservoir, where crystal fractionation and differentiation processes produced evolved magma (Fig. 8). This may have followed a hiatus in eruptive activity pre-AD 561 that allowed the magma to accumulate and evolve (cf., Gertisser and Keller, 2003), but no ages are available below. The compositional changes do not conform to a normal crystal fractionation trend, since they have lower K₂O and higher Al₂O₃ against higher SiO₂ contents (Fig. 7). Weathering is a possible explanation, but this is not consistent with other elements, because there is no associated depletion of calcium and magnesium, and enrichment of iron (Stewart et al., 2001; Fiantis et al., 2010).

Following ~100 years of repose, the next two sustained ~VEI 4 eruptions at ~AD 850 may have been triggered by influx and mixing of mafic magma into the system, as evidenced by a ~5.5 wt% drop in SiO₂ from previously erupted units (from 71.5 wt.% SiO₂ to 66.2 and 65.2 wt.% SiO₂). Mafic recharge is a common trigger of larger eruptions at stratovolcanoes (Sparks et al., 1977), and seen at nearby volcanoes, such as Merapi (Andreastuti et al., 2000; Gertisser and Keller, 2003). Evidence for this includes mafic enclaves, mixed populations of phenocrysts, variations in crystal overgrowths and strong diffusion patterns in the rims of phenocrysts (Troll et al., 2013). Mixed populations of phenocrysts were seen in the BSE images, where clinopyroxene and zoned plagioclase phenocrysts were present (Fig. 5b, d, e, f and h), and this may be evidence of magma mixing or mingling before these eruptions of Kelut at ~AD 800, 1586, 1700, 1900 and 1951, although no evidence for mixing was observed in e.g., enclaves in the deposits during fieldwork as clear evidence for mixing and mingling.

3.5.1.2 Activity from ~AD 1000 to 1400's

Another large period of repose was followed by an eruption at AD 1012 \pm 10 with a more silicic composition. This is mainly represented by PDC deposits containing both dense lava fragments and poorly vesicular clasts. This appears to represent one of many dome growth and destruction phases, with deposits consistent with either lava dome collapse, or explosive destruction. Widespread similar PDCs resulting from the collapse and growth of the Merapi volcanic edifice are observed around AD 800 to 1300 (Newhall et al., 2000).

At ~AD 1112 \pm 52, fine, thin deposits record distal small-scale PDCs (K94). They could represent lateral deposits from units on other flanks of the volcano, or thin run-outs from small-scale dome collapses (Fig. 8). During the AD 1376 and 1395 eruptions, accretionary lapilli coupled

with lithic rich ash, and angular glass shards indicate ash accretion in steam-rich plumes, or moist atmosphere (TP9). These features together are often associated with phreatomagmatic eruptions (cf. Wholetz, 1983; Houghton and Nairn, 1991; Bonadonna and Philips, 2003), but the humid tropical environment of Kelut may also lead to some of the features, e.g., accretionary lapilli. The historic records indicate that 1376 is when the first growth of a lava dome was recorded associated with a VEI 3 eruption, likely extruding through a crater lake (Table 1; Zen and Hadikusumo, 1965; GVP, 2014b). The variations in glass shard composition from this time to around ~AD 1465 indicate varying amounts of interaction between small mafic influxes mixing with a resident, evolving magma (Figs. 4 and 8). The frequency of eruptions in this period of ~400 years is higher than pre-AD 1000, indicating that periodic influxes that trigger regular mixing events maintained the system in a semi-steady state (cf. Landi et al., 2004).

3.5.1.3 Activity from ~AD 1500 to early 1900's

Two tephra fall deposits that occurred in close timing around AD 1535 \pm 66 and have more mafic compositions (~67.1 and 64.7 wt.% SiO₂) than previously erupted units. They record an intermediate magma reservoir gradually mixing with an influx of new mafic magma (Figs. 4 and 8). The most mafic composition (~64.7 wt.% SiO₂) precedes the massive, largest and coarsest sequence of tephra fall deposits recorded. This represents a recharge event, whereby overpressure likely triggered the largest eruption of Kelut to date, the VEI 5 1586 event. The variation in silica in analysed glasses from this eruption (from ~66.0 to 69.0 wt.% SiO₂; Fig. 7) may be a consequence of analysing a mixture of clasts from some very vesiculated and fragmented pumice (e.g., 5a), along with microlite rich groundmass particles (e.g., 5b and f). The large variation in compositions could be due to eruption eroding parts of the conduit, chamber and vent walls, widening the crater (e.g., Carey et al., 2007), or simply a highly zoned magma chamber erupted during incomplete mixing.

Following this, there is a regular series of thin PDC deposits resulting from dome collapses and/or short pulses of vulcanian activity during the 1700s. The compositional variation of glass (from 65.5 to 67.9 wt.% SiO₂) suggests eruptions were derived from magma undergoing quasi-steady mixing. The eruption dynamics reflect small magma pockets rising and being stalled by a vent-capping dome, or closed conduit. Slow rise rates and early degassing may have also dampened explosivity. This is similar to the series of successive VEI 2 eruptions noted the historical records (Zen and Hadikusumo, 1965; GVP, 2014b). The 1826 and 1848 PDC deposits are attributed to a larger VEI 4 eruptions. Glass shards from these units show greater surface alteration and abrasion, with some smoothed edges (Fig. 5e) from transport turbulent flows with abundant collisions (Heiken and Wohletz, 1985). Eruptions after this time, up until ~1901, must have been similar in style to those pre- AD 1535, and show near-identical deposit characteristics (Fig. 4).

3.5.1.4 Activity after 1901 to 2014

Deposits from plinian eruptions in 1919, 1951, 1996 and 1990 show more complex eruptive episodes. Clear indications of magma-water (or wet-atmosphere) interaction are evidenced by the presence of accretionary lapilli, and glass shards that have fine ash adhering to the surfaces (Fig. 5c). Fine ash adhering to the glass shards and lithic-rich ash deposits can also be produced under a hydrothermal system (cf. Tongariro, NZ, Pardo et al., 2012). Kelut has commonly had an acidic crater lake and vigorous vent-hosted hydrothermal system (Bernard and Mazot, 2004; Caudron et al., 2012). The VEI 4 eruptions likely had multiple phases, as shown by several series of granular, concentrated PDCs (e.g., K29) and tephra fall deposits, particularly in 1990 (TP23). The eruptive records indicate episodes of lava dome-growth occurred between these eruptions (see Table 1; GVP, 2014b). The 1920 dome marks the beginning of the explosive-effusive cyclic activity that remains at Kelut to this day. The composition of glass shards from this sequence of tephra (from ~68.0 to 70.5 wt.% SiO₂) reflects a magma reservoir that is continuously fractionating and differentiating with time until 1990 (Figs. 4, 6, 7 and 8). Thus, during this ~164 year period, the reservoir was unaffected by large influxes of primitive magma. Extended periods of slow lava dome effusion (e.g., 2007-2008) may allow for un-interrupted magmatic differentiation and little mixing. Slow intrusion and degassing allows little opportunity for mixing processes to take place in the upper conduit system (cf. Humphreys et al., 2006).

In the absence of chemical diversity or evidence of large-scale magma mixing, variations in post- AD 1900 eruptive styles must have another origin. Jeffery et al. (2013) suggested that the 2007-2008 dome forming episode was triggered by a subtle mafic recharge event causing mixing at shallow levels. The composition of the 2014 products is slightly less evolved than the 1990 deposits (Fig. 4), indicating that a small mafic influx may have occurred prior to the 2014 eruption. These small additions that gradually increased the volatile content, may have been enough to affect degassed magma stored in a shallow conduit, producing the dome-unroofing explosive eruption of 2014 (cf. Cronin et al., 2013; Caudron et al., 2015).

3.5.2 Eruptive frequency

Prior to AD 1000, five large eruptions occurred over an estimated ~440 years. This was the lowest eruption frequency noted (1 eruption every ~88 years). Gertisser and Keller (2003), state that periods of low eruptive frequency at Merapi are crucial in allowing magmatic differentiation. Similarly, this may be responsible for early ~AD 561 evolved glass compositions at Kelut.

Post- AD 1000 to 1919 eruptions are much more frequent, every ~35 years on average, with a complex pattern and shift in silica contents. Short periods defined by some differentiation are interrupted by approximately four periods of mafic influx (e.g., ~1112, ~1376, 1535, pre-2014). It is likely that these periodic influxes substantially altered the composition of resident magma by mixing (Cassidy et al., 2016; Figs. 4, 6, 7 and 8). The mixing events every ~200 years also acted to maintain the high frequency of eruptions observed at Kelut post- AD 1000 to ~1700. The largest

influx and mafic recharge events (e.g., pre K102 and ~AD 1535) triggered the most explosive eruptions (e.g., pre-1586). These occur less frequently, roughly every 400 years. Longer periods of repose (up to 75 years) also follow these larger events, possibly because the crustal reservoir is emptied. Eruptions of Kelut post- ~AD 1726 to 1990 appear to be tapping from a continuously differentiating magma chamber, either because there are no new influxes of primitive magma, or the influxes are small in relation to the volume of the reservoir.

Since 1919, the alternations between dome-building and explosive eruptions have a frequency of one eruption every ~12 years, with a plinian (VEI 4) eruption occurring every ~21 years. Since there is no indication of discrete magmatic influxes or complete recharge events, this cyclic pattern could thus reflect magma ascent and degassing conditions in the magma reservoir and upper conduit (see Chapter 2), or minor mafic intrusions prior to explosive sub-plinian eruptions, such as 2014 (Cassidy et al., 2016).

3.5.3 Hazard scenarios

In proximal and distal locations (≤ 7 km from the vent) all sections reveal that tephra falls from sub-plinian/vulcanian activity, and particularly falls from more explosive plinian eruptions pose a hazard. Tephra falls from larger eruptions proximal to the vent e.g., K144 from the 1586 VEI 5 eruption, and TP3 from ~AD 700 have an abundance of coarse lapilli, which can cause significant damage to buildings and infrastructure. Many of the recent (post- 1919) VEI 4 eruptions are defined by eruptions that slowly build to a climax as shown by reverse grading of deposits (1990, 2014), with multiple, complex eruptive phases. Most of these eruptions (bar 2014) show early phreatomagmatic activity and generation of PDCs that were initiated either by the marginal column collapses, or blast type associated with the destruction of a dome, followed by tephra falls. PDCs in locations proximal to the vent (< 5 km) date back to ~AD 1000, and have therefore remained a constant hazard. Lahar deposits were not observed in sections in this study, yet the eruptive history records syn- and post-eruptive lahars back to AD 1000 (Table 1; Zen and Hadikusumo, 1965; GVP, 2014b). These remain the largest hazard to proximal and distal locations due to the presence of the ephemeral crater lake at Kelut, and frequent tropical rainfall. The official hazard maps identify major risk catchments to the west, south-west, and north-west of the volcano in the proximal and distal regions, and quantify lahars as the biggest threat to human life and infrastructure (Mulyana et al., 2004; Primulyana et al., 2014; Andreastuti et al., 2017).

3.5.4 Completeness of the geological record

When investigating the stratigraphic/geological record of a volcano, it is important to evaluate the completeness and preservation of the record. In particular, how this record becomes less complete back through time, as the number of events recorded decreases as a function of time (Delinge et al., 2010; Brown et al., 2014; Kiyosugi et al., 2015; Rougier et al., 2016). Under-recording of eruptions has to be taken into consideration when estimating the eruptive frequency or recurrence

rates of large magnitude eruptions, as it can directly impact on hazard and risk assessments (Brown et al., 2014; Kiyosugi et al., 2015; Rougier et al., 2016).

Under-recording of volcanic events increases after AD 1600 (Brown et al., 2014), so it is likely that some eruptions may be missing from Kelut's historical eruptive and geological records. Although the deposits we see can be correlated to known eruptions with confidence, some probably under-represent the actual event at the volcano in terms of size and complexity of the volcanic event, where smaller magnitude eruptions in particular may be under-recorded. Some dome-forming eruptions do not leave large deposits in the stratigraphic record (e.g., the 2007-2008 dome formation has completely disappeared after the 2014 eruption), or the deposits are eroded away but subsequent activity (cf. Kiyosugi et al., 2014). There is only one historically recorded dome growth pre-1900's (in 1376), but it is highly likely that the presence of more domes are missing from the historical records, since the nature of some deposits represent dome collapse or growth stages (e.g., TP6 Fig. 4). Under-recording of some smaller eruptions (VEI 0 to 2) that have less impact on populations (Brown et al., 2014) may be responsible for the small number, or less detailed historical records available for Kelut pre-1901.

The preservation of deposits must also be considered, as this also worsens with time. Some small volume deposits (e.g., TP7 and TP8) from earlier in time (e.g., around the 1300's) are not well preserved considering both are attributed to VEI 3 eruptions. Factors including the depositional environment (e.g., riverine erosion), climate (e.g., heavy rainfall from Indonesia's tropical climate altering deposits), burial and erosion from subsequent younger eruptions, affect the preservation and alteration of deposits (Machida et al., 1997; Imura and Kobayashi, 2001; Pollard et al., 2003; Lavinge, 2004; Brown et al., 2014; Kiyosugi et al., 2015). These factors may be responsible for the partial preservation of some smaller deposits at Kelut.

Larger magnitude events (\geq VEI 4) are better recorded historically and also better preserved in the geological record (Brown et al., 2014), as clearly evidenced by the well-preserved larger volume deposits from the VEI 5 1586 eruption (TP16, Fig. 4). The geological/stratigraphic record (Fig. 4) shows 5 large (\sim VEI 4) eruptions pre- AD 1000, yet these are missing from the historical record (Table 1). Under-recording of larger eruptions further back in time, due to possibly lower population and lower literacy levels, may be responsible for these eruptions not being recorded (cf. Siebert et al., 2010). Whilst the large soil developments between these events may mean long periods of volcanic repose, it may be possible that some tephra deposits have disappeared due to erosion or burial from the younger, larger magnitude events that followed. Therefore, although the frequency of eruptions pre- AD 1000 is lower, it must be taken into account that some smaller magnitude eruptions may be missing from the geological record, and should be taken into consideration for hazard assessments, along with the possible occurrence of more frequent dome-forming eruptions.

3.6 Conclusions

The volcanological and geochemical records presented in this study reveal that the eruptive history (frequency and styles) and magmatic evolution of Kelut are complex. Varying glass shard major element compositions from tephra in the stratigraphic record at Kelut reveal that discrete influxes of mafic magma, mixing with more evolved magmas, periods of magmatic differentiation, and conduit conditions largely controlled the eruptive frequency at Kelut.

The stratigraphic sequences from four different locations presented in this study pre-date the historical eruptive records by stretching back to ~AD 560. Over a ~440 year period, activity is from ~AD 560 to 1000 is defined by five large tephra falls, with 1 eruption every ~88 years on average. The major element geochemical variations of glass shards from these eruptions are the most evolved (Figs. 4, 6, 7 and 8), indicating that lower magmatic feeding rates and longer pauses in activity resulted in periods of magmatic differentiation, and therefore resulted in more explosive eruptions. This evolutionary trend is disturbed by a recharge event detected around ~AD 700, and this recharge likely triggered two eruptions pre-AD 1000.

Activity post- AD 1000 to 1919 is defined by more frequent eruptions (1 eruption on average every ~35 years), and post-1919 to 2014 by the most frequent eruptions (1 every ~12 years), with a more complex series of PDCs and tephra falls. The geochemical variations in glass shards show a complex magmatic history that governs the periodicity and frequency of eruptions from AD 1000 to ~1726 (Figs. 4 and 8). Frequent episodes of differentiation, discrete mafic influxes every ~200 to ~450 years, and magma mixing appear to maintain the magmatic system in a quasi-steady state, providing a constant trigger for series of frequent VEI 2 to 4 eruptions. During this time period, PDCs indicate the more common formation and collapse of lava domes, and the presence of accretionary lapilli and lithic clasts also indicate that magma-water interaction likely largely controlled eruptive style, probably due to the formation of crater lakes at Kelut. Although magma mixing and differentiation processes control smaller-scale fluctuations in glass geochemistry and define periods of high-eruptive frequency (e.g., 1700's), the largest mafic recharge events appear to trigger the most explosive eruptions at Kelut, such as the 1586 VEI 5 eruption, and the two eruptions pre- AD 1000.

There are two differentiation or evolutionary magmatic trends. One does not conform to the normal crystal fractionalisation trend, around ~AD 561-700. The second is a normal differentiation trend post- AD 1726 to 1990. These post- 1726 recorded eruptions appear to be tapping into a continually evolving magma reservoir, not affected by any disturbances due to influxes of primitive magma. The first dome was recorded in 1920 following the 1919 eruption, and this therefore marks the initiation of eruptions that are cyclic between effusive dome-forming and explosive variants. Since magmatic processes such as influxes of magma do not appear to govern the transition in eruptive style (in contrast to the eruptions pre-1700's), this cyclic behaviour must depend on degassing conditions and ascent dynamics from the magma reservoir to the upper conduit.

Although it is possible that a small influx of mafic magma may have triggered the 2014 eruption, the question remains as to what is the main control on effusive-explosive eruption styles. Further work could investigate if the magma storage regions between the explosive and effusive eruptions are the same. This is in order to identify if processes, such as a fresh influxes of mafic melt, are indeed triggering the recent explosive eruptions (like past larger eruptions), or whether the lava dome is acting to trap gasses and eventually triggering the larger eruptions at Kelut.

3.7 Acknowledgements

R. Firmansyah and D. Madi are acknowledged for their assistance during fieldwork. A. Hogg and F. Petchey at the Waikato Radiocarbon Dating Laboratory are thanked for radiocarbon dating samples. S. Craven at Macquarie University is thanked for assistance in preparation of glass shards and grain mounts. I. Schipper who runs the EMP at UVW is also thanked. L. Goode is funded by a Macquarie University Research Excellence Scholarship (MQRES) (2012196) associated with an Australian Research Council Future Fellowship awarded to H. Handley (FT120100440). S. Cronin is funded by the New Zealand Natural Hazard Research Platform “Quantifying Volcanic Risks” project.

3.8 References

- Andreastuti, S.D., Alloway, B.V., and Smith, I.E.M. (2000). A detailed tephrostratigraphic framework at Merapi Volcano, Central Java, Indonesia: implications for eruption predictions and hazard assessment. *Journal of Volcanology and Geothermal Research*. 100. 51-67.
- Andreastuti, S., Widiwijayanti, C., Heriwaseso, A., and Budianto, A. (2017). Revision of hazard map considered from eruptive style and impact: the case of Kelud volcano. *Journal of Volcanology and Geothermal Research*.
- Arce, J.L., Macias, J.L., Vazquez-Selem, L. (2003). The 10.5 km plinian eruption of Nevado de Toluca volcano, Mexico: stratigraphy and hazard implications. *Geological Society of America Bulletin*. 115. 230-248.
- Badan Informasi Geospasial (BDI) (2013). Bakosurtanal (In Indonesian). Topographical map of Kelut volcano.
- Bernard, A., and Mazot, A. (2004). Geochemical evolution of the young crater lake of Kelud volcano in Indonesia. In: Wanty, R.B., and Seal II, R.B. (2004) eds. *Water-rock interaction, (WRI-11)*. London: Taylor and Francis group plc. 87- 90.
- Bonadonna, C., and Houghton, B.F. (2005). Total grain-size distribution and volume of tephra-fall deposits. *Bulletin of Volcanology*. 67. 441-456.
- Bonadonna, C., and Philips, J. (2003). Sedimentation from strong volcanic plumes. *Journal of Geophysical Research*. 108. 1-28
- Bourdier, J-L., Pratomo, I., Thouret, J-C., Boudon, G., and Vincent, P.M. (1997). Observations, stratigraphy and the eruptive processes of the 1990 eruption of Kelut volcano, Indonesia. *Journal of Volcanology and Geothermal Research*. 79. 181-203.

Chapter Three

- Branney, M.J., and Kokelaar, P. (2002). Pyroclastic density currents and the sedimentation of ignimbrites. *Geological Society, London, Memoirs*. 27.
- Brown, S.K., Crosweller, H.S., Sparks, R.S.J., Cottrell, R., Delinge, N.M., Guerrero, N.O., Hobbs, L., Kiyosugi, K., Loughlin, S.C., Siebert, L., and Takarada, S. (2014). Characterisation of the Quaternary eruption record: analysis of the Large Magnitude Explosive Volcanic Eruptions (LaMEVE) database. *Journal of Applied Volcanology*. 3. 1-22.
- Carey, R.J., Houghton, B.F., Sable, J.E., Wilson, C.J.N. (2007). Contrasting grain size and componentry in complex proximal deposits of the 1886 Tarawera basaltic Plinian eruption. *Bulletin of Volcanology*. 69. 903-926.
- Cassidy, M., Watt, S.F.L., Palmer, M.R., Trofimovs, J., Symons, W., Maclachlan, S.E., and Stinton, A.J. (2014). Construction of volcanic records from marine sediment cores: A review and case study (Montserrat, West Indies). *Earth-Science Reviews*. 138. 137-155.
- Cassidy, M., Castro, J.M., Helo, C., Troll, V.A., Deegan, F.M., Muir, D., Neave, D.A., and Mueller, S.P. (2016). Volatile dilution during magma injections and implications for volcano explosivity. *Geology*. 44. 1027-1030.
- Caudron, C., Mazot, A., and Bernard, A. (2012). Carbon dioxide dynamics in Kelud volcanic lake. *Journal of Geophysical Research*. 117. 1-11.
- Caudron, C., Taisne, B., Garces, M., Alexis, L.P., and Mialle, P. (2015). On the use of remote infrasound and seismic stations to constrain the eruptive sequence and intensity for the 2014 Kelud eruption. *Geophysical Research Letters*. 6614-6621.
- Cioni, R., Marianelli, P., Santacroce, R., and Sbrana, A. (2000). *Plinian and Subplinian Eruptions*. In: Encyclopedia of Volcanoes. Eds. Sigurdsson, H., Houghton, B., Rymer, H., McNutt, S., and Stix, J. Academic Press. p477 – 494.
- Clynne, M.A., Calvert, A.T., Wolfe, E.W., Evarts, R.C., Fleck, R.J., and Lanphere, M.A. (2008). The Pleistocene eruptive history of Mount St. Helens, Washington, from 300,000 to 12,800 years before present. *U.S. Geological Survey Professional Paper*. 1750. 1-35.
- Colonge Radiocarbon Calibration & Paleoclimate Research Package (2003-2007). *The CalPal Online Radiocarbon Calibration, University of Colonge, Germany*. <http://www.calpal-online.de>
- Cronin, S.J., Lube, G., Dayudi, D.S., Sumarti, S., Subrandiyo, S., Surono. (2013). Insights into the October-November 2010 Gunung Merapi eruption (Central Java, Indonesia) from the stratigraphy, volume and characteristics of its pyroclastic deposits. *Journal of Volcanology and Geothermal Research*. 261. 244-259.
- Damaschke, M., Cronin, S.J.C., Holt, K.A., Bebbington, M.S., and Hogg, A.G. (2017). A 30,000 year high-precision eruption history for the andesitic Mt. Taranaki, North Island, New Zealand. *Quaternary Research*. 87. 1-23.
- De Bélizal, E., Lavigne, F., Gaillard, J.C., Grancher, D., Pratomo, I., and Komorowski, J.C. (2012). The 2007 eruption of Kelut volcano (East Java, Indonesia): Phenomenology, crisis management and social response. *Geomorphology*. 136. 165-175.
- Delinge, N.I. Coles, S.G., Sparks, R.S.J. (2010). Recurrence rates of large explosive volcanic eruptions. *Journal of Geophysical Research*. 115.

- Donoghue, S.L., Vallance, J., Smith, I.E.M., and Stewart, R.B. (2006). Using geochemistry as a tool for correlating proximal andesitic tephra: case studies from Mt Rainier (USA) and Mt Ruapehu (New Zealand). *Journal of Quaternary Science*. 22. 395-410.
- Druitt, T.H., Edwards, L., Mellors, R.M., Pyle, D.M., Sparks, R.S.J., Lanphere, M., Davies, M., and Barriero, B. (1999). Santorini volcano. *Geological Society of London Memoirs*. 19. 1-176.
- Fiantis, D., Nelson, M., Shamshuddin, J., Goh, T.B., and Van Ranst, E. (2010). Determination of the geochemical weathering indices and trace element content of new volcanic ash deposits from Mt. Talang (West Sumatra) Indonesia. *Eurasian Soil Science*. 43. 1477-1485.
- Fink, J.H. (1987). The emplacement of silicic domes and lava flows. *Geological Society of America*. 212. 37.
- Gertisser, R., and Keller, J. (2003). Temporal variation in magma composition at Merapi Volcano (Central Java, Indonesia): magmatic cycles during the past 2000 years of explosive activity. *Journal of Volcanology and Geothermal Research*. 123. 1-23.
- Goode, L.R., Handley, H.K., and Cronin, S.J. (in press). Insights into eruption dynamics from the 2014 pyroclastic deposits of Kelut volcano, Java, Indonesia and implications for future hazards. *Journal of Volcanology and Geothermal Research – Kelud and Sinabung Special Edition*.
- Global Volcanism Program (GVP) (2008). Report on Kelut (Indonesia). In: Wunderman, R. (ed.), Bulletin of the Global Volcanism Network, 33:3. Smithsonian Institution. Available: <http://dx.doi.org/10.5479/si.GVP.BGVN200803-263280>.
- Global Volcanism Program (GVP) (2012). Report on Kelut (Indonesia). In: Wunderman, R. (ed.), Bulletin of the Global Volcanism Network, 37:3. Smithsonian Institution. Available: <http://dx.doi.org/10.5479/si.GVP.BGVN201203-263280>
- Global Volcanism Program (GVP). (2014). Report on Kelut (Indonesia). In: Wunderman, R. (ed.), Bulletin of the Global Volcanism Network, 39:2. Smithsonian Institution. Available: <http://dx.doi.org/10.5479/si.GVP.BGVN201402-263280>.
- Global Volcanism Program (GVP). (2014b). Eruptive History. In: Kelut Eruption Page. Smithsonian Institution. Accessed March 2015. Available: <http://www.volcano.si.edu/volcano.cfm?vn=263280>
- Gómez-Vazquez, A., De la Cruz-Reyna, S., Mendoza-Rosas, A.T. (2016). The ongoing dome emplacement and destruction cyclic process at Popocatepetl volcano, Central Mexico. *Bulletin of Volcanology*. 78. 58.
- González, M.B., Ramirez, J.J., Navarro, C. (2002). Summary of the historical eruptive activity of Volcán De Colima, Mexico 1519-2000. *Journal of Volcanology and Geothermal Research*. 117. 21-46.
- Heiken, G., and Wohletz, K. (1985). *Volcanic Ash* (2nd eds). University California Press. 52, 122, 162.
- Houghton, B.F., and Nairn, I.A. (1991). The 1976-1982 Strombolian and phreatomagmatic eruptions of White Island: New Zealand: eruptive and depositional mechanisms at a 'wet' volcano. *Bulletin of Volcanology*. 54. 25-49.
- Humphreys, M.C.S., Blundy, J., and Sparks, R.S.J. (2006). Magma evolution and open-system processes at Shiveluch volcano: insights from phenocryst zoning. *Journal of Petrology*. 47. 2303-2334.

Chapter Three

- Imura, R., and Kobayashi, T. (2001). Geological map of Kirishima volcano. Geological Survey of Japan (in Japanese with English abstract).
- Jeffery, A.J., Gertisser, R., Troll, V.R., Jolis, E.M., Dahren, B., Harris, C., Tindle, A.G., Preece, K., O'Driscoll, B., Humaida, H., and Chadwick, J.P. (2013). The pre-eruptive magma plumbing system of the 2007-2008 dome-forming eruption of Kelut volcano, East Java, Indonesia. *Contributions to Mineralogy and Petrology*. 166. 275-308.
- Kiyosugi, K., Connor, C., Sparks, R.S.J., Crosweller, H.S., Brown, S.K., Siebert, L., Wang, T., and Takarada, S. (2015). How many explosive eruptions are missing from the geological record? Analysis of the quaternary record of large magnitude explosive eruptions in Japan. *Journal of Applied Volcanology*. 4. 1-15.
- Klug, C., Cashman, K.V., and Bacon, C.R. (2002). Structure and physical characteristics of pumice from the climactic eruption of Mount Mazama (Crater Lake), Oregon. *Bulletin of Volcanology*. 64. 486-501.
- Kristiansen, N.I., Prata, A.J., Stohl, A., and Carn, S.A. (2015). Stratospheric volcanic ash emissions from the 13 February 2014 Kelut eruption. *Geophysical Research Letters*. 42, 588-596.
- Landi, P., Metrich, N., Bertagnini, A., and Rosi, M. (2004). Dynamics of magma mixing and degassing recorded in plagioclase at Stromboli (Aeolian Archipelago, Italy). *Contributions to Mineralogy and Petrology*. 147. 213-227.
- Lavinge, F. (2004). Rate of sediment yield following small-scale volcanic eruptions: a quantitative assessment at the Merapi and Semeru stratovolcanoes, Java, Indonesia. *Earth Surface Process Landforms*. 29. 1045-1058.
- Lowe, D.J (2011). Tephrochronology and its application: a review. *Quaternary Geochronology*. 6: 107-153.
- Lube, G., Cronin, S.J., Thouret, J.-C., Surono (2011). Kinematic characteristics of pyroclastic density currents at Merapi and controls on their avulsion from natural and engineered channels. *Geological Society of America Bulletin*. 123. 1127-1140.
- Lube, G., Breard, E.C.P., Cronin, S.J., Procter, J.N., Brenna, M., Moebis, A., Pardo, N., Stewart, R.B., Jolly, A., Fournier, N. (2014). Dynamics of surges generated by hydrothermal blasts during the 6 August 2012 Te Maari eruption, Mt. Tongariro, New Zealand. *Journal of Volcanology and Geothermal Research*. 286. 348-366.
- Luhr, J.F., Navarro-Ochoa, C., and Savov, I.P. (2010). Tephrochronology, petrology and geochemistry of Late-Holocene pyroclastic deposits from Volcán de Colima, Mexico. *Journal of Volcanology and Geothermal Research*. 197. 1-32.
- Machida, H., Yamazaki, H., Arai, F., and Fujiwara, O. (1997). Omine Pyroclastic flow deposits: A marker tephra for the study of evolution of the Japan Northern Alps. *Journal of Geography*. 3. 432-439. (In Japanese).
- Machida, H. (1999). The stratigraphy, chronology and distribution of distal marker-tephras in and around Japan. *Global of Planetary Change*. 21. 71-94.
- Maeno, F., Nakada, S., Yoshimoto, M., Shimano, T., Hokanishi, N., Zaennudin, A., and Iguchi, M. (2017). A sequence of a plinian eruption preceded by dome destruction at Kelud volcano, Indonesia, on February 13, 2014, revealed from tephra fallout and pyroclastic density current deposits. *Journal of Volcanology and Geothermal Research*. <http://dx.doi.org/10.1016/j.jvolgeores.2017.03.002>

- Mulyana, A.R., Nasution, A., Martono, A., Sumpena, A.D., Purwoto, and Santoso, M.S. (2004). Peta Kawasan Rawan Bencana Gunungapi Kelud, Propinsi Jawa Timur (Volcanic hazards map of Kelud volcano, East Java Province), Pusat Vulkanologi dan Mitigasi Bencana Geologi, Badan Geologi, Departemen Energi dan Sumber Daya Mineral. Scale 1:100,000, 1 plate.
- Newhall, C.G., Bronto, S., Alloway, B., Banks, N.G., Bahar, I., del Marmol, M.A., Hadisantono, R.D., Holcomb, R.T., McGeehin, J., Miksic, J.N., Rubin, M., Sayudi, S.D., Sukhyar, R., Andreastuti, S., Tilling, R.I., Torley, R., Trimble, D., and Wirakusumah, A.D. (2000). 10,000 years of explosive eruptions of Merapi Volcano, Central Java: archaeological and modern implications. *Journal of Volcanology and Geothermal Research*. 100. 9-50.
- Pardo, N., Cronin, S.J., Palmer, A., Procter, J., Smith, I. (2012). Andesitic Plinian eruptions at Mt. Ruapehu: quantifying the uppermost limits of eruptive parameters. *Bulletin of Volcanology*. 74. 1161-1185.
- Pardo, N., Avellán, D.R., Macías, J.A., Scolamacchia, T., and Rodríguez, D. (2008). The ~1245 yr BP Asososca Maar: New advances on recent volcanic stratigraphy of Managua (Nicaragua) and hazard implications. *Journal of Volcanology and Geothermal Research*. 176. 493-512.
- Pardo, N., Cronin, S.J., Nemeth, K., Brenna, M., Schipper, C.I., Breard, E., White, J.D.L., Procter, J., Stewart, B., Agustin-Flores, J., Moebis, A., Zernack, A., Kereszturi, K., Lube, G., Auer, A., Neall, v., and Wallace, C. (2014). Perils in distinguishing phreatic from phreatomagmatic ash; insights into mechanisms of the 6 August 2012 Mt. Tongariro eruption. *Journal of Volcanology and Geothermal Research*. 286. 397-414.
- Pollard, A.M., Blockley, S.P.E., and Ward, K.R. (2003). Chemical alteration of tephra in the depositional environment: theoretical stability modelling. *Journal of Quaternary Science*. 18. 385-394.
- Pratomo, I. (1992). Etude de l'éruption de 1990 du volcan Kelut (Java- Est Indonesie): son apport à l'interprétation de l'activité historique du volcan. Unpublished PhD Thesis, Blaise Pascal Clermont-Ferrand II.
- Primulyana, S., Hariwaseso, A., Zaenuddin, A., Budianto, A. (2014). Peta Kawasan Rawan Bencana Gunungapi Kelud, Propinsi Jawa Timur (Volcanic hazards map of Kelud volcano, East Java Province), Pusat Vulkanologi dan Mitigasi Bencana Geologi, Badan Geologi, Kementerian Energi dan Sumber Daya Mineral. Scale 1:100,000, 1 plate.
- Prueher, L.M., and Rea, D.K. (2001). Tephrochronology of the Kamchatka-Kurile and Aleutian arcs: evidence for volcanic episodicity. *Journal of Volcanology and Geothermal Research*. 106. 67-84.
- Roobol, M.J., and Smith, A.L. (1976). Mount Pelée, Martinique: A pattern of alternating eruptive styles. *Geology*. 4. 521-524.
- Rougier, J., Sparks, S.R., and Cashman, K.V. (2016). Global recording rates for large eruptions. *Journal of Applied Volcanology*. 5. 1-10.
- Siebe, C., and Macías, J.L. (2006). Volcanic Hazards in the Mexico City metropolitan area from eruptions at Popocatepetl, Nevado de Toluca, and Jocotitlán stratovolcanoes and monogenetic scoria cones in the Sierra Chichinautzin Volcanic Field. *Geological Society of America*. 402.
- Siebert, L., Simkin, T., and Kimberly, P. (2010). *Volcanoes of the World*, 3rd Edition. University of California Press, Berkeley.
- Smith, A.L., Roobol, M.J., Schellekens, J.H., and Mattioli, G.S. (2007). Prehistoric stratigraphy of the Soufrière Hills-South Soufrière Hills volcanic complex, Montserrat, West Indies. *Journal of Geology*. 115. 115-127.

- Sparks, R.S.J., Sigurdsson, H., and Wilson, L. (1977). Magma mixing: a mechanism for triggering acid explosive eruptions. *Nature*. 267. 315-318.
- Sparks, R.S.J., and Young, S.R. (2002). The eruption of Soufrière Hills Volcano, Montserrat (1995-1999): overview of scientific results. *Geological Society, London, Memoirs*. 21. 45-69.
- Stewart, R.B., Capo, R.C., and Chadwick, O.A. (2001). Effects of rainfall on weathering rate, base cation provenance, and Sr isotope composition of Hawaiian soils. *Geochimica et Cosmochimica Acta*. 65. 1087-1099.
- Sulpizio, R., Lucchi, F., Forni, F., Massaro, S., and Tranne, C. (2016). Unravelling the effusive-explosive transitions and the construction of a volcanic cone from geological data: The example of Monte dei Porri, Salina Island (Italy). *Journal of Volcanology and Geothermal Research*. <http://dx.doi.org/10.1016/j.jvolgeores.2016.06.024>
- Torres-Orozco, R., Cronin, S.J., Pardo, N., and Palmer, A.S. (2017a). New insights into Holocene eruption episodes from deposit sequences at Mt. Taranaki (Egmont), New Zealand. *Bulletin of Volcanology*. 79:3.
- Torres-Orozco, R., Cronin, S.J., Damaschke, M., and Pardo, N. (2017b). Diverse dynamics of Holocene mafic-intermediate Plinian eruptions at Mt. Taranaki (Egmont), New Zealand. *Bulletin of Volcanology*. 79:76. 1-27.
- Troll, V.R., Deegan, F.M., Jolis, E.M., Harris, C., Chadwick, J.P., Gertisser, R., Schwarzkopf, L.M., Borisova, A.Y., Bindeman, I.N., Sumarti, S., & Preece, K. (2013). Magmatic differentiation processes at Merapi Volcano: inclusion petrology and oxygen isotopes. *Journal of Volcanology and Geothermal Research*. 261. 38-49.
- Turner, M.B., Cronin, S.J., and Smith, I.E.M. (2008) Eruption episodes and magma recharge events in andesitic systems, Mt Taranaki, New Zealand. *Journal of Volcanology and Geothermal Research*. 177. 1063-1076.
- Turner, M.B., Cronin, S.J., Bebbington, M.S., Smith, I.E.M., and Stewart, R.B. (2009). Integrating records of explosive and effusive activity from proximal and distal sequences: Mt. Taranaki, New Zealand. *Quaternary International*. 246. 364-373.
- VSI, CVGHM (Volcanological Survey of Indonesia, Center for Volcanology and Geological Hazard Mitigation) (2014). G. Kelud, Jawa Timur: Sejarah Letusan (Historical Eruptions). Data Dasar Gunungapi (Volcano Data). Badan Geologi (In Indonesian). <http://www.vsi.esdm.go.id/index.php/gunungapi/data-dasar-gunungapi/538-g-kelud>
- Waikato Radiocarbon Dating Laboratory. (2017). [AMS Processing Technical Report. Radiocarbon Dating Laboratory, University of Waikato.](#)
- Walker, G.P.L. (1981). Plinian eruptions and their products. *Bulletin of Volcanology*. 44. 221-240.
- Westercamp, D. and Traineau, H. (1983). The past 5,000 years of volcanic activity at Mt. Pelee Martinique (F.W.I): Implications for assessment of volcanic hazards. *Journal of Volcanology and Geothermal Research*. 17. 159-185.
- Wohletz, K.H. (1983). Mechanisms of hydrovolcanic pyroclast formation: grain size, scanning electron microscopy and experimental studies. *Journal of Volcanology and Geothermal Research*. 17. 31-63.
- Zen, M.T., and Hadikusumo, D. (1965). The future danger of Mt. Kelut (Eastern Java – Indonesia). *Bulletin Volcanologique*. 28. 275-282.

4. The pre-eruptive magma storage system of the 1990 and 2014 Plinian, and 2007-2008 effusive dome-forming eruptions at Kelut volcano, Indonesia: insights into cyclic transitions in eruptive style

Louise R. Goode¹, Heather K. Handley¹, Chris W. Firth¹, Simon P. Turner¹, Shane J. Cronin², Mirzam Abdurrachman³

¹Department of Earth and Planetary Sciences, Macquarie University, Sydney, NSW 2109, Australia.

²School of Environment, University of Auckland, Private Bag 92019, Auckland 1142, New Zealand.

³Department of Geological Engineering, Bandung Institute of Technology, Bandung 40132, Indonesia.

4.1 Abstract

Kelut volcano, Indonesia, exhibits changes in eruptive styles from cyclic effusive to explosive variants. Since 1920, lava dome-forming episodes are followed by a single, explosive, dome-destroying eruption that occurs every ~21 years. The 1990 eruption was explosive in nature, followed by an emergence of a lava dome 17 years later in 2007-2008. This lava dome was present for 7 years until it was destroyed in the most recent 2014 explosive eruption. Currently the driving forces behind, and processes governing the explosivity of eruptions such as the 1990 and 2014 explosions are unknown. Therefore, studies on the petrography, geochemistry, mineralogy and the pre-eruptive magma storage conditions of these two most recent VEI 4 eruptions are investigated, particularly comparing these eruptive products to that of 2007-2008 dome effusion eruption at Kelut volcano.

Mineral assemblages for all eruptions are similar, and comprise of plagioclase, clinopyroxene, orthopyroxene and titanomagnetite. Amphibole is only found in one 2014 sample. The same mineral assemblages are observed in glomerocryst clots in all samples. The complex textures of the minerals include plagioclase with single or multiple sieve-textured zones, and clinopyroxenes that mantle orthopyroxenes with resorbed cores. Complex oscillatory zonation patterns show large, sometimes up to 40 mol.% variations in anorthite from core to rim, with <10 % variations between individual zones in the 1990 and 2014 plagioclase, and are dominantly normally zoned. Major and trace elements of the 1990, 2007-2008 and 2014 eruptions are homogeneous in composition, limited to 54-55 wt. % SiO₂, and identify a singular magmatic source. Clinopyroxenes in equilibrium with the basaltic andesite bulk-rock composition gave reliable thermobarometry estimations for all eruptions. Average temperatures (~1030 °C) for clinopyroxene crystallisation are comparable between all eruptions. Pressure estimates reveal crystallisation from 14 to 2 km, with two dominant storage regions at ~5 and 11 km depth for clinopyroxene crystallisation for all eruptions, where they are stalled at the lithological boundaries in the crust. This, coupled with the homogeneity in bulk-rock compositions and variety of mineral textures suggests that a complex interplay of processes are occurring in the magma plumbing system beneath Kelut. Open-system processes dominate interactions between various parts of the plumbing system. Regular, discrete injections of volatile-rich, mafic magmas at depth mean that frequent mixing events with a shallower, resident, more evolved magma are recorded in anorthite and Fe fluctuations in some plagioclase. These injections mobilise earlier-crystallised orthopyroxene and plagioclase, and the interaction of magmas results in resorbed cores. The continuous small influxes of this magma allow for efficient mixing and thermal buffering of the system at shallower levels, and is responsible for the homogeneity of the bulk-rock, and complexity observed in the sieve-textures and zoning in plagioclase. Remobilisation from depth, and remelting of cumulate xenoliths and glomerocryst clots is also responsible for buffering the magmatic system.

The results show little variation temporally, and thus the storage conditions and pre-eruptive processes for the explosive 1990 and 2014 eruptions, and effusive 2007-2008 eruption are the

same. Therefore, this suggests that the magmatic processes taking place between these eruptions, such as discrete additions of volatile-rich, mafic magma into the system, and magma mixing, were not substantial enough to drive the more explosive eruptions at Kelut. Therefore, the transitions in eruptive style are likely attributed to other physical processes that are of greater influence on the eruptive style. The gradual addition of volatiles into the magma from mafic influxes, coupled with the 7-year presence of a conduit-capping lava dome will have inhibited volatile escape. This results in eventual magma overpressure, driving magma ascent and subsequently causes an explosive eruption. The interplay between the addition of volatiles, and the ability of those volatiles to escape is responsible for the variation in eruptive styles at Kelut for the past ~100 years.

Key words: Kelud, lava dome, explosive, plinian, effusive, homogeneity, sieve-textures, oscillatory zoning, storage regions

4.2 Introduction

Mineralogical and petrological studies of large volcanic eruptions are important in revealing, characterising and understanding the processes occurring in the magmatic system at depth. Records held in the textural variations and chemistry of the rocks and minerals can be utilised to unravel magmatic processes, such as crystal fractionation, magma recharge, magma mixing, volatile dissolution and crustal assimilation (Sparks et al., 1977; Davidson and Tepley, 1997; Blundy and Cashman, 2001; Couch et al., 2001; Gertisser and Keller, 2003; Humphreys et al., 2006; Chadwick et al., 2007; Troll et al., 2013; Cassidy et al., 2016). An understanding of such processes is vital in order to characterise the evolution of the magma plumbing system, and how this governs the style of eruptions, particularly in the context of transitions in eruptive styles.

Volcanoes worldwide commonly exhibit changes in eruptive styles from effusive to explosive variants, such as the Soufrière Hills volcano, West Indies (e.g., Druitt et al., 2002; Edmonds and Herd, 2007), Stromboli, Italy (e.g., Ripepe et al., 2005, 2007), Shiveluch, Kamchatka (e.g., Dirksen et al., 2006; Van Manen et al., 2012; Zharinov and Demyanchuk, 2013), Novarupta, Alaska (e.g., Adams et al., 2006; Nguyen et al., 2014), Mount Taranki, New Zealand (e.g., Platz et al., 2007), Colima, Mexico (e.g. Zobin et al., 2002; Varley and Taran, 2003; Lavallée et al., 2012), and regionally such as Merapi volcano (e.g., Preece et al., 2014, 2016). Reasons attributed to the transition in eruptive behaviour are those that contribute to eventual magma chamber overpressure and a subsequent explosive eruption, and include; the rate of magma supply and increases in magma flow rate, (Woods and Koyaguchi, 1994), influxes of mafic magma, mixing events (Sparks et al., 1977), chemical differences resulting in changes to magma viscosity and rheology with crystallisation of the magma (Edmonds and Herd, 2007), and the exsolution of gases and gas flux (Cashman and Blundy, 2000; Ripepe et al., 2005; Adams et al., 2006), fragmentation of magma, and changes in magma ascent rates (Castro and Gardner, 2008; Preece et al., 2016). Textural and petrological analysis of explosive and effusive activity can determine the pre- and syn-eruptive crystallisation and degassing processes to analyse driving forces behind the eruptions. These are established by analysing the whole rock major and trace elemental compositions, mineral compositions and thermobarometry of samples from the different eruptions as case studies.

Such transition in eruptive styles is also observed at Kelut volcano, in East Java, Indonesia (Fig. 1). Since 1920, lava dome forming eruptions occur on average every ~33 years. Each dome-forming episode is followed by a single, explosive (VEI 4), dome-destroying eruption that occurs every ~21 years on average. The formation and subsequent destruction of the dome appears to be cyclic at Kelut. However, there are earlier indications of dome growth much earlier in 1379 (Zen and Hadikusumo, 1965; Bourdier et al., 1997; Jeffery et al., 2013). The most recent eruption of Kelut in 2014 was an explosive plinian volcanic explosivity index (VEI) 4 eruption, similar to the last explosive eruption in 1990 (also VEI 4), and destroyed the pre-existing 2007-2008 lava dome (GVP, 2014). Past studies on Kelut have only focused on the 1990 and 2007-2008 eruptions. The pyroclastic deposits of the explosive 1990 eruption was investigated by Bourdier

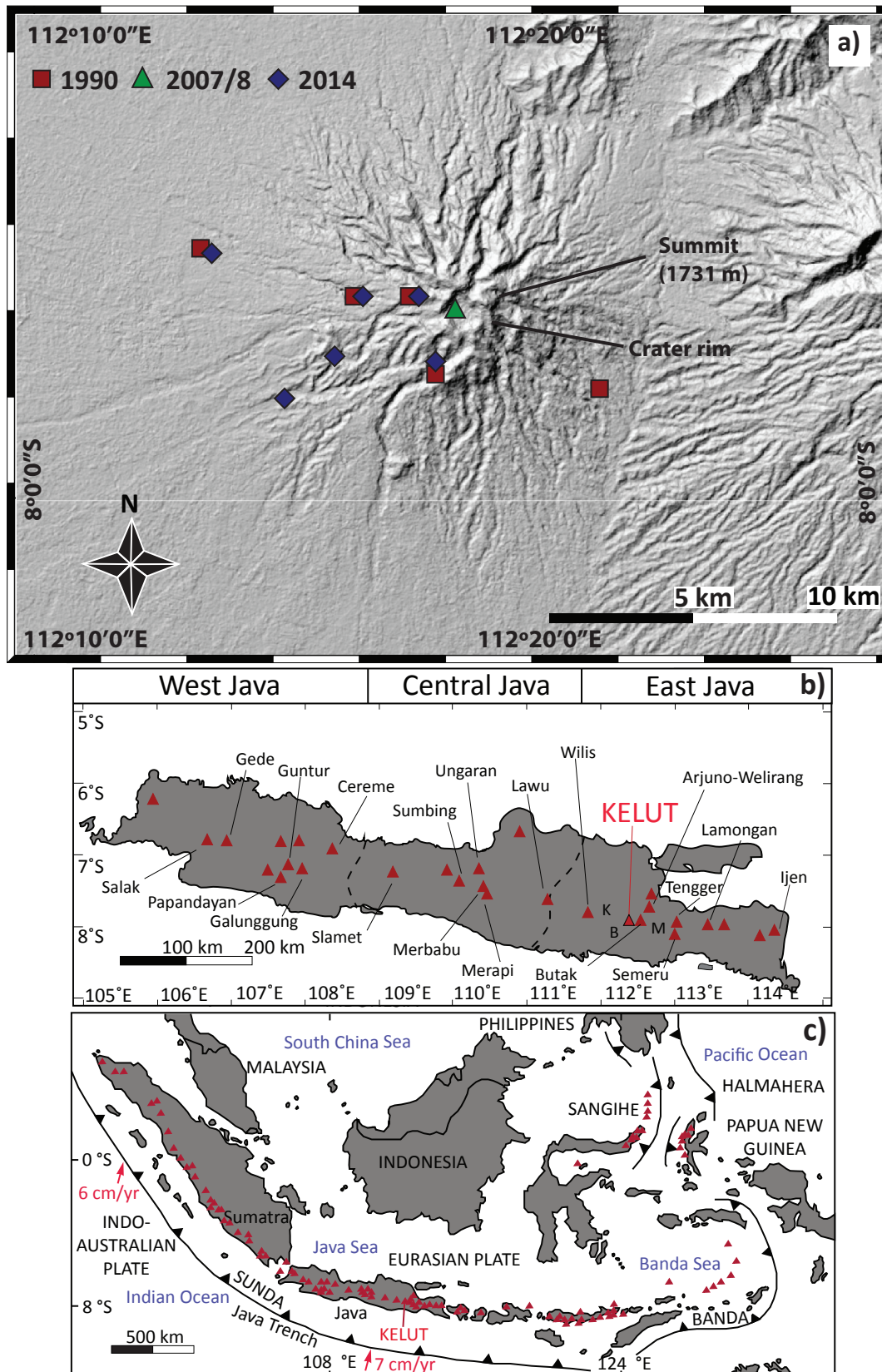


Figure 1: Maps showing Kelut, Java island, and the surrounding general tectonic setting. a) Digital Elevation Model of Kelut, with sample locations marked. Red circles indicate 1990 eruption sample location, green triangles from the 2007-2008 eruption sample location, and blue diamonds from the 2014 eruption sample location. b) Island of Java with volcanoes marked by red triangles (after GVP, 2015), showing the location of Kelut volcano. Letters show the locations of major population centres K – Kediri, B – Blitar and M – Malang around Kelut. c) Map of the general tectonic setting of the Sunda Arc and surrounds (modified after Gertisser & Keller, 2003; Handley et al., 2014).

et al. (1997), and an in depth study of the petrology and mineralogy of the 2007-2008 effusive, 8-month long lava dome eruption by Jeffery et al. (2013). However, the driving forces behind and processes governing the explosivity of eruptions such as the 1990, and the most recent 2014 episodes are unknown. Therefore, studies on the petrography and mineralogy of these two most recent explosive VEI 4 eruptions are needed, particularly comparing these eruptive products to that of 2007-2008 dome effusion eruption at Kelut volcano. Petrological and mineralogical studies on other Indonesian volcanoes e.g., Merapi (Chadwick et al., 2007; Costa et al., 2013; Preece et al., 2014), Krakatau (Dahren et al., 2013), Gede (Handley et al., 2010), and Ijen (Handley et al., 2007) to name a few, indicate that the magma plumbing systems are complex, and involve a complex interplay of magmatic processes such as recharge, mixing and crustal assimilation, that govern the style and recurrence of eruptions. Kelut is one of the most hazardous and active volcanoes in Java (Bourdier et al., 1997; van Bergen et al., 2000; Jeffery et al., 2013), therefore detailed petrological, mineralogical and geochemical studies are vital in order to better understand the driving forces behind higher magnitude eruptions.

This paper presents new petrographic, mineralogical and geochemical data on deposits of the 2014 explosive eruption, which are compared with new data on the 1990 explosive and 2007-2008 dome forming eruptions. The data are used to determine: 1) the pre-eruptive magma plumbing system dynamics, for example storage and crystallisation depths of magma for each eruption, and 2) understanding what drives the transitions in eruption styles at Kelut, and add this into the context of understanding the full range of eruptive behaviour that Kelut can produce.

4.2.1 Geological and tectonic setting

Kelut volcano is located on the island of Java in the Sunda arc subduction system, which includes 78% of Indonesia's active volcanoes and stretches over 3000 km from the Andaman Islands to Flores in the Banda Sea (Hamilton, 1979; Hall, 2002; Fig. 1). The Indo-Australian plate is being subducted beneath the Eurasian plate, at a rate of around 6-7 cm/yr⁻¹ (Hamilton, 1979). Detailed accounts of the tectonic setting are given by van Bemmelen (1949), Hamilton (1979) and Hall (2002, 2011). Present day active volcanism on Java has been grouped into three distinct regions: West, Central and East Java (Fig. 1). This is largely based on major structural and tectonic divisions, magma petrogenesis, and volcano morphology associated with significant crustal boundaries (e.g., Hall et al., 2002; Smyth et al., 2005, 2007; Handley, 2006; Clements et al., 2009; Handley et al., 2014).

Kelut, in eastern Java, is located ~70 km west of the Semeru-Bromo-Tengger massif, and ~210 km east of Merapi volcano (Fig. 1). Wheller et al. (1987) suggest that the area between Merapi and Kelut is an extinct sector of the arc, containing the volcanoes of Wilis and Lawu that only experience solfataric activity and have not erupted since 1885. Therefore Kelut marks the eastern continuation of volcanism. The volcano is thought to lie on a basement of Cretaceous arc/ophiolitic material, overlain by 8-11 km of volcanoclastic crustal sediments, and shallow marine

clastic sediments and carbonates (Smyth et al., 2005; Smyth et al., 2008). The basaltic andesite stratovolcano of Kelut was constructed by several lava flows and lava domes, pyroclastic density current (PDCs), tephra falls, and lahar deposits (Wirakusumah, 1991; GVP, 2014). The currently active crater sits within a horseshoe-shaped caldera on the west side of the volcano, and periodically holds a summit crater-lake (Jeffery et al., 2013).

4.2.2 Eruptive and geologic history

Kelut has erupted 34 times since AD 1000 (Siebert et al., 2011; GVP, 2014a), typically with VEI 3 to 4 subplinian and plinian eruptions, although a VEI 5 eruption occurred in 1586 (Zen and Hadikusumo, 1965; De B lizar et al., 2012; GVP, 2014). A pattern of lava dome growth and subsequent destruction of the dome by an explosive eruption has been observed over the last century. A VEI 4 explosive eruption in 1919 was followed by effusive lava dome growth in 1920 (Zen and Hadikusumo, 1965; Hadikusumo, 1974; GVP, 2014). This lava dome was destroyed in 1951 by a VEI 4 explosive eruption (GVP, 2014). Following another VEI 4 eruption in 1966, a dome was also recorded in the crater 1 year later. The 1967 lava dome was destroyed 23 years later by the 1990 VEI 4 explosive eruption (Bourdier et al., 1997; GVP, 2014). Due to the lack of detailed eruption history pre-1901, it is possible that this pattern of alternating effusive and explosive eruptions existed in the past but the less explosive, smaller-scale lava dome effusions were not recorded. Several remnant andesitic lava domes surround the summit area of Kelut (Wirakusumah, 1991) suggesting that there were more periods of dome effusion other than those recorded in the eruptive records. Full details of Kelut's eruptive history are given in Chapters 2 and 3.

The 1990 eruption destroyed the 1967 lava dome and also the surrounding summit area. The opening stage of the eruption on 10 February 1990 was marked by several short, and discrete phreatomagmatic explosions, followed by a main plinian eruption lasting around 4 hours (GVP, 1990; GVP, 1990a; Bourdier et al., 1997). The chronology of the eruption, including the deposits and eruption dynamics are well documented by Bourdier et al. (1997). Widespread PDC, tephra fall and syn-eruptive lahar deposits were studied (Bourdier et al., 1997a). In April of the same year, an embryonic dome was observed in the crater bottom, but this was soon submerged by a crater lake (Bourdier et al., 1997).

No eruptive activity was recorded at Kelut from the 1990 eruption until November 2007, when increased seismic activity and an increase in lake water temperature accompanied the extrusion of a lava dome in the crater lake. This lava dome continued to grow until May 2008 to a volume of approximately $3.5 \times 10^7 \text{ m}^3$, almost completely displacing the crater lake (GVP, 2008; Siebert et al. 2011; GVP, 2012; Jeffery et al. 2013).

The subsequent VEI 4 eruption on 13 February 2014, followed a 6-year period of quiescence. The eruption disrupted approximately 40 flights across the Asia-Pacific area due to the south-west dispersal of the eruption column. Ash fallout occurred up to 240 km west, north, and south of the

volcano (GVP, 2014; Kristiansen et al., 2015). A total of seven fatalities were reported due ash accumulating on roofs, causing roof collapse in the Malang region (GVP, 2014). This was the most recent eruption of Kelut to date. The 2014 eruption had an initial small-scale explosion followed by a more powerful second explosion, with an entire eruption duration of approximately 4 hours (GVP, 2014; Caudron et al., 2015; Kristiansen et al., 2015; Chapter 2). Small phreatic eruptions continued to occur until 20 February 2014 (GVP, 2014). This eruption was similar in style, and the volume of erupted material to the 1990 eruption (0.10 km³ in 2014, 0.13 km³ in 1990; GVP, 2014a), with PDCs, tephra falls (and south-west dispersal of the eruptive column) and syn- and post-eruptive lahars. Figure 2 shows a compiled stratigraphic section of the 2014 eruptive deposits from which 3 major eruptive stages are identified. Stage 1 is identified as the onset eruptive phase, marked by an initial small magnitude explosion, earliest reports suggest this explosion occurred around 22:30, lasting only ~15 to 30 minutes (Chapter 2; Caudron et al., 2015; Nakashima et al., 2016), producing low run-out PDCs. Stage 2 is identified as the start of the second, larger magnitude, plinian explosion that followed the first, earliest reported at 23:00, and lasting until around 01:00 local time, which also produced PDCs. The final stage of the 2014 eruption (stage 3) is identified as when the eruption reached the climax around 01:00 to 02:00 local time, producing pumice-rich tephra falls.

Kelut volcanic rocks are calc-alkaline basaltic andesites and andesites (Kemmerling, 1921; Whitford, 1975; Zaennudin et al., 1987; Bourdier et al., 1997; Jeffery et al., 2013). The eruptions have become gradually more mafic in composition over time from andesite to basaltic andesite, although no time constraints exist as to when this transition occurred (Jeffery et al., 2013). However, the longer eruptive sequence shows compositional changes from glass shards from ~64 to 72 wt.% SiO₂ over a ~1500 year period, governed by periodic magma mixing due to mafic influxes and recharge events (Chapter 3). The typical phenocryst assemblage of the 2007-2008 lava dome consists of plagioclase, orthopyroxene, clinopyroxene and magnetite. Amphibole is present in the more silica-rich samples and is also common in gabbroic cumulate nodules (Jeffery et al., 2013). Textural disequilibrium, such as resorbed or rounded cores and rims, reverse and oscillatory zoning, and sieve-textured cores, are commonly observed in the minerals, similar to those described in other Javanese volcanic rocks, e.g., Gede and Merapi (Whitford, 1975; Handley et al., 2010; Costa et al., 2013). A detailed investigation into the textures and mineral chemistry of the 2007-2008 dome samples, along with crystal size distribution (CSD) analysis, and major and trace element data, suggested that pre-eruptive magma mixing, and decompression-driven resorption, degassing and crystallisation plus crustal assimilation occurred prior to the extrusion of the 2007-2008 dome (Jeffery et al., 2013).

4.3 Methodology and analytical techniques

Petrographic studies were conducted on 22 thin sections of juvenile rocks to determine textural characteristics and phenocryst abundance, size and shape. These include 15 samples from the

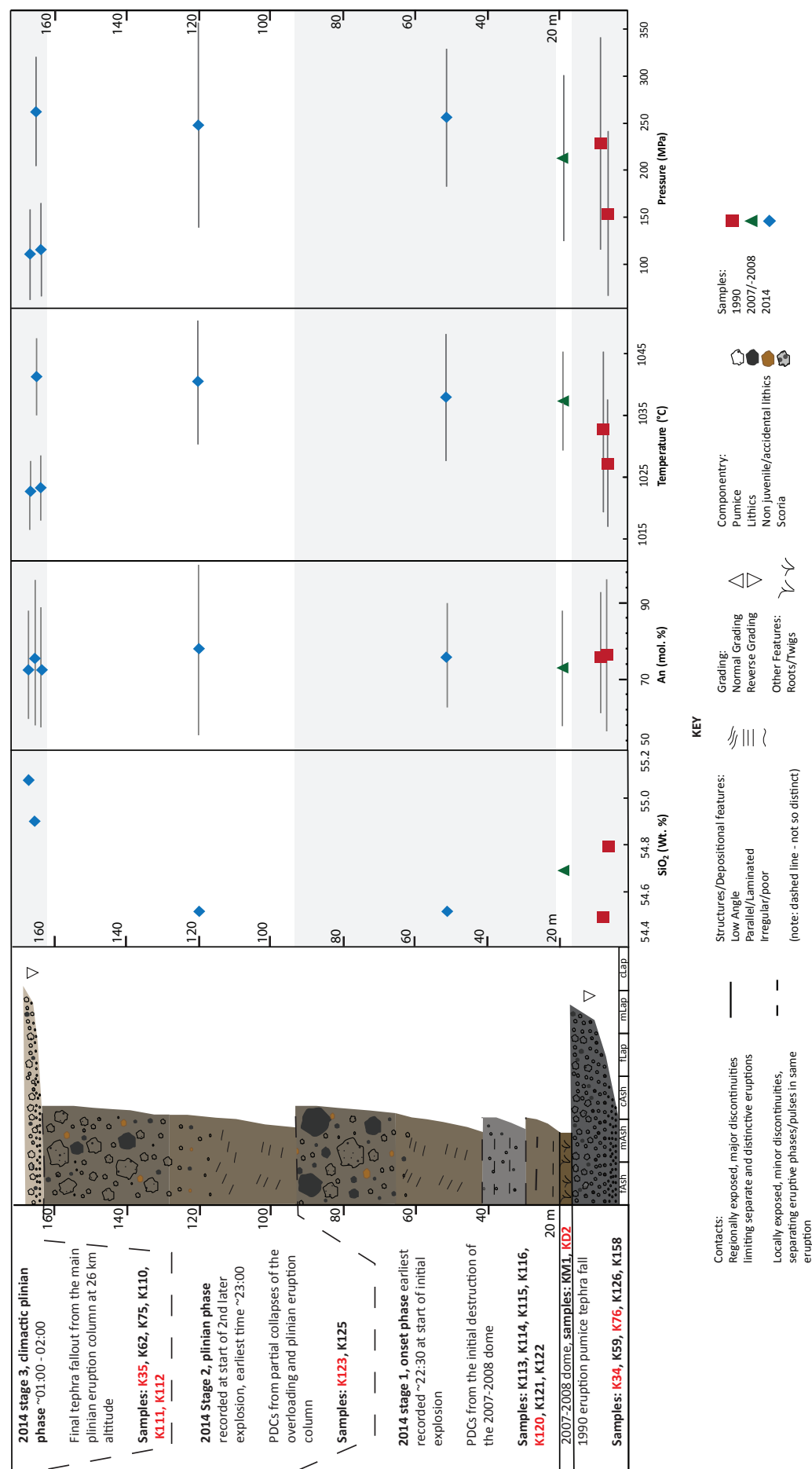


Figure 2: Overall variation in geochemistry, temperature and pressure estimates with height in the stratigraphic succession of deposits, from the 1990 to 2007-2008 to 2014 eruptions. Times reported for the stages of the 2014 eruptions are in local time. See key for an explanation of bedding structures and componentry for each layer. SiO₂ (wt.%) values are from whole rock major element data. Anorthite (An, mol.%) contents are from average plagioclase analyses for each sample, with error bars showing the standard deviation. Temperature and pressure estimates were calculated using the clinopyroxene-liquid barometer (Neave and Putirka, 2017) and thermometer (Putirka, 2008), displaying the average and standard deviation as error bars.

2014 eruption, five from the 1990 eruption, and two from the 2007-2008 lava dome eruption. A petrographic description of all samples is given in Supplementary Table 1, Appendix C. Modal proportions of minerals, vesicles and groundmass glass were calculated using JMicro Vision software. Representative samples of the different stages of the 2014 eruption (tephra falls and PDC samples; see Supplementary Table 1 for the chronology of units), the 1990 and the 2007-2008 eruptions were then chosen for mineral analyses: one PDC sample from 2014 stage 1 (K120), one PDC sample from 2014 stage 2 (K123), and 3 tephra fall samples from stage 3 of the 2014 eruption (K111, K112, K35); two 1990 tephra fall deposits (K34, K76); and one 2007-2008 lava dome clast (KD2). Mineral analyses were performed on carbon-coated polished slides. The major element contents of plagioclase, clinopyroxene, orthopyroxene and Fe-Ti oxides were analysed using CAMECA SX100 electron microprobes (EMP) at the Macquarie University GeoAnalytical facility, Australia, and at the Research School of Earth Sciences, Australian National University (ANU), Australia. Spot and line analyses were taken using a 5 μm beam, an acceleration voltage of 15 kV and beam current of 10-20 nA on each instrument. Spot and line analyses on two of each phenocryst for each sample that were previously analysed were repeated on the second instrument in a nearby location at the same running conditions. These results were compared, and all compositions were within 1 standard deviation of each other to ensure all data is comparable. Standard names used to calibrate the instruments, along with detection limits are included in Supplementary Table 2, Appendix C. Silicate minerals and pure metals were routinely analysed in-run as secondary standards to monitor accuracy and precision during analyses. Each point analysis peak counting times was run for a total of around 4.5 minutes for silicate minerals, and around 6.5 minutes for metal oxides to ensure minimum error in detection limits on both instruments. Ferric iron contents were estimated using the stoichiometric methods of Lindsley (1983) for pyroxenes and Droop (1987) for spinel.

Whole rock major element contents and trace element concentrations were determined for 16 selected pumice lapilli fragments (greater than 1 mm) from the 2014 tephra falls (K35, K75, K62, K112) and PDCs (K113, K115, K116, K120, K123, K125), the 1990 tephra falls (K34, K59, K76, K158), one PDC (KD3) and the 2007-2008 lava dome (KD2). Samples are described in Supplementary Table 1, Appendix C. Clasts were sonicated in deionised water several times until clean then slowly dried. Weathered surfaces were removed before the sample was crushed to a fine powder in an agate mill. Glass discs were prepared and fused with a lithium metaborate/tetraborate flux, and analysed for whole rock major element contents by X-ray fluorescence (XRF) spectrometry on a PANalytical Axios 1KW WDXRF spectrometer at Macquarie University GeoAnalytical (MQGA), Australia. Loss on ignition was reported as the weight difference after ignition for 2 hours at 1,000°C. Dissolved rock powders were analysed for trace element concentrations using an Agilent 7500 series instrument by inductively coupled plasma mass spectrometry (ICP-MS) calibrated using international rock standards BCR-2. Accuracy and precision was checked by analysing BIR-1 and BHVO-2 internal standards routinely in-run, and the samples were also run twice. All analysed elements are within 2σ of published standard values. Drift was corrected with

a spike containing Li6, Ar, Rh and In. Trace elemental analyses were also undertaken the MQGA at Macquarie University.

4.4 Results

4.4.1 Petrography and Mineralogy

Full petrographic descriptions of the 1990, 2007-2008 and 2014 rocks are presented in Supplementary Table 1, Appendix C. The mineral modes, grain size, and types of groundmass and mineral textures of samples selected for mineral chemical analysis are given in Table 1. Classification of mineral textures, zoning patterns and grain size are described in Tables 2 (plagioclase), 3 (clinopyroxene), and 4 (orthopyroxene). Samples from three different stages of the 2014 eruption (as discussed in Section 2): stage 1, K120; stage 2, K123; stage 3, K111, K112, K35, two samples from the 1990 eruption (K34, K76), and one from the 2007-2008 lava dome (KD2) were selected for further geochemical analyses. Representative mineral chemistry is shown in Tables 5 (plagioclase), 6 (clinopyroxene), 7 (orthopyroxene), 8 (titanomagnetite), and 9 (amphibole). All mineral chemistry and end member calculations are presented in the Supplementary Table 2, Appendix C.

4.4.2 General petrography of the 2014, 1990 and 2007-2008 samples

Phenocryst (>300 to 2500 μm) and microphenocryst (>100 to 300 μm) populations of the 2014, 1990 and 2007-2008 samples are comparable. The 2014 samples consist of plagioclase (groundmass and vesicle free, ≤ 78 vol.%), clinopyroxene (≤ 9 vol.%), orthopyroxene (≤ 9 vol.%), and titanomagnetite (≤ 6 vol.%), with rare or absent amphibole (present only in 2014 sample K123). The 1990 samples have similar overall mineral assemblages (minus amphibole), textural features and crystal sizes to the 2014 samples. The 2007-2008 lava dome predominantly consists of plagioclase (63 vol.%), with higher amounts of clinopyroxene and orthopyroxene than the 2014 and 1990 samples (at 15 and 16 vol.%, respectively). Amphibole is not present in the 2007-2008 samples.

The juvenile 2014 and 1990 pumice tephra fall and PDC samples are porphyritic, glomeroporphyritic and vitrophyric in texture. They contain are large, coalesced bubbles up to 4000 μm in length, with some smaller vesicles <100 μm long. Vesicles can make up to 40 vol.% of the 2014 and 1990 samples (Table 1). Crystal contents in 1900 and 2014 samples make up ≤ 50 vol.% of samples, with groundmass totalling ≤ 40 vol.% of samples. Therefore the groundmass textures in most 2014 and 1990 tephra fall and PDC samples fall into Types 1 and 2 (Table 1; Fig. 3d). Groundmass texture Type 1 describes a dominantly glassy groundmass (≥ 30 vol.% of sample), with large vesicles ~ 500 to 2000 μm in length (Fig. 3). Microphenocrysts in Type 1 samples include plagioclase, clinopyroxene, titanomagnetite and very rarely orthopyroxene. Plagioclase microlites are also present (Fig. 3d). Type 2 groundmass texture is characterised by a dominance in larger sized vesicles (≤ 4000 μm) with some smaller vesicles (<100 μm), and less groundmass

Table 1: Location and petrographic description of all samples

Table 1. Locational and petrographic description of air samples																														
Eruption	Deposit type	Sample	Sample Location (°S, °E)	Mineral modes						Grain Size	Groundmass Type Type 1 Type 2 Type 3	Plagioclase Type 1 Type 2 Type 3				Clinopyroxene Type 1 Type 2 Type 3 Type 4				Orthopyroxene Type 1 Type 2 Type 3 Type 4				Titanomagnetite Type 1 Type 2		Glomerocryst Type 1 Type 2 Type 3				
				Plag	Cpx	Opx	Titmag	Amph	G.mass			Vesicles	Melt inclusions	Type 1	Type 2	Type 3	Type 4	Type 1	Type 2	Type 3	Type 4	Type 1	Type 2	Type 3	Type 4		Type 1	Type 2		
1990	Fall	K34	7°56'09.65" 112°16'57.92"	33.2	3.9	4.0	2.7	0.0	33.8	21.5	0.8	Plag: 2200 - 200µm (micro ≤100µm); Cpx: 1700 - 350µm; Opx 1500 - 400µm; Oxides: 300 - <100µm	x	x	x	x	x	x	x	x	x	x	x	x	x	x	x	x		
1990	Fall	K76	7°55'36.28" 112°14'30.18"	23.8	2.6	2.7	1.7	0.0	30.2	38.7	0.4	Plag: 2000 - 250µm; Cpx: 800 - 300µm; Opx: 1200 - 350µm; Oxides: 250µm	x	x	x	x	x	x	x	x	x	x	x	x	x	x	x	x		
2007-2008	Lava dome	KD2	7°56'16.29" 112°18'9.95"	38.9	9.0	9.9	3.9	0.0	30.8	7.5	0.0	Plag: 2300 - 150µm; Cpx: 2000 - 150µm; Opx: 1900 - 200µm; Oxides: 200µm	x	x	x	x	x	x	x	x	x	x	x	x	x	x	x	x	x	
2014	PDC	K120	7°57'19.21" 112°17'47.81"	24.4	9.6	2.5	1.1	0.0	36.5	25.0	0.9	Plag: 1500 - 150µm; Cpx: 2000 - 200µm; Opx: 750 - 200µm; Oxides: 150µm	x	x	x	x	x	x	x	x	x	x	x	x	x	x	x	x	x	x
2014	PDC	K123	7°57'19.20" 112°17'47.80"	35.3	8.1	4.1	3.0	0.1	27.4	21.8	0.2	Plag: 1100 - 150µm; Cpx: 1500 - 300µm; Opx: 1100 - 250µm; Oxides: 200µm	x	x	x	x	x	x	x	x	x	x	x	x	x	x	x	x	x	x
2014	Fall	K111	7°57'53.1" 112°15'19.32"	18.0	4.6	2.8	2.2	0.0	27.9	43.7	0.9	Plag: 900 - 250µm; Cpx: 900 - 250µm; Opx: 800 - 450µm; Oxides: 250µm	x	x	x	x	x	x	x	x	x	x	x	x	x	x	x	x	x	x
2014	Fall	K112	7°57'53.1" 112°15'19.32"	24.3	4.3	3.4	2.4	0.0	24.3	40.6	0.6	Plag: 1200 - 150µm; Cpx: 2200 - 200µm; Opx: 850 - 200µm; Oxides: 150µm	x	x	x	x	x	x	x	x	x	x	x	x	x	x	x	x	x	x
2014	Fall	K35	7°56'09.65" 112°16'57.92"	30.0	5.0	4.5	1.9	0.0	33.2	24.8	0.6	Plag: 1600 - 150µm; Cpx: 2500 - 200µm; Opx: 2000 - 250µm; Oxides: 300µm	x	x	x	x	x	x	x	x	x	x	x	x	x	x	x	x	x	x

Included are type of groundmass present in each sample (see text for description), and the textures of the minerals plagioclase (see Table 2), clinopyroxene (see Table 3), orthopyroxene (see Table 4), titanomagnetite and type of glomerocrysts present in each sample. Range of crystal sizes presented for each mineral. Noticeable features of each sample from the different eruption dates (2014, 2007-2008, 1990) discussed in text.

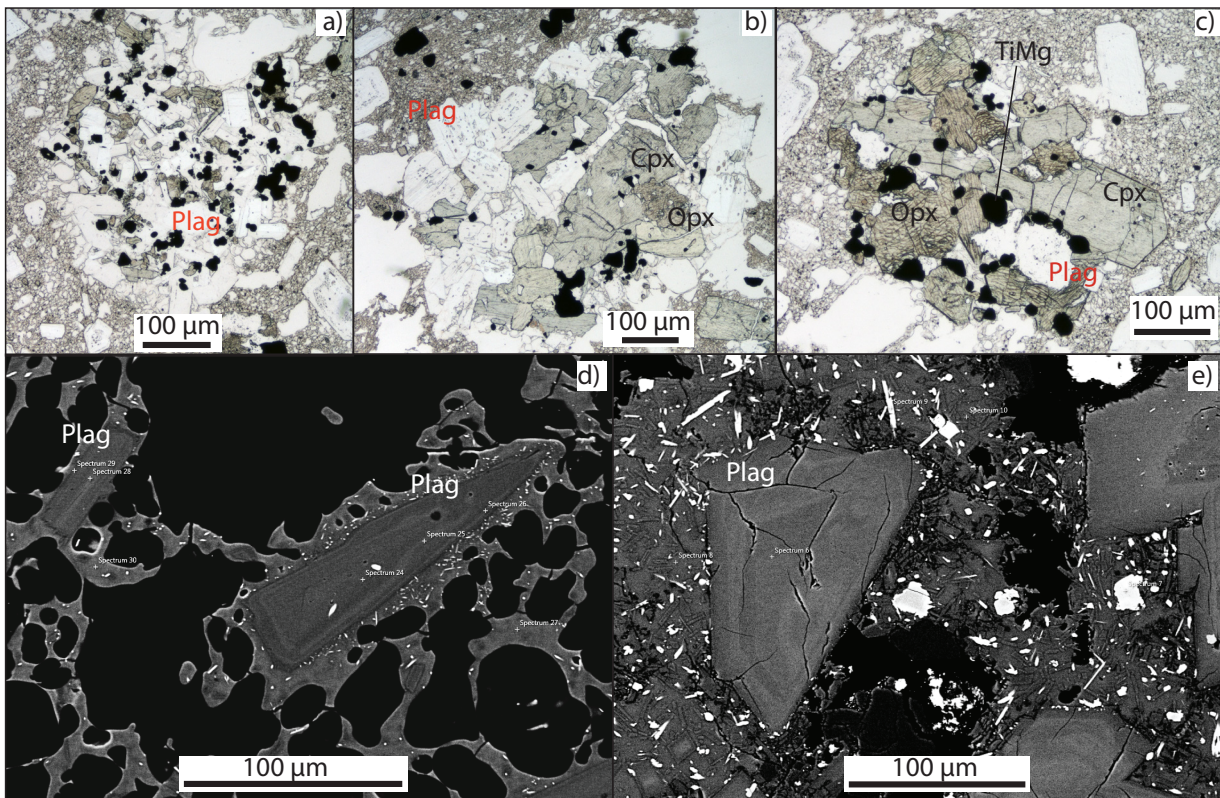


Figure 3: Photomicrographs of glomerocryst and groundmass textures from Kelut samples. a – c are photomicrographs taken on a polarizing microscope at x10 zoom in PPL. a) Glomerocryst Type 1 is plagioclase dominated with lesser clinopyroxene, orthopyroxene and titanomagnetite, from sample K34 (1990). b) Type 2 glomerocryst, is clinopyroxene dominated and from sample K35 (2014). c) Type 3 glomerocryst is orthopyroxene dominated, and is from sample K35 (2014). d and e are SEM images to portray the difference in vesicle rich versus microcrystalline rich groundmass between d) sample K76 (1990) groundmass Type 1, with a small zoned plagioclase microlite. e) Groundmass Type 3 in sample KD2 (2007-2008) which has a higher content of fine grained microlites of plagioclase, clinopyroxene and orthopyroxene and microphenocrysts of plagioclase.

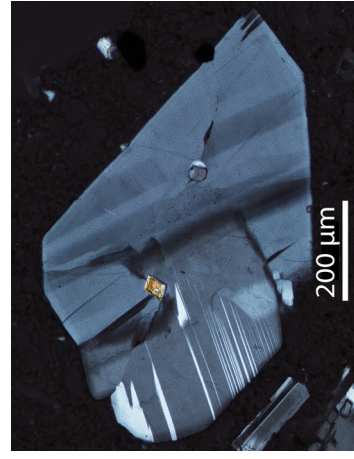
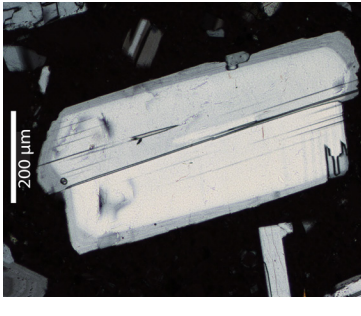
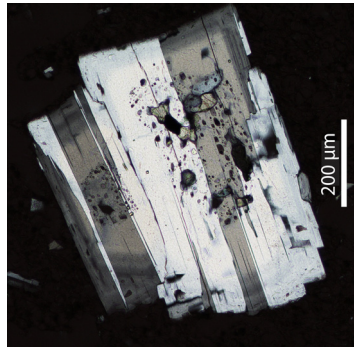
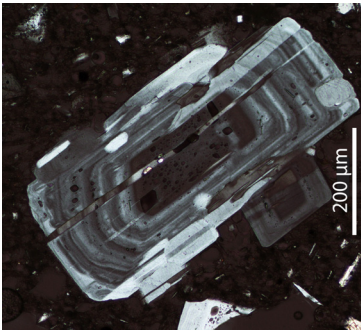
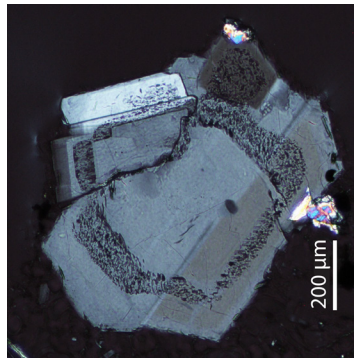
glass (≤ 30 vol.%). Some vesicles in this texture type are elongated and wispy in appearance, especially when deformed around the shape of a phenocryst. The groundmass glass also appears less devitrified as it is lighter in colour. Vesicles are larger, and phenocrysts are less common in this texture than Type 1, at 27-34 vol.%, to 35-50 vol.% respectively across samples (Table 1). Microphenocrysts and microlites of the same minerals are present in Type 2 groundmass, but it is overall less microcrystalline than Type 1 due to the presence of smaller vesicles.

The two samples of the 2007-2008 lava dome (KM1 and KD2) are porphyritic and glomeroporphyritic, although generally more phaneritic than the explosive samples (2014 and 1990 eruptions). The 2007-2008 lava dome samples are denser than the pumice samples, containing less vesicles (< 10 vol.%), and are more crystalline than Types 1 and 2, with 62 vol.% phenocrysts (compared to 27-50 vol.% of 2014 and 1990 samples), and a more microcrystalline groundmass than the 2014 and 1990 samples (31 vol.%; Fig. 3e; Table 1). Therefore, Type 3 groundmass characterises these samples. There is a greater abundance of microphenocrysts and microlites in Type 3, due to the presence of fewer vesicles (Fig. 3e). This groundmass type is exclusive to

Table 2: Main texture descriptions and classification of plagioclase phenocrysts

Type	1			2	3
	a	b	c		
Texture	Sieve textured in the mid and/or rims of phenocrysts with clear cores. Most common texture over all samples. Normal and lamellar twins. Euhedral to subhedral phenocrysts.	Sieve textured in the cores and the mid and rims of phenocrysts. Often in cores and just rims; cores and mid only; or both. Normal and lamellar twins. Euhedral to subhedral.	Sieve textured cores only. If show high degrees of resorption then have more inclusions of pyroxene and iron titanomagnetite. Can be fractured, euhedral and subhedral.	Zoned crystals, completely unresorbed, no inclusions. Can be fractured. Often mid sized and euhedral (unless fractured), and commonly seen in microphenocrysts and microlites. Normal and lamellar twins.	No zoning, common lamellar and growth twins, can have syreate textures. Rarely included, often lath shaped, euhedral. Only seen in smaller crystals (microphenocrysts and microlites)
Zoning	Commonly oscillatory and normally zoned; rarely display reverse, discontinuous and sector zoning.	Normally and oscillatory zoning most common; Reverse zoning most commonly seen in this texture, but still rarely seen. Few sector and convolutedly zoned phenocrysts.	Discretely zoned, often only in outer rims showing normal zonation; Very rarely reversely zoned	Normally zoned. Never exhibit reverse zoning. Can show convolute, sector and discontinuous zonation.	
Inclusions	Melt; melt with cpx ; melt with opx	Melt; opx; cpx; melt with opx; melt with cpx	Melt; cpx; melt and opx; melt and opx; melt, opx and cpx; melt and FeOx; All	n/a	n/a
Size	2000 - 500µm	1200 - 700µm	2200 - 150µm	800 - <100µm	300 - <100µm

Photomicrograph



Plagioclase textures above are found in samples from the 2014, 1990 and 2007-2008 eruptions. Details include zoning patterns, inclusions, size ranges (>300 µm phenocrysts; 300 - 100 µm microphenocrysts; <100 µm microlites). Photomicrographs of each texture type taken on a polarizing microscope at x10 zoom. Note the scale differs on each. Type 1a - sample K111 (2014; XPL); type 1b - sample K34 (1990; XPL); type 1c - sample K35 (2014; XPL); type 2 - sample K123 (2014; XPL); type 3 - sample K35 (2014; XPL).

the 2007-2008 lava dome samples. Microlites in the 1990 and 2014 rocks consist of elongated, lath-shaped plagioclase ($\leq 100\ \mu\text{m}$ in length). Whereas, in the lava dome samples plagioclase, clinopyroxene, orthopyroxene and titanomagnetite occur as microphenocrysts, and all silicate minerals occur as microlites (Fig. 3e).

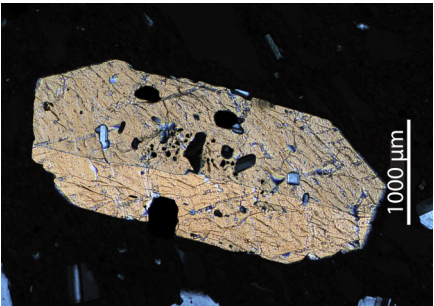
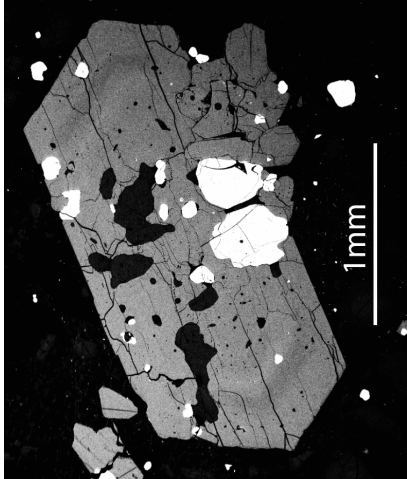
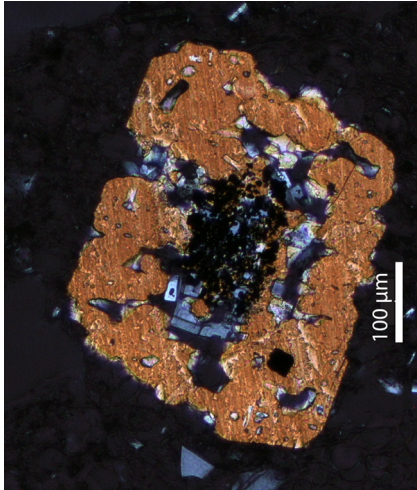
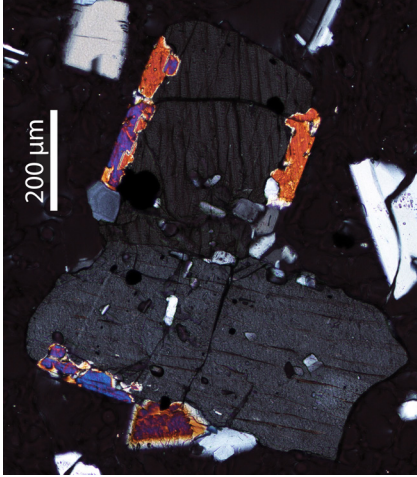
Glomerocrysts or intergrowing crystal clots are observed in all but five 2014 samples, and in all 1990 and 2007-2008 samples. The glomerocrysts display similar overall mineral assemblages, dominated by plagioclase (Type 1; Fig. 3a), clinopyroxene (Type 2; Fig 3b), or orthopyroxene (Type 3; Fig. 3c). Glomerocryst Types 1 and 2 are the most common, whereas Type 3 is less commonly observed in the 2014 samples. Type 3 glomerocrysts are absent from the 1990 samples and the 2007-2008 lava dome samples.

4.4.2.1 Plagioclase

Plagioclase crystals ($300\text{--}2200\ \mu\text{m}$) in all samples are dominantly euhedral to subhedral, and are fractured in some 1990 and 2014 samples. Some crystals from 1990 and 2014 samples appear to have partly rounded crystal edges and irregular shapes. The textural descriptions that characterise plagioclase phenocrysts are presented in Table 2. Type 1 Plagioclase texture is characterised by phenocrysts with resorption or sieve textures, and can be simply or oscillatory zoned, with normal and reverse patterns (Table 2). Type 1a shows sieve textures in the mid regions or rims of phenocrysts with clear cores. These phenocrysts often have larger scale variations in anorthite content associated with larger zoned regions. Type 1b shows sieve textures in the cores, mid regions, and rims of phenocrysts, and display more subtle variations in anorthite due to complex oscillatory zoning patterns. Type 1c plagioclase shows sieve or ‘spongy’ textures in the cores only, with large variations in anorthite from the core to rim of the phenocrysts. Type 2 plagioclase texture is characterised by unresorbed phenocrysts with only normally zoned patterns. Type 3 plagioclase texture shows unzoned with common lamellar twins (Table 2).

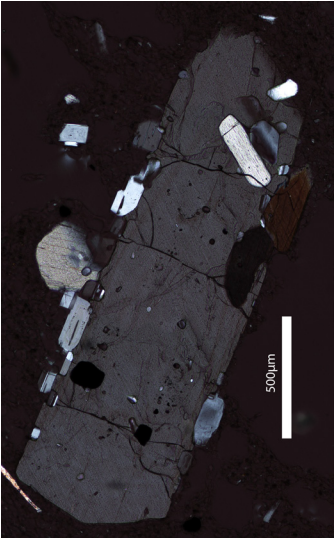
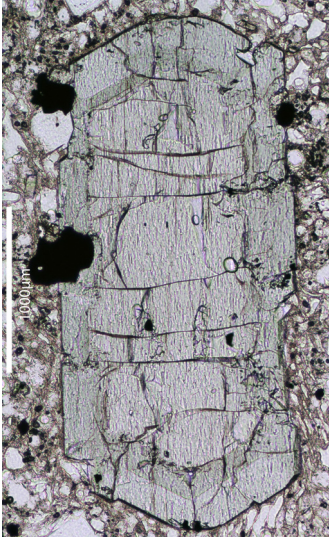
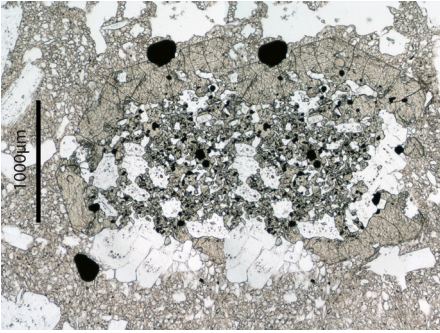
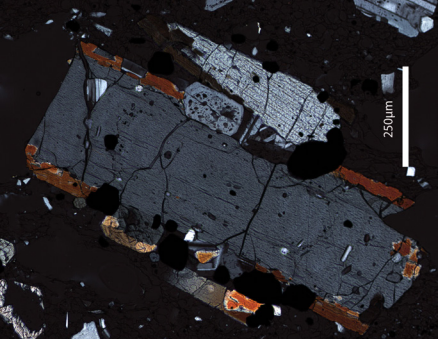
All plagioclase crystal textures are observed in all the samples from all eruptions (Tables 1 and 2), apart from one 1990 sample with an absence texture Type 3. The texture Type 1a and b of plagioclase phenocrysts is in the highest abundance throughout all the 2014 and 1990 samples. Plagioclase Type 2 is also fairly commonly observed. In the 2007-2008 lava dome plagioclase texture Type 1 (specifically Types 1a and 1b) is the most common observed, like that of the 2014 and 1990 plagioclase. Plagioclase less commonly is as heavily included by glass than the 2014 and 1990 samples. Plagioclase texture Type 2 is therefore slightly more commonly seen in the 2007-2008 lava dome samples. Type 3 is present as microphenocrysts and microlites across all samples ($\leq 300\ \mu\text{m}$). Clinopyroxene, orthopyroxene and titanomagnetite are observed as inclusions in plagioclase, dominantly in texture Type 1c.

Table 3: Main texture descriptions and classification of clinopyroxene.

Type	1	2	3	4
Texture	Often single phenocrysts, often twinned. Heavily included, rarely have no inclusions. Euhedral. No or little chemical variation in crystal. Can be fractured. Rarely have phenocrysts touching opx phenocrysts.	Single phenocrysts, or can have growths with opx phenocrysts, often twinned and faintly zoned. Can have sieve textures in the cores and mid/rims, or just cores. Rarely have no inclusions. Euhedral and subhedral. Can be fractured.	Heavily altered/resorbed and embayed. Sometimes has relict opx in the centre poikilitic texture. Can be faintly zoned. Subhedral to anhedral (if completely resorbed).	Forms rims around opx, either on all crystal faces or partially. Often lath shaped, longer in length.
Zoning	n/a	Normal and reversely zoned; concentrically zoned.	Faintly normally and reversely zoned	n/a
Inclusions	Melt; titanomagnetite only; plagioclase and titanomagnetite; plagioclase, titanomagnetite and cpx; plagioclase, titanomagnetite, cpx and opx.	Melt; titanomagnetite only; plagioclase and titanomagnetite; plagioclase, titanomagnetite and cpx; plagioclase, titanomagnetite, cpx and opx.	Melt; plagioclase and titanomagnetite	Rare titanomagnetite and plagioclase
Size	2500 - 2500µm	2500 - 11000µm	2000 - 3500µm	850 - 2000µm
Photo				

Clinopyroxene textures above are found in samples from the 2014, 1990 and 2007-2008 eruptions. Details include zoning patterns, inclusions, size ranges (>300 µm phenocrysts; 300 - 100 µm microphenocrysts; <100 µm microlites). Photomicrographs of each texture type taken on a polarizing microscope at x10 zoom. Note the scale differs on each. Type 1 - K34 (1990; XPL); type 2 - K76 (1990; BSE SEM image); type 3 - sample K112 (2014; XPL); type 4 - sample KD2 (2007-2008; XPL).

Table 4: Main texture descriptions and classification of orthopyroxene.

Type	1	2	3	4
Texture	Single phenocrysts, euhedral and often larger. Negligible chemical variation in the crystals. No melt inclusions. Often twinned	Single phenocrysts, or often growths with cpx phenocrysts, faintly zoned. Euhedral. Rare. Have high relief and alteration. Often twinned.	Heavily altered/resorbed and embayed. If heavily resorbed reacted completely to cpx. Often poikilitic textured. Can be faintly zoned. Subhedral to anhedral (if completely resorbed).	Phenocrysts with cpx rims. Often completely surrounded by cpx (on all crystal faces), or partially. Can see replacement in stages from opx to cpx - some of the opx is very altered by cpx and completely anhedral.
Zoning	n/a	Normally and reversely zoned, rarely faintly concentrically zoned.	Faintly normally and reversely zoned	Opx itself can be faintly concentrically zoned
Inclusions	Titanomagnetite and plagioclase; titanomagnetite; plagioclase	Titanomagnetite and plagioclase; titanomagnetite; plagioclase	Titanomagnetite and plagioclase; titanomagnetite; plagioclase	Rare titanomagnetite and plagioclase
Size	2300 - 400µm	1500 - 250µm	2100 - 400µm	850 - 200µm
Photo				

Orthopyroxene texture above are found in samples from the 2014, 1990 and 2007-2008 eruptions. Details include zoning patterns, inclusions, size ranges (>300 µm phenocrysts; 300 - 100 µm microphenocrysts; <100 µm microlites). Photomicrographs of each texture type taken on a polarizing microscope at x10 zoom. Note the scale differs on each. Type 1: type 1 - sample K35 (2014; XPL); type 2 - sample K123 (2014; PPL); type 3 - sample K34 (1990; PPL); type 4 - sample K76 (1990; XPL).

Table 5: Representative plagioclase analyses (wt. % oxide) with end members (mol. %)

Eruption	1990	1990	2007-2008	2014	2014	2014	2014	2014
Sample	K34	K76	KD2	K120	K123	K111	K112	K35
SiO ₂	50.5	49.5	50.4	49.3	50.3	48.1	50.5	50.8
TiO ₂	/	0.04	0.00	0.03	/	/	0.05	/
Al ₂ O ₃	30.4	31.1	31.3	32.1	31.3	32.2	31.1	29.9
FeO	0.53	0.63	0.55	0.57	0.57	0.58	0.58	0.54
MnO	/	0.01	0.01	0.01	0.02	/	/	/
MgO	0.04	0.04	0.06	0.01	0.01	0.04	0.02	0.04
CaO	14.6	15.1	13.8	14.8	13.6	16.3	13.7	14.4
Na ₂ O	3.56	3.18	3.75	2.98	3.59	2.58	3.57	3.91
K ₂ O	0.04	0.05	0.09	0.05	0.08	0.04	0.07	0.09
Total	99.7	99.6	100.0	99.8	99.4	99.8	99.6	99.7
End Members								
An	74.4	75.7	72.0	75.5	78.4	73.4	76.0	73.8
Ab	25.2	24.0	27.6	24.0	21.3	26.3	23.6	26.0
Or	0.33	0.39	0.42	0.50	0.30	0.31	0.38	0.31

4.4.2.2 Clinopyroxene and orthopyroxene

Clinopyroxene and orthopyroxene phenocrysts in 2014 samples varies from 200 to 2000 μm , up to 1500 μm in 1990 samples and up to 1900 μm in 2007-2008 samples. The textural descriptions that characterise clinopyroxene and orthopyroxene phenocrysts are presented in Tables 3 and 4 respectively. Type 1 clinopyroxene and orthopyroxene textures are characterised by single, twinned, unzoned phenocrysts with some inclusions of plagioclase and titanomagnetite. Clinopyroxene and orthopyroxenes are most commonly observed texture Types 1 and 2 across all samples. Phenocrysts are euhedral and subhedral. Larger phenocrysts ($\geq 1700 \mu\text{m}$) are observed in the 2007-2008 dome sample compared to the 2014 and 1990 samples (typically 200 to 2500 μm and 300 to 1700 μm long, respectively). Type 2 texture for both minerals describes those phenocrysts that are slightly concentrically zoned, although orthopyroxene is generally more uniform in composition. Type 3 texture describes phenocrysts of clinopyroxene and orthopyroxene that contain abundant inclusions (see Tables 3 and 4 for details), or partially or completely resorbed either just at the cores of phenocrysts or throughout the entire crystal. This texture is present in one 1990 sample, four of the 2014 samples, and all of the 2007-2008 samples (Table 1). Type 4 texture is characterised by clinopyroxene that mantles orthopyroxene, either partially on some crystal faces, or completely surrounds the orthopyroxene on all faces. This is more commonly observed in the 2007-2008 samples than the 1990 and 2014 samples (Table 1).

4.4.2.3 Titanomagnetite and amphibole

Titanomagnetite (3-8 vol.%) is present in all samples as microphenocrysts and inclusions in all other minerals. It is more abundant in the 2007-2008 samples than the explosive 1990 and 2014 samples. A single, subhedral amphibole (500 μm long) with inclusions of plagioclase and titanomagnetite is observed in only one sample (K123 from the 2014 eruption).

4.4.3 Mineral chemistry of the 2014, 1990 and 2007-2008 samples

4.4.3.1 Plagioclase

Representative analyses for all plagioclase in all samples are included in Table 5, and ternary classification plots in Figure 4a, b and c. Histograms of plagioclase composition show unimodal distributions of An content in the 2014 samples (Fig. 5). Stage 1 (Fig. 5d), stage 2 (Fig. 5e), and stage 3 (Fig. 5f-h) samples show weakly positively skewed An contents. Anorthite contents in the two 1990 samples show similar ranges to 2014 samples, and both have maximum peaks at 71-75 mol.% An (Fig. 5a, b). K34 (1990) however shows a slightly boarder distribution in composition (Fig. 5a) when compared to K76 (1990) (Fig. 5b) and the 2014 samples. Plagioclase anorthite contents in the effusive 2007-2008 dome sample also show a unimodal distribution, but do not extend to the high An contents observed in the 1990 and 2014 samples (Fig. 5c). The anorthite content of plagioclase cores in several of the 2014 samples and K34 from 1990 show a wide variation in composition, whereas core compositions are more restricted towards higher An contents in K76 from 1990. Plagioclase rims in all 2014 and 1990 samples generally show lower calcium contents relative to the cores, consistent with normal zonation patterns across all samples (Fig. 5). Microlites in the 2014 samples are generally more calcic than the plagioclase rims in

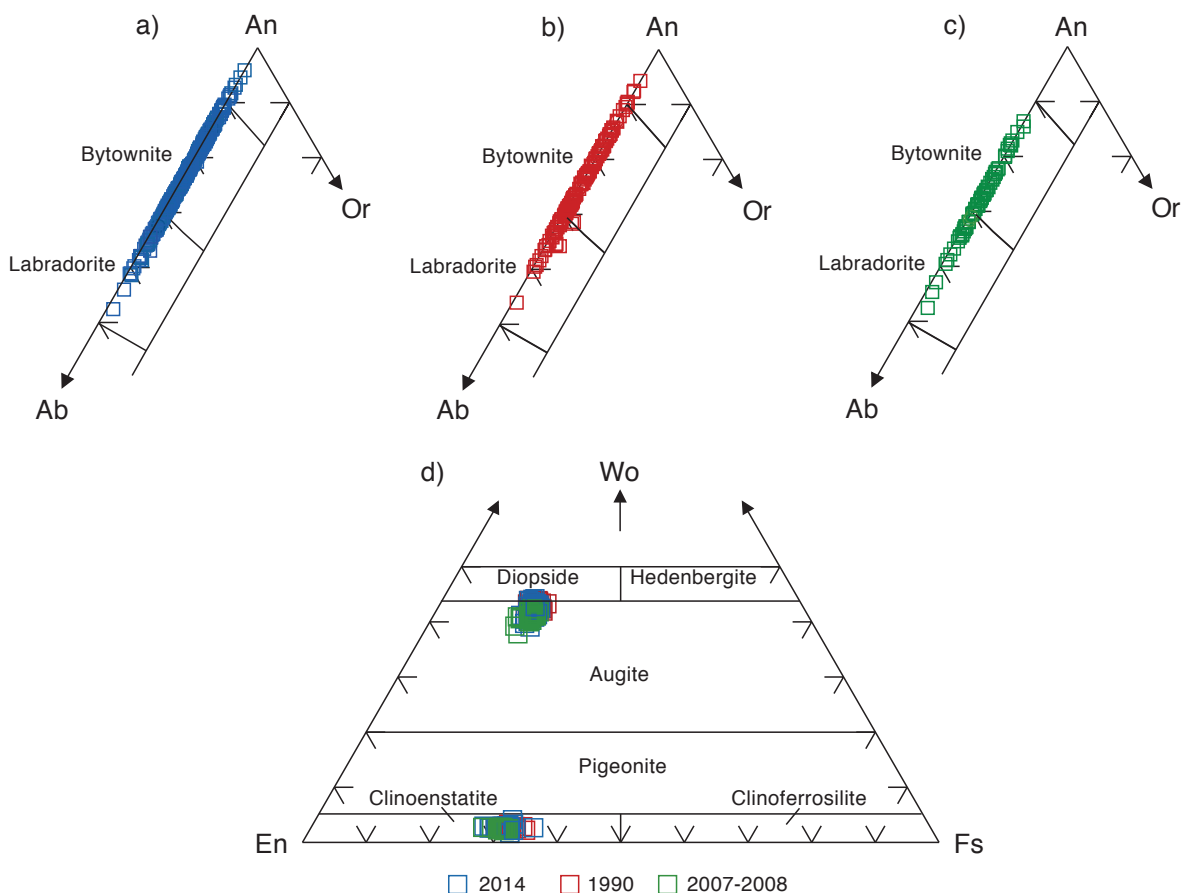


Figure 4: Ternary classification plots of a) analysed plagioclase from the 2014 eruption. b) Analysed plagioclase from the 1990 eruption. c) Analysed plagioclase from the 2007-2008 eruption. d) Analysed clinopyroxenes from all samples (see key) are all augite in composition. All analysed orthopyroxenes from all samples are exclusively clinoenstatite in composition.

Supplementary tables provided in Electronic Appendix C

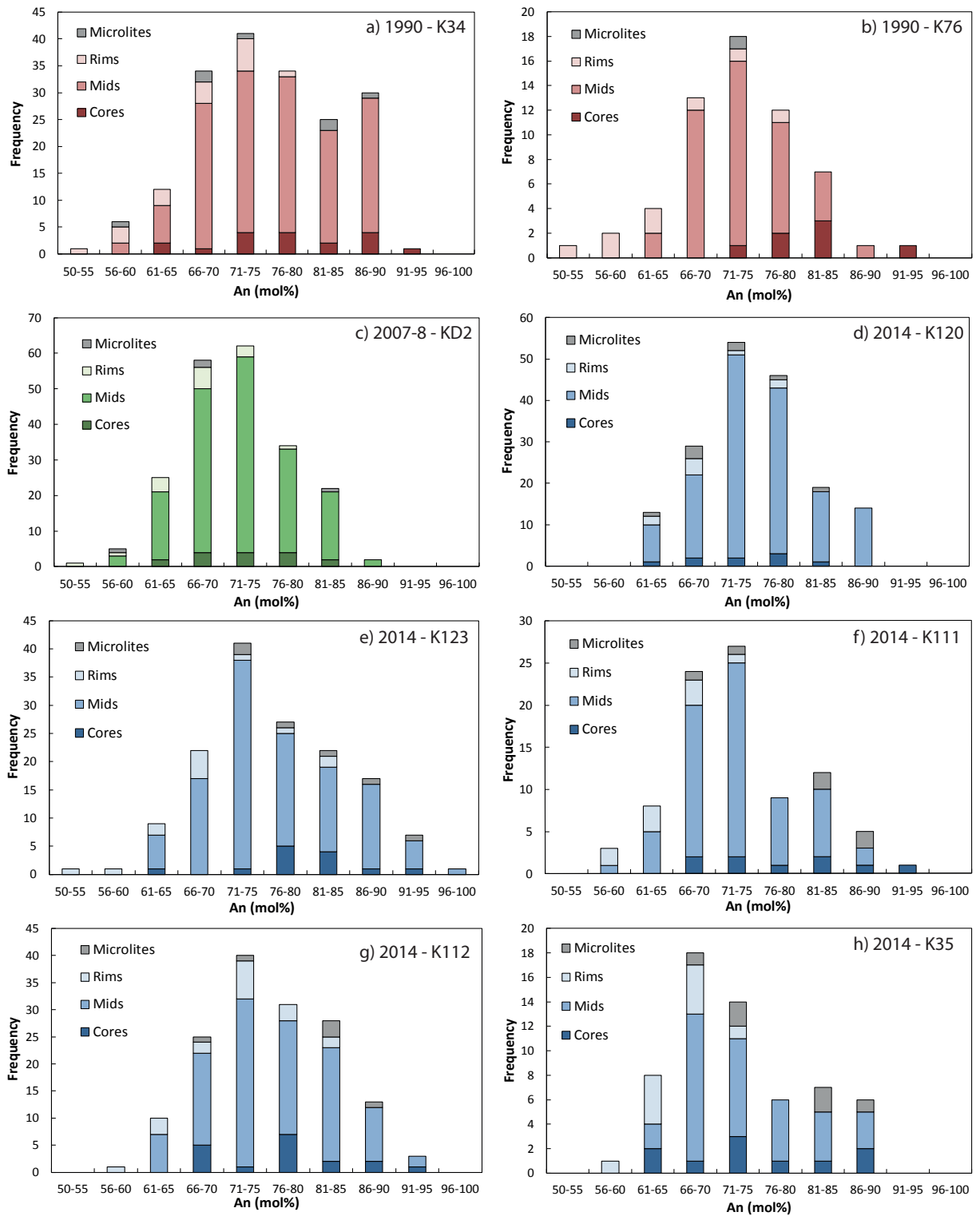


Figure 5: Frequency histograms of An contents (mol.%) of plagioclase phenocryst cores, mid regions, rims and microlites in each sample. 1990 eruptions are the red histograms (a) K34 $n = 193$, b) K76 $n = 74$, 2007-2008 lava dome is the green histogram (c) KD2 $n = 212$, 2014 eruptions are the blue histograms (d) K120 $n = 173$, e) K123 $n = 158$, f) K111 $n = 89$, g) K112 $n = 157$, h) K35 $n = 79$).

the same sample, but show a wide variability in anorthite content from An 67-92 mol.% (Fig. 5). Microlites in the 1990 samples are slightly less calcic than those in the 2014 samples (60–87 mol.% An). Microlites in the 2007-2008 dome sample show variable An mol.% from 56-86 and generally less calcic compositions compared to microlites in the explosive 1990 and 2014 samples.

Plagioclase across all samples shows complex oscillatory and simple normal and reverse zoning patterns (Fig. 6). Normal and oscillatory zoning patterns are most commonly observed in plagioclase from the 2014 and 1990 eruptions than the 2007-2008 eruption (Fig. 6), and most commonly in plagioclase texture Types 1 and 2 (Fig. 7). Plagioclase texture Types 1a, 1b and 1c display normal, reverse and simple and oscillatory zoning trends in phenocrysts with a variation in the fluctuation of anorthite contents between types (Figs. 7a, b and 8b). Plagioclase texture Type 2 from 1990 and 2014 samples display only normal zoning patterns (Table 1; Figs. 7c and 8a), with some microphenocrysts also showing normal zoning patterns. Plagioclase shows large compositional ranges from as little as

~1 up to ~30 mol.% in anorthite (An) content in the grains of in the 2014 and 1990 samples from core to rim in Texture types 1 and 2 (Figs. 7 and 8a). Phenocrysts with texture Type 2 also commonly show a sharp decrease in calcium towards the rim (Fig. 8a). Plagioclase in the 2007-2008 sample is more frequently reversely zoned than the explosive samples (Figs. 6 and 8c). Variations from core to rim of normal and reversely zoned 2007-2008 plagioclase are around 1-20 mol.% An (Fig. 8b), less variation than that seen in the 2014 and 1990 samples (Fig. 8c).

Fluctuations in FeO generally do not mirror the zonation patterns observed in plagioclase (Figs. 7a, b). However, in some 2014 and 1990 samples an increase An is accompanied by a slight increase in FeO in the outer mid regions to the rim of phenocrysts (Fig. 7c). FeO profiles in the 2007-2008 lava dome sample do not mirror the zoning of calcium (Fig. 8c). However, FeO can

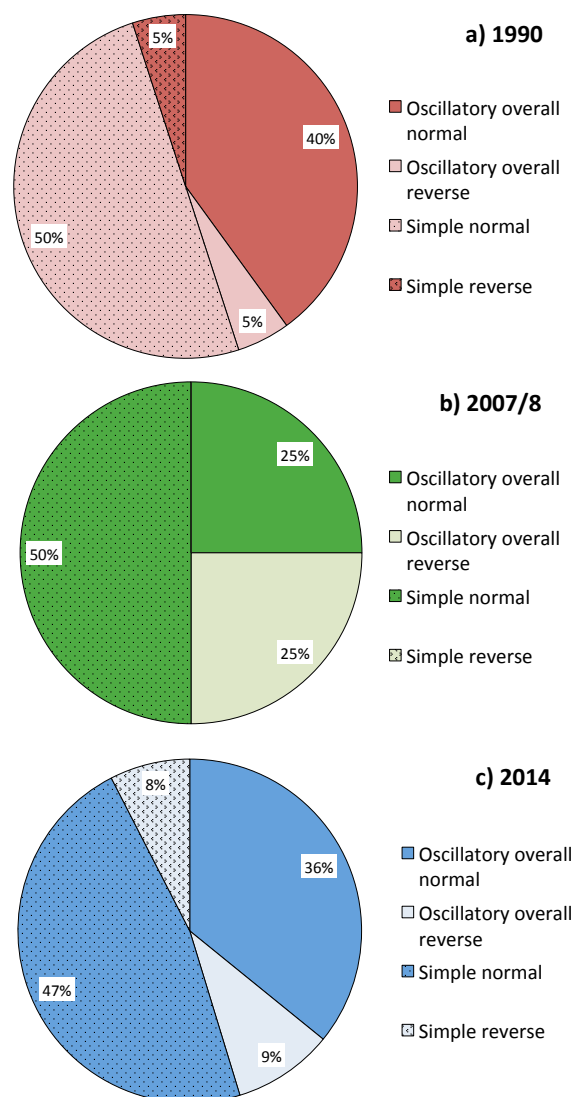


Figure 6: Pie charts of the abundance (%) of plagioclase phenocrysts with oscillatory or simple zoning patterns, with type of chemical zoning pattern (normal or reverse based on Anorthite content variation) in a) 1990 samples, b) 2007-2008 samples, and c) 2014 samples.

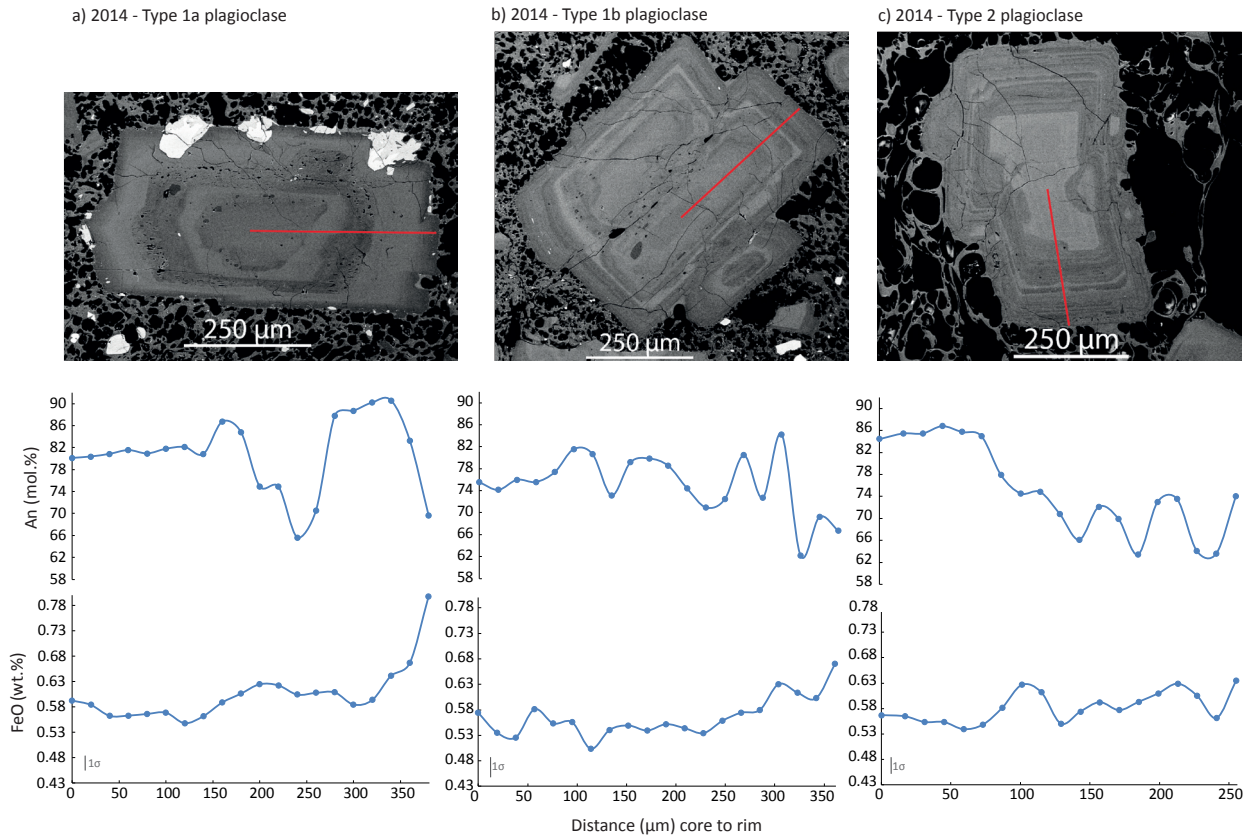


Figure 7: Variations in An (mol.%), FeO (wt.%; with 1σ error bar) across plagioclase phenocrysts (starting from the core to the rim) from 2014 samples. a) phenocryst from sample K120, texture Type 1a, and b) phenocrysts are from sample K123, texture Type 1b with oscillatory zoning, and c) phenocryst from sample K112, texture Type 2 and oscillatory zoned. Standard error for anorthite content is ~ 1 wt.% for all samples, and is ~ 0.03 wt.% for FeO on plagioclase analyses.

mirror a decrease in anorthite from mid regions to the rims, unlike that observed in the 1990 and 2014 plagioclase profiles (Figs. 7 and 8).

4.4.3.2 Clinopyroxene

All clinopyroxene crystals from all eruptions are exclusively augite in composition (using the Morimoto et al., 1988 classification; Table 6 and Fig. 4d). Most 2014 samples show unimodal distributions in Mg# for clinopyroxene analyses (Figs. 9f, g and h). However, Stage 1 clinopyroxene shows a bimodal distribution Mg# (Fig. 9d) with the lowest and highest Mg# values observed in all 2014 samples. Stage 2 clinopyroxene displays higher Mg# values overall (Mg# 76-80; Fig. 9e). Samples from the final eruptive Stage show larger variations in Mg# from 73-80 (Figs. 9f, g and h). K112 from this Stage has the lowest Mg# range from 73-78 (Fig. 9g). 1990 clinopyroxene shows maximum peaks in Mg# at 76-77 in both samples, and are very similar to 2014 samples (Fig. 9a and b), and both profiles are skewed towards higher Mg#. When compared to 2014 clinopyroxene, 1990 plots similarly to analyses from clinopyroxene in samples from Stage 3 of the 2014 eruption (Fig. 9f and h). Normal and reverse zonation patterns are seen in all samples, however the Mg# varies only by 2 in a single phenocryst (normally 75-77). 2007-2008 clinopyroxene analyses show a relatively uneven unimodal distribution in Mg# (Fig. 9c), with a slightly wider variation from

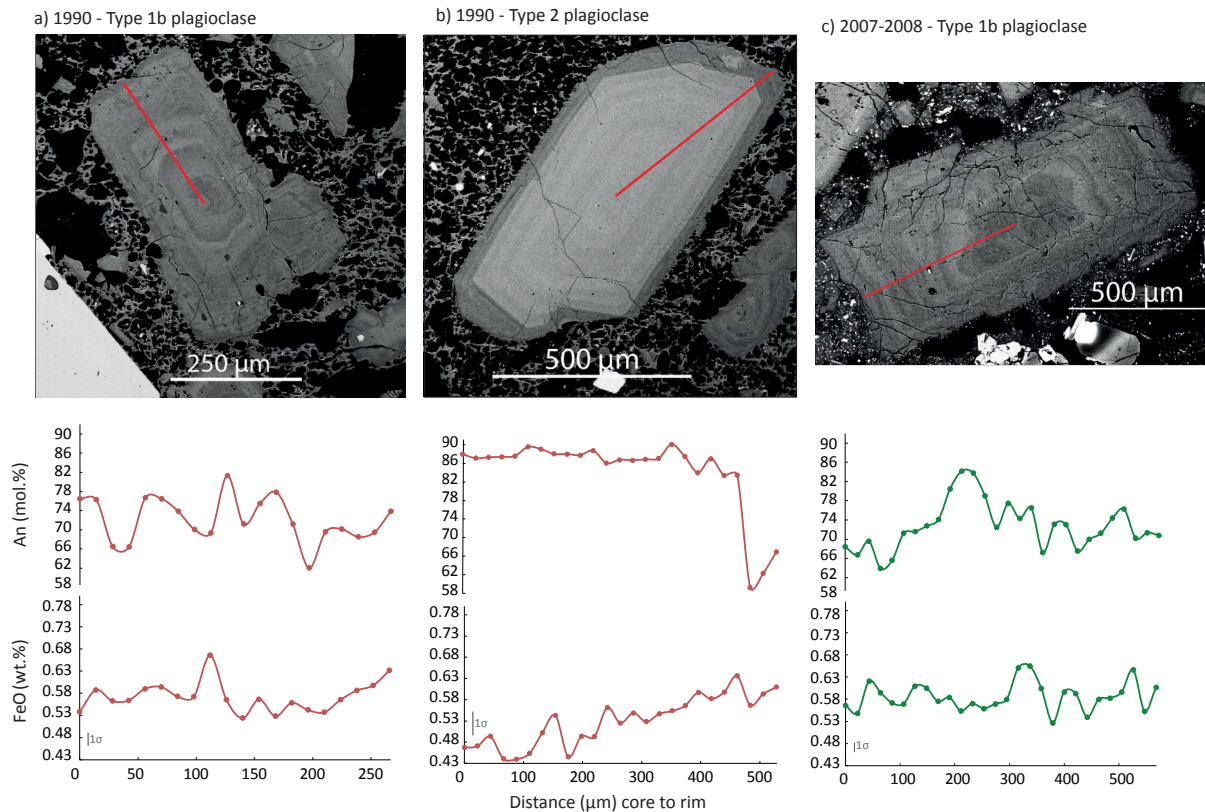


Figure 8: Variations in An (mol.%), FeO (wt.%; with 1 σ error bar) plagioclase phenocrysts (starting from the core to the rim) from a) 1990 eruption, phenocryst is from sample K34, texture Type 1b. B) 1990 eruption, phenocryst is from sample K34, texture Type 2, and c) 2007-2008 dome eruption, phenocryst is from sample KD2, texture Type 1b. Standard error for anorthite content is ~1-1.5 wt.% for 1990 samples, and is ~0.03-0.06 wt.% for FeO on plagioclase analyses. Standard error for anorthite content is ~1 wt.% for the 2007-2008 sample, and is ~0.02 wt.% for FeO on plagioclase analyses.

Mg# 72-79, like that of 1990 sample K76. Mg# in clinopyroxene is higher than in orthopyroxene in all Kelut samples (Figs. 9, 10).

The composition of most 2014 clinopyroxene phenocrysts varies very little between En 42-46 mol.% to Wo 41-44 mol. %, and straddles across the 1990 and 2007-2008 clinopyroxene phenocrysts (Fig. 10a-e). 1990 clinopyroxene overall generally cluster towards higher Wo (mol.%), with lower En (mol.%) than most samples (Fig. 9). 2007-2008 eruption clinopyroxene phenocrysts are similar to and overlap that of the 2014 eruption (Fig. 10). They are however generally higher En and lower Wo (mol.%) contents than 2014 and 1990 eruption samples, the latter of which cluster towards higher Wo and lower En (mol.%). Clinopyroxene as inclusions, glomerocrysts and microlites show similar concentrations in all samples. 2014 intergrown clinopyroxene (without glomerocryst textures) shows similar compositions to single phenocrysts (Fig. 10). Clinopyroxene as inclusions in plagioclase and orthopyroxene show very little geochemical variation in samples (Fig. 10b). Clinopyroxene in glomerocrysts, touching clinopyroxene-orthopyroxene, and as microphenocrysts show similar chemical variations as phenocrysts (Figs. 9 and 10).

Table 6: Representative clinopyroxene analyses (wt. % oxide) with end members (mol. %)

Eruption	1990	1990	2007-2008	2014	2014	2014	2014	2014
Sample	K34	K76	KD2	K120	K123	K111	K112	K35
SiO ₂	52.22	51.49	53.15	52.56	51.95	51.91	51.90	51.89
TiO ₂	0.33	0.38	0.34	0.39	0.16	0.38	0.37	0.40
Al ₂ O ₃	1.72	2.01	1.70	1.83	1.16	1.88	1.93	2.01
FeO	9.63	9.44	9.70	9.54	9.08	9.23	9.52	9.34
MnO	0.54	0.45	0.49	0.51	0.62	0.48	0.49	0.45
MgO	14.61	14.46	15.26	14.84	14.61	14.48	14.89	14.65
CaO	20.58	20.63	19.78	19.99	21.72	20.91	20.34	20.80
Na ₂ O	0.30	0.33	0.28	0.25	0.26	0.31	0.28	0.34
K ₂ O	/	/	/	/	/	0.01	/	/
Total	99.93	99.18	100.70	99.90	99.56	99.59	99.73	99.88
End members								
En	42.8	43.1	44.5	43.9	43.5	43.1	43.8	43.3
Fs	15.7	15.4	15.4	16.5	15.7	15.3	15.6	15.2
Wo	43.8	43.7	41.4	43.0	44.4	43.6	42.1	43.6

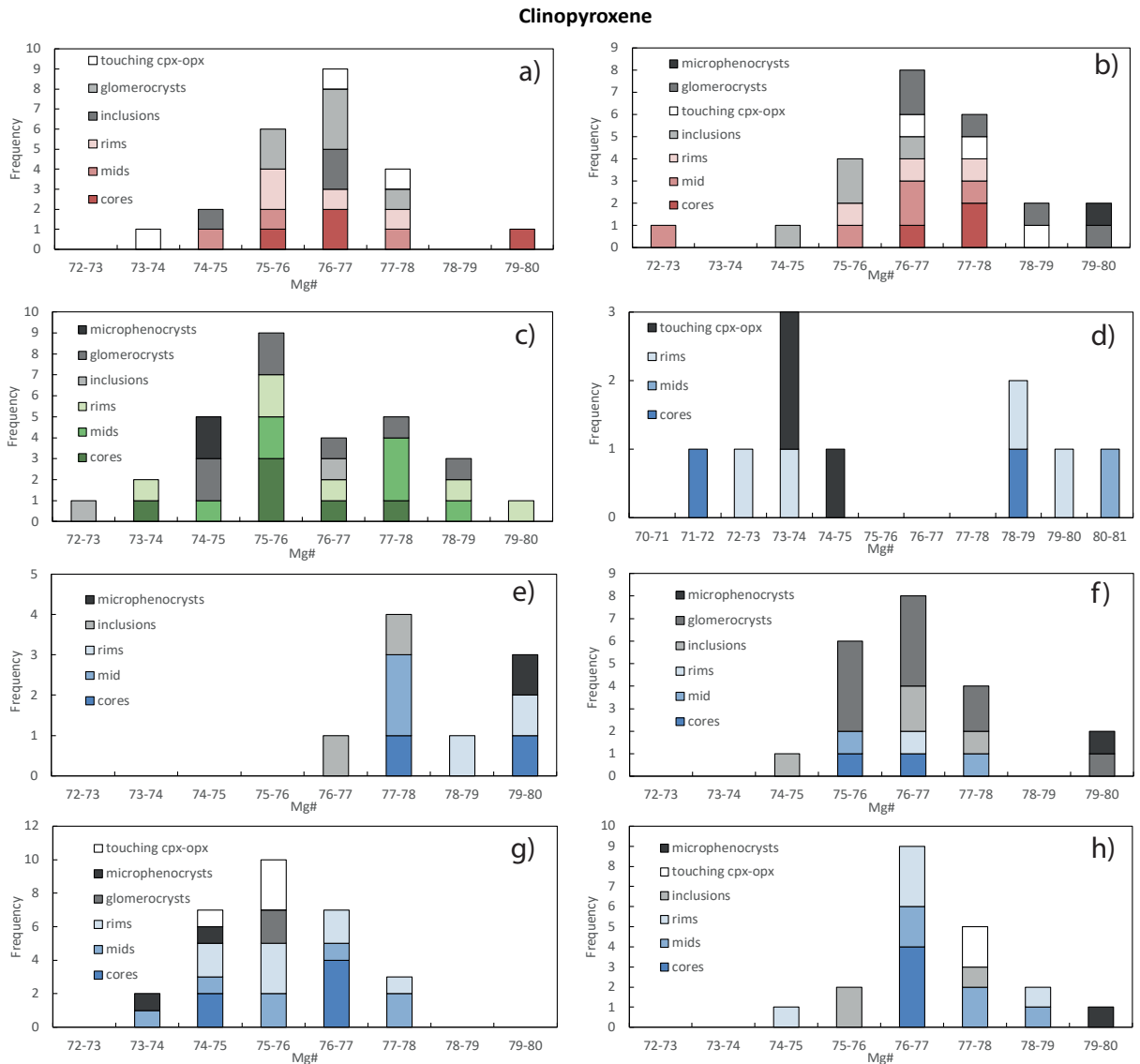


Figure 9: Frequency histograms of Mg# values in clinopyroxene cores, mid regions, rims, glomerocrysts, inclusions, and touching cpx-opx analyses. 1990 sample analyses a) K34 n = 23, b) K76 n = 24. 2007-2008 dome sample analyses c) KD2, n = 30. 2014 sample analyses d) K120 n = 10, e) K123 n = 9, f) K111 n = 21, g) K112 n = 29, h) K35 n = 20.

4.4.3.3 Orthopyroxene

Orthopyroxene crystals across all samples are enstatites using the Morimoto et al. (1988) classification scheme (Table 7; Fig. 4d). There are no significant geochemical differences between individual 2014 orthopyroxene phenocrysts, varying by around 2-7 in Mg# (Fig. 10). Unimodal distributions of Mg# in orthopyroxene are seen in all samples (Fig. 10) apart from K111 (Stage 3, Fig. 10f). 1990 orthopyroxene shows maximum peaks in Mg# of 65-67 in both samples (Fig. 10a, b). 1990 orthopyroxene analyses generally shows less range in Mg# (from 65-68) than 2014 samples. 2014 and 1990 orthopyroxene as microphenocrysts, in glomerocrysts and as inclusions are very similar in composition. 2007-2008 orthopyroxenes have similar, unimodal distributions in Mg# values to that of 1990 and 2014 eruption samples, but are slightly higher, up to 71 (Fig. 10c). Mg# in analysed orthopyroxenes are less than the clinopyroxenes (Fig. 9).

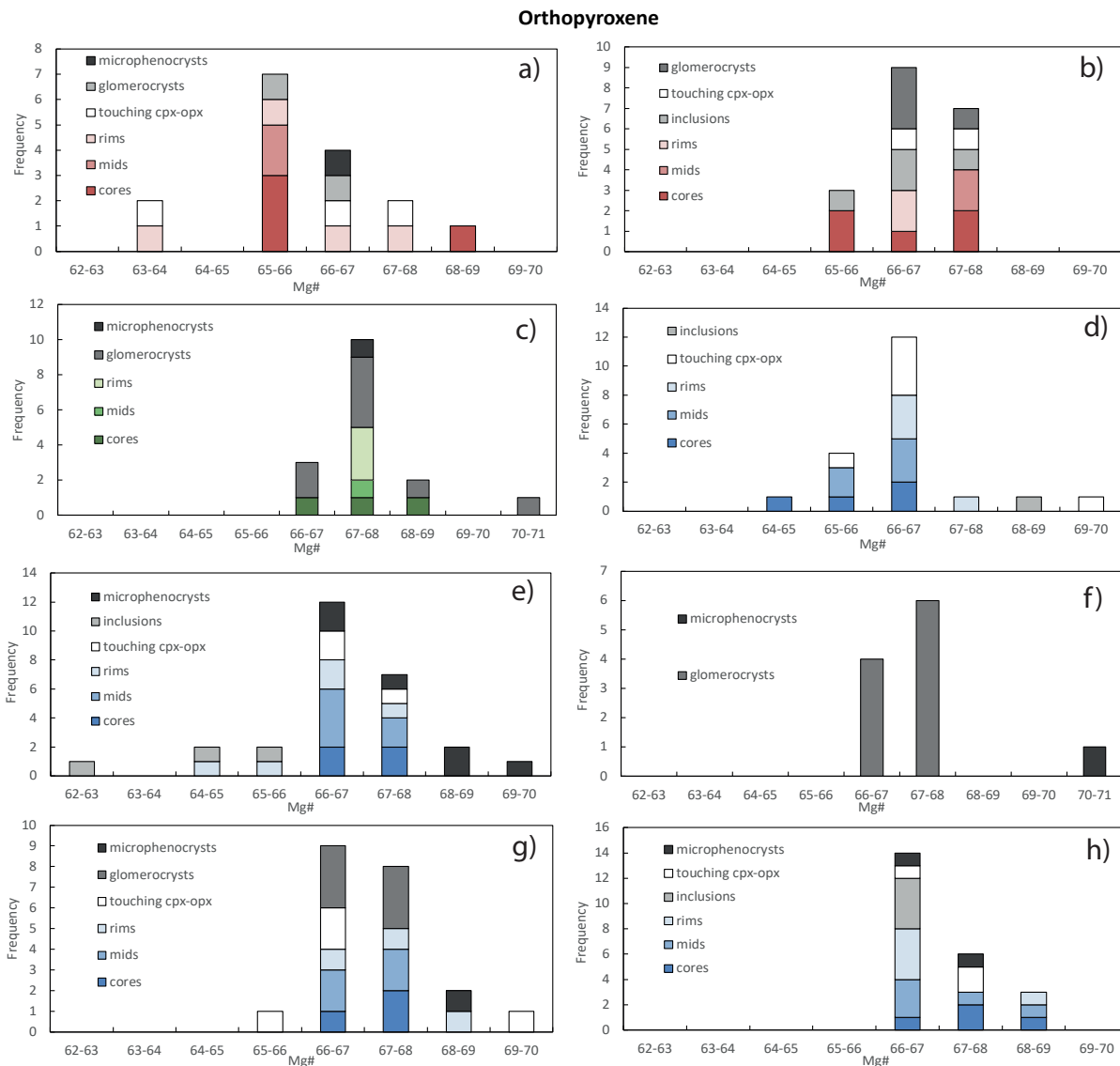


Figure 10: Frequency histograms of Mg# values in orthopyroxene cores, mid regions, rims, glomerocrysts, inclusions, and touching opx-cpx analyses. 1990 sample analyses a) K34 n = 16, b) K76 n = 19. 2007-2008 dome sample analyses c) KD2 n = 16. 2014 sample analyses d) K120 n = 20, e) K123 n = 27, f) K111 n = 11, g) K112 n = 21, h) K35 n = 23.

Table 7: Representative orthopyroxene analyses (wt. % oxide) and end members (mol. %)

Eruption	1990	1990	2007-2008	2014	2014	2014	2014	2014
Sample	K34	K76	KD2	K120	K123	K111	K112	K35
SiO ₂	53.27	53.04	53.36	52.70	53.10	53.35	53.55	54.37
TiO ₂	0.19	0.22	0.19	0.19	0.15	0.19	0.16	0.13
Al ₂ O ₃	0.98	1.05	1.14	1.06	0.94	1.03	0.96	1.08
FeO	19.85	18.96	19.43	19.55	18.89	18.67	19.06	17.13
MnO	0.89	0.84	0.92	0.92	0.79	0.87	0.90	0.69
MgO	23.46	23.51	24.40	24.16	24.23	23.48	23.87	24.93
CaO	1.39	1.43	1.43	1.38	1.45	1.40	1.40	1.55
Na ₂ O	/	0.01	/	0.02	/	0.04	/	0.06
K ₂ O	/	/	/	/	/	/	/	/
Total	100.03	99.04	100.87	99.97	99.55	99.02	99.89	99.94
End members								
En	66.1	66.7	63.4	67.0	66.3	67.0	67.1	67.1
Fs	31.1	30.4	33.8	30.3	30.6	30.2	30.2	30.0
Wo	2.86	2.91	2.78	2.68	3.06	2.85	2.77	2.96

Like clinopyroxene, the composition of orthopyroxene varies very little from En 64-69 mol. % to Fs 28-34 mol.% in all samples from all eruptions (Fig 11. f-j). 1990 orthopyroxene phenocrysts generally show similar end member contents to the 2014 samples, but cluster towards slightly less elevated En (mol. %), and slightly more Fs (mol. %; Fig. 11). 2007-2008 orthopyroxenes generally show less range in En and Fs (mol.%), sitting in between values from 1990 and 2014 analyses (Fig. 11). Orthopyroxene as inclusions varies slightly more than phenocrysts, from En 62-68 mol.% to Fs 28-35 mol.% across all samples (Fig. 11f). In 2014 and 1990 glomerocrysts and touching orthopyroxene-clinopyroxene (not in glomerocrysts), orthopyroxene show very similar compositions as singular phenocrysts (Fig. 11). 2007-2008 glomerocryst analyses show slightly more enriched En mol.% and less Fs (mol.%) than that of the 2014 and 1990 samples, by up to 5 mol.% En and Fs (Fig. 11). Microphenocrysts across all samples show the highest Mg# values, however all orthopyroxene compositions remain very similar across all 2014 samples.

4.4.3.4 Titanomagnetites and amphibole

Titanomagnetites are ubiquitous and show limited compositional variation (Table 8), with greater proportions of Fe³⁺ (~ 50 mol.%), with less Fe²⁺ (40 mol.%), and minor titanium (~ 9 mol.%), and similar ratios of Fe²⁺/Fe³⁺ (0.54 to 0.57). The single amphibole (Table 9) is classified as magnesiohastingsite using the Leake et al. (1997) classification scheme.

4.4.4 Summary of the main petrographic features

Plagioclase is the most abundant mineral in volcanic rocks from all eruption periods (Table 1). Plagioclase phenocrysts commonly show sieve-textures (Type 1; Table 2; Figs. 7 and 8) and are rarely homogeneous in composition. An is varied across phenocryst cores, mid regions, and rims of texture Types 1 and 2 (Fig. 5), with normal oscillatory and simple zoning patterns most commonly observed across all samples (Figs. 5-8). Type 2 phenocrysts are always normally zoned from core to rim. Plagioclase in the 2007-2008 dome samples have more frequent reverse zoning than the 1990 and 2014 samples (Fig. 6). The 1990 and 2014 plagioclase show a greater variation in

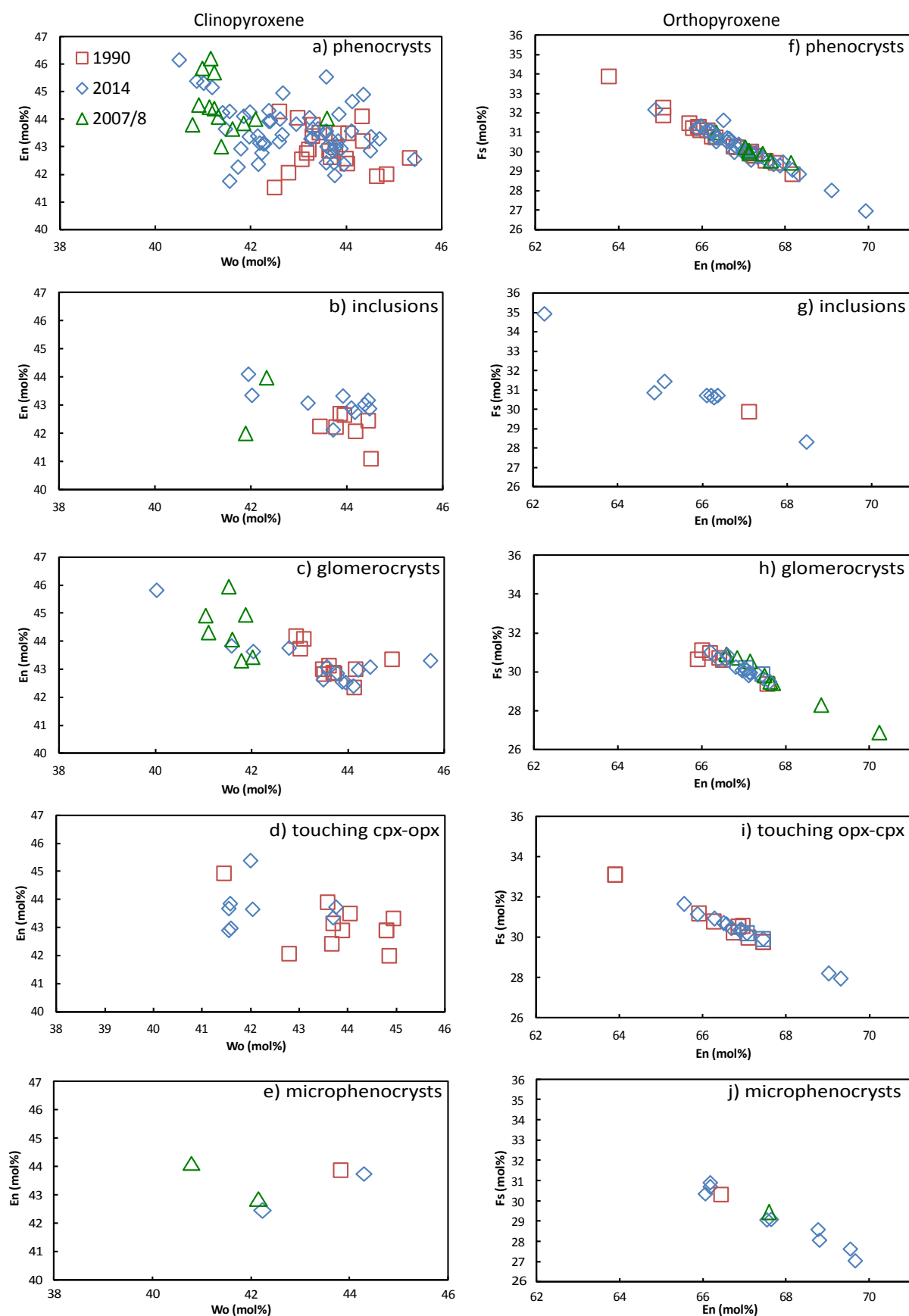


Figure 11: End member variation plots of clinopyroxene and orthopyroxene. a – e) Plots of En versus Wo for clinopyroxene phenocrysts (a), inclusions, (b) glomerocrysts (c), touching cpx-opx (d), and microphenocrysts (e). f – j) Plots of En versus Fs for orthopyroxene phenocrysts (f), inclusions (g), glomerocrysts (h), touching opx-cpx (i) and microphenocrysts (j).

Supplementary tables provided in Electronic Appendix C

Table 8: Representative titanomagnetite analyses (wt. % oxide) and end members (mol. %)

Eruption	1990	1990	2007-2008	2014	2014	2014	2014	2014
Sample	K34	K76	KD2	K120	K123	K111	K112	K35
SiO ₂	0.09	0.07	0.08	0.08	0.08	0.12	/	0.08
TiO ₂	8.66	8.86	9.03	8.87	9.22	8.41	8.82	8.69
Al ₂ O ₃	2.93	2.85	2.84	2.96	2.52	2.97	3.05	2.83
FeO	35.0	34.2	35.3	35.2	34.3	34.0	33.7	34.4
Fe ₂ O ₃	48.5	46.9	47.9	48.9	48.4	46.6	48.2	47.1
MnO	0.53	0.57	0.41	0.56	0.46	0.53	0.57	0.55
MgO	2.37	2.29	1.66	2.11	2.27	2.31	2.19	2.24
CaO	0.01	0.04	/	/	/	0.02	/	0.01
Na ₂ O	/	0.02	/	/	/	/	/	0.01
P ₂ O ₅	/	0.02	/	/	/	0.01	/	/
Cr ₂ O ₃	/	0.02	0.07	0.05	0.05	0.05	0.06	0.01
NiO	/	0.02	/	/	0.01	0.01	/	0.07
Total	98.09	95.84	97.32	98.74	97.31	95.04	96.60	95.98
End members								
FeO	40.6	40.9	40.9	40.6	40.1	40.8	39.9	40.8
Fe ₂ O ₃	50.2	49.6	49.8	50.4	50.7	49.8	51.1	49.9
TiO ₂	9.20	9.36	9.34	9.00	9.22	9.37	9.04	9.33

Table 9: Representative amphibole analyses from sample K123 (wt. % oxide)

Eruption	2014	2014	2014	2014	2014
Sample	K123	K123	K123	K123	K123
SiO ₂	44.11	44.62	44.65	44.59	44.46
TiO ₂	1.90	1.55	1.66	1.93	1.59
Al ₂ O ₃	9.73	9.43	9.45	9.71	9.37
FeOt	15.54	15.48	15.59	15.81	15.60
MnO	0.39	0.43	0.43	0.39	0.42
MgO	13.32	13.40	13.20	13.58	13.45
CaO	11.23	11.17	11.24	11.45	11.36
Na ₂ O	1.78	1.74	1.73	1.80	1.70
K ₂ O	0.31	0.30	0.29	0.30	0.29
Total	98.32	98.12	98.24	99.56	98.23

plagioclase anorthite content from core to rim than in the 2007-2008 samples (Figs. 7 and 8). FeO in plagioclase from 1990 and 2014 samples always increases slightly in the outer mid regions to rims of phenocrysts, even if calcium does not also increase (Figs. 7, 8). In 2007-2008 plagioclase, there is little variation throughout, and not always an increase in FeO in the outer regions of the phenocrysts (Fig. 8). Microlite An compositions are varied (Fig. 5), showing generally lower An contents in the 1990 and 2007-2008 (56-90 An mol.%) samples compared to the 2014 samples (66-95 An mol.%). Although, there are fewer microlites in the explosive 1990 and 2014 samples compared to the effusive 2007-2008 samples.

Clinopyroxene is modally more abundant than orthopyroxene in the 2014 and 2007-2008 samples, but in almost equal proportions in the 1990 samples (Table 1). Clinopyroxene is often observed mantling orthopyroxene (Tables 1, 3 and 4) and some clinopyroxenes and orthopyroxenes have abundant inclusions of glass or plagioclase. Some clinopyroxenes and orthopyroxenes are the largest, elongated phenocrysts in samples ($\leq 2200 \mu\text{m}$). Clinopyroxenes in the 1990 and 2007-2008 volcanic rocks show distinct compositions, and the 2014 clinopyroxene compositions overlap the

1990 and 2007-2008 clinopyroxenes (Fig. 11). A similar pattern is observed in orthopyroxene composition (Fig. 11), although there is a more restricted variation in composition. A few 2014 orthopyroxenes display higher En and lower Fs contents compared to the 1990 and 2007-2008 samples (except for glomerocrysts, Fig. 10h).

4.4.5 Major and trace element geochemistry

Major and trace element data are given in Table 10 and presented in Figures 12, 13 and 14. Whole rock loss on ignition (LOI) values are slightly higher in the 1990 (up to 0.8) samples than the 2014 samples (up to 0.2) (Table 10). The 2014, 2007-2008 and 1990 volcanic rocks show similar, and highly restricted variation in major element contents, with only 1 wt% variation in SiO₂ content overall (54.7 to 55.5 wt%) and are classified as low-K basaltic andesites (Fig. 12a). CaO, MgO and Fe₂O₃ contents show a negative trend with SiO₂ (Figs. 12c-d and g). TiO₂ content shows little variation in the Kelut volcanic rocks (Fig. 12d). Na₂O and K₂O show a positive correlation with SiO₂ in the 2014, 2007-2008 and 1990 volcanic rocks (Fig. 12b and h). Al₂O₃ content shows more scattered variation with SiO₂ (Fig. 12e). Major and trace element compositional variation is extremely limited throughout the different stages of the 2014 eruption, and between eruptions, i.e. from 1990 to 2014 (Figs. 2 and 12).

Chondrite-normalised REE patterns for the 2014, 2007-2008 and 1990 volcanic rocks show little variation between the eruptive periods (Figs. 13a and b). The rocks display minor enrichment in LREE relative to chondrite and relatively flat HREE profiles. The La/Lu ratios in the 1990 (21), 2007-2008 (20), and 2014 (20) rocks are almost identical. The different samples from the 2014 eruption show very minor variation in REE patterns. There is a pronounced positive Eu anomaly in data from all eruption years (Figs. 13a and b). The new 2007-2008 dome data presented in this study are indistinguishable from the type of data presented by Jeffery et al. (2013) for the 2007-2008 lava dome samples (grey dashed lines). However the new data show higher positive Eu anomalies. A multi-element normal mid-ocean ridge basalt (N-MORB) -normalised diagram shows similar patterns for the 2014, 1990 and 2007-2008 samples (Figs. 13c, d). Samples are enriched in concentrations of large ion lithophile elements (LILE) Rb, Ba, and Sr. There is also enrichment of high field strength elements (HFSE) Pb, Th and U relative to N-MORB concentrations. HFSE elements Nb and Ta show depletion relative to N-MORB, and create a pronounced trough in the pattern, typical of island arc volcanic rocks. The MREE and HREE are also depleted relative to N-MORB, displaying flat profiles. The 2007-2008 dome data from Jeffery et al. (2013) show lower and more variable Pb concentrations compared to the new 2007-2008 data presented here. No correlation is observed between europium anomaly and silica content (Fig. 14a). The 2014 and 2007-2008 samples appear to have a slightly higher Eu anomalies than the 1990 samples. A slight positive correlation is observed between Eu and Sr (Fig. 14b).

Table 10: Major elements (Wt. %) and trace elements (ppm) of 1990, 2007-2008 and 2014 Kelut samples

Eruption	1990	1990	1990	1990	1990	2007/8	2014	2014	2014	2014	2014	2014	2014	2014	2014	2014
Sample	K34	K59	K76	K158	KD3	KD2	K113	K115	K116	K120	K123	K125	K35	K62	K75	K112
Deposit type	Fall	Fall	Fall	Fall	Flow	Lava	Flow	Flow	Flow	Flow	Flow	Flow	Fall	Fall	Fall	Fall
SiO ₂	54.7	55.5	54.9	55.7	54.9	54.9	54.7	55.0	55.1	54.8	54.7	55.5	55.4	54.9	54.9	55.1
Al ₂ O ₃	18.7	19.3	19.0	19.3	19.1	19.0	18.7	19.2	18.9	18.8	18.6	18.8	19.0	18.9	18.8	19.4
Fe ₂ O ₃	8.90	8.40	8.80	8.60	8.90	8.90	9.20	8.60	8.80	9.40	9.30	8.80	8.80	8.90	9.20	8.50
MgO	4.00	3.50	3.90	3.50	3.80	3.80	4.00	3.60	3.90	4.10	4.10	3.80	3.70	3.80	4.10	3.60
CaO	9.20	9.00	9.10	8.80	9.20	9.20	9.30	9.10	9.10	9.00	9.30	9.00	9.20	9.10	9.40	9.30
Na ₂ O	3.00	3.10	3.00	3.00	2.90	3.00	2.90	3.00	3.00	3.00	2.90	3.00	3.00	3.00	2.90	3.10
K ₂ O	0.60	0.70	0.60	0.70	0.60	0.60	0.60	0.70	0.70	0.60	0.60	0.70	0.70	0.60	0.60	0.60
TiO ₂	0.60	0.60	0.60	0.60	0.60	0.60	0.70	0.60	0.60	0.70	0.70	0.60	0.60	0.60	0.60	0.60
MnO	0.20	0.20	0.20	0.20	0.20	0.20	0.20	0.20	0.20	0.20	0.20	0.20	0.20	0.20	0.20	0.20
P ₂ O ₅	0.20	0.20	0.20	0.20	0.20	0.20	0.20	0.20	0.20	0.30	0.20	0.20	0.20	0.20	0.10	0.20
Total	100	100	100	100	100	100	100	100	100	100	100	100	100	100	100	100
LOI	0.1	0.3	0.2	0.8	0.3	<0.1	0.2	<0.1	<0.1	0.2	0.1	<0.1	<0.1	<0.1	<0.1	0.2
Li	8.78	8.95	9.00	11.0	10.2	9.70	9.10	10.6	10.2	10.2	10.1	10.4	9.00	9.10	8.90	9.10
Be	0.70	0.70	0.70	1.00	0.80	0.80	0.70	1.00	1.00	1.00	1.00	1.00	0.70	0.70	0.70	0.70
Sc	23.0	19.0	21.0	21.0	24.0	22.0	22.0	22.0	23.0	23.0	25.0	23.0	21.0	20.0	23.0	20.0
Ti	3966	3713	3787	4082	4346	4161	4029	4286	4236	4422	4375	4282	3845	3927	4042	3727
V	181	160	166	172	194	184	181	188	188	188	198	186	168	175	181	164
Cr	15.5	15.2	15.0	15.0	17.0	13.7	14.1	17.0	14.0	16.0	14.0	14.0	12.5	15.0	14.0	16.0
Mn	1546	1466	1571	1697	1715	1643	1620	1624	1702	1771	1753	1687	1535	1561	1587	1506
Co	20.2	18.0	19.4	20.0	22.3	21.0	20.5	20.0	21.0	22.0	23.0	21.0	18.8	19.9	20.2	18.8
Ni	8.20	6.50	6.90	7.30	7.80	7.40	7.60	7.60	7.70	8.40	8.20	7.60	7.30	7.30	7.60	6.90
Cu	47.0	43.1	43.3	52.9	51.4	46.5	32.8	71.3	55.7	61.6	58.1	62.0	58.3	49.6	69.6	48.6
Zn	60.3	59.0	60.2	60.4	59.5	57.6	60.7	62.9	63.5	66.5	65.0	61.5	60.1	61.1	65.8	56.2
Ga	15.1	15.4	14.9	16.3	16.1	15.4	15.4	16.3	16.1	15.9	16.0	16.0	15.2	15.0	15.0	15.1
Rb	13.2	14.0	13.1	15.0	14.5	13.8	12.9	13.5	14.2	13.4	13.7	15.2	14.2	13.1	12.7	13.0
Sr	575	592	581	644	632	629	589	621	610	598	611	620	595	581	584	605
Y	17.7	17.8	17.6	19.5	19.7	18.2	17.7	18.7	18.8	17.9	19.1	19.5	18.8	17.3	18.0	17.1
Zr	49.0	51.6	49.2	58.0	54.0	51.7	48.5	54.2	52.9	50.2	50.5	55.8	52.2	48.8	48.5	48.1
Nb	1.20	1.20	1.20	1.40	1.30	1.20	1.10	1.30	1.30	1.20	1.20	1.30	1.20	1.20	1.20	1.10
Mo	1.00	1.00	1.00	1.10	1.00	1.00	1.00	1.10	1.00	1.10	1.00	1.10	1.00	1.00	1.00	1.00
Cd	0.10	0.10	0.10	0.10	0.10	0.10	0.10	0.10	0.10	0.10	0.10	0.10	0.10	0.10	0.10	0.10
Cs	1.10	1.10	1.10	1.20	1.10	1.10	1.00	1.20	1.10	1.10	1.10	1.20	1.20	1.10	1.10	1.00
Ba	460	486	468	532	508	476	452	499	495	462	475	514	497	464	462	463
La	5.50	6.00	5.50	6.40	9.40	5.50	5.30	5.70	5.90	5.40	5.60	6.20	6.00	5.70	5.50	5.40
Ce	12.9	13.4	12.9	14.9	13.8	13.1	12.6	13.8	13.5	12.9	13.3	14.2	13.7	12.8	12.9	12.5
Pr	1.70	1.80	1.70	2.00	1.90	1.80	1.70	1.80	1.80	1.80	1.80	1.90	1.90	1.70	1.70	1.70
Nd	8.30	8.60	8.40	9.50	9.10	8.50	8.20	8.80	8.90	8.50	8.80	9.30	8.90	8.40	8.50	8.20
Sm	2.30	2.30	2.30	2.60	2.50	2.30	2.30	2.40	2.40	2.30	2.40	2.50	2.40	2.30	2.30	2.20
Eu	0.90	1.00	0.90	1.00	1.00	1.00	0.90	1.00	1.00	1.00	1.00	1.00	1.00	0.90	1.00	1.00
Tb	0.40	0.40	0.40	0.50	0.50	0.40	0.40	0.50	0.50	0.40	0.50	0.50	0.50	0.40	0.40	0.40
Gd	2.60	2.60	2.60	2.90	2.80	2.60	2.60	2.70	2.80	2.60	2.80	2.90	2.80	2.60	2.70	2.60
Dy	2.70	2.70	2.70	2.90	2.90	2.70	2.60	2.80	2.90	2.70	2.90	2.90	2.80	2.70	2.80	2.60
Ho	0.60	0.60	0.60	0.70	0.60	0.60	0.60	0.60	0.60	0.60	0.60	0.60	0.60	0.60	0.60	0.60
Er	1.70	1.70	1.70	1.90	1.90	1.70	1.70	1.80	1.80	1.80	1.90	1.90	1.80	1.70	1.80	1.70
Yb	1.70	1.70	1.70	1.90	1.80	1.70	1.70	1.80	1.80	1.70	1.80	1.90	1.80	1.70	1.80	1.70
Lu	0.30	0.30	0.30	0.30	0.30	0.30	0.30	0.30	0.30	0.30	0.30	0.30	0.30	0.30	0.30	0.30
Hf	1.30	1.40	1.40	1.50	1.40	1.40	1.30	1.50	1.40	1.30	1.40	1.50	1.40	1.40	1.40	1.30
Ta	0.10	0.10	0.10	0.10	0.10	0.10	0.10	0.10	0.10	0.10	0.10	0.10	0.10	0.10	0.10	0.10
Pb	8.80	9.20	9.10	10.30	9.30	8.10	8.60	9.30	9.30	8.70	8.90	9.60	9.60	9.00	9.00	8.80
Th	1.00	1.10	1.00	1.10	1.00	1.00	1.00	1.00	1.00	0.90	1.00	1.10	1.10	1.00	1.00	1.00
U	0.40	0.40	0.40	0.40	0.40	0.40	0.40	0.40	0.40	0.40	0.40	0.40	0.40	0.40	0.40	0.40

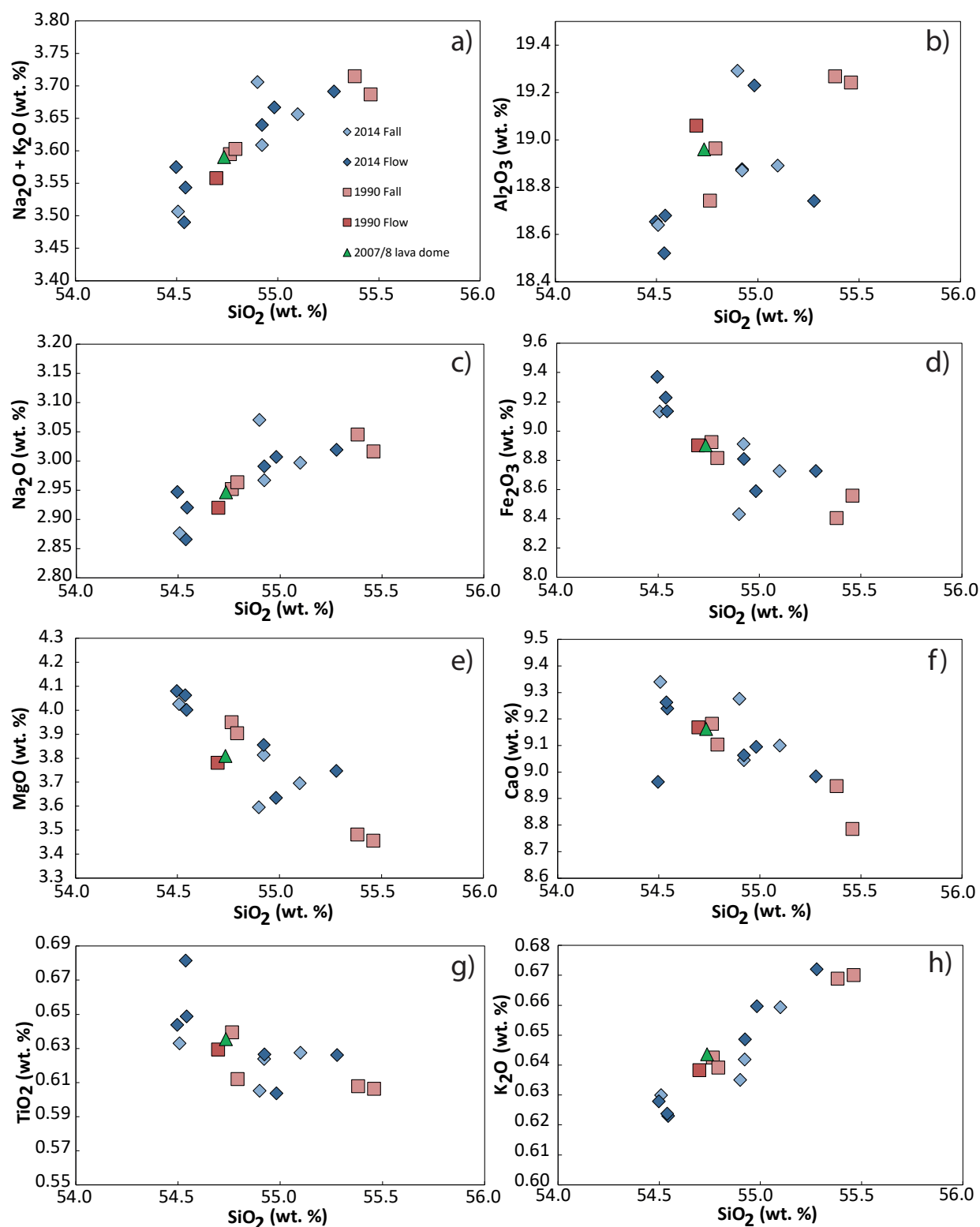


Figure 12: Harker plots for whole rock major element analyses. a) a total alkali silica diagram displaying whole rock analyses for 2014, 2007-2008, and 1990 eruptions of Kelut volcano using Le Maitre et al. (1989). Plots b - e show Al_2O_3 , Fe_2O_3 (given as total iron), MgO , CaO , Na_2O , K_2O and TiO_2 against SiO_2 .

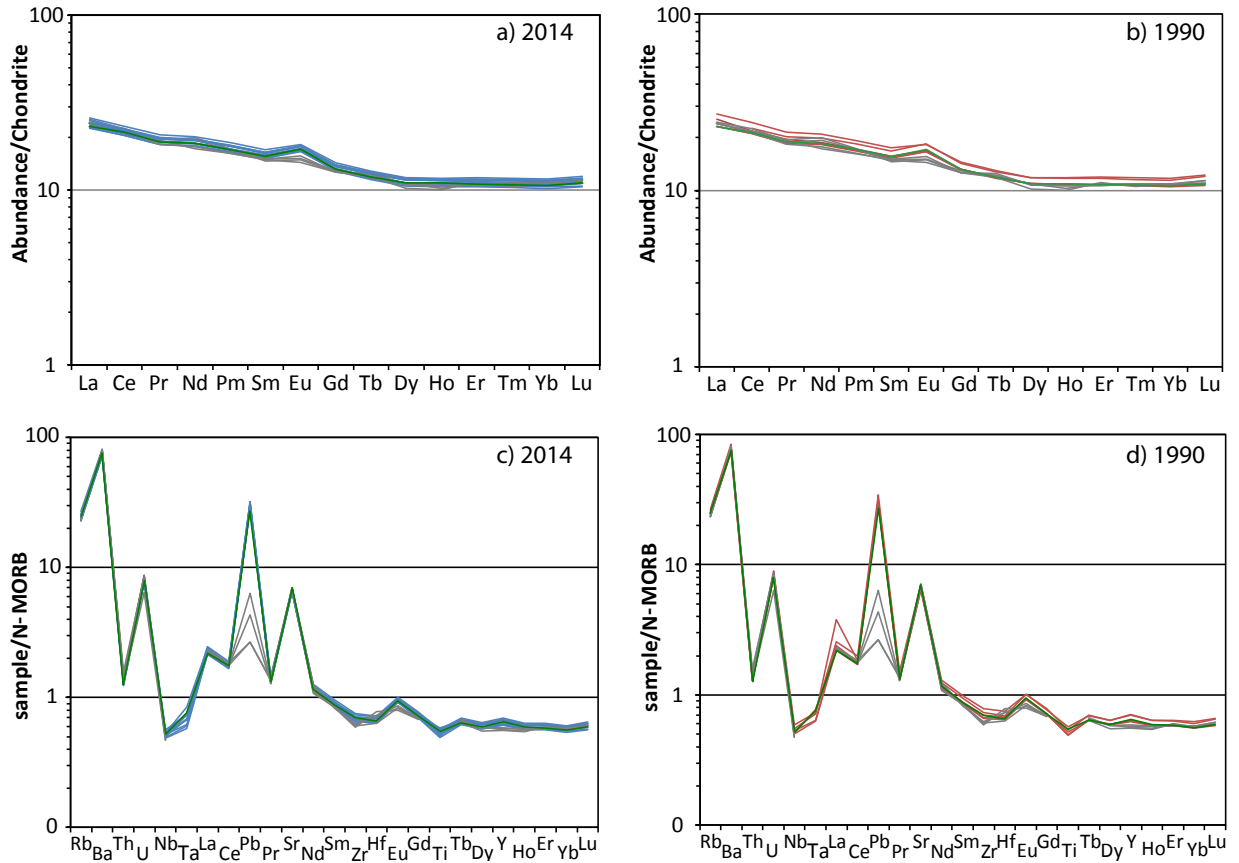


Figure 13: Chondrite normalized rare earth element diagram of Kelut rocks a) 2014 eruption samples b) 1990 eruption samples. N-MORB normalized multi-element spider diagrams of c) 2014 eruption samples and d) 1990 eruption samples. N-MORB and Chondrite values from Sun and McDonough (1989). In both plots, the dashed grey lines represent data from the 2007-2008 dome published in Jeffery et al. (2013) for comparison.

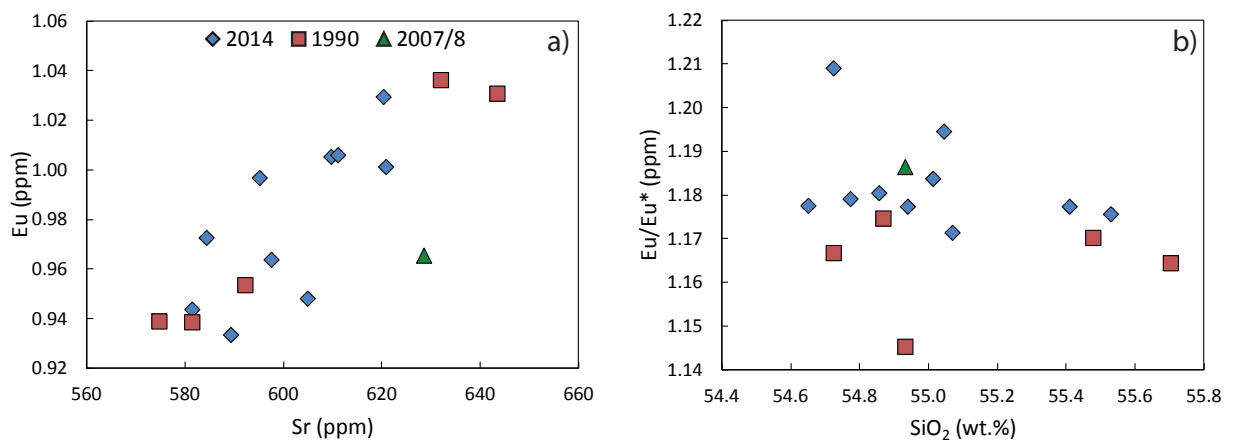


Figure 14: Trace element whole rock data plots all plotted for 1990, 2007-2008 and 2014 samples of a) Eu versus Sr, and b) Eu anomaly (Eu/Eu^*) versus SiO_2 .

4.5 Discussion

4.5.1 Determination of pre-eruptive magma storage conditions

4.5.1.1 Amphibole pre-eruptive pressure, temperature and water estimates

The amphibole geothermobarometer by Ridolfi and Renzulli (2012) has been used on the only amphibole in the 2014 sample (K123) to determine equilibration pressures and temperatures, and H_2O content (wt.%). This has been applied in order to determine H_2O_{melt} estimates. The amphibole records temperatures of 798-813 °C (average = 807 °C, $n = 5$, $1\sigma = 7$ °C) and pressures (with 10% relative error) from 205-219 MPa (average = 209 MPa, $n = 5$, $1\sigma = 6$ MPa). Application of the hygrometer provides H_2O_{melt} estimates between 5.7-5.9 wt.% (average = 5.8 wt.%, $n = 5$, $1\sigma = 0.1$ wt.%). Jeffery et al. (2013) calculated pressures from amphibole bearing xenoliths at a higher pressure of 603 MPa on average, and a higher H_2O_{melt} content by ~3 wt.% at 8.1 to 8.6 wt.% for the mid-crustal system, suggesting that a hydrous melt was fed into the system pre-2007-2008 eruption.

4.5.1.2 Pyroxene pre-eruptive pressure and temperature estimates

The compositions of touching clinopyroxene-orthopyroxene minerals were used in the two-pyroxene thermobarometer of Putirka (2008), however, they did not satisfy the test for equilibrium $K_D[\text{FeMg}]$. Therefore, it is assumed that cotectic crystallisation of the pyroxenes did not occur, and these were not in equilibrium at the time of crystallisation.

The clinopyroxene-melt barometer of Neave and Putirka (2017; Standard error estimates (SEE) = 140 MPa), and thermometer of Putirka (2008; Equation 33, SEE = 45 °C) were used as they produce more accurate results than previous versions (cf. Putirka 2003, 2008 - Equations 32c, 32d). An input of 4.0 wt.% H_2O_{melt} is used as this is typical for arc magmas (e.g., Plank et al., 2013; Preece et al., 2014), and the estimations of temperature and pressure equilibration presented below are using this water content. The pressure and temperature estimations paired with higher H_2O_{melt} content from amphibole hygrometry (5.8 wt.%) are quoted as comparison. The compositions of analysed clinopyroxene rims for each sample from the 2014, 1990 and 2007-2008 eruptions were paired with a combination of melt compositions. For the 2014 samples the liquid composition used includes: 1) dacitic groundmass glass from Chapter 3 (K35), 2) clinopyroxene compositions with the plagioclase-hosted melt inclusion compositions from this study, 3) 2014 melt inclusions from Cassidy et al. (2016), and 4) groundmass glass compositions from Cassidy et al. (2016) for the 2014 eruption (dacitic in composition), and 5) the 3 whole rock 2014 samples from this study (K35, K75, K112). For the 1990 samples, the liquid composition used includes; 1) groundmass glass from Chapter 3, (K34), 2) clinopyroxene compositions with the plagioclase-hosted melt inclusion compositions from this study, the 3) Jeffery et al. (2013) 1990 whole rock, and 4) 3 whole rock compositions from 1990 samples from this study (K34, K59, K76). Jeffery et al. (2013) whole rock compositions are used to aid comparison in P-T estimates, particularly for the 2007-2008 lava

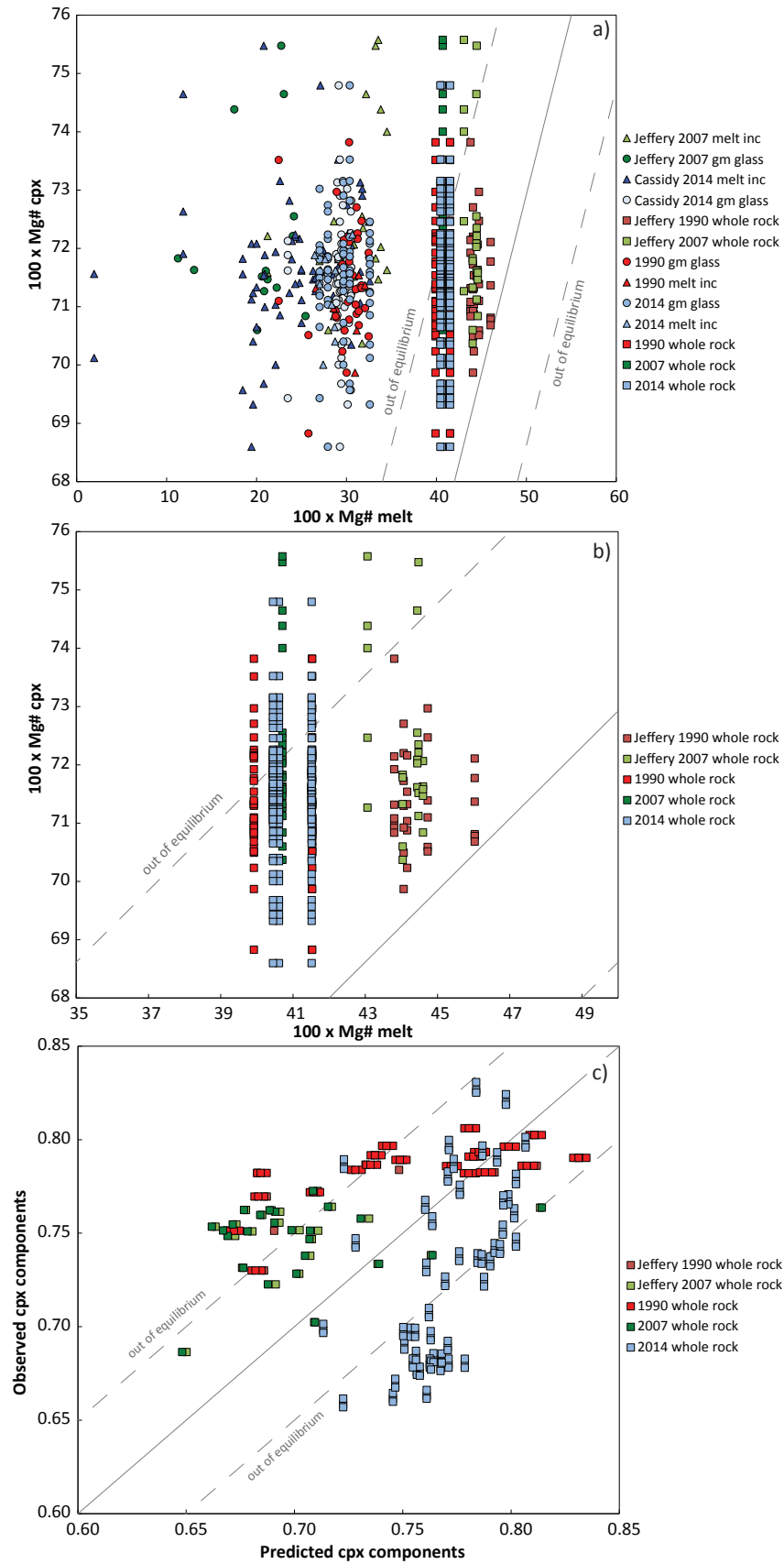


Figure 15: a) Test for equilibrium using the $K_D[\text{FeMg}]$ between clinopyroxene and melt close to the ideal of 0.28 (Putirka, 2008). Gm in key is groundmass. Melt inc is melt inclusions. b) Zoomed in part of those in and close to equilibrium, those paired with whole rock analyses are within this range, and therefore selected as most likely to have equilibrated with clinopyroxenes. c) Plot of predicted versus observed clinopyroxene component (diopside-hedenbergite; DiHd) as a further equilibrium test for whole rock, showing good fit as associated melt.

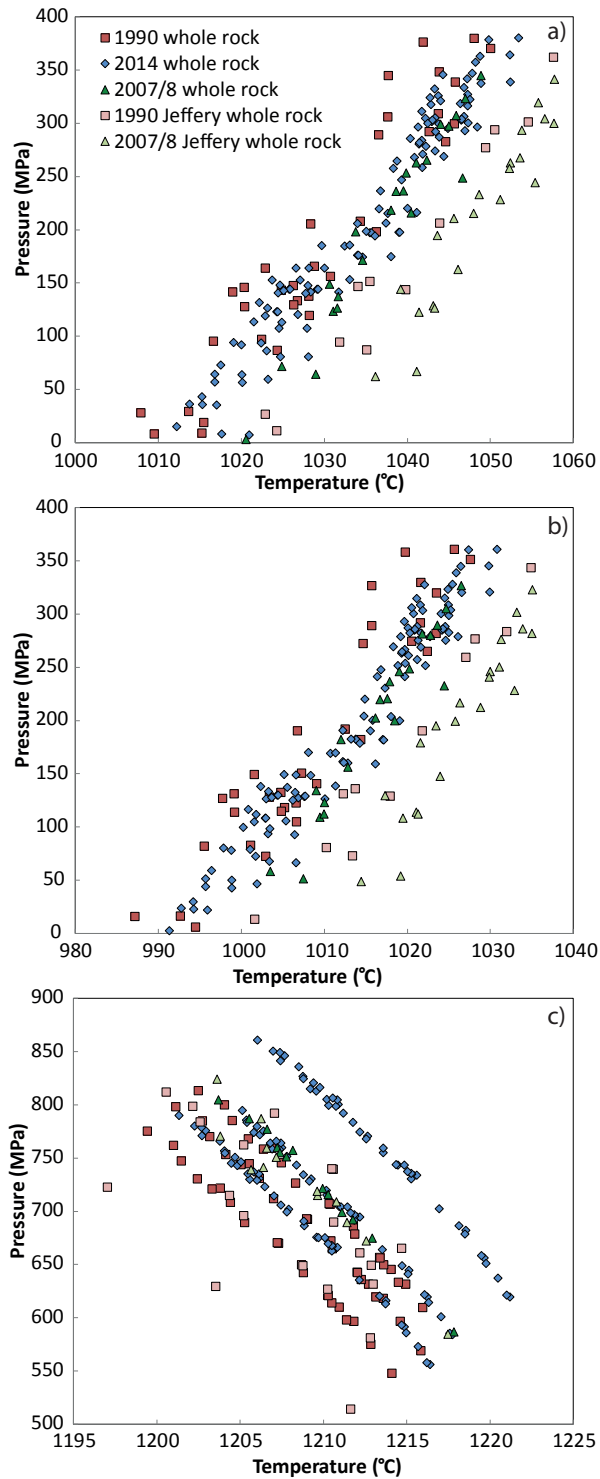


Figure 16: a-b) Pressure versus temperature estimations for clinopyroxene-melt equilibration for clinopyroxenes from 2014, 2007-8, 1990 with whole rock from this study used as melt compositions, and 2007-8 and 1990 with Jeffery et al. (2013) whole rock used as melt compositions with an input of a) 4 wt.% $\text{H}_2\text{O}_{\text{melt}}$ b) input of 5.8 wt.% $\text{H}_2\text{O}_{\text{melt}}$ from amphibole hygrometry. c) Pressure versus temperature estimations for plagioclase-melt equilibration for rims of plagioclase from 2014, 2007-8, 1990 with whole rock from this study used as melt compositions, and 2007-8 and 1990 with Jeffery et al. (2013) whole rock used as melt compositions, with an input of pressures from clinopyroxene-melt barometry.

Supplementary tables provided in Electronic Appendix C

dome. For the 2007-2008 lava dome sample (KD2), the liquid composition used include: 1) groundmass glass, 2) melt inclusions (both rhyolitic), and 3) whole rock compositions from Jeffery et al. (2013) lava dome material, 4) one whole rock from the lava dome sample from this study (KD2).

The calculated $K_D[\text{FeMg}]$ of the melts (13 options) are compared in Figure 15a and 15b as a further test of equilibrium. Only 206 combinations of the whole rock used as melt compositions with 1990, 2007-2008 and 2014 compositions are in the ideal $K_D[\text{FeMg}] = 0.28 \pm 0.08$ interval, and only these options are assumed to represent the melt in equilibrium with analysed clinopyroxenes at positive pressure estimates (cf. Putirka 2008). This is due to the melt inclusions and groundmass glass compositions not being mafic enough to satisfy the Mg/Fe equilibrium, and the ideal liquid compositions here have Mg# of 40-42. Further refinement of chosen equilibrium couples was performed using the predicted versus observed clinopyroxene components diopside-hedenbergite (DiHd; Putirka, 2008). 172 data points are in equilibrium (Fig. 15c) with the whole rock composition as melt, and these were used for thermobarometry estimations. The clinopyroxenes from the 2014 samples are only in equilibrium with whole rock 2014 compositions from this study. This suggests that clinopyroxene crystallised early when the melt was still close to the bulk-rock composition (cf. Costa et al., 2013). Clinopyroxenes with greater than Mg# 72 are not in equilibrium with the melt (Fig. 15).

The Neave and Putirka (2017) and Putirka (2008) models gives equilibration

temperature estimates for the 2014 clinopyroxenes of 1012-1053 °C (average = 1035 °C, $n = 96$, $1\sigma = 11$ °C; Fig. 16). The barometer-calculated, equilibration pressures for the 2014 clinopyroxenes are 7-380 MPa (average = 208 MPa, $n = 96$, $1\sigma = 100$ MPa; Fig. 16a). There is restricted temporal variation in temperature and pressures in the 2014 samples (Fig. 2), and all variation is within the standard estimated error of the barometer and thermometer.

The clinopyroxenes from the 1990 samples below Mg# 72-73 are only in equilibrium with our 1990 samples whole rock compositions, and the 1990 whole rock data from Jeffery et al. (2013) with clinopyroxenes with Mg# below 74 (Fig. 15). Equilibrated temperature values with our whole rock composition vary from 1008-1050 °C (average = 1030 °C, $n = 28$, $1\sigma = 12$ °C; Fig. 16). Equilibrated temperature values using Jeffery et al. (2013) 1990 whole rock compositions as the liquid are slightly higher, and range from 1023-1058 °C (average = 1040 °C, $n = 13$, $1\sigma = 11$ °C). On average this falls within error of the thermometer (SEE = 45 °C).

The clinopyroxenes in the 2007-2008 lava dome samples with Mg# below 72 are only in equilibrium with 2007-2008 whole rock compositions as input melt from this study, and Jeffery et al. (2013) 2007-2008 dome whole rock with clinopyroxenes below Mg# 74 (Fig. 15). Equilibrated temperature estimates from our whole rock compositions with 2007-2008 clinopyroxenes are 1020-1049 °C (average = 1038 °C, $n = 22$, $1\sigma = 8$ °C; Fig. 16). Pressure estimates vary from 3-345 MPa (average = 207 MPa, $n = 22$, $1\sigma = 91$ MPa). Clinopyroxenes in the 2007-2008 lava dome samples in equilibrium with melt compositions using Jeffery et al. (2013) published 2007-2008 lava dome whole rock data have slightly higher temperature estimates from 1036-1058 °C with lower melt-water content (average = 1049 °C, $n = 13$, $1\sigma = 7$ °C).

At higher melt-water content given by amphibole hygrometry (5.8 wt.% H_2O_{melt}) equilibration pressures and temperatures are comparable to that at 4 wt.% H_2O_{melt} . The temperature of equilibration for all clinopyroxenes across all samples drops by an average of 21 °C, although still within error of the thermometer (SEE = 45 °C), and the average equilibration pressure drops by ~6 MPa, also well within the error of the barometer (Fig. 16b).

4.5.1.3 Plagioclase-melt pre-eruptive pressure and temperature estimates

The plagioclase-melt thermobarometer of Putirka (2008) has been applied to the rims of plagioclase phenocrysts. This thermobarometer requires input of pressures, whereby the average pressure for each sample was taken from the clinopyroxene-melt barometer. The same clinopyroxene-liquid paired combinations were applied to the plagioclase-liquid model (Putirka, 2008) using Equation 24a as the thermometer (SEE = 36 °C). The barometer (Equation 25a) is viewed with much scepticism (cf. Putirka, 2008), due to large error values (SEE = 247 MPa) but can give an idea of pressure estimations. Of these combinations whole rock data used as liquid composition from this study were in equilibrium (for all samples), as were Jeffery et al. (2013) whole rock for 1990 and 2007-2008 samples ($n = 232$). All other combinations did not satisfy the equilibrium conditions of $KD[\text{AbAn}]$ at 0.1 ± 0.05 for temperatures below 1050 °C, and 0.28 ± 0.11 for temperatures above

1050 °C (cf. Putirka, 2008). On this basis, only compositions between An 63-83 mol.% were suitable for thermometry. This suggests that the rims of plagioclase phenocrysts in equilibrium with the bulk rock melt crystallised from a relatively mafic magma, rather than a dacitic magma, as melt inclusions and groundmass glass were not in equilibrium with plagioclase at the time of crystallisation. However, anorthite content does not always increase towards the rims of plagioclase in the 1990 and 2014 samples, not supporting this theory (Fig. 6). Yet increases in FeO in the outer rims of 2014 plagioclase phenocrysts (Fig. 6) is a more subtle suggestion of a discrete mafic influx before eruption.

Equilibration temperature estimates for the 2014 samples range from 1201-1221 °C (average = 1212 °C, $n = 127$, $1\sigma = 5$ °C; Figs. 2 and 16c). Calculated pressures range from 556-861 MPa (average = 723 MPa, $n = 127$, $1\sigma = 71$ MPa). Equilibration temperature estimates for the 1990 plagioclase paired with 1990 whole rock compositions from this study range from 1199-1216 °C (average = 1209 °C, $n = 59$, $1\sigma = 4$ °C). Calculated pressures range from 548-814 MPa (average = 686 MPa, $n = 59$, $1\sigma = 66$ MPa). The 2007-2008 equilibration temperature estimates using whole rock compositions from this study range from 1204-1218 °C (average = 1218, $n = 13$, $1\sigma = 4$), slightly higher than the 1990 and 2014 plagioclase temperature estimates. Equilibration pressures range from 587-805 MPa (average = 729 MPa, $n = 13$, $1\sigma = 58$ MPa). Temperature estimates for the 2007-2008 dome samples using Jeffery et al. (2013) whole rock compositions show very similar, overlapping results. Temperature estimates for the 1990 samples using Jeffery et al. (2013) whole rock compositions show very similar results (Fig. 16c). The three distinct arrays in pressure and temperature of the 1990 and 2014 samples reflect plagioclase being paired with the three, slightly different, bulk rock compositions.

4.5.2 Depth of magma crystallisation and storage beneath Kelut

The pressure estimates acquired from the barometric models give estimation of the depths of the magma plumbing system and any storage zones. Pressures were translated to depths, using a crustal density of 2640 kg/m³, inferred by the crustal stratigraphy of Java (Smyth et al., 2005, 2007). Clinopyroxene and amphibole models give a region of crystallisation ranging from 0-15 km depth. Equilibrated pressures give depth estimates for amphibole growth in a shallow region of crystallisation at ~8 km. Depth estimates for crystallisation of the 2014 clinopyroxenes range from 0.3-14.7 km (average = 8.1 km, $n = 116$, $1\sigma = 3.9$ km), with dominant growth regions at 5-6 and 11-12 km (Fig. 17a).

The 1990 clinopyroxene paired our whole rock melt composition gives a range depth estimates of around 0.4-14.0 km (average = 6.8 km, $n = 35$, $1\sigma = 4.4$ km). The dominant growth region is around 5-6 km (Fig. 17b). The 1990 clinopyroxenes equilibrated with Jeffery et al. (2013) 1990 whole rock melt composition provide crystallisation depth estimates of around 0.5-13.3 km (average = 6.7 km, $n = 12$, $1\sigma = 4.0$ km).

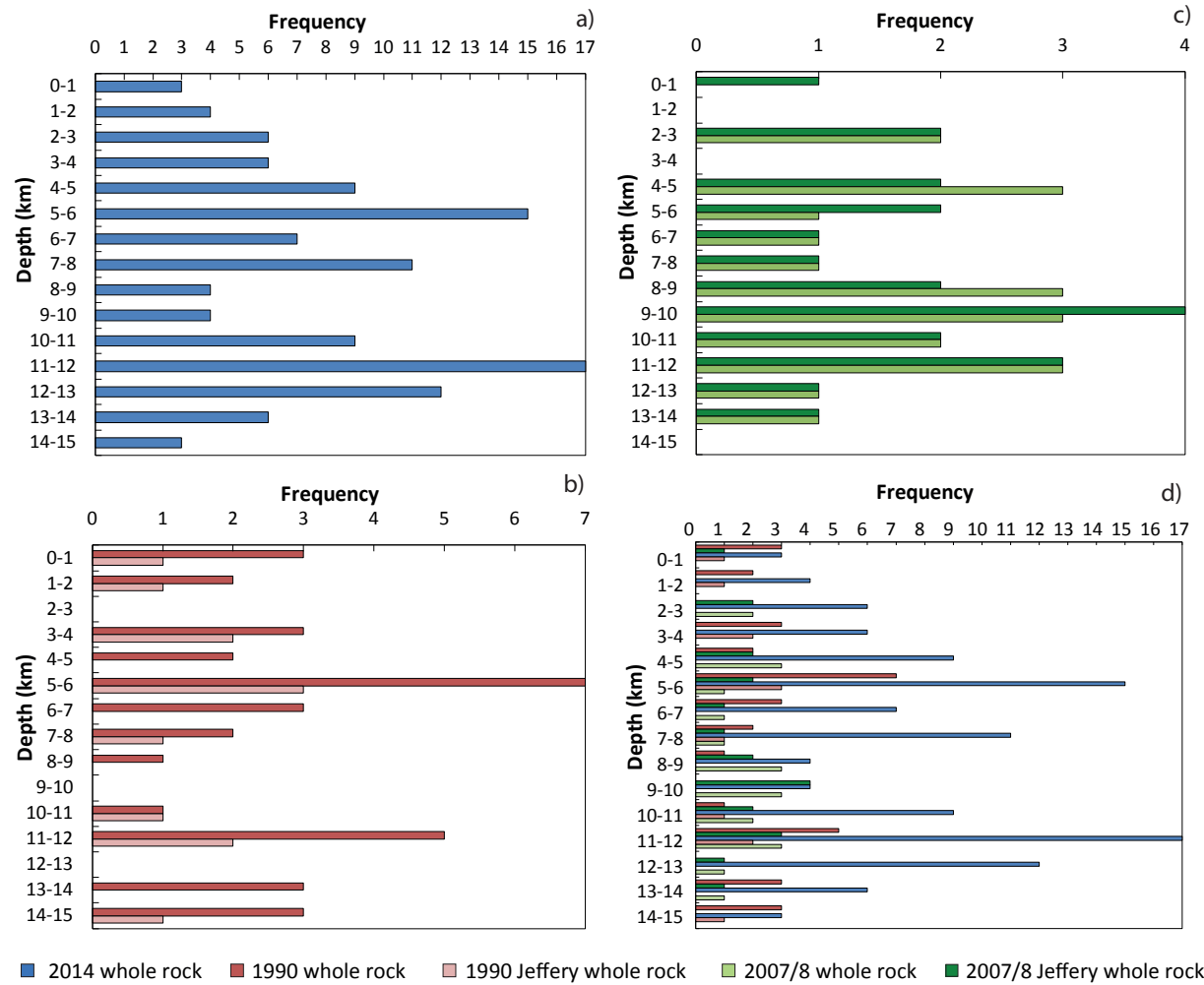


Figure 17: Frequency histograms of number of analyses showing the most populous depth regions calculated from pressure estimates from clinopyroxene-melt thermobarometry. a) Frequency of 2014 clinopyroxene crystallisation depth estimations with whole rock melt compositions from this study. b) Frequency of 1990 clinopyroxene crystallisation depth estimations with whole rock melt compositions from this study, and with Jeffery et al. (2013) 1990 whole rock. c) Frequency of 2007-2008 clinopyroxene crystallisation depth estimations with whole rock melt compositions from this study, and with Jeffery et al. (2013) 2007-8 whole rock, and d) Frequency of clinopyroxene crystallisation depth estimations from all equilibrated samples and combinations.

The pressure estimates of the 2007-2008 clinopyroxenes paired with our 2007-2008 whole rock compositions give depths of clinopyroxene growth ranging from 0.1-13.3 km (average = 8.0 km, $n = 22$, $1\sigma = 3.5$ km; Fig. 17c). Pressures from models using 2007-2008 clinopyroxene paired with Jeffery et al. (2013) lava dome whole rock compositions gives similar depths of clinopyroxene crystallisation.

The range of depths of clinopyroxene crystallisation indicate that there are multiple storage zones in the upper crust beneath Kelut (Figs. 17d and 18) and range from ~0 to ~14 km. The first clearly defined peaks in crystallisation of clinopyroxene in the 2014 and 1990 samples at ~5 km depth, although there is a spread from 2-8 km across all 2014, 2007-2008 and 1990 samples, with a second deeper at around 11 km depth across all samples, with spread from around 10-13 km. (Fig. 17a, b, c, d).

Calculated depths for the 2007-2008 lava dome are concurrent with that estimated by Jeffery et al. (2013) indicating two storage regions around ~4-5 and 8-12 km. Temperatures of plagioclase equilibration thermometry at 1199-1221 °C indicate that the majority of plagioclase crystallisation occurs within the mid-deep crustal region for all Kelut eruptions. Geophysical data corroborate the estimated shallow crystallisation regions determined by thermobarometry. Hidayati et al. (2009) state that swarms of volcano-tectonic (VT) earthquakes before the 2007-2008 eruption originated from a 5 km shallow reservoir. This is consistent with our estimate of the depth clinopyroxene crystallisation at 2-6 km. These observations only record shallow processes associated with the movement of magma to the surface before an eruption, so any detections movement from of deeper magma storage regions are not recorded. Regionally, Krakatau and Merapi volcanoes also have multi-level magma storage systems (Dahren et al., 2012; Costa et al., 2013; Preece et al., 2014). Krakatau has multi-level crystallisation of plagioclase at depths of 23-28 km, and 3-7 km, with clinopyroxenes crystallising at a depth of 7-12 km (Dahren et al., 2012). It is suggested that Merapi magma has multiple, interconnected crystallisation zones, with a deep reservoir at 30 km, an intermediate reservoir at 13 km, and a shallow reservoir <10 km depth, with most crystallisation of amphibole, clinopyroxene and plagioclase at intermediate to shallow storage zones (Chadwick et al., 2007; Costa et al., 2013; Preece et al., 2014), similar to that observed at Kelut. At Merapi, deeper crystallisation depth estimations are obtained from the clinopyroxene rims that have slightly higher, more primitive Al contents (Costa et al., 2013). This is also observed at Kelut, with high-Al rims crystallising at depths of around ~13 km, and low-Al rims crystallising at depths of around ~2 km. Therefore, it is suggested that the rims of these crystals fractionated from a slightly more primitive magma at greater depths, when the melt was still close to bulk-rock composition (although still in equilibrium). Jeffery et al. (2013) propose that stalling and crystallisation at deeper chamber levels (~8-11 km) occurs as a result of density differences at the boundary between metamorphosed basement material and upper volcanic material (cf. Smyth et al., 2005, 2008). This also supports the presence of multi-level storage and crystallisation regions at Kelut.

4.5.3 Discrete mafic influxes resulting in magma mixing and convection

In addition to the presence of multi-storage and crystallisation regions at Kelut, there is evidence to suggest that multiple discrete injections of mafic magma result in volatile injection and increase, and convective mixing of magmas prior to each eruption. The presence of sieve textured zones in Type 1 plagioclase phenocrysts across all samples suggests that these phenocrysts came into contact with melt rich in volatiles (e.g., H₂O, CO₂), causing rapid dissolution of pre-existing plagioclase, and trapping of melt onto the surface of the crystal (cf. Tepley et al., 1999, 2000; Ginibre et al., 2002a; Cassidy et al., 2016). Dissolution textures observed in plagioclase at Shiveluch, Stromboli and Fuego volcanoes are stated to be the result of this process (cf. Anderson, 1984; Landi et al., 2004; Humphreys et al., 2006). Therefore, the presence of multiple sieve-textures in different zones (e.g., Types 1a and 1b; Figs. 7 and 8) of the crystal may be the result of successive inputs of

volatile rich, mafic magma, hinting that repetitive dissolution-crystallisation processes take place (e.g., Landi et al., 2004), and that convective mixing events took place over some time, prior to each eruption (e.g., Jeffery et al., 2013; Cassidy et al., 2016). Phases that are heavily resorbed, such as plagioclase with ‘spongy’ sieve textured cores (texture Type 1c; Table 2) likely originated from deeper depths from more mafic end member magmas, and were then transported to shallower regions where they are then dispersed and mixed into more evolved magmas (e.g., Dungan and Rhodes, 1978; Tsuchiyama, 1985; Davidson and Tepley, 1999; Jeffery et al., 2013).

In addition, many of the Type 3 ‘spongy’ orthopyroxenes are heavily resorbed and replaced by clinopyroxene and plagioclase, which suggests that orthopyroxene therefore may have originated from a previous crystallisation from older magmas. These orthopyroxenes were likely eventually remobilised to shallower levels, where subsequent crystallisation of clinopyroxene occurred (cf. Jeffery et al., 2013). The presence of more mafic clinopyroxenes than orthopyroxenes, and the fact that touching pyroxene pairs are not in equilibrium suggests that they did not fractionate from a melt of the same composition, and did not crystallise cotectically. Additionally, nucleation of clinopyroxene mantling orthopyroxene (Tables 3, 4) can also indicate that an influx of a hotter magma, and convective self-mixing will have induced a temperature increase (e.g., Handley et al., 2010; Jeffery et al., 2013). This is supported by the crystallisation of higher-Al clinopyroxenes at deeper depths. The composition of 2014 pyroxene end-members (Fig. 11) generally overlaps that of the 1990 and 2007-2008 end-members. This could also indicate that mixing and recycling of previously crystallised clinopyroxenes occurred prior to the 2014 eruption.

Variations in anorthite content are observed from the cores to the rims of plagioclase phenocrysts in all eruptions (Figs. 5, 7 and 8). Variations in the compositional zonation of plagioclase can also be attributed to mixing events and convection in the magma chamber. Those phenocrysts with oscillatory zonation patterns (e.g., Figs. 7b, c, and 8b, c) with <10 mol.% anorthite fluctuations in each zone likely record the long term effects of convection in the chamber (e.g., Ginibre et al., 2002a). Convection processes of this scale are sustained by regular, repetitive influxes of mafic magma increasing turbulence in the chamber (cf. Shore and Fowler, 1996; Stewart and Fowler, 2001; Ginibre et al., 2002a). Plagioclase with abrupt large-scale variations in anorthite by ~ >20 mol.% between zones (e.g., Figs. 7a and 8a) more likely record larger influxes of magma that may also trigger subsequent mixing (e.g., Vance, 1962; Ginibre et al., 2002a; Landi et al., 2004).

Stewart and Fowler (2001) suggest that the rims of plagioclase grow shortly before the eruption, and reflect the composition of the melt at that time. The 2007-2008 reversely zoned phenocrysts do not show a large variation in An from core to rim (~68 to 70 mol.% An; Fig. 8c), so the variation is not significant enough to attribute the inverse zoning to large influx of primitive melt, and fluctuations are likely the result of a convecting magma, or repetitive discrete recharges and mixing. However, the fact that most of the phenocrysts are overall normally zoned in anorthite content (Figs. 5, 6, 7 and 8) shows that a large influx of mafic magma did not precede the 2014 eruption. In 1990 and 2014 plagioclase phenocrysts, changes FeO can increase with An,

or have a negative correlation, where An is depleted at the rims FeO increases (Figs. 7, 8). This may be the result of these zones coming into contact with a more discrete primitive, Fe rich melt during mixing or recharge (e.g., Troll and Schmincke, 2002; Ginibre et al., 2002b). However, the fluctuations are not large enough to support a large mafic recharge event prior to the eruption, as supported by anorthite zonation. Therefore, it may be possible that the iron rich zone or crystals may have come into contact with crustal contaminated melts. Chadwick et al. (2007) and Jeffery et al. (2013) propose the origin of such observations in Merapi and 2007-2008 plagioclase is due to the interaction between the upper crustal volcanoclastic sediment, crustal limestones or calc-silicate material with the melt.

4.5.4 Efficient mixing, and thermal and chemical buffering of magma

Kelut bulk rock compositions from the 1990, 2007-2008 and 2014 samples are very homogeneous, with ~1 wt.% variation SiO_2 (Fig. 12). This, coupled with similar trace elemental trends (Fig. 13) suggests that all samples from all eruptions are cogenetic. All elements lie generally (apart from Al) on a normal single array fractional crystallisation trend of the observed mineral assemblage. This is supported by the mineral modes in all samples, since plagioclase is the most populous mineral, followed by clinopyroxene and orthopyroxene (Table 1). Such homogeneities in magma chambers are often governed by effective and thorough thermal and compositional convectional mixing (cf. Murphey et al., 2000; Lindsay et al., 2001; Hauber et al., 2009). This suggests that the homogeneity of Kelut lavas may also be induced by latent heat buffering of the magma around 1030 °C at mid-crustal regions (as revealed by clinopyroxene-liquid equilibria), leading to rapid equilibration and crystal fractionation throughout the reservoir by roughly 40 % of the observed mineral phases. This would also require discrete, incremental input of magmas that are compositionally similar over time. Hauber et al. (2009) suggests that such latent heat buffering induces a ‘mushification’ stage of crystal rich magmas and extended storage periods. Eventual periodic and intermittent influxes of mafic magma cannot penetrate this overlying crystal mush, and therefore underplate the hot magma. The new injection of gas and thermal rejuvenation eventually leads to stirring, mobilisation and partial remelting of the crystal mush, redistributing xenocrysts throughout the multi-level magma chamber, mixing the system and buffering it to a constant composition (e.g., Couch et al., 2001; Miller et al., 2007). This may be the case for Kelut, as evidenced by the presence of glomerocryst clusters (Fig. 3, Table 1) and deep crustal xenoliths/cumulates in the 2007-2008 lava dome (Jeffery et al., 2013) acting as a buffer to the magmatic system.

Additionally, the periodic small influxes of volatile rich magmas act to lower the viscosity of magma, and therefore can produce more turbulent flow regimes, triggering efficient mixing with a resident high-viscosity magma (e.g., Kazahaya et al., 1994; Lejeune et al., 1999; Landi et al., 2004). This may also explain the homogeneity of clinopyroxene compositions between individual phenocrysts and clinopyroxenes in glomerocrysts (Fig. 9), and why high-Al clinopyroxene rims

and rims of plagioclase phenocrysts are in equilibrium with a basaltic-andesite 54-55 wt.% SiO₂ melt (the composition of the bulk rock), and not a more evolved, differentiated melt.

Since plagioclase is the most dominant mineral in all samples (up to 39 %), a decrease in aluminium with increasing silica should be observed in the bulk rock. However, there is a scatter in Al₂O₃ with SiO₂ (Fig. 12e). This suggests accumulation of plagioclase into the melt, either from previous crystallisation or glomerocryst (specifically Type 1) and xenolith clusters may have occurred at Kelut, and does not represent primary compositions of the melt (cf. Fournelle and Marsh, 1991). This is also supported by a positive Eu anomaly across all samples (Fig. 13) (e.g., Vukadinovic, 1993). However, the scattered array of Sr, Eu, and Eu anomaly with SiO₂ in Figure 14 does not support a simple accumulation of plagioclase (cf. Vukadinovic, 1993). Multi-level in-situ crystallisation and incorporation of plagioclase in a convecting, well-buffered magma chamber may be responsible for such observations.

4.5.5 Silicic magma at shallowest chamber regions

Injections of mafic, hotter magma below an initially homogeneous magma batch may also lead to eventual stratification of the magma chamber (e.g., Huppert et al., 1982; Ruprecht et al., 2008). Evidence from clinopyroxene-liquid thermobarometry and depth estimates suggest that the low-Al rims of clinopyroxene crystallise at shallower chamber regions of 1-2 km. Dense crystals and more mafic magmas accumulate at the lower parts of the magma reservoir (e.g., high-Al clinopyroxene at Kelut), whilst more silicic melt and lower density phases (e.g., low-An plagioclase at Kelut) rest near the roof (Hauber et al., 2009). Cassidy et al. (2016) suggest that the dacitic 2014 melt inclusions were trapped in the shallow levels of the chamber, not upon ascent. Texture Type 2 plagioclase crystals without sieve textures presented here are proposed to have stayed separate from boundary of interaction between the mixing and rejuvenating melts, or may have grown from a shallower (<5 km) reservoir, or pockets of the magma chamber (i.e. near the walls and surface) that were not as thoroughly mixed. Therefore, in this shallow crustal storage region, it is likely that the chamber is less affected by the efficient mixing of the resident magma with the periodic influxes of mafic magma (cf. Métrich et al., 2001; Landi et al., 2004).

Further evidence for an evolved magma at shallow levels is from lower An contents (\geq 56 mol.%) of microlites in samples (e.g., K34, K120, Fig. 5). The tiny, sub-100 μ m lath shaped microlites present in the groundmass of 2014 and 1990 samples suggests they formed at lower pressures during ascent in the conduit, or at very shallow levels from more evolved rhyolitic/dacitic melt compositions, without significant time for crystallisation during rapid ascent (Blundy and Cashman, 2001). The larger microlites in the 2007-2008 lava dome likely formed at elevated pressures in the magma chamber, with enough time for the larger microlites to grow (Couch et al., 2003; Fig. 4c). Large microlites may also grow during ascent, emplacement, or after emplacement during cooling, since the dome grew gradually over 8 months, the cooling rates may have been slow enough for larger microlites to grow. However, there is a wide range of An in microlites from

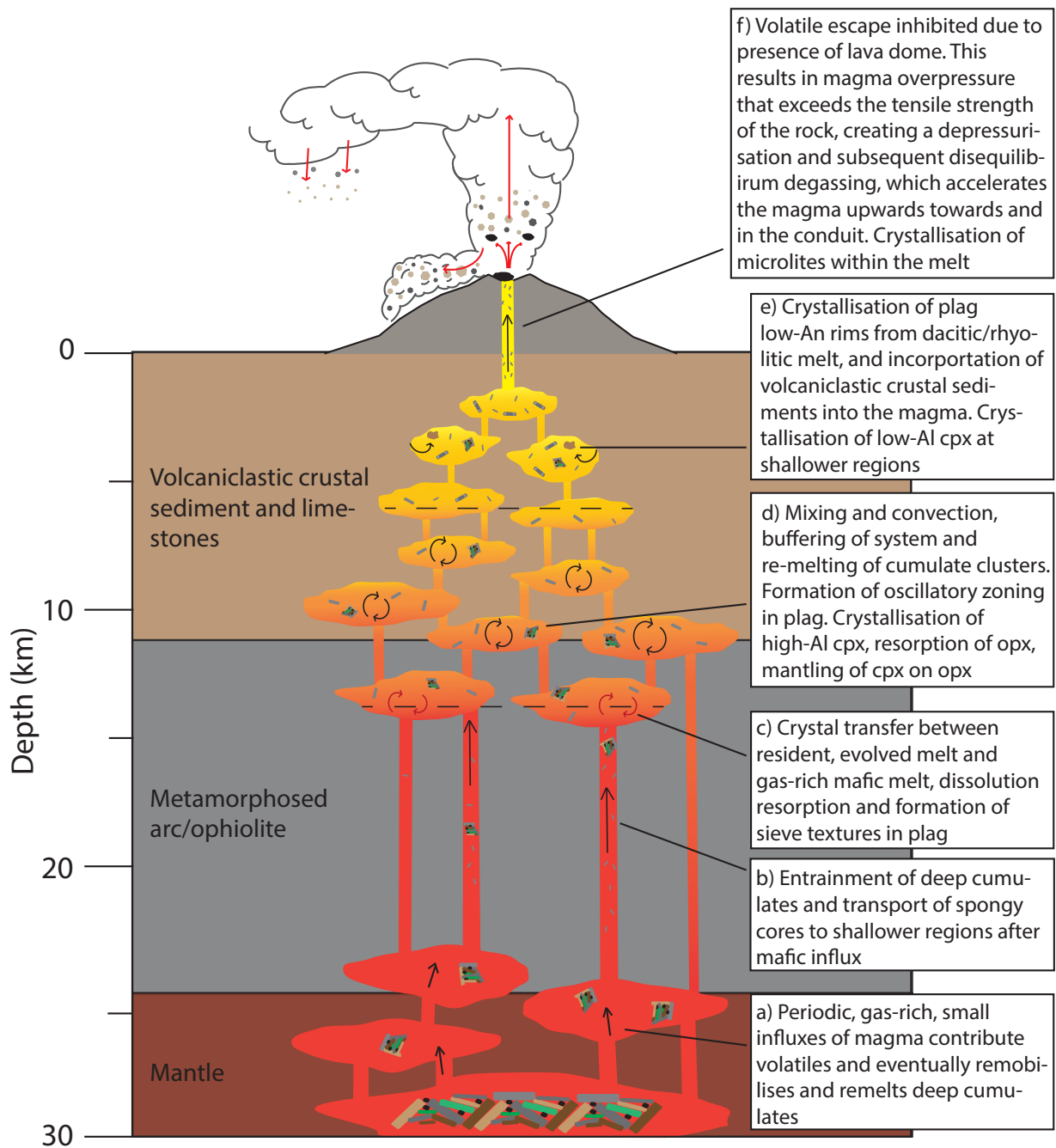


Figure 18: Petrogenetic model for the 2014 eruption of Kelut volcano based on results from this study integrated with that from Jeffery et al. (2013), and using information on the crustal structure beneath Kelut from Smyth et al. (2005, 2008). The same model may be applicable for the 1990 eruption model. Dark brown crystals indicate amphibole phenocrysts, light brown are orthopyroxene (opx), green are clinopyroxene (cpx), grey and plagioclase (plag), and black are titanomagnetites. Red magma indicates that of low SiO_2 , and yellow is higher SiO_2 . See text for discussion.

most samples (Fig. 4). Some high-An microlites (≤ 95 mol.%) seen in the 1990 and 2014 samples may also be an indication of a small mafic influx inducing mixing prior to the eruption (e.g., Couch et al., 2003). The wide range of anorthite content in microlites of one 1990 (K34), the 2007-2008, and all 2014 samples may be explained by small scale, late-stage mixing and buffering of the system prior to the eruptions.

4.5.6 Petrogenetic summary and model for Kelut magmas

The variety of mineral textures and homogeneity in bulk-rock compositions suggest that a complex interplay of processes are occurring in the magma plumbing system at Kelut (Fig. 18). Since the results show little variation temporally, this model can be applied for magma storage conditions prior to the 1990, 2007-2008 and 2014 eruptions.

The deepest portions of the magma chamber (~25-30 km depth) are proposed by Jeffery et al. (2013) to be the origin of primitive magmas that form the cumulate xenoliths with calcic plagioclase, clinopyroxene, orthopyroxene, olivine and amphibole (Fig. 18a). The presence of these cumulates in the 2007-2008 lavas in Jeffery et al. (2013), and glomerocryst clusters in this study, suggests that these cumulates have eventually been remobilised, or possibly crystallised at different storage levels. It is proposed that discrete, regular influxes of similar composition of gas-rich magma (Fig. 18a) eventually allowed for the redistribution, stirring and transportation of these crystals to a shallower storage region in the crust (e.g., Hauber et al., 2009; Fig. 18b). In addition, these regular influxes of magma will have contributed to the volatile content of the magma, without causing an eruption. Orthopyroxenes (Type 3; Table 4) and plagioclase (Type 1b, c; Table 2) with 'spongy' cores represent crystals undergoing accelerated thermal resorption (e.g., Troll et al., 2004). They likely originated from an earlier crystallisation event, and were incorporated into the mafic intruding magmas (Fig. 18c), eventually transported to shallower, more evolved regions. This supports a staged ascent and crystallisation of orthopyroxene and plagioclase.

Most crystallisation occurs at the mid- to upper-crustal storage levels, where the ascending magmas eventually stall and convect for some time around 8-10 km due to density differences between the surrounding rock (Fig. 18d, e). The higher-Al clinopyroxenes crystallising from a more primitive bulk-rock magma compositions (basaltic andesite rather than dacitic/rhyolitic), suggest partial crystallisation occurred at deeper depths of ~12-14 km (c.f. Costa et al., 2013). Mixing and interaction of the more gas-rich, primitive magma, with a stalled, more evolved resident magma at these levels allows for the formation of clinopyroxenes that mantle orthopyroxenes (Handley et al., 2010), and formation of sieve textures in plagioclase zones (Dungan and Rhodes, 1978; Tsuchiyama, 1985; Fig. 18c, d). The presence of rhyolitic and dacitic melt inclusions in the sieve textured regions indicates that the evolution of magma occurred in this mid-crustal zone, similar to that proposed by Jeffery et al. (2013) and Cassidy et al. (2016). The presence of complex oscillatory zonation patterns in plagioclase also supports that efficient magma mixing processes occurred during discrete influx events (cf. Dungan and Rhodes, 1978; Tsuchiyama, 1985; Landi et al., 2004).

Small- and large-scale oscillatory variations in anorthite content in plagioclase across all samples also suggest dissolution and movement of crystals occurred within in a convecting magma. It also suggests that there were regular influxes of new, volatile-rich magma that triggered mixing with the shallow, more evolved magma (e.g., Shore and Fowler, 1996; Stewart and Fowler, 2001; Troll and Schminke, 2002; Landi et al., 2004). Some of the sieve textures and zoning in plagioclase may be the result of repetitive dissolution-crystallisation processes taking place, as a result of rapid degassing driven by water exsolution when the phenocrysts comes into contact with a melt rich in volatiles (e.g., Landi et al., 2004). This also supports the postulation that discrete, volatile-rich magmas were periodically injected into the system. Cassidy et al. (2016) report crystallisation of plagioclase for the 2014 samples occurred around 1010 – 1090 °C, this fits our model better, and suggests most plagioclase crystallisation occurs at mid-crustal levels in a mixing magma chamber (Fig. 18d). These temperature estimates are within error of our clinopyroxene-liquid crystallisation temperatures, it is likely that estimations from our plagioclase-melt thermometry are too high (at around 1200 °C).

With time, it is likely that the xenoliths and glomerocrysts were remelted and recycled into the magma, acting to buffer the system to a constant basaltic-andesite composition (e.g., Couch et al., 2001; Lindsay et al., 2001; Miller et al., 2007; Fig. 18d), and is reflected in the homogeneity in the bulk-rock compositions of Kelut (Figs. 12, 13, 14). Remelting and recycling of xenoliths may provide a source for accumulating plagioclase, and variations in Sr, Eu and aluminium likely reflect a complex system where both plagioclase accumulation and fractionation are occurring. Continuous, small, and periodic gas-rich, mafic influxes, mixing and convection in the magma chamber over time are also responsible for buffering the temperature of the system (O'Hara, 1977), and of clinopyroxene crystallisation at ~1030 °C within a range of 2-13 km, and even in shallower regions (Fig. 18d, e). Similar crystallisation and storage regions have been observed regionally at Merapi and Krakatau volcanoes (Dahren et al., 2012; Costa et al., 2013; Preece et al., 2014, 2016).

Another peak in clinopyroxene crystallisation at shallower pressures indicates that further fractionation of lower-Al clinopyroxene occurred around ~5 km, where there is more influence of mixing with a more evolved magma (Fig. 18e). Cassidy et al. (2016) suggest that the 2014 melt inclusions were trapped within the shallow levels of the magma reservoir, and not upon ascent. It is likely that certain portions of the magma chamber (i.e. near the walls and upper chamber) were not as thoroughly mixed. Those plagioclase crystals without sieve textures are proposed to have stayed separate from boundary of interaction between the mixing and rejuvenating melts, or may have grown from a shallower (5 km) reservoir. Jeffery et al. (2013) proposed that these crystals might have been residing in a magma pocket, or being located at the top of the storage chamber. Along the conduit margins and walls of the chamber there is a temperature gradient which favours crystallisation of less calcic plagioclase from more evolved melts, less affected by the mixing processes at that time. Eventually, incorporation of these crystals into the melt by further mixing

processes can explain why such variation is seen in plagioclase compositions (Métrich et al., 2001; Landi et al., 2004).

However, the normal zonation patterns of anorthite in plagioclase from 1990 and 2014 samples indicate that a significant magma influx likely did not occur prior to the eruption. Rims of the plagioclase phenocrysts may have crystallised from shallower depths where the more evolved magma has been less affected by mixing and convection, and therefore will not record a late, discrete influx of magma to deeper chamber levels. Jeffery et al. (2013) propose that at these shallow levels (8-11 km depth), scouring and incorporation of the chilled margin facies occurs. This includes volcanoclastic crustal sediments and limestones (Smyth et al., 2005) contaminating melt, and may be responsible for the increase in FeO in the outer mid regions and rims of plagioclase phenocrysts (Fig. 18e).

Although there are no significant petrographic indicators for why the 1990 and 2014 eruptions were more explosive than the 2007-2008 eruption, Cassidy et al. (2016) propose that a small injection of H₂O-rich magma prior to the 2014 eruption increased the viscosity of the melt, contributing to the high explosivity of the eruption. The range of textures and zoning patterns observed in the phenocrysts, particularly plagioclase, and the homogeneity of the bulk rocks between eruptions suggest that efficient mixing of the chamber was taking place, due to periodic inputs of mafic, gas-rich magma and remelting of cumulate xenoliths. This has also been observed at steady state volcanic systems (e.g., Stromboli, Métrich et al., 2001; Landi et al., 2004), however Kelut is not in such a system. The cyclicity in formation and destruction of domes may be linked to differences in volatile content of magmas, but the chemistry of the different eruptive products is largely comparable. This suggests that there is no or little difference in the storage of the magmas prior to each eruption. The discrete, regular mafic influxes will not have been significant in volume to trigger an explosive event, and instead contributed volatiles into the magma. The lack of microlites, coupled with the high intensity of the 2014 eruption, suggests that the 2014 magma ascended rapidly (Chapter 2; Cassidy et al., 2016; Fig. 18f). Late-stage, small-scale mixing and convection prior to the 2014 eruption is supported by the presence of microlites with a range in high-An contents. The presence of some microlites with low-An contents suggests that these microlites crystallised rapidly upon ascent from this shallower, more evolved magma (Cashman, 1992; Blundy and Cashman, 2001).

It appears that shallow physical controls have a greater influence and drive the contrasting styles of eruptive activity at Kelut. The small, regular influxes of magma mafic magma to the system will also have contributed volatiles into the magma during the transition between effusive and explosive activity at Kelut. Due to the presence of the 2007-2008 lava dome these magmatic volatiles cannot escape at shallow levels for a period of over ~7 years whilst the dome was present. This results in eventual magma overpressure that exceeds the tensile strength of the rock, and drives magma upwards and a subsequent explosive eruption.

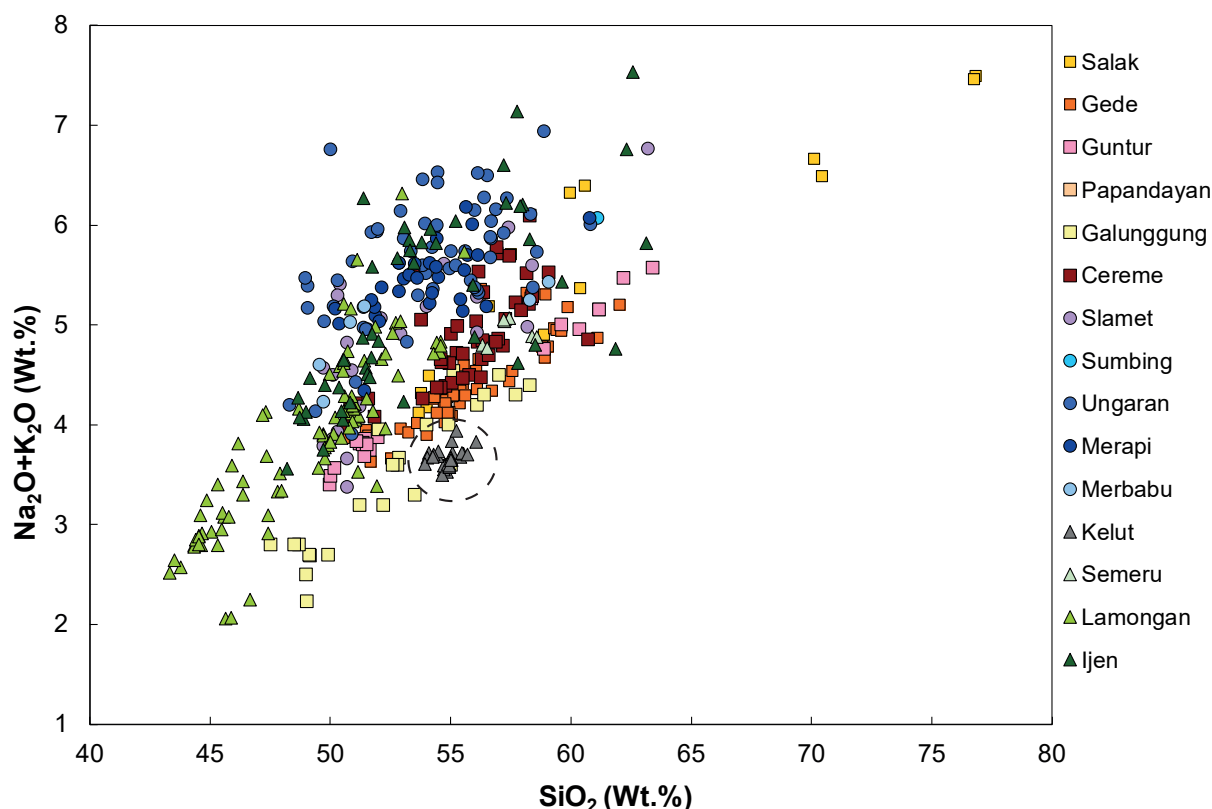


Figure 19: Total alkali silica of whole-rock compositions of Javan volcanoes for regional comparison. West Javan volcanoes are shown with squares, Central Javan with circles, and East Javan with triangles; Salak (Handley et al., 2008), Gede (Handley et al., 2010, 2011), Papandayan (Whitford, 1975; Whitford et al., 1981; White and Patchett, 1984; Woodhead et al., 2001), Guntur (Edwards, 1990), Galunggung (Whitford, 1975; Gerbe et al., 1992; Turner and Foden, 2001), Cereme (Edwards, 1990), Slamet (Vukadinovic and Sutawidjaja, 1995), Sumbing (Whitford, 1975; Woodhead et al., 2001), Ungaran (Whitford, 1975; Claproth, 1989; Woodhead et al., 2001), Merbabu (Gertisser, unpublished), Merapi (Woodhead et al., 2001; Troll et al., 2013; Handley et al., 2014), Kelut (this study; Jeffery et al., 2013), Semeru (Whitford, 1975; Carn and Pyle, 2001; Woodhead et al., 2001), Lamongan (Whitford, 1975; Carn and Pyle, 2001; Woodhead et al., 2001) and Ijen (Handley et al., 2007).

4.5.7 Regional and longer-term geochemical comparison

Whole rock compositions of Kelut 1990, 2007-2008 and 2014 lavas have a very homogenous range compared to volcanoes regionally from West, Central and East Java (Fig. 19, dashed circle). Kelut has geochemical signature similar to West Javanese volcanoes, and has higher silica with alkaline compositions than other East Javanese volcanoes, although the range is much larger in Semeru, Lamongan and Ijen volcanoes. Although Merapi appears to have a similar storage and crystallisation regions as Kelut, the suite of compositions from volcanic rocks is much more diverse, although this spans over a much longer timescale (up to ~2000 years). The homogeneity in samples may be due to a lack of temporally constrained geochemical data, i.e., only from the last 24 years and 3 eruptions.

As explored in Chapter 3, the longer-term view of Kelut shows a much more heterogeneous composition in the groundmass glasses of samples dating back to ~AD 560. Specific longer periods of inactivity allow for periods of differentiation, some discrete mafic influxes, and episodes

complete magma recharge. Such recharge episodes occur prior to, and likely trigger the largest eruptions, i.e. the 1586 VEI 5 eruption, and are unlike that of recent cyclic eruption styles (post-1920). Chapter 3 states that the composition of groundmass glasses during this time period show an incremental evolution and continued crystal fractionation of the petrogenetic assemblage with time, revealing that the system was unaffected by large mafic influxes for ~100 years. This is in agreement with this chapter, where the cyclicity in eruptive behaviour cannot be contributed to large mafic influxes or recharge events.

4.5.8 Regional and global eruptive patterns

Patterns in the transition of explosive eruptions to lava dome building are commonly seen at other arc volcanoes worldwide. Regionally, past eruptive behaviour at Merapi volcano consists of VEI 1 to 3 eruptions, and is renowned for its dome growth and collapse initiated block and ash flow deposits (BAFs; Newhall et al., 2000; Andreastuti et al., 2000; Gertisser and Keller, 2003; Cronin et al., 2013). The eruption of Merapi in 2006 consisted of an effusive dome growing period, with some gravitational dome collapse forming BAFs. In contrast, Merapi erupted explosively (VEI 4) in 2010, destroying the 2006 dome, shortly followed by rapid growth of a new dome (Gertisser et al., 2012; Cronin et al., 2013; Preece et al., 2014). This was the second most deadly eruption of Merapi to date due to the volume and number of PDCs and BAFs recorded (Cronin et al., 2013). Such PDCs are comparatively larger and more destructive than that at Kelut. The transition in effusive-explosive volcanism at Merapi is attributed to magma ascent rates, magma influx, and open- and closed-system degassing processes, since there is geochemical homogeneity between eruptions, similar to Kelut (Preece et al., 2014, 2016). The more recent eruptive cycles of lava dome growth and explosions at Colima volcano have been recorded in detail from 1998-2010. A period of dome extrusion occurred from 2007-2011 shortly after a small explosive eruption. In January 2013 a short explosive eruption occurred, destroying the dome and creating a new pit crater (Robin et al., 1991; Lavallée et al., 2012). Shortly after a new dome was growing at the summit in April 2013. Explosive eruptions at this volcano are attributed to an absence of continued gas flux because of the viscous, crystal-rich nature of the magma, acting to trap gases, leading to rapid decompression and fragmentation of magma (Lavallée et al., 2012). Timescales of this eruptive cycle of a short, violent event with a long, effusive event are much shorter, where dome extrusion occurs over a few years, compared to much longer periods at Kelut of ~7 to 31 years. Similarly, the Soufriere Hills volcano, Montserrat experiences the same cyclic nature of effusive to explosive eruptions. This is defined by moderate levels of dome growth, followed by lower level activity and the onset of the destruction of the dome due to collapse, preceded by a larger vulcanian explosive eruption (e.g., 1995-1997; Druitt et al., 2002; Edmonds and Herd, 2007). The transition to effusive behaviour is attributed to the development of permeable shear zones allowing gas release and relief of overpressure (Edmonds and Herd, 2007). Cyclic lava dome growth and destruction has occurred since 1980 accompanied with explosive activity at Shiveluch volcano, Kamchatka (Dirksen et al., 2006; Humphreys et al., 2006; Van Manen et al.,

2012; Zharinov and Demyanchuk, 2013). Thick pyroclastic flows as a result of the destruction of parts of the dome due to an explosive eruption were recorded from 2010-2013 (Ovsyannikov and Manevich, 2010). Unlike at Kelut, sectors of the dome here are progressively destroyed over a period of a few years, and not by a single, forceful explosive eruption. Similar conclusions to those attributed to the effusive-explosive transitions at Merapi can be attributed to Kelut. Using these better-studied volcanoes experiencing the same style of eruptions, a framework of future studies for Kelut volcano can be built. Such studies on volatile loss and ascent rates of magma can contribute further to the establishing of drivers of explosive volcanism.

4.6 Conclusions

The Kelut 1990, 2007-2008 and particularly the 2014 eruptive products provide evidence for a complex, open, magma plumbing system. All magmas are similar in terms of bulk compositions, mineral assemblages, and textural features. Most crystallisation occurs within multi-level (~2 and 14 km), multi-pocket, mid-crustal to upper-crustal storage zones. The main magma storage levels coincide with the lithological and density boundaries in the crust, and acted to stall the magma. Texturally complex plagioclase with small- and large-scale oscillatory zonation patterns and sieve-textures suggests that convection and multiple mixing of magmas takes place within this region. Pockets of shallower, more evolved older dacitic to rhyolitic magma are mixing with discrete, periodic, gas-rich, hotter, mafic influxes. This is supported by the presence of dacitic and rhyolitic pockets of melt comprising the sieve textured zones in plagioclase phenocrysts. These sieve textures are formed by volatile driven dissolution when phenocrysts come into contact with a melt rich in volatiles (Landi et al., 2004). Compositional homogeneity of the bulk rocks means that buffering and stalling of system for some time around ~1030 °C occurred. The movement, incorporation and partial remelting of crustal cumulates and glomerocryst clots into the recharging melt, and the regular, discrete, gas-rich recharge events to the system allowed for this to happen. This also adds to the textural diversity of 2014 eruptive products. Spongy cores of orthopyroxene and plagioclase indicate that the ascent of these phenocrysts was staged. These heavily resorbed phases originate from crystallisation of deeper, mafic melts, and when dispersed into more evolved melts resorption takes place. This also results in the formation of clinopyroxenes that mantle orthopyroxenes. Normal zonation of Anorthite, combined with Fe-rich areas in the mid regions to the outer rims of plagioclase phenocrysts indicates that recycling of crustal, volcanoclastic material took place, similar to that described by Jeffery et al. (2013). Scatter in aluminium, Sr, and a pronounced Eu anomaly support accumulation of plagioclase, whereas mineral modes support fractionation of plagioclase. It is proposed that both fractionation and accumulation of plagioclase occur within this magma system.

The homogeneity of bulk rock compositions and range in crystal textures of the 1990, 2007-2008 and 2014 samples suggests that continuous, discrete, volatile rich injections allow for efficient mixing and buffering of the magma system. The lack of significant differences in the

chemistry of the samples suggest the storage of the magmas from the 1990, 2014 and 2007-2008 magmas remain the same, and that the explosive (1990, 2014) and effusive (2007-2008) variants of eruptions are controlled by either the volatile content of the magma, or external processes. The lack of microlites in the 2014 and 1990 samples, when compared to the 2007-2008 dome samples suggest that the magma ascended too rapidly to allow crystallisation. This contributed to the explosivity of the 1990 and 2014 eruptions. Cassidy et al. (2016) propose that an injection of H₂O-rich magma raised the viscosity of the melt prior to the 2014 eruption, leading to a more explosive eruption. Other authors suggest that physical processes may be responsible for the transition in eruptive styles (e.g., Caudron et al., 2015; Nakashima et al., 2017). This conforms with the homogeneity in chemistry presented in this study, and the apparent cyclic pattern in eruptive activity can be attributed to degassing processes. The regular small influxes of mafic melt will have contributed to the increased volatile content of the magma, without causing an eruption. When coupled with the presence of a dome (e.g., 2007-2008 eruption) that inhibits volatile release for ~7 years, this will contribute to eventual magma overpressure that exceeds the tensile strength of the rock and depressurises the magma. This triggers disequilibrium degassing and rapid ascent of magma, and hence a more explosive eruption. However, other explosive eruptions at Kelut in the past appear to be driven by mixing, due to large mafic recharge events following periods of quiescence (Chapter 2). Further geophysical measurements and investigations into the volatile content of magmas, and magma ascent rates will be needed in order to continue to elucidate what exactly drives larger eruptions at Kelut.

4.7 Acknowledgements

Reza Firmansyah and Dermadi Madi from Bandung Institute of Technology are thanked for their assistance during fieldwork. Peter Wieland and David Adams at Macquarie University, and Robert Rapp at ANU are thanked for their analytical support. L. Goode is funded by an International Macquarie University Research Excellence Scholarship (iMQRES) (2012196) associated with an Australian Research Council Future Fellowship awarded to H. Handley (FT120100440). S. Cronin is funded by the New Zealand Natural Hazard Research Platform “Quantifying exposure to volcanic hazards” project.

4.8 References

- Adams, N.K., Houghton, B.F., Fagents, S.A., and Hildreth, W. (2006). The transition from explosive to effusive eruptive regime: The example of the 1912 Novarupta eruption, Alaska. *GSA Bulletin*. 118. 620-634.
- Anderson, A.T. (1984). Probable relations between plagioclase zoning and magma dynamics, Fuego volcano, Guatemala. *American Mineralogist*. 69. 660-676.
- Andreastuti, S.D., Alloway, B.V., and Smith, I.E.M. (2000). A detailed tephrostratigraphic framework at Merapi Volcano, Central Java, Indonesia: implications for eruption predictions and hazard assessment. *Journal of Volcanology and Geothermal Research*. 100. 51-67.

Chapter Four

- Blundy, J., and Cashman, K.V. (2001). Magma ascent and crystallisation at Mount St. Helens, 1980-1986. *Contributions to Mineralogy and Petrology*. 140. 631-650.
- Bourdier, J-L., Pratomio, I., Thouret, J-C., Boudon, G., and Vincent, P.M. (1997). Observations, stratigraphy and the eruptive processes of the 1990 eruption of Kelut volcano, Indonesia. *Journal of Volcanology and Geothermal Research*. 79. 181-203.
- Bourdier, J-L., Thouret, J-C., Pratomio, I., Vincent, P.M., and Boudon, G. (1997a). Volcanic hazards at Kelut volcano (Java island, Indonesia): lessons learned from the 1990 eruption. *Geomaterials*. 324. 961-968.
- Carn, S.A., and Pyle, D.M. (2001). Petrology and geochemistry of the Lamongan Volcanic Field, East Java, Indonesia: Primitive Sunda Arc magmas in an extensional tectonic setting? *Journal of Petrology*. 42. 1643-1683.
- Cashman, K.V. (1992). Groundmass crystallisation of Mount St. Helens dacite, 1980-1986: a tool for interpreting shallow magmatic processes. *Contributions to Mineralogy and Petrology*. 109. 431-449.
- Cashman, K., and Blundy, J. (2000). Degassing and crystallisation of ascending andesite and dacite. *Philosophical Transactions of the Royal Society*. 358.
- Cassidy, M., Cole, P.D., Hicks, K.E., Varley, N.R., Peters, N., and Lerner, A.H., (2015). Rapid and slow: Varying magma ascent rates as a mechanism for Vulcanian explosions. *Earth and Planetary Science Letters*. 420. 73-84.
- Cassidy, M., Castro, J.M., Helo, C., Troll, V.R., Deegan, F.M., Muir, D., Neave, D.A., and Mueller, S.P. (2016). Volatile dilution during magma injections and implications for volcano explosivity. *Geology*. 44. 1027-1030.
- Castro, J.M., Gardner, J.E. (2008). Did magma ascent rate control the explosive-effusive transition at the Inyo volcanic chain, California? *Geology*. 36. 279-282.
- Caudron, C., Taisne, B., Garces, M., Alexis, L.P., and Mialle, P. (2015). On the use of remote infrasound and seismic stations to constrain the eruptive sequence and intensity for the 2014 Kelud eruption. *Geophysical Research Letters*. 6614-6621.
- Chadwick, J.P., Troll, V.R., Ginibre, C., Morgan, D., Gertisser, R., Waight, T.E., and Davidson, J.P. (2007). Carbonate assimilation at Merapi Volcano, Java, Indonesia: insights from crystal isotope stratigraphy. *Journal of Petrology*. 48. 1793-1812.
- Claproth, R. (1989). Petrography and geochemistry of volcanic rocks from Ungaran, Central Java, Indonesia. Unpublished PhD thesis, Department of Geology, University of Wollongong, Australia.
- Clements, B., Hall, R., Smyth, H.R., and Cottam, M.A. (2009). Thrusting of a volcanic arc: a new structural model for Java. *Petrological Geoscience*. 15. 159-174.
- Coote, A.C., and Shane, P. (2016). Crystal origins and magmatic system beneath Ngauruhoe volcano (New Zealand) revealed by plagioclase textures and compositions. *Lithos*. 260. 107-119.
- Costa, F., Andreastuti, S., Bouvet de Maisonneuve, C., and Pallister, J.S. (2013). Petrological insights into the storage conditions, and magmatic processes that yielded the centennial 2010 Merapi explosive eruption. *Journal of Volcanology and Geothermal Research*. 261. 209-235.

- Couch, S., Sparks, R.S.J., and Carroll, M.R. (2001). Mineral disequilibrium in lavas explained by convective self-mixing in open magma chambers. *Nature*. 411. 1037-1039.
- Couch, S., Harford, C.L., Sparks, R.S.J., and Carroll, M.R. (2003). Experimental constraints on the conditions of formation of highly calcic plagioclase microlites at the Soufriere Hills volcano, Montserrat. *Journal of Petrology*. 44. 1455-1475.
- Cronin, S.J., Lube, G., Dayudi, D.S., Sumarti, S., Subrandiyo, S., Surono. (2013). Insights into the October-November 2010 Gunung Merapi eruption (Central Java, Indonesia) from the stratigraphy, volume and characteristics of its pyroclastic deposits. *Journal of Volcanology and Geothermal Research*. 261. 244-259.
- Dahren, B., Troll, V.R., Andersson, U.B., Chadwick, J.P., Gardner, M.F., Jaxybulatov, K., and Koulakov, I. (2012). Magma plumbing beneath Anak Krakatau volcano, Indonesia: evidence for multiple magma storage regions. *Contributions to Mineralogy and Petrology*. 163. 631-651.
- Davidson, J.P., and Tepley, F.J. (1997). Recharge in volcanic systems: evidence from isotopic profiles of phenocrysts. *Science*. 275. 826-829.
- De B  lizar, E., Lavigne, F., Gaillard, J.C., Grancher, D., Pratomo, I., and Komorowski, J.C. (2012). The 2007 eruption of Kelut volcano (East Java, Indonesia): Phenomenology, crisis management and social response. *Geomorphology*. 136. 165-175.
- Dirksen, O., Humphreys, M.C.S., Pletchov, P., Melnik, O., Demyanchuk, Y., Sparks, R.S.J., and Mahony, S. (2006). The 2001-2004 dome-forming eruption of Shiveluch volcano, Kamchatka: Observation, petrological investigation and numerical modelling. 155. 201-226.
- Droop, G.T.R. (1987). A general equation for estimating Fe³⁺ concentrations in ferromagnesian silicates and oxides from microprobe analyses, using stoichiometric criteria. *Mineralogical Society*. 51. 431-435.
- Druitt, T.H., and Kokelaar, B.P. eds., (2002). The eruption of Soufriere Hills volcano, Montserrat, from 1995 to 1999. Geological Society of London.
- Dungan, M.A., and Rhodes, J.M. (1978). Residual glasses and melt inclusions in basalts from DSDP Legs 45 and 46: evidence for magma mixing. *Contributions to Mineralogy and Petrology*. 67. 417-431.
- Edmonds, M., and Herd, R.A. (2007). A volcanic degassing event at the explosive-effusive transition. *Geophysical Research Letters*. 34.
- Edwards, C.M.H. (1990). Petrogenesis of tholeiitic, calc-alkaline and alkaline volcanic rocks, Sunda arc, Indonesia. Unpublished PhD thesis, Royal Holloway, University of London, UK.
- Fournelle, J., and Marsh, B.D. (1991). Shishaldin volcano: Aleutian high-alumina basalts and the question of plagioclase accumulation. *Geology*. 19.
- Gerbe, M.-C., Gourgaud, A., Sigmarsson, O., Harmon, R.S., Joron, J.-L., and Provost, A. (1992). Mineralogical and geochemical evolution of the 1982-1983 Galunggung eruption (Indonesia). *Bulletin of Volcanology*. 54. 284-298.
- Gertisser, R., and Keller, J. (2003). Temporal variations in magma composition at Merapi Volcano (Central Java, Indonesia): magmatic cycles during the past 2000 years of explosive activity. *Journal of Volcanology and Geothermal Research*. 123. 1-23.

Chapter Four

- Gertisser, R., Charbonnier, S.J., Keller, J., Quidelleur, X. (2012). The geological evolution of Merapi volcano, Central Java, Indonesia. *Bulletin of Volcanology*. 74. 1213-1233.
- Ginibre, C., Kronz, A., Wörner, G. (2002a). High-resolution quantitative imaging of plagioclase composition using accumulated backscattered electron images: new constraints on oscillatory zoning. *Contributions to Mineralogy and Petrology*. 142. 436-448.
- Ginibre, C., Wörner, G., and Kronz, A. (2002b). Minor- and trace-element zoning in plagioclase: implications for magma chamber processes at Paríacota volcano, northern Chile. *Contributions to Mineralogy and Petrology*. 142. 300-315.
- Global Volcanism Program (GVP) (1990). Report on Kelut (Indonesia). In: McClelland, L. (ed.), *Bulletin of the Global Volcanism Network*, 15:1. Smithsonian Institution. Available: <http://dx.doi.org/10.5479/si.GVP.BGVN199001-263280>.
- Global Volcanism Program (GVP) (1990a). Report on Kelut (Indonesia). In: McClelland, L. (ed.), *Bulletin of the Global Volcanism Network*, 15:9. Smithsonian Institution. Available: <http://dx.doi.org/10.5479/si.GVP.BGVN199009-263280>.
- Global Volcanism Program (GVP) (2008). Report on Kelut (Indonesia). In: Wunderman, R. (ed.), *Bulletin of the Global Volcanism Network*, 33:3. Smithsonian Institution. Available: <http://dx.doi.org/10.5479/si.GVP.BGVN200803-263280>.
- Global Volcanism Program (GVP) (2012). Report on Kelut (Indonesia). In: Wunderman, R. (ed.), *Bulletin of the Global Volcanism Network*, 37:3. Smithsonian Institution. Available: <http://dx.doi.org/10.5479/si.GVP.BGVN201203-263280>.
- Global Volcanism Program (GVP). (2014). Report on Kelut (Indonesia). In: Wunderman, R. (ed.), *Bulletin of the Global Volcanism Network*, 39:2. Smithsonian Institution. Available: <http://dx.doi.org/10.5479/si.GVP.BGVN201402-263280>.
- Global Volcanism Program (GVP). (2014a). Eruptive History. In: Kelut Eruption Page. Smithsonian Institution. Accessed March 2015. Available: <http://www.volcano.si.edu/volcano.cfm?vn=263280>
- Global Volcanism Program (GVP) (2014c). Smithsonian Institution. The Indonesia Region. Accessed March 2014. Available: <http://www.volcano.si.edu/region.cfm?rn=6>
- Hadikusumo, D. (1974). The rise and drop of Mt. Kelut crater bottom after paroxysmal eruptions. *Tectonophysics*. 23. 341-347.
- Hall, R. (2002). Cenozoic geological and plate tectonic evolution of SE Asia and the SW Pacific: computer-based reconstructions, model and animations. *Journal of Asian Earth Science*. 20. 353-431.
- Hall, R. (2011). Australia-SE Asia collision: plate tectonics and crustal flow. In: Hall, R., Cottam, M.A., and Wilson, M.E.J. (eds): *The SE Asian gateway: history and tectonics of Australia-Asia collision*. Geological Society of London Special Publication. 75 – 109.
- Hamilton, W. (1979). Tectonics of the Indonesian Region. US Geological Survey Professional Paper. 1078.1-50
- Handley, H.K. (2006). Geochemical and Sr-Nd-Hf-O isotopic constraints on volcanic petrogenesis at the Sunda Arc, Indonesia. PhD Thesis, Durham University, UK. <http://etheses.dur.ac.uk/2670/>

- Handley, H.K., Macpherson, C.G., Davidson, J.P., Berlo, K., and Lowry, D. (2007). Constraining fluid and sediment contributions of subduction-related magmatism in Indonesia: Ijen Volcanic Complex, Indonesia. *Journal of Petrology*. 48. 1155-1183.
- Handley, H.K., Davidson, J.P., and Macpherson, C.G. (2008). Untangling differentiation in arc lavas: constraints from unusual minor and trace element variations at Salak Volcano, Indonesia. *Chemical Geology*. 255. 360-376.
- Handley, H.K., Macpherson, C.G., and Davidson, J.P. (2010). Geochemical and Sr-O isotopic constraints on magmatic differentiation at Gede Volcanic Complex, West Java, Indonesia. *Contributions to Mineralogy and Petrology*. 159. 885-908.
- Handley, H.K., Blichert-Toft, J., Gertisser, R., Macpherson, C.G., Turner, S.P., Zaennudin, A., and Abdurrachman, M. (2014). Insights from Pb and O isotopes into along-arc variations in subduction inputs and crustal assimilation for volcanic rocks in Java, Sunda arc, Indonesia. *Geochemica et Cosmochimica Acta*. 139. 205-226.
- Handley, H.K., Reagan, M., Gertisser, R., Preece, K., Berlo, K., Barclay, J., Herd, R. (2018). Timescales of magma ascent and degassing and the role of crustal assimilation at Merapi volcano, Indonesia: constraints from uranium-series and Sr-Nd-Pb isotopic compositions in volcanic rocks of the 2006 and 2010 eruptions. *Geochimica et Cosmochimica Acta*. 222. 34-52.
- Hidayati, S., Basuki, A., Kristianto, Mulyana, I. (2009). Emergence of lava dome for the crater lake of Kelud volcano, East Java. *Jurnal Geologi Indonesia*. 4. 229-238.
- Huber, C., Bachmann, O., and Magna, M. (2009). Homogenization processes in silicic magma chambers by stirring and mushification (latent heat buffering). *Earth and Planetary Science Letters*. 283. 38-47.
- Humphreys, M.C.S., Blundy, J., and Sparks, R.S.J. (2006). Magma evolution and open-system processes at Shiveluch volcano: insights from phenocryst zoning. *Journal of Petrology*. 47. 2303-2334.
- Huppert, H.E., Sparks, R.S.J., and Turner, J.S. (1982). Effects of volatiles on mixing in calcalkaline magma systems. *Nature*. 332. 554-557.
- Jeffery, A.J., Gertisser, R., Troll, V.R., Jolis, E.M., Dahren, B., Harris, C., Tindle, A.G., Preece, K., O'Driscoll, B., Humaida, H., and Chadwick, J.P. (2013). The pre-eruptive magma plumbing system of the 2007-2008 dome-forming eruption of Kelut volcano, East Java, Indonesia. *Contributions to Mineralogy and Petrology*. 166. 275-308.
- Kazahaya, K., Shinohara, H., and Saito, G. (1994). Excessive degassing of Izu-Oshima volcano: magma convection in a conduit. *Bulletin of Volcanology*. 56. 207-216.
- Kemmerling, G.L.L (1921). De Uitbarsting van den G.Keleot in den nacht van den 19 den op den 20 sten Mei 1919. *Vulc. Meded, II. Landsdrukkerij – Welterreden*.
- Kristiansen, N.I., Prata, A.J., Stohl, A., and Carn, S.A. (2015). Stratospheric volcanic ash emissions from the 13 February 2014 Kelut eruption. *Geophysical Research Letters*. 42, 588-596.
- Landi, P., Métrich, N., Bertagnini, A., and Rosi, M. (2004). Dynamics of magma mixing and degassing recorded in plagioclase at Stromboli (Aeolian Archipelago, Italy). *Contributions to Mineralogy and Petrology*. 147. 213-227.

Chapter Four

- Lavallée, Y., Varley, N.R., Alatorre-Ibarguengoitia, M.A., Hess, K.U., Kueppers, U., Mueller, S., Richard, D., Scheu, B., Spieler, O., Dingwell, D.B. (2012). Magmatic architecture of dome-building eruptions at Volcan de Colima, Mexico. *Bulletin of Volcanology*. 74. 249-260.
- Leake, B.E., Woolley, A.R., Arps, C.E.S., Birch, W.D., Gilbert, M.C., Grice, J.D., Hawthorne, F.C., Kato, A., Kisch, H.J., Nickel, E.H., Rock, N.M.S., Schaumacher, J.C., Smith, D.C., Stephenson, N.C.N., Ungeretti, L., Whittaker, E.J.W., and Youzhi, G. (1997). Nomenclature of amphiboles: report on the subcommittee on amphiboles of the international mineralogical association, commission on new minerals and mineral names. *Canadian Mineralogist*. 35. 219-246.
- Lejeune, A.M., Bottinga, Y., Trull, T.W., Richet, P. (1999). Rheology of bubble-bearing magmas. *Earth and Planetary Science Letters*. 166. 71-84.
- Lindsay, J.M., Schmitt, A.K., Trumbull, R.B., de Silva, S.L., and Emmermann, R. (2001). Magmatic evolution of the La Pacana caldera system, Central Andes, Chile: compositional variation of the two cogenetic, large-volume felsic ignimbrites. *Journal of Petrology*. 42. 459-486.
- Lindsley, D.H. (1983). Pyroxene thermometry. *American Mineralogist*. 68. 477-493.
- Métrich, N., Bertagnini, A., Landi, P., and Rosi, M. (2001). Crystallisation driven by decompression and water loss at Stromboli volcano (Aeolian Islands, Italy). *Journal of Petrology*. 42. 1471-1490.
- Miller, J.S., Matzel, J.E.P., Miller, C.F., Burgess, S.D., and Miller, R.B. (2007). Zircon growth and recycling during the assembly of large, composite arc plutons. *Journal of Volcanology and Geothermal Research*. 162. 282-299.
- Morimoto, N., Fabries, J., Ferguson, A.K., Ginzburg, I.V., Ross, M., Seifert, F.A., Zussman, J., Aoki, K., and Gottardi, G. (1988). Nomenclature of pyroxenes. *Mineral Mag.* 52. 535-550.
- Nakamichi, H., Iguchi, M., Triastuty, H., Hendrasto, M., and Mulyana, I. (2017). Differences of precursory seismic energy release for the 2007 effusive dome-forming and 2014 plinian eruptions at Kelud volcano, Indonesia. *Journal of Volcanology and Geothermal Research*. <http://dx.doi.org/10.1016/j.jvolgeores.2017.08.004>
- Neave, D., and Putirka, K.D. (2017). A new clinopyroxene-liquid barometer, and implications for magma storage pressures under Icelandic rift zones. *American Mineralogist*. 102. 777-794.
- Nelson, S.T., and Montana, A. (1992). Sieve-textured plagioclase in volcanic rocks produced by rapid decompression. *American Mineralogist*. 77. 1242-1249.
- Newhall, C.G., Bronto, S., Alloway, B., Banks, N.G., Bahar, I., del Marmol, M.A., Hadisantono, R.D., Holcomb, R.T., McGeehin, J., Miksic, J.N., Rubin, M., Sayudi, S.D., Sukhyar, R., Andreastuti, S., Tilling, R.I., Torley, R., Trimble, D., and Wirakusumah, A.D. (2000). 10,000 years of explosive eruptions of Merapi Volcano, Central Java: archaeological and modern implications. *Journal of Volcanology and Geothermal Research*. 100. 9-50.
- Nguyen, C.T., Gonnermann, H.M., and Houghton, B.F. (2014). Explosive to effusive transition during the largest volcanic eruption of the 20th century (Novarupta 1912, Alaska). *Geology*. 42. 702-706.
- O'Hara, M.J. (1977). Geochemical evolution during fractional crystallisation of a periodically refilled magma chamber. *Nature*. 266. 503-507.

- Ovsyannikov, A. and Manevich, A. (2010). Eruption Shiveluch in October 2010. Bulletin of Kamchatka Regional Association (Educational-Scientific Center); Earth Sciences (In Russian). IV&S FEB RAS, Petropavlovsk-Kamchatka (2010). 2. No. 16, ISSN 1816-5532.
- Plank, T., Kelley, K.A., Zimmer, M.A., Hauri, E.H., and Wallace, P.J. (2013). Why do mafic arc magmas contain ~4 wt.% water on average? *Earth and Planetary Science Letters*. 364. 168-179.
- Platz, T., Cronin, S.J., Cashman, K.V., Stewart, R.B., and Smith, I.E.M. (2007). Transition from effusive to explosive phases in andesite eruptions – A case-study from the AD1655 eruption of Mt. Taranaki, New Zealand. 161. 15-34.
- Preece, K., Gertisser, R., Barclay, J., Berlo, K., Herd, R.A., Edinburgh Ion Microprobe Facility. (2014). Pre- and syn-eruptive degassing and crystallisation processes of the 2010 and 2006 eruptions of Merapi volcano, Indonesia. *Contributions to Mineralogy and Petrology*. 168. 1-25.
- Putirka, K.D. (2008). Thermometers and barometers for volcanic systems. *Reviews in Mineralogy & Geochemistry*. 69. 61-120.
- Ripepe, M., Marchetti, E., Ulivieri, G., Harris, A., Dehn, J., Burton, M., Caltabiano, T., and Salerno, G. (2005). Effusive to explosive transition during the 2003 eruption of Stromboli volcano. *Geology*. 33. 341-344.
- Ripepe, M., Marchetti, E., and Ulivieri, G. (2007). Infrasonic monitoring at Stromboli volcano during the 2003 effusive eruption: Insights on the explosive and degassing process of an open conduit system. *Journal of Geophysical Research*. 112.
- Robin, C., Camus, G., Gourgaud, A. (1991). Eruptive and magmatic cycles at Fuego de Colima volcano (Mexico). *Journal of Volcanology and Geothermal Research*. 45. 209-225.
- Ruprecht, P., Bergantz, G.W., and Dufek, J. (2008). Modeling of gas-driven magmatic overturn: Tracking of phenocryst dispersal and gathering during magma mixing. *Geochemistry, Geophysics and Geosystems*. 9. 1-20.
- Shore, M., and Fowler, A.D. (1996). Oscillatory zoning in minerals: a common phenomemon. *Canadian Mineralogist*. 34. 1111-1126.
- Siebert, L., Simkin, T., and Kimberly, P. (2011). *Volcanoes of the World*. 3rd Ed. University of California Press: Los Angeles. 83-102.
- Smyth, H., Hall, R., Hamilton, J., and Kinny P. (2005). East Java: Cenozoic basins, volcanoes and ancient basement. In: 30th Annual Convention of the Indonesian Petroleum Association. Jakarta, Indonesia: Indonesian Petroleum Association. 251-266.
- Smyth, H.R., Hamilton, P.J., Hall, R., and Kinny, P.D. (2007). The deep crust beneath island arcs: Inherited zircons reveal a Gondwana continental fragment beneath East Java, Indonesia. *Earth and Planetary Science Letters*. 258. 269 – 282.
- Smyth, H.R., Hall, R., and Nichols, G.J. (2008). Cenozoic volcanic arc history of East Java, Indonesia: The stratigraphic record of eruptions on an active continental margin. *The Geological Society of America, special paper*. 436. 199-221
- Sparks, R.S.J., Sigurdsson, H., and Wilson, L. (1977). Magma mixing: a mechanism for triggering acid explosive eruptions. *Nature*. 267. 315-318.

Chapter Four

- Stewart, M.L., and Fowler, A.D. (2001). The nature and occurrence of discrete zoning in plagioclase from recently erupted andesitic volcanic rocks, Montserrat. *Journal of Volcanology and Geothermal Research*. 106. 243-253.
- Tepley, F.J., Davidson, J.P., Tilling, R.I., and Arth, J.G. (2000). Magma mixing, recharge and eruption histories recorded in plagioclase phenocrysts from El Chichón volcano, Mexico. *Journal of Petrology*. 41. 1397-1411.
- Tepley, F.J., Davidson, J.P., and Clynnne, M.A. (1999). Magmatic interactions as recorded in plagioclase phenocrysts of Chaos Crags, Lassen Volcanic Center, California. *Journal of Petrology*. 40. 787-806.
- Troll, V.R., and Schmincke, H-U. (2002). Magma mixing and crustal recycling recorded in ternary feldspar from compositionally zoned peralkaline ignimbrite 'A', Gran Canaria, Canary Islands. *Journal of Petrology*. 43. 243-270.
- Troll, V.R., Donaldson, C.H., Emelus, C.H. (2004). Pre-eruptive magma mixing in ash-flow deposits of the Tertiary Rum Igneous Centre, Scotland. *Contributions to Mineralogy and Petrology*. 147. 722-739.
- Troll, V.R., Deegan, F.M., Jolis, E.M., Harris, C., Chadwick, J.P., Gertisser, R., Schwarzkopf, L.M., Borisova, A.Y., Bindeman, I.N., Sumarti, S., and Preece, K. (2013). Magmatic differentiation processes at Merapi volcano: inclusion petrology and oxygen isotopes. *Journal of Volcanology and Geothermal Research*. 261. 38-49.
- Tsuchiyama, A. (1985). Dissolution kinetics of plagioclase in the melt of a system diopside-albite-anorthite and origin of dusty plagioclase in andesites. *Contributions to Mineralogy and Petrography*. 89. 1-16.
- Turner, S., and Foden, J. (2001). U, Th, and Ra disequilibria, Sr, Nd and Pb isotope and trace element variations in Sunda arc lavas: predominance of a subducted sediment component. *Contributions of Mineralogy and Petrology*. 142. 43-57.
- Van Bemmelen, R.W. (1949). *The Geology of Indonesia and Adjacent Archipelago*. Government Printing Office: The Hague. 1-150.
- Vance, J. (1962). Zoning in igneous plagioclase; normal and oscillatory zoning. *American Journal of Science*. 260. 746-760.
- Van Manen, S.M., Blake, S., and Dehn, J. (2012). Satellite thermal infrared data from Shiveluch, Kliuchevskoi, and Karymsky, 1993-2008: effusion, explosions and the potential to forecast ash plumes. *Bulletin of Volcanology*. 74. 1313-1335
- Varley, N.R., and Taran, Y.A. (2003). Degassing processes of Popocatepetl and Volcán de Colima, Mexico. In: Oppenheimer, C., Pyle, D.M and Barclay, J. (eds) *Volcanic degassing*. Geological Society, London. 263-280.
- Vukadinovic, D. (1993). Are Sr enrichments in arc basalts due to plagioclase accumulation? *Geology*. 21. 611-614.
- Vukadinovic, D., and Sutawidjaja, I. (1995). Geology, mineralogy and magma evolution of Gunung Slamet Volcano, Java, Indonesia. *Journal of Southeast Asian Earth Sciences*. 11. 135-164.
- White, W.M., and Patchett, J. (1984). Hf-Nd-Sr isotopes and incompatible element abundances in island arcs: implications for magma origins and crustal-mantle evolution. *Earth and Planetary Science Letters*. 67. 167-185.

- Whitford, D.J. (1975). Strontium isotopic studies of volcanic rocks of the Sunda Arc, Indonesia and their petrogenetic implications. *Geochim. Cosmochim. Acta*. 39. 1287-1302.
- Whitford, D.J., White, W.M. and Jezek, P.A (1981). Neodymium isotopic composition of Quaternary island arc lavas from Indonesia. *Geochemica et Cosmochimica Acta*. 45. 989-995.
- Wirakusumah, A.D. (1991). Some studies of the volcanology, petrology and structure of Mt. Kelut, East Java, Indonesia. PhD Thesis, Victoria University, Wellington, New Zealand.
- Woodhead, J.D., Hergt, J.M., Davidson, J.P and Eggins, S.M. (2001). Hafnium isotope evidence for 'conservative' element mobility during subduction processes. *Earth and Planetary Science Letters*. 192. 331-346.
- Woods, A.W., and Koyaguchi, T. (2004). Transitions between explosive and effusive eruptions of silicic magmas. *Nature*. 370. 641-644.
- Zaennudin, A., Dana, I., Wahyudin, D., and Hadisantono, R.D. (1987). Laporan Kemajuan Tahap III Pemetaan Gunungapi Kelut Jawa Timur. Unpublished report, Volcanological Survey of Indonesia.
- Zen, M.T., and Hadikusumo, D. (1965). The future danger of Mt. Kelut (Eastern Java – Indonesia). *Bulletin Volcanologique*. 28. 275-282.
- Zharinov, N.A., and Demyanchuk, Y.V. (2013). Large explosive eruptions of Shiveluch volcano, Kamchatka resulting in partial destruction of the extrusive dome (February 28, 2005 and October 27, 2010). *Journal of Volcanology and Seismology*. 7. 131-144.
- Zobin, V.M., Luhr, J.F., Taran, Y.A., Breton, M., Cortes, A., De La Cruz-Reyna, S., Dominguez, T., Galindo, I., Gavilanes, J.C., and Muniz, J.J. (2002). Overview of the 1997-2000 activity of Volcan de Colima, Mexico. *Journal of Volcanology and Geothermal Research*. 117. 1-19.

5. Conclusions and Future Work

This thesis has developed short-term and long-term volcanological and geochemical records for Kelut volcano that did not previously exist. The data was used to gain a deeper understanding of eruption dynamics, patterns in eruptive activity, and magmatic drivers of recent and past eruptions at Kelut. This thesis specifically aimed to determine the following objectives:

1. Improve the understanding of eruption dynamics of intermediate composition explosive eruptions from deposition records at Kelut;
2. Build long-term detailed and combined records of volcanology, geochronology and geochemistry in order to understand how Kelut's eruptive behaviour has varied over time;
3. Use petrography, mineralogy and geochemistry to gain insight into the magma plumbing system dynamics, storage regions and pre-eruptive magmatic processes that influence the style and magnitude of eruptions; and
4. Establish the pattern and frequency of eruptive activity over time at Kelut, particularly the recurrence of large eruptions, and determine how this aids in eruption forecasting and identifying potential hazards.

5.1 Improving the understanding of eruption dynamics from deposits of single explosive eruptions at Kelut

Due to the lack of stratigraphic and volcano-sedimentologic studies of deposits from largest-scale explosive eruptions at Kelut, this research firstly focused on identifying the physical characteristics (size, grain size distribution, componentry) and stratigraphic relationships of the 2014 eruption, presented in Chapter 2. The stratigraphic relationships of the >VEI 3 eruption sequences were presented in Chapter 3. Determining the timing of eruptive events through an eruptive episode is important in placing constraints on the mechanisms, processes and dynamics of the eruption, and this investigated from stratigraphy and sedimentary characteristics of pyroclastic deposits of large explosive eruptions.

5.1.1 The 2014 eruption of Kelut

The 2014 eruption of Kelut was well observed and the chronology of the eruptive episodes was well documented. The investigation into the stratigraphy and deposit characteristics in Chapter 2 provided key insight and a better framework for understanding the dynamics and timing of eruptive events. Chapter 2 specifically focused on an in-depth sedimentological study of the deposits (see Figure 4, Chapter 2) from the most recent 2014 plinian eruption, directly compared to observational accounts of the eruption chronology, in order to elucidate a dynamic framework for the eruption, revealing that the eruption had three stages (Figure 10, Chapter 2). As the eruption

progressed, the characteristics of both pyroclastic density current (PDC) and tephra fall deposits reflect a 4-hour sustained eruption that became progressively more powerful during its course. Specifically, the first PDC deposits reflected the early destruction of the pre-existing 2007-2008 lava dome by explosions. The subsequent PDC deposits in Stage 2 reflected an increase in the flux of magma, due to conduit and vent widening, and the incorporation of dense blocks into the basal margins of the column. These deposits were associated with a large explosion that occurred approximately ~15-30 minutes after the initial dome-destruction. The PDC deposits from both eruptive stages emplaced thick lobes of pumice rich PDC deposits, emplaced through eruptive transport processes, ponding within the main valleys. The deposits are comparable to other similar eruptions, with early highly concentrated, lithic-rich PDCs, followed by pumice-rich PDCs. The final pumice-lapilli falls reflected sedimentation from a sustained ~26 km high eruption column. At this stage rapid expansion of the gas-rich magma was most efficient, and indicated the climax of the eruption was reached. This work contributed an improved understanding of the 2014 eruption, by piecing together an imperfect observation record and chronological framework with details of the pyroclastic deposits. Together, these provided a more robust understanding of the dynamics of the 2014 eruption. The scale and style of the 2014 eruption are comparable to that of the previous similar explosive eruption of Kelut that occurred in 1990 as described by Bourdier et al. (1997).

5.1.2 Other older large explosive eruptions of Kelut

The eruptive record at Kelut shows evidence of several VEI 4 to 5 eruptions that were closely investigated, and reported in Chapter 3. Here a well-constrained stratigraphic record of the older eruptive deposits at Kelut were studied, whereby large eruptive events were easily identified due to their deposit size, coarseness and sedimentary characteristics. Key features and mapping was used to correlate units from site to site. The largest eruptive events (e.g. 1586 (VEI 5)) in the stratigraphic record were clearly identified by larger volume deposits, and were easily correlated with key identifiable deposit characteristics (e.g., massive, coarse-pumice lapilli; see Figure 2, Chapter 3). The pre-2014 deposits of these larger (\geq VEI 3) eruptions vary from large sets of tephra falls to intricate bed sets of PDC deposits (see Figure 4, Chapter 3). This indicated that the past eruptive behaviour of Kelut was complex, and geochemical investigations into the interplay of deep and shallow magmatic processes was needed in order to determine drivers of this activity. Such tephrochronological studies like those undertaken at Merapi (Gertisser and Keller, 2003), and Mt. Taranaki, New Zealand (Turner et al., 2008; Torres-Orozco et al., 2017), are long overdue at Kelut to better characterise the volcanic and magmatic history, where the frequency, scale and composition of eruptives varies over time.

5.2 Variation in Kelut's eruptive behaviour and magmatic processes from a series of eruptions

Radiocarbon dating of charcoal in deposits from the well-constrained stratigraphic sequences recorded eruptive activity that pre-dates the historical records of volcanism at Kelut (see Table 1, Chapter 3). In Chapter 3, a total of 25 separate eruptive events from ~AD 560 to 2014 were recorded for the first time at Kelut (see Figure 4, Chapter 3). The next focus of this thesis was to characterise and understand the temporal geochemical variations in eruptive record, in relation to the complex interplay of magmatic processes, including defining periods of magmatic differentiation, mafic/fresh magma influx, recharge events, and mixing of magmas (see Figures 4 and 8, Chapter 3). These processes governed the variable periodicity and frequency of eruptions at Kelut pre-AD 1826. Similar processes are envisaged to have controlled the variation in eruptive behaviour at Merapi (Andreastuti et al., 2000; Gertisser and Keller, 2003), Colima, Mexico (Luhr et al., 2010) and Hekla, Iceland (Larsen and Eriksson, 2007).

5.2.1 Pre-eruptive influences on the magma system; large recharge versus small influxes of magma and eruption triggers

Figure 1 shows a summary of all pathways and scenarios of magmatic influences on eruptive behaviour at Kelut. The oldest, pre-AD 1000 eruptions at Kelut were represented by large tephra falls from infrequent ~VEI 4 eruptions, with long periods of repose between each. These eruptions were fed by some of the most evolved composition (70-72 wt.% SiO₂) magmas, where the eruptions were tapping a differentiated, shallower magma reservoir, previously undisturbed by large primitive recharge events for many years, although an exact timescale is to be determined. The first three eruptions ~AD 560 are represented by pathway A in blue on Figure 1. Five influxes of mafic magma were recorded after this sequence of eruptions, every ~200 to 450 years, the first at ~AD 700 (see Figures 4 and 8, Chapter 3). The two eruptions pre-AD 1000, around ~AD 700 and 850 are represented by pathway B on Figure 1. From AD 1000, regular, small influxes of new magma maintained the system in a quasi-steady state via mixing with the differentiating, residual magma, and also maintaining periods of high eruptive rates, represented by pathway C on Figure 1. Activity post-AD 1000 to 1919 at Kelut records more frequent eruptions than earlier (every ~35 years), with behaviour that varied from vulcanian to plinian in style, including clear periods of dome-destruction. However, the largest mafic recharge events, such as that recorded pre-1586 eruption (pathway B, Fig. 1), appeared to trigger the more explosive eruptions at Kelut and evacuation of the magma chamber without time for efficient mixing (Fig. 1). This is the case for other large eruptions, such as those at Tarawera volcanic complex, New Zealand (Okareka eruption; Shane et al., 2008), Paríacota volcano, Chile (Ginibre et al., 2007), and the Bishop magma system, California (Wark et al., 2007). This was followed by the longest ~75 year long period of repose due to magma replenishment, where the magma was undisturbed for some time after allowing for differentiation. In other cases, recharge, coupled with magma mixing is a well-documented eruption trigger (e.g. Sparks et al., 1977; Davidson and Tepley, 1997) at

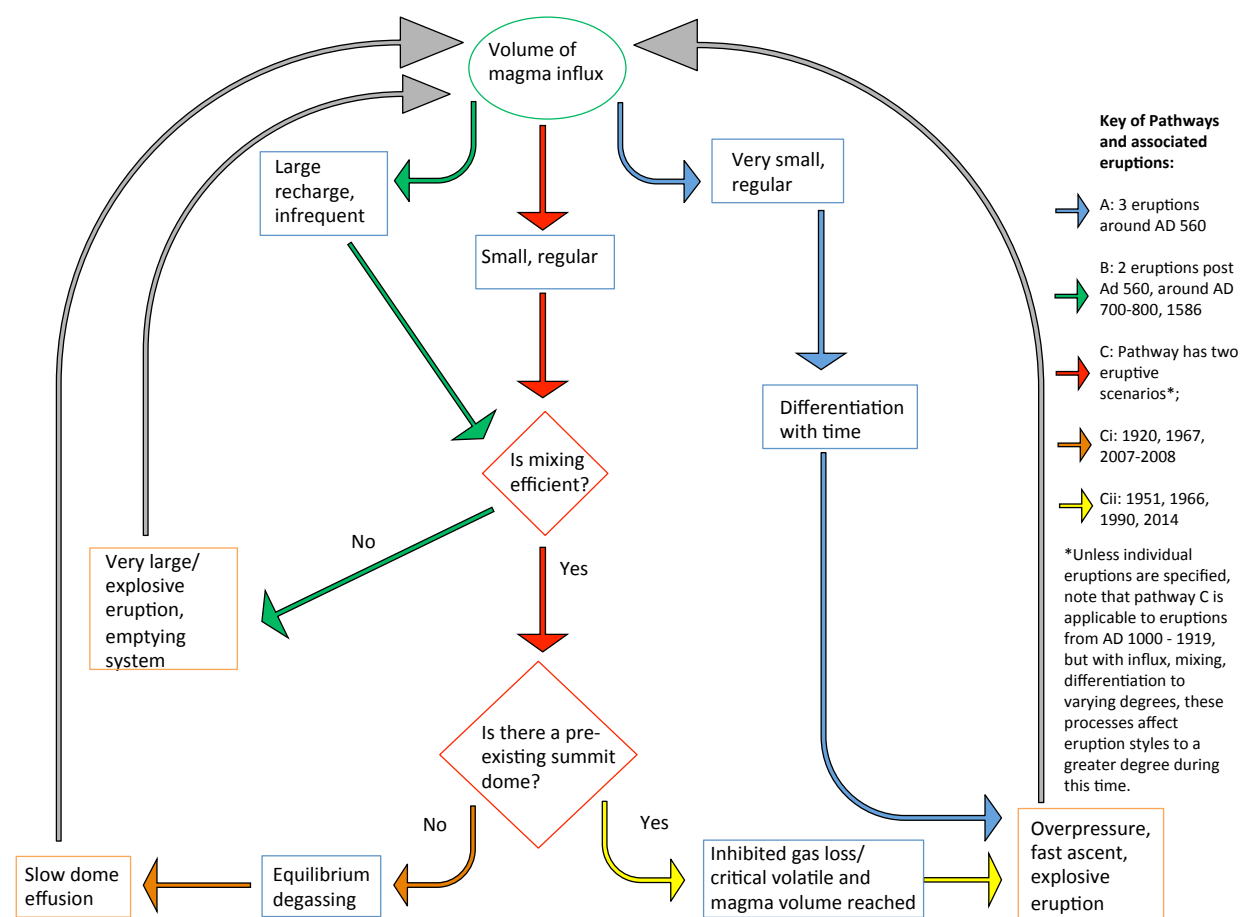


Figure 1: Summarising flow chart of the main magmatic and eruptive scenarios at Kelut. Green is the starting scenario, representing the magmatic system, and orange represent the outcomes of processes. See key eruptions associated for each colour coded pathway. See text for further discussion.

many volcanoes worldwide, such as Soufriere Hills volcano, Montserrat (Devine et al., 1998) Mt. Hood, USA (Kent et al., 2010) and Santorini, Italy (Parks et al., 2012). It was clear that the rates of magma supply, such as sporadic large recharge events, versus small regular influxes control eruption volume and style at Kelut (Fig. 1; e.g., Caricchi et al., 2014).

From around ~1826 to 1990, eruptions at Kelut appeared to be continuously tapping a reservoir that was showing incremental increases in silica content (from 64 to 71 wt.% SiO₂) (see Figures 4 and 8, Chapter 3). It seemed that these magmas were unaffected by large fresh influxes of magma that trigger mixing processes, similar to that envisaged by Humphreys et al. (2006) at Shiveluch volcano. Hence, magmatic processes did not largely account for the observed transitions in explosive-effusive eruptive styles from 1919 onwards, although between 1990 and 2014 a small influx of gas-rich mafic magma may have triggered the most recent eruption. Therefore, a comparative petrological and mineralogical study of the products from explosive and effusive eruptions was vital in order to determine if magmatic processes are governing this cyclic behaviour.

5.3 A deeper understanding of pre-eruptive magma storage regions

Chapter 4 presented the petrology, geochemistry and mineralogy of the 1990 and 2014 plinian eruptions, and the 2007-2008 effusive lava-dome forming eruption, to identify any possible variations in magma storage regions and give insights into processes governing eruptive style. This thesis revealed that the mineral assemblages, textures, zoning patterns, and the composition of the bulk-rock (major and trace elements) of all the eruptions are comparable. Thermobarometry for all eruptions identified two dominant regions at ~5 and 11 km depth for clinopyroxene crystallisation, although crystallisation occurs within the mid- to upper-crustal regions at ~14 to 2 km, similar to other Indonesian volcanoes Krakatau (Dahren et al., 2012) and Merapi (Costa et al., 2013). The ascending magmas eventually stalled around 8-10 km, controlled by the presence of lithological and density boundaries of the surrounding crust, before further shallow crystallisation occurred (see Figure 18, Chapter 4).

5.3.1 Pre-eruptive processes providing insights into the magmatic system

Higher-Al clinopyroxenes crystallised from more primitive bulk-rock magma compositions at depths of ~14-12 km, suggesting that a mafic influx occurred, similar to Merapi volcano before the 2010 eruption (Costa et al., 2013). Mixing of this primitive magma with a more evolved resident magma allowed for the formation of clinopyroxenes that mantle orthopyroxenes. In addition, the formation of plagioclase with multiple sieve-textured zones, and small (~10 mol.%) and large scale (up to 40 mol.%) variations in anorthite content between oscillatory zones, and from core to rim of plagioclase phenocrysts suggests mixing and convection was efficient for some time, whereby turbulence was sustained by regular influxes of magma. Troll et al. (2013) and Couch et al. (2001) suggest similar processes occurred at Merapi and the Soufriere Hills volcano. The homogeneity in bulk-rock compositions (54-55 wt.% SiO₂) for all eruptions also revealed that pre-eruptive processes for the eruptions were the same. It is likely that the regular, small injections of mafic, gas-rich magma over time allowed for efficient mixing with a resident, evolved gas-poor magma (pathway C, Fig. 1). Similar processes are responsible for the textural observations and homogeneity of erupted rocks at Stomboli (Landi et al., 2004), and Yasur volcanoes (Firth et al., 2014). The continuous influxes of magma, and remobilisation and melting of cumulate material allowed for thermal buffering of the system (around 1030 °C) at shallow levels over time from 1990 to 2014 (see Figure 18, Chapter 4 for an overview of all processes). Regular influxes and mixing were also observed at longer timescales in the overall evolution of the magma plumbing system and compositional variations in glass shards at Kelut (Fig. 1) (see Chapter 3).

5.3.2 Degassing conditions between effusive and explosive eruptions

Due to the homogeneity between effusive and explosive eruptive rocks in 1990, 2014 and 2007-2008 samples, this study indicated that magma influx and mixing can not solely control the transitions in eruptive style at Kelut, similar to conclusions reached for explosive eruptions at Merapi volcano (Costa et al., 2013; Preece et al., 2014, 2016). Other processes, such as increased volatile content,

rapid degassing and fragmentation of a volatile rich magma, and rapid ascent of the magma are of greater influence on the eruptive styles at Kelut volcano. Explosive eruptions at Merapi volcano are controlled by rapid magma ascent rates and inhibited exsolution of gases (Preece et al., 2014). Effusive eruptions at the Soufriere Hills volcano are attributed to the formation of permeable shear zones allowing for gas release (Edmonds and Herd, 2007). At Colima and Merapi it is suggested that explosive eruptions occurred as a result of inhibited gas release, due to the presence of a pre-existing dome (Robin et al., 1991; Lavallée et al., 2012; Girona et al., 2015), and at Novarupta, Alaska it is suggested that permeable outgassing is responsible for effusive phases (Nguyen et al., 2014). It is suggested in Chapters 2 and 4 that the magma degassing conditions in the shallow magma reservoir and upper conduit were determined by the presence of the dome capping the conduit before explosive eruptions, similar to other volcanoes worldwide (Merapi, Shiveluch, Soufriere Hills volcano, Colima) (Pathways Ci and Cii, Fig. 1). This acted to trap gases that were being added by the small, regular influxes of volatile rich melt, eventually leading to magma overpressure and causing the magma to quickly ascend and fragment in the conduit, contributing to the explosivity of the 2014 eruption. It is also likely that these regular, small influxes were adding to a chamber that already is at maximum capacity, pressurising the magma to a critical limit, and hence contributing to the more explosive eruption (Bower and Woods, 1997; Chiodini et al., 2016) (Pathway Cii, Fig. 1). Since the compositions of glass shards from the eruptions of 1919 to 1990 reflect a magma chamber that is continuously differentiating with time (see Chapter 3), mafic influxes or recharge events may not be large enough to trigger the more explosive episodes. This indicates that the interplay between the addition of volatiles and the ability of volatile escape (or entrapment caused by a conduit-capping lava dome) may be responsible for the variation in eruptive styles for over ~100 years at Kelut.

5.4 Possibility of tectonic triggered eruptions

Regional faulting and tectonic events can change a stress field around a volcano, acting to change volcanic activity and seismicity, and can trigger magmatic overpressure and explosive eruptions (Linde and Sacks, 1998; West et al., 2005; Manga and Brodsky, 2006). This has been known to trigger eruptions at Pinatubo, Philippines (1991) and Kilauea, Hawaii (1975) (Tilling et al., 1976; Bautista et al., 1996). Regionally, it is stated that a 6.4 magnitude earthquake that occurred syn-eruptions at Merapi and Semeru volcanoes in Java in 2006 triggered the enhanced output of erupted material. Earthquakes can therefore affect an on-going eruption (e.g., Harris and Ripepe, 2007). It is therefore possible that regional tectonic activity may initiate larger eruptions, or sustain ongoing eruptions at Kelut, as this could produce magmas of variable composition.

5.5 Eruptive frequency at Kelut

An understanding of eruptive patterns and potential hazards was obtained from the frequency of explosive eruptions. The behavioural eruptive patterns and hazards that arise from eruptions were approached throughout Chapters 2, 3 and 4. As discussed in Chapter 3, the older sequence

of eruptions showed a pattern of infrequent (~88 year-intervals), larger eruption, until around AD 1000, when eruptions became more frequent to 1919 (every ~35 years). This is similar to Merapi volcano, where periods of high eruptive frequency during the past ~2000 years of activity were sustained by frequent influxes of mafic magma (Gertisser and Keller, 2003). The most explosive eruptions were followed by the longest periods of repose of up to 75 years, where the magma chamber was replenishing. These chapters also discussed when the cyclic nature of effusive-explosive eruptions was first recorded, at around 1920, although there were earlier indications of dome growth and collapse in the stratigraphic records. Eruptions episodes occurred every 7 to 31 years until the most recent in 2014. It appeared that the presence of a lava dome eventually lead to overpressure and an explosive, plinian eruption, which occurs every ~21 years on average.

5.5.1 The current state of the magmatic system at Kelut

Based on the typical cycles of eruptive activity at Kelut, it is expected that the next eruption may involve a decadal period of lava dome effusion through the crater lake if this eruptive pattern continues. Periods of lava dome effusion (e.g., 2007-2008) were often accompanied by months of precursory seismic activity that increases gradually over time and suddenly drops before extrusion of magma, accompanied by an increase in the flux of CO₂ and other gases in the lake. Similar observations are precursory signs at other volcanoes with crater lakes, such as El Chichón, Mexico (Jácome Paz et al., 2015). In addition, the presence of the vent-hosted hydrothermal system may allow for passive, continuous degassing, as was the case prior to the effusive 2007-2008 episode (Caudron et al., 2012). In contrast, the most explosive episodes of Kelut (e.g., 2014) were preceded by a rapid acceleration of seismic activity and a larger build-up of energy, hence a more forceful eruption (e.g, Caudron et al., 2015; Nakamichi et al., 2017). In the past, it is suggested that large recharge events may trigger more explosive eruptions (Chapter 3), indicating the need for monitoring deep seismic activity and the movement of large volumes of magma from depth (Chouet, 1996). If a large recharge event were to occur in the future, this could disrupt the current pattern of cyclic activity, so the potential of a repeated larger (e.g., VEI 5) eruption occurring cannot be ruled out. Therefore close monitoring of the flux of gases (e.g., CO₂, SO₂) and movement of magma at shallow levels as indicated by seismic activity is vital (as discussed in Chapter 2).

5.6 Implications for hazard analysis

Since eruptions of Kelut have such devastating effects due to high populations in close proximity to the volcano (see Figure 2, Chapter 1), this framework of past and recent eruptive activity is necessary to aid in the forecasting and recurrence of the timing of explosive events, as identified in each Chapter. The major risk catchments have, and remain to be, those located to the north-west, west, and south-west of the volcano. In the most explosive eruptions that produce a large volume of material, such as 1586, 1990 and 2014, lahars remain the primary hazard to life in distal and proximal locations, due to the presence of the crater lake, and also from secondary rain-triggered lahars. PDCs in recent and older eruptions ran out ≤ 7 km from the volcano, with more voluminous

deposits in proximal locations. Tephra falls were dispersed radially in proximal locations, and distally fine-ash is spread by the south-westerly prevailing winds as far as Yogyakarta (~215 km) to the west. Although this understanding had already existed at the volcano, and many comprehensive hazard maps had been produced, the channelisation of the 2014 PDCs, and post-eruptive lahars down river valleys to the west and south of the volcano mean that the hazard maps must be, and recently have been updated since the eruption.

5.7 Summary and broader implications of this work

This thesis further contributed further to studies concerning the magmatic drivers behind the 1990 and 2007-2008 eruptions. It also provided new insights into the eruption chronology, behaviour and magmatic drivers of the 2014 eruption. This thesis highlighted that the volcanological and geochemical temporal frameworks of Kelut volcano are complex, whereby multiple magmatic processes at depth such as mixing, differentiation, and influxes of magma largely govern eruptive behaviour (Fig.1) from ~AD 560 to 1800's. In addition, large mafic recharge events also appeared to trigger the largest eruptions at Kelut (e.g., 1586), and these were followed by the longest periods of repose (75 years). However, this thesis recognised that in more recent times since 1920, and particularly from 1990 to 2014, the explosive-effusive transitions in eruptive behaviour every ~12 years appear to be attributed to degassing processes and external conditions, rather than compositional variations in the magma. The homogeneity of the 2007-2008 effusive, and 1990 and 2014 explosive samples is attributed to efficient mixing processes with regular, small influxes of mafic, volatile-rich magma. Although in this case, magmatic drivers were not sufficient to trigger the more explosive eruptions. The presence of the lava dome is interpreted as the major control on degassing processes, contributing to the subsequent more explosive eruptions by gas overpressure. Although the frequency and pattern of recent eruptions suggest that the next may be a period of prolonged dome growth, the likelihood of a large, cataclysmic eruption possibly triggered by complete mafic recharge event must be considered in hazard analysis regionally. Close and consistent geophysical and seismic monitoring, surface deformation, and gas flux measurements are vital to assessing whether an explosive eruption is imminent, and to avoid eruptive crises and damage to human infrastructure. The understanding of what controls patterns in eruptive behaviour overtime provided by this thesis will assist in not only mitigating volcanic hazards at Kelut, but at other volcanoes regionally and worldwide.

Many volcanoes across various magmatic systems around the world have transitions between explosive and effusive behaviour, and long, complex eruptive histories. Therefore, the type of detailed, chronologically well-constrained volcanological, petrological and geochemical approach used in this study can be applied to other understudied, highly active, and hazardous volcanoes worldwide with long-eruptive histories. The findings of this thesis contributed to and illustrated broader themes that include; 1) the dynamics and chronology of single large eruptions can be very variable and complex with multiple deposits and eruptive stages, 2) magmatic controls on the frequency of large eruptions (e.g., mafic recharge, influxes, mixing), whereby mafic recharge

and mixing can trigger very explosive eruptions, 3) the recognition of transitions in effusive to explosive eruptions, and what drives this behaviour, specifically that magmatic drivers may not always be sufficient enough to trigger explosive eruptions, and 4) explosive eruptions may be triggered from magmatic overpressure due to inhibited gas loss from the presence of a conduit-capping dome. This was important to developing our understanding of the complexities of volcanic systems, particularly of those in Java, and specifically into what mechanisms and processes trigger the abrupt variations in eruptive style, and drivers of the largest and most explosive eruptions at volcanoes worldwide.

5.8 Future directions and research suggestions

The work in this thesis highlighted the magmatic drivers behind temporal variations in eruption frequency at styles at Kelut volcano. As discussed in Chapter 4, what remains unknown are the exact driving forces behind the transition in eruptive styles, and what exactly triggered the recent explosive eruptions at Kelut. Therefore further suggested areas for research include:

- A further textural analysis of microlites and comparison between the 2007-2008 and 2014 eruptions can further quantify and assess ascent processes, and elucidate short timescales of ascent in the conduit (e.g., Blundy et al., 2006; Costa et al., 2013; Preece et al., 2013).
- Further to this, decompression and permeability experiments specific to Kelut, such as quantification of ascent rates or volatile exsolution obtained by examining the growth of natural microlites and vesicles, against those formed under specific starting pressures and temperature conditions. Continuous decompression versus a stepped decompression can simulate whether the ascent paths are stalled or continuous in the Kelut system (e.g., Mangan and Sisson, 2000; Couch et al., 2001).
- Analyses of vesicles, volatiles, and light lithophile elements in melt inclusions of plagioclase and clinopyroxenes, like those conducted at Merapi volcano, to further quantify and understand the driving forces behind the more explosive versus effusive eruptions (e.g., Blundy and Cashman, 2005; Preece et al., 2014, 2016).
- Establishing the timescales of magmatic processes at depth similar to that undertaken at the Soufriere Hills volcano (e.g., Humphreys et al., 2010), and via e.g., diffusion profiles of Mg in olivine. Such processes identified include mixing, mafic influx, and crystal growth prior to effusive-explosive eruptions. This can provide valuable long- and short-term insights into timing of processes prior to eruption and can help in monitoring of Kelut volcano, specifically before explosive eruptions (e.g., Costa and Dungan, 2005; Costa et al., 2008, 2013).
- Investigate if regional tectonics had any influence on triggering eruptions, and increasing the volume of eruptions at Kelut (e.g., Harris and Ripepe, 2007).

- Stratigraphic, geochronological and geochemical studies on other East Javan volcanoes that do not currently exist. Such volcanoes regionally are Semeru and the Bromo-Tengger system, and worldwide volcanoes such as Mayon and Bulusan volcanoes in the Philippines. These volcanoes have long and complex eruptive histories similar to Kelut. These studies will further existing studies on these volcanic centres (cf. Van Gerven and Pichler, 1995; Siswawidjoyo et al., 1997; Thouret et al., 2007; Solikhin et al., 2012).
- Further geochemical and isotopic analyses (such as oxygen, Sr, Nd, Hf and Pb; U, Th and Ra disequilibria) of other East-Javan arc lavas (e.g., Wilis, Lawu, Semeru, Bromo, Tengger caldera) and more detailed of Kelut, to further constrain the relative importance of, for example, magmatic differentiation, crustal assimilation and contamination at shallow levels, and/or the subducted input of crustal material (e.g., Turner and Foden, 2001; Gertisser and Keller, 2003a; Chadwick et al., 2007; Smyth et al., 2007; Handley et al., 2007, 2014, 2018; Troll et al., 2013).
- Microdrilling of plagioclase to detect changes of insitu Sr, Nd and Pb isotopes across oscillatory zoned phenocrysts at Kelut and other Javan volcanoes. These are indicators of shallow-level open system processes important in magma evolution and modelling that may have previously been overlooked (e.g., Ginibre et al., 2002; Chadwick et al., 2007).
- Close monitoring of the output of gases from the crater lake between eruptions (e.g., SO₂), since explosivity is linked to the build up of pressure between eruptions. In addition, measurements on the permeability of rock types can determine the how volatiles exsolve and are lost from the magma, and reveal how eruptions may be explosive or effusive (e.g., Varley and Taran, 2003; Burgisser and Gardner, 2004).

5.9 References

- Andreastuti, S.D., Alloway, B.V., and Smith, I.E.M. (2000). A detailed tephrostratigraphic framework at Merapi Volcano, Central Java, Indonesia: implications for eruption predictions and hazard assessment. *Journal of Volcanology and Geothermal Research*. 100. 51-67.
- Arce, J.L., Macias, J.L., Vazquez-Selem, L. (2003). The 10.5 km plinian eruption of Nevado de Toluca volcano, Mexico: stratigraphy and hazard implications. *Geological Society of America Bulletin*. 115. 230-248.
- Bautista, B.C., Bautista, L.P., Stein, R.S., Barcelona, E.S., Punongbayan, R.S., Laguerta, E.P., Rasdas, A.R., Ambubuyog, G., and Amin, A.Q. (1996). Relationship of regional and local structures of Mount Pinatubo activity, In: *Fire and Mud*, Newhall, C.G., and Punongbayan, R.S. (eds). University of Washington Press, Seattle. 351-370.
- Blundy, J., and Cashman, K. (2005). Rapid decompression-driven crystallisation recorded by melt inclusions from Mount St. Helens volcano. *Geology*. 33. 793-796.
- Blundy, J., Cashman, K., and Humphreys, M. (2006). Magma heating by decompression-driven crystallisation beneath andesite volcanoes. *Nature*. 443. 76-80.

- Bourdier, J-L., Pratomio, I., Thouret, J-C., Boudon, G., and Vincent, P.M. (1997). Observations, stratigraphy and the eruptive processes of the 1990 eruption of Kelut volcano, Indonesia. *Journal of Volcanology and Geothermal Research*. 79. 181-203.
- Bower, S.M., and Woods, A.W. (1997). Control of magma volatile content and chamber depth on the mass erupted during explosive volcanic eruptions. *Journal of Geophysical Research*. 102. 10273-10290.
- Burgisser, A., and Gardner, J.E. (2004). Experimental constraints on degassing and permeability in volcanic conduit flow. *Bulletin of Volcanology*. 67. 42-56.
- Calder, E.S., Sparks, R.S.J., and Gardeweg, M.C. (2000). Erosion, transport and segregation of pumice and lithic clasts in pyroclastic flows inferred from ignimbrite at Lascar Volcano, Chile. *Journal of Volcanology and Geothermal Research*. 104. 201-235.
- Caricchi, L., Annen, C., Blundy, J., Simpson, G., and Pinel, V. (2014). Frequency and magnitude of volcanic eruptions controlled by magma injection and buoyancy. *Nature Geoscience*. 7. 126-130.
- Carey, R.J., Houghton, B.F., Sable, J.E., Wilson, C.J.N. (2007). Contrasting grain size and componentry in complex proximal deposits of the 1886 Tarawera basaltic Plinian eruption. *Bulletin of Volcanology*. 69. 903-926.
- Caudron, C., Mazot, A., and Bernard, A. (2012). Carbon dioxide dynamics in Kelud volcanic lake. *Journal of Geophysical Research*. 117. 1-11.
- Caudron, C., Taisne, B., Garces, M., Alexis, L.P., and Mialle, P. (2015). On the use of remote infrasound and seismic stations to constrain the eruptive sequence and intensity for the 2014 Kelud eruption. *Geophysical Research Letters*. 6614-6621.
- Chadwick, J.P., Troll, V.R., Ginibre, C., Morgan, D., Gertisser, R., Waight, T.E., & Davidson, J.P. (2007). Carbonate assimilation at Merapi Volcano, Java, Indonesia: insights from crystal isotope stratigraphy. *Journal of Petrology*. 48. 1793-1812.
- Chiodini, G., Paonita, A., Aiuppa, A., Costa, A., Caliro, S., Prospero, D.M., Acocella, V and Vandemeulebroek, J. (2016). Magmas near the critical degassing pressure drive volcanic unrest towards a critical state. *Nature Communications*. Doi:10.1038/ncomms13712.
- Chouet, B.A. (1996). Long-period volcano seismicity: its source and use in eruption forecasting. *Nature*. 380. 309-316.
- Costa, F., and Dungan, M. (2005). Time scales of magmatic assimilation from diffusion modelling of multiple elements in olivine. *Geology*. 33. 837-840.
- Costa, F., Dohmen, R., and Chakraborty, S. (2008). Time scales of magmatic processes from modelling the zoning patterns of crystals. *Reviews in Mineralogy and Geochemistry*. 69. 545-594.
- Costa, F., Andreastuti, S., Bouvet de Maisonneuve, C., and Pallister, J.S. (2013). Petrological insights into the storage conditions, and magmatic processes that yielded the centennial 2010 Merapi explosive eruption. *Journal of Volcanology and Geothermal Research*. 261. 209-235.
- Couch, S., Sparks, R.S.J., and Carroll, M.R. (2001). Mineral disequilibrium in lavas explained by convective self-mixing in open magma chambers. *Nature*. 411. 1037-1039.

Chapter Five

- Cronin, S.J., Lube, G., Dayudi, D.S., Sumarti, S., Subrandiyo, S., Surono. (2013). Insights into the October-November 2010 Gunung Merapi eruption (Central Java, Indonesia) from the stratigraphy, volume and characteristics of its pyroclastic deposits. *Journal of Volcanology and Geothermal Research*. 261. 244-259.
- Dahren, B., Troll, V.R., Andersson, U.B., Chadwick, J.P., Gardner, M.F., Jaxybulatov, K., and Koulakov, I. (2012). Magma plumbing beneath Anak Krakatau volcano, Indonesia: evidence for multiple magma storage regions. *Contributions to Mineralogy and Petrology*. 163. 631-651.
- Devine, J.D., Murphy, M.D., Rutherford, M.J., Barclay, J., Sparks, R.S.J., Carroll, M.R., Young, S.R., and Gardner, J.E. (1998). Petrologic evidence for pre-eruptive pressure-temperature conditions, and recent reheating of andesitic magma erupting at the Soufriere Hills volcano, Montserrat, W.I. *Geophysical Research Letters*. 25. 3669-3672.
- Edmonds, M., and Herd, R.A. (2007). A volcanic degassing event at the explosive-effusive transition. *Geophysical Research Letters*. 34.
- Firth, C.W., Handley, H.K., Cronin, S.J., and Turner, S.P. (2014). The eruptive history and chemical stratigraphy of a post-caldera, steady-state volcano: Yasur, Vanuatu. *Bulletin of Volcanology*. 76.
- Gertisser, R., and Keller, J. (2003). Temporal variations in magma composition at Merapi Volcano (Central Java, Indonesia): magmatic cycles during the past 2000 years of explosive activity. *Journal of Volcanology and Geothermal Research*. 123. 1-23.
- Gertisser, R., & Keller, J. (2003a). Trace element and Sr, Nd, Pb and O isotope variations in medium-K and high-K volcanic rocks from Merapi Volcano, Central Java, Indonesia: evidence for the involvement of subducted sediments in Sunda arc magma genesis. *Journal of Petrology*. 44. 457 – 489.
- Ginibre, C., Wörner, G., and Kronz, A. (2002b). Minor- and trace-element zoning in plagioclase: implications for magma chamber processes at Paríacota volcano, northern Chile. *Contributions to Mineralogy and Petrology*. 142. 300-315.
- Girona, T., Costa, F., and Schubert, G. (2015). Degassing during quiescence as a trigger of magma ascent and volcanic eruptions. *Scientific Reports*. 5. 18212.
- Handley, H.K., Macpherson, C.G., Davidson, J.P., Berlo, K., & Lowry, D. (2007). Constraining fluid and sediment contributions to subduction-related magmatism in Indonesia: Ijen Volcanic Complex. *Journal of Petrology*. 48. 1155-1183.
- Handley, H.K., Blichert-Toft, J., Gertisser, R., Macpherson, C.G., Turner, S.P., Zaennudin, A., and Abdurrachman, M. (2014). Insights from Pb and O isotopes into along-arc variations in subduction inputs and crustal assimilation for volcanic rocks in Java, Sunda arc, Indonesia. *Geochimica et Cosmochimica Acta*. 139. 205-226.
- Handley, H.K., Reagan, M., Gertisser, R., Preece, K., Berlo, K., Barclay, J., Herd, R. (2018). Timescales of magma ascent and degassing and the role of crustal assimilation at Merapi volcano, Indonesia: constraints from uranium-series and Sr-Nd-Pb isotopic compositions in volcanic rocks of the 2006 and 2010 eruptions. *Geochimica et Cosmochimica Acta*. 222. 34-52.
- Harris, A.J.L., and Ripepe, M. (2007). Regional earthquake as a trigger of enhanced volcanic activity: Evidence from MODIS thermal data. *Geophysical Research Letters*. 34.

- Humphreys, M.C.S., Blundy, J., and Sparks, R.S.J. (2006). Magma evolution and open-system processes at Shiveluch volcano: insights from phenocryst zoning. *Journal of Petrology*. 47. 2303-2334.
- Humphreys, M.C.S., Edmonds, M., Christopher, T., and Hards, V. (2010). Magma hybridisation and diffusive exchange recorded in heterogeneous glasses from Soufriere Hills volcano, Montserrat. *Geophysical Research Letters*. 37.
- Jácome Paz, M.P, Taran, Y., Inguaggiato, S., and Collard, N. (2015). CO₂ flux and chemistry of El Chichón crater lake (Mexico) in the period of 2013-2015: Evidence for enhanced volcano activity. *Geophysical Research Letters*. 127-134.
- Kent, A.J.R., Darr, C., Koleszar, A.M., Salisbury, M.J., and Cooper, K.M. (2010). Preferential eruption of andesitic magmas through recharge filtering. *Nature Geoscience*. 3. 631-636.
- Landi, P., Metrich, N., Bertagnini, A., and Rosi, M. (2004). Dynamics of magma mixing and degassing recorded in plagioclase at Stromboli (Aeolian Archipelago, Italy). *Contributions to Mineralogy and Petrology*. 147. 213-227.
- Larsen, G., and Eiriksson, J. (2007). Late Quaternary terrestrial tephrochronology of Iceland – frequency of explosive eruptions, type and volume of tephra deposits. *Journal of Quaternary Science*. 23. 109-120.
- Lavallée, Y., Varley, N.R., Alatorre-Ibarguenoitia, M.A., Hess, K.U., Kueppers, U., Mueller, S., Richard, D., Scheu, B., Spieler, O., Dingwell, D.B. (2012). Magmatic architecture of dome-building eruptions at Volcan de Colima, Mexico. *Bulletin of Volcanology*. 74. 249-260.
- Luhr, J.F., Navarro-Ochoa, C., and Savov, I.P. (2010). Tephrochronology, petrology and geochemistry of Late-Holocene pyroclastic deposits from Volcán de Colima, Mexico. *Journal of Volcanology and Geothermal Research*. 197. 1-32.
- Manga, M., and Brodsky, E. (2006). Seismic triggering of eruptions in the far field: volcanoes and geysers. *Annual Review of Earth and Planetary Sciences*. 34. 263-291.
- Mangan, M., and Sisson, T. (2000). Delayed, disequilibrium degassing in rhyolite magma: decompression experiments and implications for explosive volcanism. *Earth and Planetary Science Letters*. 183. 441-455.
- Nakamichi, H., Iguchi, M., Triastuty, H., Hendrasto, M., and Mulyana, I. (2017). Differences of precursory seismic energy release for the 2007 effusive dome-forming and 2014 plinian eruptions at Kelud volcano, Indonesia. *Journal of Volcanology and Geothermal Research*. <http://dx.doi.org/10.1016/j.jvolgeores.2017.08.004>
- Nguyen, C.T., Gonnermann, H.M., and Houghton, B.F. (2014). Explosive to effusive transition during the largest volcanic eruption of the 20th century (Novarupta 1912, Alaska). *Geology*. 42. 702-706.
- Parks, M.M., Biggs, J., England, P., Mather, T.A., Nomikou, P., Palamartchouk, K., Papanikolaou, X., Paradissis, D., Parsons, B., Pyle, D.M., Papatakis, C., and Zacharis, V. (2012). Evolution of Sanotrinini volcano dominated by episodic and rapid fluxes of melt from depth. *Nature Geoscience*. 5. 749-754.
- Preece, K., Barclay, J., Gertisser, R., Herd, R.A. (2013). Textural and micro-petrological variations in eruptive products of the 2006 dome-forming eruption of Merapi volcano, Indonesia: implications for sub-surface processes. *Journal of Volcanology and Geothermal Research*. 261. 98-120.

Chapter Five

- Preece, K., Gertisser, R., Barclay, J., Berlo, K., Herd, R.A., Edinburgh Ion Microprobe Facility. (2014). Pre- and syn-eruptive degassing and crystallisation processes of the 2010 and 2006 eruptions of Merapi volcano, Indonesia. *Contributions to Mineralogy and Petrology*. 168. 1-25.
- Preece, K., Gertisser, R., Barclay, J., Charbonnier, S.J., Komorowski, J-C., and Herd, R.A. (2016). Transitions between explosive and effusive phases during the cataclysmic 2010 eruption of Merapi volcano, Java, Indonesia. *Bulletin of Volcanology*. 78. 54.
- Robin, C., Camus, G., Gourgaud, A. (1991). Eruptive and magmatic cycles at Fuego de Colima volcano (Mexico). *Journal of Volcanology and Geothermal Research*. 45. 209-225.
- Siswowidjoyo, S., Sudarsono, U., & Wirakusumah, A.D. (1997). The threat of hazards in the Semeru volcano region in East Java, Indonesia. *Journal of Asian Earth Sciences*. 15. 185-194.
- Shane, P., Nairn, I.A., Smith, V.C, Darragh, M., Beggs, K., and Cole, J.M. (2008). Silicic recharge of multiple rhyolite magmas by basaltic intrusion during the 22.6 ka Okareka Eruption Episode, New Zealand. *Lithos*. 103. 527-549.
- Smyth, H.R., Hamilton, P.J., Hall, R., & Kinny, P.D. (2007). The deep crust beneath island arcs: Inherited zircons reveal a Gondwana continental fragment beneath East Java, Indonesia. *Earth and Planetary Science Letters*. 258. 269 – 282.
- Sparks, R.S.J., Sigurdsson, H., and Wilson, L. (1977). Magma mixing: a mechanism for triggering acid explosive eruptions. *Nature*. 267. 315-318.
- Sparks, R.S.J., Self, S., and Walker, G.P.L. (1973). Products of ignimbrite eruptions. *Geology*. 1. 115-118.
- Solikhin, A., Thouret, J-C., Gupta, A., Harris, A.J.L., & Liew, S.C. (2012). Geology, tectonics, and the 2002-2003 eruption of the Semeru volcano, Indonesia: Interpreted from high-spatial resolution satellite imagery. *Geomorphology*. 138. 364-379.
- Tilling, R.I., Koyanagi, R.Y., Lipman, P.W., Lockwood, J.P., Moore, J.G., and Swanson, D.A. (1976). Earthquake and related catastrophic events, Island of Hawaii, November 29, 1975: A preliminary report. *US Geological Survey*. 740. 33
- Thouret, J-C., Lavigne, F., Suwa, H., Sukatja, B., & Surono. (2007). Volcanic hazards at Mount Semeru, East Java (Indonesia), with emphasis on lahars. *Bulletin of Volcanology*. 70. 221-244.
- Torres-Orozco, R., Cronin, S.J., Pardo, N., and Palmer, A.S. (2017). New insights into Holocene eruption episodes from deposit sequences at Mt. Taranaki (Egmont), New Zealand. *Bulletin of Volcanology*. 79:3.
- Troll, V.R., Deegan, F.M., Jolis, E.M., Harris, C., Chadwick, J.P., Gertisser, R., Schwarzkopf, L.M., Borisova, A.Y., Bindeman, I.N., Sumarti, S., & Preece, K. (2013). Magmatic differentiation processes at Merapi Volcano: inclusion petrology and oxygen isotopes. *Journal of Volcanology and Geothermal Research*. 261. 38-49.
- Turner, S., & Foden, J. (2001). U, Th and Ra disequilibria, Sr, Nd and Pb isotope and trace element variations in Sunda arc lavas: predominance of a subducted sediment component. *Contributions to Mineralogy and Petrology*. 142. 43 – 57.
- Turner, M.B., Cronin, S.J., and Smith, I.E.M. (2008) Eruption episodes and magma recharge events in andesitic systems, Mt Taranaki, New Zealand. *Journal of Volcanology and Geothermal Research*. 177. 1063-1076.

- Varley, N.R., and Taran, Y.A. (2003). Degassing processes of Popocatépetl and Volcán de Colima, Mexico. In: Oppenheimer, C., Pyle, D.M and Barclay, J. (eds) Volcanic degassing. *Geological Society, London*. 263-280.
- Van Gerven, M., & Pichler, H. (1995). Some aspects of volcanology and geochemistry of the Tengger Caldera, Java, Indonesia: eruption of a K-rich tholeiitic series. *Journal of Southeast Asian Earth Sciences*. 11. 125-133.
- Wark, D.A., Hildreth, W., Spear, F.S., Cherniak, D.J., and Watson, E.B. (2007). Pre-eruption recharge of the Bishop magma system. *Geology*. 35. 235-238.

Appendix A: Supplementary Data for Chapter Three

Eruption frequency, style and composition variations at Kelut volcano, Indonesia, based on 1500 years of tephra records

Louise R. Goode, Heather K. Handley, Shane J. Cronin, Mirzam Abdurrachman

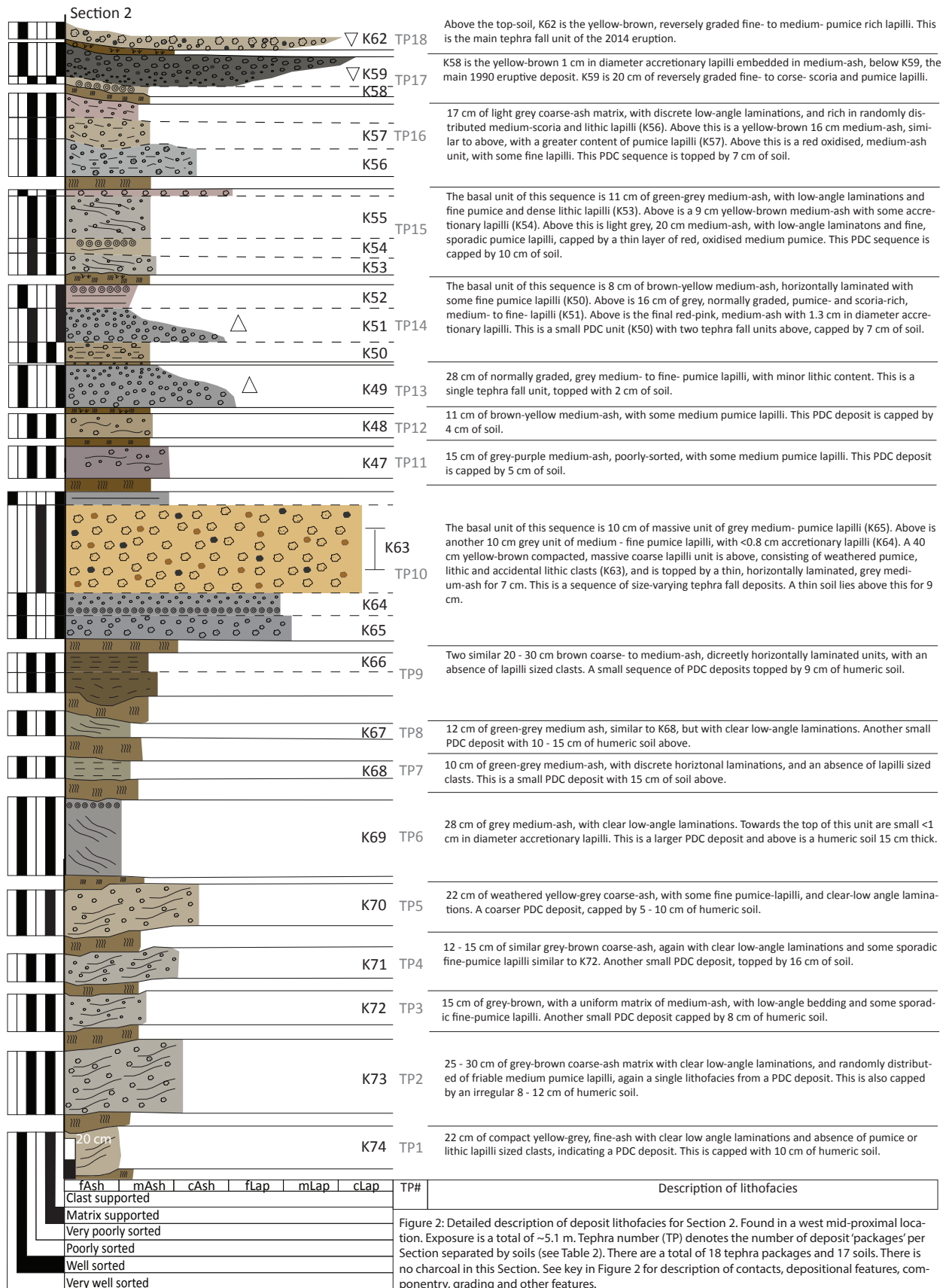
Supplementary Figure 1: Stratigraphy and deposit descriptions for Section 1

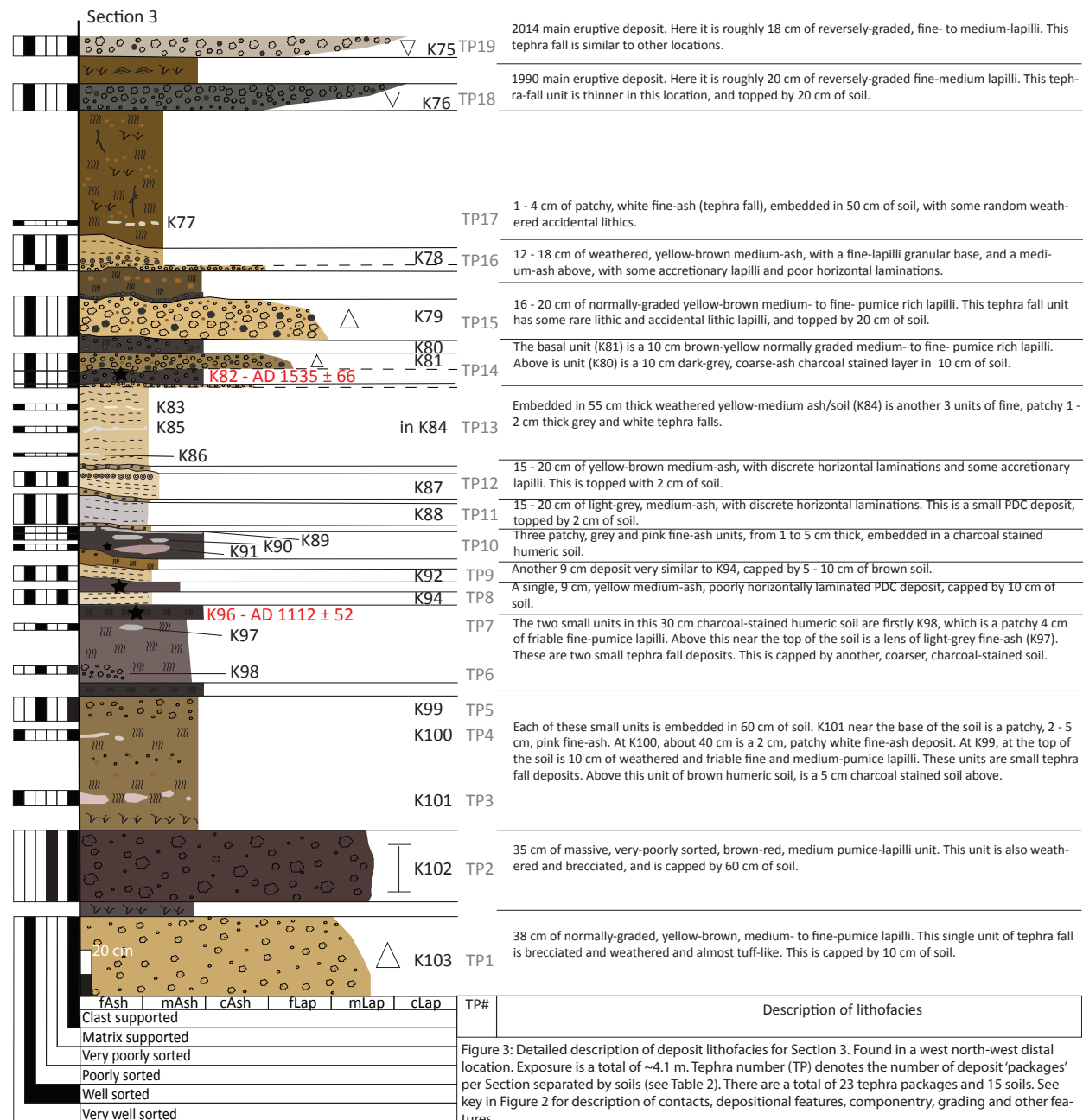
Supplementary Figure 2: Stratigraphy and deposit descriptions for Section 2

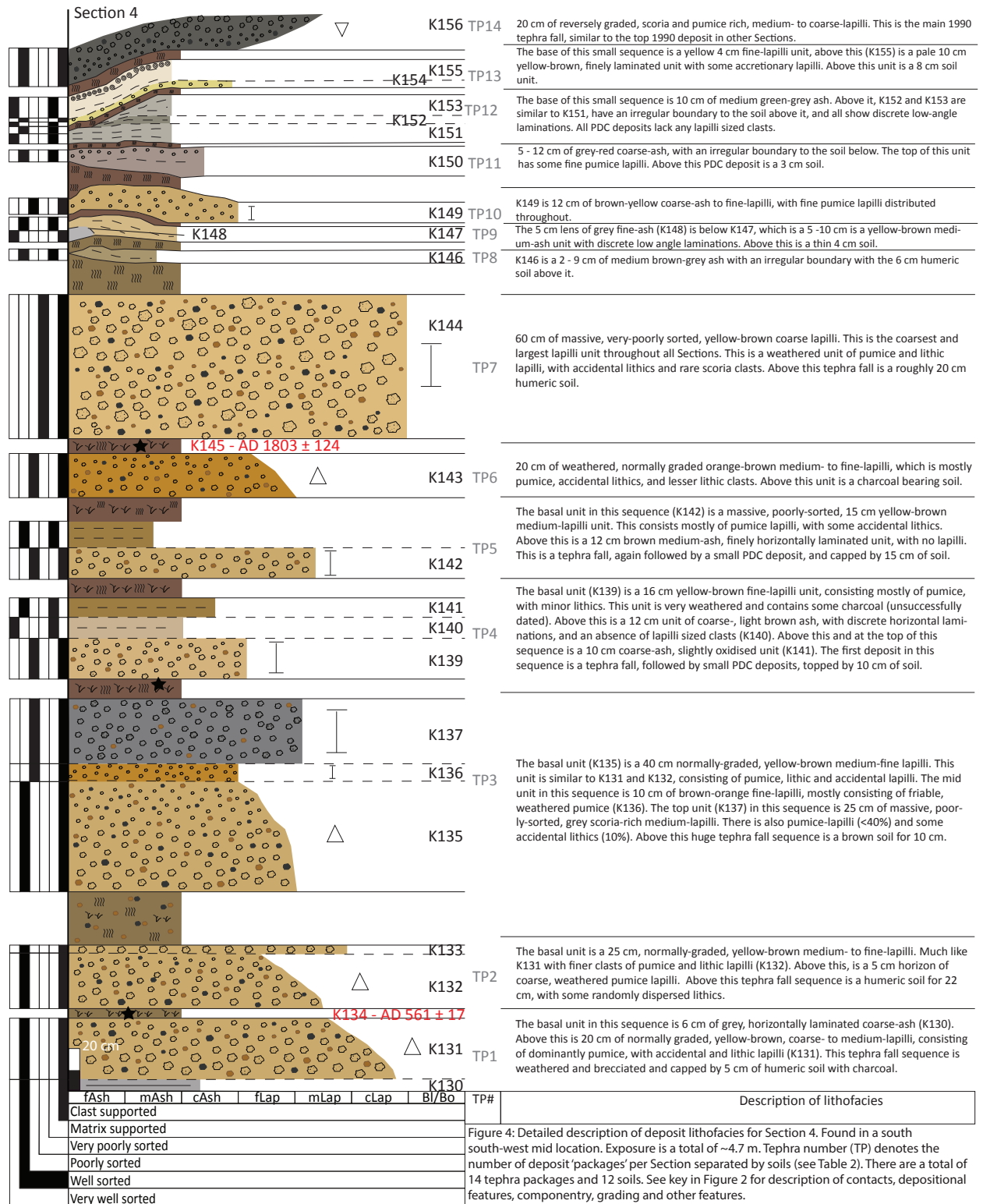
Supplementary Figure 3: Stratigraphy and deposit descriptions for Section 3

Supplementary Figure 4: Stratigraphy and deposit descriptions for Section 4









Electronic Appendices

Electronic Appendix A

Chapter Two: Insights into eruption dynamics from the 2014 pyroclastic deposits of Kelut volcano, Java, Indonesia, and implications for future hazards

Louise R. Goode, Heather K. Handley, Shane J. Cronin, Mirzam Abdurrachman

Supplementary Table 1: Raw values for the grain size distribution, componentry, modal grain size, median grain size/diameter ($Md\phi$), and standard deviations/sorting coefficient ($\sigma\phi$) for the 2014 pyroclastic deposits.

Electronic Appendix B

Chapter Three: Eruption frequency, style and composition variations at Kelut volcano, Indonesia, based on 1500 years of tephra records

Louise R. Goode, Heather K. Handley, Shane J. Cronin, Mirzam Abdurrachman

Supplementary Table 1: Major elemental analyses of glass shards by EMP.

Electronic Appendix C

Chapter Four: The pre-eruptive magma storage system of the 1990 and 2014 Plinian, and 2007-2008 effusive dome-forming eruptions at Kelut volcano, Indonesia: insights into cyclic transitions in eruptive style

Louise R. Goode, Heather K. Handley, Chris W. Firth, Simon P. Turner, Shane J. Cronin, Mirzam Abdurrachman

Supplementary Table 1: Petrography description of all thin sections, with crystallisation assemblage, mineral modes, textures, grain size, groundmass type and description, types of textures of phenocrysts present, and description of sample overall.

Supplementary Table 2: EMP analyses of plagioclase, clinopyroxene, orthopyroxene, titanomagnetite and amphibole for Kelut samples.

Supplementary Table 1: Raw values for the grain size distribution, componentry, modal grain size, median grain size/diameter (Mdφ), and standard deviations/sorting coefficient (σφ) for the 2014 pyroclastic deposits.
Median grain size/diameter and standard deviations/sorting coefficients using the technique given in Folk and Ward, 1957.

Unit	Sample	Modal φ	Mdφ	σφ	Component	Grain Size											
						-6 φ 63.0 - 31.5 mm	-5 φ 31.5 - 16.0 mm	-4 φ 16.0 - 8.0 mm	-3 φ 8.0 - 4.0 mm	-2 φ 4.0 - 2.0 mm	-1 φ 2.0 - 1.0 mm	0 φ 1.00 mm - 500 μm	1 φ 500 - 250 μm	2 φ 250 - 125 μm	3 φ 125 - 63 μm	4 φ 63 - 32 μm	5 φ <32 μm
3-TF	K35	-3 φ	-3.7	0.04	Pumice (light grey)				25.46	10.97	3.04	1.50					
					Pumice (darker grey/brown)				3.25	1.46	0.70	0.04					
					Pumice (oxidised)					0.09	0.02	0.02					
					Scoria				0.54	0.18	0.21	0.02					
					Crystals (single free)							0.19					
					Crystals (aggregates)						0.12	0.65					
					Lithics (dark grey)					2.10	1.11	0.50					
					Lithics (light grey)				2.17	0.37	0.30	0.81					
					Lithics (brown)					0.09	0.07	0.02					
					Lithics (oxidised)					0.09		0.02					
					No componentry data			11.53	26.62				3.68	0.65	0.29	0.21	0.27
					Total wt. %	0.00	11.53	26.62	31.43	15.36	5.57	3.79	3.68	0.65	0.29	0.21	0.27
3-TF	K62	-3 φ	/	/	Pumice (light grey)				20.57	16.85	7.66	4.96					
					Pumice (darker grey/brown)				2.40	0.45	0.09						
					Pumice (oxidised)				0.80	0.31	0.66	0.21					
					Scoria				0.80	0.36	1.00						
					Crystals (single free)						0.17	1.42					
					Crystals (aggregates)						0.66	2.13					
					Lithics (dark grey)				0.27	1.07	1.12	0.83					
					Lithics (light grey)				2.40	1.47	0.89	1.11					
					Lithics (brown)					0.18	0.03						
					Lithics (oxidised)				0.27		0.11						
					No componentry data			20.73					6.66	0.51	0.21	0.14	0.09
					Total wt. %	0.00	0.00	20.73	27.51	20.67	12.39	10.66	6.66	0.51	0.21	0.14	0.09
3-TF	K75	-5 φ	/	/	Pumice (light grey)				4.41	7.30	7.25	4.75					
					Pumice (darker grey/brown)					0.12							
					Pumice (oxidised)				0.35	0.59	0.39	0.15					
					Scoria												
					Crystals (single free)							0.81					
					Crystals (aggregates)						0.18	1.06					
					Lithics (dark grey)					0.47	0.96	0.45					
					Lithics (light grey)				1.06	1.33	1.71	1.41					
					Lithics (brown)												
					Lithics (oxidised)				0.18	0.41	0.29	0.15					
					No componentry data	14.16	33.31	10.26					5.60	0.54	0.12	0.10	0.07
					Total wt. %	14.16	33.31	10.26	6.00	10.23	10.78	8.79	5.60	0.54	0.12	0.10	0.07
3-TFa	K110	1 φ	0.9	4.04	Pumice (light grey)							1.09	8.57	6.59	3.05		
					Pumice (darker grey/brown)							0.28	0.52	0.25	0.47		
					Pumice (oxidised)							0.01	0.17	0.12	0.09		
					Scoria												
					Crystals (single free)							0.56	9.26	6.40	4.10		
					Crystals (aggregates)							3.55	28.64	3.51	1.15		
					Lithics (dark grey)							0.17	0.09				
					Lithics (light grey)							0.45	0.61				
					Lithics (brown)							0.05					
					Lithics (oxidised)							0.06	0.44				

3-TFb	K111	0 φ	0.9	1.32	No componentry data											11.84	7.04
					Total wt. %	0.00	0.00	0.00	0.00	0.00	6.22	48.28	16.87	8.86	11.84	7.04	
					Pumice (light grey)					6.20	12.38	17.04					
					Pumice (darker grey/brown)				0.76	2.11	2.04	4.76					
					Pumice (oxidised)					0.40		0.23					
					Scoria					0.53	1.48	0.61					
					Crystals (single free)							3.07					
					Crystals (aggregates)					0.26	0.34	7.37					
					Lithics (dark grey)							3.63	5.53				
					Lithics (light grey)					0.53	11.58	6.07					
					Lithics (brown)					0.26	0.34	0.31					
					Lithics (oxidised)												
					3-Tf	K112	−3 φ	−3.2	−2.26	No componentry data							10.49
Total wt. %	0.00	0.00	0.00	0.76						10.29	31.79	44.99	10.49	0.53	0.31	0.16	0.05
Pumice (light grey)				29.29						26.26	3.37	0.06					
Pumice (darker grey/brown)				5.60						4.26	0.41						
Pumice (oxidised)				1.87						0.53	0.15	0.02					
Scoria										0.53	0.26	0.01					
Crystals (single free)										0.35		0.05					
Crystals (aggregates)				0.00						0.00	0.00	0.00					
Lithics (dark grey)										0.89	0.59	0.01					
Lithics (light grey)				4.30						3.90	0.32	0.01					
Lithics (brown)											0.06						
Lithics (oxidised)										0.53	0.03	0.00					
2-oPS1	K113	1 φ	0.5	5.41						No componentry data			16.19				0.13
					Total wt. %	0.00	0.00	16.19	41.06	37.26	5.20	0.14	0.13	0.18	0.14	0.07	0.05
					Pumice (light grey)				3.72	6.92	4.85	7.45					
					Pumice (darker grey/brown)					0.48							
					Pumice (oxidised)				0.74	0.72	1.01	0.66					
					Scoria					0.24	0.13						
					Crystals (single free)							0.50					
					Crystals (aggregates)							0.23	1.82				
					Lithics (dark grey)				0.74	2.03	1.52	0.52					
					Lithics (light grey)				0.74	0.84	0.77	1.35					
					Lithics (brown)					0.12		0.01					
					Lithics (oxidised)						0.11						
					2-oPS2	K114	2 φ	1	5.96	No componentry data							25.71
Total wt. %	0.00	0.00	0.00	5.96						11.34	8.63	12.31	25.71	24.56	9.22	1.75	0.30
Pumice (light grey)				3.30						5.12	3.78	5.06					
Pumice (darker grey/brown)										0.16	0.14						
Pumice (oxidised)				0.55						0.48	0.40	0.62					
Scoria											0.26						
Crystals (single free)												0.23					
Crystals (aggregates)												1.61					
Lithics (dark grey)										0.64	0.86	0.94					
Lithics (light grey)				0.55						0.64	0.60	0.74					
Lithics (brown)											0.14						
Lithics (oxidised)										0.16	0.17	0.14					
2-oPDCa	K115	3 φ	2.3	7.3						No componentry data							24.69
					Total wt. %	0.00	0.00	0.00	4.40	7.20	6.35	9.33	24.69	28.76	15.79	3.43	0.16
					Pumice (light grey)							1.37	1.47	3.75	4.60		

3-TF	K116	-3 φ	-3.2	-0.14	Pumice (darker grey/brown)														
					Pumice (oxidised)						0.08	0.18	0.24	0.99					
					Scoria														
					Crystals (single free)						0.43	3.85	12.00	22.02					
					Crystals (aggregates)						0.89	3.79	6.46	3.29					
					Lithics (dark grey)						0.36	0.37							
					Lithics (light grey)						0.49	0.86	0.96						
					Lithics (brown)														
					Lithics (oxidised)						0.02								
					No componentry data										1.15				
					No componentry data					2.00	2.04						22.55	3.30	
					Total wt. %	0.00	0.00	0.00	0.00	2.00	2.04	3.64	10.50	23.41	32.05	22.55	3.30		
					Pumice (light grey)					29.36	21.39	7.50	2.44						
					Pumice (darker grey/brown)						0.50								
					Pumice (oxidised)					0.59	0.50	0.38	0.16						
1-PS1	K120	1 φ	1.1	6.85	Scoria							0.29							
					Crystals (single free)							0.14	0.07						
					Crystals (aggregates)								0.88						
					Lithics (dark grey)					1.76	1.00	1.20	0.32						
					Lithics (light grey)					2.35	3.17	0.53	0.48						
					Lithics (brown)						0.50								
					Lithics (oxidised)						0.67	0.43							
					No componentry data						7.97	11.03		2.02	1.01	1.27	0.66	0.15	
					Total wt. %	0.00	7.97	11.03	34.06	27.73	10.48	4.35	2.02	1.01	1.27	0.66	0.15		
					Pumice (light grey)					2.01	2.39	5.81	8.70						
					Pumice (darker grey/brown)						0.10								
					Pumice (oxidised)					0.22	0.33	0.26	1.10						
					Scoria						0.24								
					Crystals (single free)							0.04	0.10	8.14					
					Crystals (aggregates)							0.07	1.24	5.31					
					Lithics (dark grey)					0.78	1.15	0.91	2.65						
1-PSL	K121	2 φ	1.6	6.93	Lithics (light grey)					1.00	1.04	1.11	2.74						
					Lithics (brown)						0.03								
					Lithics (oxidised)						0.09								
					No componentry data									22.34	19.08	9.05	1.78		
					Total wt. %	0.00	0.00	0.00	0.00	4.02	5.47	9.43	28.65	22.34	19.08	9.05	1.78		
					Pumice (light grey)					1.55	1.03	3.26	3.45	8.06	8.36	5.86			
					Pumice (darker grey/brown)						0.08								
					Pumice (oxidised)					0.07	0.38	0.12	0.2	1.23	0.94				
					Scoria						0.05								
					Crystals (single free)							0.12		7.49	8.95				
					Crystals (aggregates)							0.20	1.22	3.45	5.77	3.48			
					Lithics (dark grey)					0.48	0.63	0.77	3.91	4.85	1.25				
					Lithics (light grey)					0.76	0.73	0.73	2.25	2.53	2.41				
					Lithics (brown)						0.03								
					Lithics (oxidised)					0.52	0.10			0.34	0.48				
					No componentry data											12.33	2.68		
1-PS2	K122	2 φ	1.5	6.78	Total wt. %	0.00	0.00	0.00	2.06	2.34	5.46	6.41	17.87	30.57	23.37	12.33	2.68		
					Pumice (light grey)							5.12	12.47	15.71	5.12				
					Pumice (darker grey/brown)														
					Pumice (oxidised)							0.11	0.19	0.27	0.69				

1-PDC(a)	K123	2 φ	0.8	7.09	Scoria													
					Crystals (single free)							0.25	2.88	4.01	9.54			
					Crystals (aggregates)							1.39	4.03	6.28	3.46			
					Lithics (dark grey)							0.71	1.25	1.00				
					Lithics (light grey)							0.60	1.25	3.14				
					Lithics (brown)													
					Lithics (oxidised)													
					No componentry data										1.64	1.31		
					No componentry data							0.90	2.85				10.69	4.87
					Total wt. %	0.00	0.00	0.00	0.00	0.90	2.85	8.18	22.06	32.05	20.12	10.69	4.87	
					Pumice (light grey)					5.84	5.28	4.64	4.66	11	14.31	4.46		
					Pumice (darker grey/brown)										1.18			
					Pumice (oxidised)					0.65	0.29	0.18	0.38					
					Scoria													
					Crystals (single free)								0.50	1.34	2.06	6.56		
					Crystals (aggregates)								2.19	4.67	3.43	2.87		
					Lithics (dark grey)					1.30	0.49	0.76	0.48		0.43			
					Lithics (light grey)					0.65	1.37	1.00	0.53	1.52	1.68	0.43		
					Lithics (brown)						0.10	0.06						
					Lithics (oxidised)					0.65	0.29	0.15		0.42				
No componentry data												5.58	1.63					
Total wt. %	0.00	0.00		3.35	9.08	7.83	7.19	8.74	18.95	23.09	14.32	5.58	1.63					
1-oPSL	K44	2 φ	1.6	6.78	Pumice (light grey)							3.12	12.17	10.77	5.34			
					Pumice (darker grey/brown)													
					Pumice (oxidised)							0.21	0.09	0.34	0.54			
					Scoria													
					Crystals (single free)							0.30	2.68	3.31	10.19			
					Crystals (aggregates)							1.44	3.93	12.98	3.22			
					Lithics (dark grey)							0.76	2.65					
					Lithics (light grey)							0.70	2.15	2.19				
					Lithics (brown)													
					Lithics (oxidised)										1.79	1.45		
					No componentry data							2.10					12.12	3.26
					Total wt. %	0.00	0.00		0.00	0.00	0.00	2.10	6.53	23.66	31.38	20.74	12.12	3.26
					Pumice (light grey)								2.16	12.62	8.21	5.12		
					Pumice (darker grey/brown)								0.62		0.74			
					Pumice (oxidised)								0.53	0.09	0.29	0.21		
					Scoria													
					Crystals (single free)								0.47	2.35	13.35	9.65		
					Crystals (aggregates)								1.13	4.63	9.93	5.57		
					Lithics (dark grey)								0.26	1.05				
					Lithics (light grey)								0.90	1.04	1.96	0.43		
Lithics (brown)																		
Lithics (oxidised)											0.33							
No componentry data								1.30				9.54	5.43					
Total wt. %	0.00	0.00		0.00	0.00	0.00	1.30	6.07	21.77	34.82	20.98	9.54	5.43					
1-PDC* Matrix	K40	1 φ	1.3	7.13	Pumice (light grey)													
					Pumice (darker grey/brown)													
					Pumice (oxidised)													
					Scoria										0.48			

2-PDC* Matrix	K37	2 φ	1.5	6.86	Crystals (single free)						0.54	3.12	6.76	9.67			
					Crystals (aggregates)						1.92	4.65	5.13	2.96			
					Lithics (dark grey)						1.71	3.21					
					Lithics (light grey)						1.23	3.45	4.45	2.76			
					Lithics (brown)												
					Lithics (oxidised)									0.90			
					No componentry data					3.50	1.98				9.76	2.10	
					Total wt. %	0.00	0.00	0.00	0.00	3.50	1.98	10.20	27.03	24.69	18.59	9.76	2.10
					Pumice (light grey)							6.13	11.81	15.09	4.37		
					Pumice (darker grey/brown)												
					Pumice (oxidised)						0.20				0.32		
					Scoria												
					Crystals (single free)						0.34	3.42	4.66	11.34			
					Crystals (aggregates)						1.80	5.09	5.38	5.98			
					Lithics (dark grey)						0.45	0.98					
					Lithics (light grey)						0.68	1.34	0.16				
					Lithics (brown)												
					Lithics (oxidised)									0.32	0.13		
					No componentry data					1.56	3.26					11.40	3.62
					Total wt. %	0.00	0.00	0.00	0.00	1.56	3.26	9.60	22.64	25.61	22.14	11.40	3.62

Supplementary Table 1: Major elemental analyses of glass shards by EMP. Uncertainties reported as standard deviations (SD)

Sample	No.	CaO	TiO ₂	Na ₂ O	MgO	P ₂ O ₅	SiO ₂	Al ₂ O ₃	K ₂ O	MnO	FeO	Cl	SO ₃	Total
K2	9	5.20	0.15	4.37	1.22	0.10	64.6	16.5	1.41	0.14	4.29	0.14	0.01	98.1
K2	10	4.86	0.22	4.28	1.43	0.16	64.8	15.5	1.62	0.19	4.99	0.15	0.04	98.3
K2	11	4.05	0.22	4.13	1.23	0.12	65.8	15.4	1.69	0.15	4.61	0.15	0.00	97.5
K2	13	4.56	0.19	3.55	1.32	0.08	65.2	15.4	1.65	0.21	4.47	0.16	0.00	96.7
K2	14	4.07	0.19	3.83	1.44	0.16	66.1	15.4	1.72	0.08	4.58	0.13	0.02	97.7
K2	15	4.10	0.21	4.19	1.39	0.12	64.2	15.0	1.68	0.11	4.93	0.13	0.01	96.0
K2	16	3.91	0.17	4.23	1.27	0.12	66.8	15.7	1.65	0.17	4.51	0.11	0.02	98.6
K2	17	4.02	0.19	3.91	1.19	0.08	66.9	15.1	1.66	0.11	4.47	0.17	0.03	97.8
K2	18	3.75	0.19	3.86	1.16	0.07	67.4	15.3	1.78	0.13	4.11	0.15	0.01	97.9
K2	19	3.85	0.21	3.37	1.36	0.07	66.3	15.0	1.72	0.14	4.66	0.17	0.01	96.9
K2	21	4.11	0.23	4.13	1.40	0.15	66.0	15.2	1.65	0.15	4.75	0.17	0.04	97.9
K2	22	4.03	0.21	4.24	1.32	0.09	65.9	15.2	1.64	0.11	4.39	0.15	0.02	97.2
Average SD		4.21	0.20	4.01	1.31	0.11	65.8	15.4	1.66	0.14	4.56	0.15	0.02	97.6
		0.44	0.02	0.31	0.10	0.03	0.98	0.40	0.09	0.04	0.25	0.02	0.01	
K4	35	3.93	0.21	3.79	1.48	0.01	67.1	15.0	1.51	0.17	4.53	0.12	0.00	97.8
K4	37	3.68	0.18	3.46	1.06	0.04	68.6	15.1	1.74	0.12	4.14	0.18	0.00	98.2
K4	39	4.10	0.21	3.74	1.36	0.10	66.4	15.7	1.61	0.16	4.74	0.17	0.01	98.3
K4	40	3.79	0.20	3.71	1.14	0.03	68.9	15.0	1.75	0.16	4.08	0.14	0.01	98.8
K4	47	3.37	0.24	3.77	1.24	0.09	68.1	14.7	1.86	0.06	4.74	0.16	0.01	98.3
K4	48	3.54	0.23	4.25	1.02	0.10	68.5	14.9	1.82	0.14	4.05	0.18	0.00	98.7
K4	49	3.70	0.20	4.43	0.91	0.04	69.1	15.5	1.70	0.14	3.65	0.12	0.01	99.4
K4	50	3.13	0.24	3.52	0.90	0.08	69.6	14.1	1.91	0.14	4.17	0.16	0.01	98.0
K4	51	4.24	0.19	3.74	1.48	0.13	65.4	15.1	1.70	0.14	4.97	0.19	0.02	97.3
K4	52	4.27	0.21	4.25	1.35	0.15	66.2	15.6	1.68	0.12	4.67	0.13	0.02	98.6
K4	53	3.51	0.18	3.81	1.15	0.03	67.4	15.0	1.87	0.09	4.19	0.16	0.03	97.4
K4	57	5.28	0.18	3.90	1.74	0.13	65.6	16.0	1.29	0.15	4.39	0.12	0.01	98.7
K4	59	3.98	0.24	3.94	1.26	0.13	66.9	15.3	1.70	0.15	4.43	0.16	0.02	98.2
Average SD		3.89	0.21	3.87	1.24	0.08	67.5	15.2	1.70	0.13	4.36	0.15	0.01	98.3
		0.54	0.02	0.29	0.24	0.05	1.38	0.47	0.17	0.03	0.36	0.02	0.01	
K7	70	5.57	0.25	4.03	1.64	0.09	62.2	16.5	1.46	0.14	5.71	0.14	0.01	97.7
K7	72	4.07	0.21	3.48	1.29	0.13	66.7	15.7	1.69	0.14	4.60	0.16	0.03	98.1
K7	73	4.61	0.23	3.66	1.44	0.13	64.9	15.4	1.66	0.15	5.47	0.15	0.02	97.8
K7	75	3.87	0.23	3.99	1.31	0.10	67.2	15.4	1.67	0.05	4.63	0.12	0.01	98.5
K7	77	4.90	0.22	3.73	1.53	0.06	65.4	15.7	1.52	0.19	4.96	0.18	0.03	98.4
K7	78	4.65	0.19	3.72	1.53	0.17	65.7	15.7	1.54	0.14	5.18	0.18	0.04	98.6
K7	79	4.46	0.21	3.67	1.44	0.06	65.8	15.9	1.67	0.15	4.72	0.15	0.03	98.2
Average SD		4.59	0.22	3.75	1.45	0.11	65.4	15.8	1.60	0.14	5.04	0.15	0.02	98.2
		0.56	0.02	0.19	0.12	0.04	1.63	0.37	0.09	0.04	0.43	0.02	0.01	
K9	82	4.99	0.22	3.79	1.37	0.10	64.3	16.4	1.47	0.10	4.42	0.13	0.00	97.3
K9	83	4.27	0.23	4.19	1.28	0.09	66.0	15.4	1.61	0.08	4.54	0.17	0.02	97.8
K9	84	4.18	0.21	4.23	1.29	0.08	66.8	15.5	1.67	0.13	4.52	0.15	0.01	98.8
K9	85	4.32	0.20	4.29	1.32	0.09	66.8	15.8	1.60	0.16	4.71	0.14	0.01	99.4
K9	86	4.11	0.24	3.85	1.34	0.09	66.9	15.3	1.75	0.08	4.72	0.16	0.00	98.5
K9	87	4.69	0.23	4.12	1.46	0.15	65.4	15.5	1.70	0.11	5.00	0.15	0.00	98.5
K9	88	4.61	0.22	3.66	1.50	0.10	64.5	15.7	1.52	0.14	4.78	0.14	0.00	96.8

K9	89	3.76	0.19	3.57	1.26	0.11	67.4	15.0	1.77	0.13	4.61	0.14	0.00	98.0
K9	90	3.99	0.23	4.18	1.24	0.11	66.9	15.6	1.73	0.11	4.27	0.10	0.01	98.5
K9	91	3.91	0.21	3.59	1.31	0.10	67.2	15.6	1.72	0.11	4.37	0.16	0.01	98.3
K9	93	4.09	0.24	3.64	1.32	0.09	66.8	15.8	1.63	0.12	4.50	0.17	0.05	98.4
	Average	4.26	0.22	3.92	1.34	0.10	66.3	15.6	1.65	0.12	4.59	0.15	0.01	98.2
	SD	0.37	0.02	0.29	0.08	0.02	1.09	0.35	0.10	0.02	0.21	0.02	0.01	
K10	104	3.29	0.22	4.03	1.13	0.11	68.9	14.1	1.78	0.13	4.57	0.13	0.01	98.4
K10	105	2.91	0.27	3.99	0.38	0.16	70.1	14.1	2.05	0.10	3.30	0.19	0.04	97.5
K10	106	4.22	0.20	3.44	1.28	0.11	66.9	15.4	1.58	0.15	4.74	0.17	0.02	98.3
K10	107	4.24	0.21	3.22	1.34	0.09	66.7	15.2	1.63	0.17	4.75	0.17	0.02	97.7
K10	108	5.08	0.25	3.69	1.21	0.16	63.5	16.3	1.41	0.11	5.20	0.13	0.01	97.1
K10	109	4.18	0.21	3.64	1.33	0.08	67.3	15.8	1.52	0.18	4.65	0.15	0.03	99.1
K10	111	3.99	0.18	4.37	0.29	0.08	67.9	16.2	1.68	0.10	2.48	0.12	0.01	97.4
K10	112	3.44	0.20	4.33	0.28	0.15	69.7	15.5	1.84	0.13	2.46	0.15	0.03	98.2
	Average	3.92	0.22	3.84	0.91	0.12	67.6	15.3	1.69	0.14	4.02	0.15	0.02	97.9
	SD	0.68	0.03	0.41	0.49	0.03	2.08	0.85	0.20	0.03	1.10	0.03	0.01	
K11	115	4.81	0.18	4.02	1.33	0.10	65.3	16.2	1.48	0.14	4.34	0.09	0.01	98.1
K11	117	4.29	0.20	4.31	1.16	0.08	66.8	16.0	1.42	0.14	4.30	0.12	0.02	98.8
K11	118	4.13	0.15	3.28	1.33	0.14	66.9	15.9	1.45	0.11	4.39	0.12	0.00	97.9
K11	120	3.85	0.21	3.57	1.17	0.09	67.5	15.4	1.69	0.11	4.21	0.12	0.03	98.0
	Average	4.27	0.18	3.79	1.25	0.10	66.6	15.9	1.51	0.12	4.31	0.12	0.02	98.2
	SD	0.40	0.02	0.46	0.10	0.03	0.93	0.33	0.12	0.02	0.08	0.01	0.01	
K12	130	4.69	0.17	3.96	1.37	0.08	66.2	15.6	1.49	0.13	4.44	0.17	0.01	98.2
K12	131	4.47	0.18	3.92	1.32	0.05	67.0	15.7	1.61	0.21	4.77	0.15	0.00	99.3
K12	132	4.74	0.23	3.50	1.55	0.12	66.0	16.2	1.47	0.13	4.77	0.15	0.06	98.8
K12	133	4.61	0.25	3.35	1.62	0.12	66.2	16.4	1.56	0.20	4.62	0.10	0.03	99.0
K12	134	4.10	0.19	3.35	1.31	0.08	67.8	15.6	1.63	0.18	4.10	0.12	0.02	98.4
K12	136	4.30	0.20	3.85	1.21	0.08	67.5	15.0	1.51	0.18	4.55	0.15	0.00	98.5
K12	137	3.92	0.19	3.71	1.22	0.10	67.2	15.1	1.61	0.17	4.36	0.15	0.00	97.6
K12	139	4.45	0.19	4.02	1.37	0.07	66.6	15.3	1.49	0.03	5.09	0.15	0.01	98.8
K12	140	4.72	0.24	4.13	1.42	0.06	66.8	15.5	1.50	0.24	4.95	0.16	0.04	99.7
K12	141	4.68	0.19	3.94	1.27	0.10	66.9	15.4	1.58	0.25	4.78	0.15	0.02	99.2
K12	142	3.94	0.22	3.91	1.18	0.07	67.4	15.5	1.61	0.09	4.35	0.13	0.03	98.3
K12	143	5.01	0.21	3.78	1.65	0.04	65.3	15.7	1.44	0.22	5.19	0.13	0.02	98.6
K12	144	4.99	0.26	3.76	1.85	0.14	64.2	15.9	1.44	0.10	5.28	0.11	0.01	98.1
K12	145	5.17	0.21	3.62	1.77	0.16	64.6	16.5	1.37	0.17	5.17	0.10	0.02	98.9
K12	146	4.25	0.19	3.84	1.23	0.08	66.9	15.9	1.55	0.12	4.18	0.12	0.00	98.3
K12	147	4.59	0.22	3.41	1.71	0.14	65.5	16.0	1.53	0.14	5.37	0.15	0.00	98.8
K12	148	3.87	0.22	3.34	1.34	0.01	67.6	15.1	1.66	0.16	4.47	0.17	0.00	97.9
K12	149	4.11	0.19	3.39	1.47	0.09	67.2	15.5	1.51	0.23	4.84	0.16	0.01	98.7
	Average	4.48	0.21	3.71	1.44	0.09	66.5	15.7	1.53	0.16	4.74	0.14	0.02	98.6
	SD	0.39	0.02	0.26	0.21	0.04	1.03	0.44	0.08	0.06	0.38	0.02	0.02	
K14	150	4.78	0.26	3.66	1.84	0.12	64.9	16.3	1.47	0.17	5.18	0.10	0.01	98.8
K14	151	4.61	0.24	3.43	1.48	0.10	66.8	16.0	1.58	0.13	4.85	0.17	0.01	99.4
K14	153	4.65	0.20	4.02	1.41	0.06	66.2	15.5	1.47	0.18	4.78	0.15	0.00	98.6
K14	154	4.52	0.18	3.68	1.48	0.13	66.0	15.9	1.58	0.13	4.88	0.13	0.01	98.6
K14	156	5.26	0.20	4.16	1.18	0.07	65.4	16.9	1.36	0.17	4.14	0.12	0.00	98.9
K14	157	4.71	0.23	3.88	1.50	0.13	66.6	16.0	1.54	0.21	4.98	0.15	0.01	99.8

K14	159	4.37	0.22	3.42	1.51	0.15	66.3	15.8	1.60	0.15	4.78	0.14	0.01	98.4
	Average	4.70	0.22	3.75	1.49	0.11	66.0	16.0	1.52	0.16	4.80	0.14	0.01	98.9
	SD	0.28	0.03	0.28	0.19	0.03	0.67	0.45	0.09	0.03	0.32	0.02	0.01	
K18	9	4.39	0.19	3.72	1.31	0.13	65.9	15.4	1.61	0.12	4.74	0.14	0.00	97.6
K18	10	4.40	0.21	3.57	1.32	0.05	66.0	15.4	1.45	0.04	4.80	0.16	0.04	97.4
K18	11	4.02	0.21	3.39	1.45	0.07	65.8	14.9	1.70	0.18	4.86	0.16	0.01	96.7
K18	12	3.88	0.18	3.99	1.18	0.07	65.6	15.2	1.62	0.08	4.24	0.15	0.03	96.2
K18	14	4.05	0.17	3.29	1.29	0.14	65.8	15.4	1.59	0.11	4.66	0.12	0.01	96.6
K18	15	3.99	0.21	3.79	1.25	0.10	66.8	15.4	1.69	0.11	4.39	0.12	0.01	97.8
K18	17	4.85	0.27	3.32	1.63	0.12	64.2	15.5	1.40	0.15	5.23	0.17	0.05	96.8
K18	18	4.52	0.18	3.74	1.43	0.13	65.3	15.6	1.65	0.08	4.84	0.11	0.00	97.6
K18	21	4.18	0.23	3.96	1.25	0.07	66.0	15.5	1.61	0.11	4.56	0.15	0.03	97.6
	Average	4.25	0.21	3.64	1.34	0.10	65.7	15.4	1.59	0.11	4.70	0.14	0.02	97.1
	SD	0.31	0.03	0.27	0.14	0.03	0.70	0.20	0.10	0.04	0.29	0.02	0.02	
K20	23	4.16	0.19	3.70	1.31	0.10	66.6	15.5	1.46	0.15	4.59	0.15	0.01	97.8
K20	25	4.41	0.20	3.91	1.25	0.06	65.9	15.2	1.57	0.10	4.65	0.15	0.04	97.4
K20	26	3.98	0.22	4.32	1.23	0.03	66.3	15.3	1.63	0.13	4.35	0.13	0.00	97.7
K20	27	4.55	0.20	3.85	1.28	0.09	65.6	15.9	1.46	0.07	4.84	0.12	0.02	98.0
K20	28	3.97	0.20	3.95	0.91	0.08	64.3	15.5	1.40	0.09	3.51	0.14	0.03	94.1
K20	30	4.85	0.20	4.09	0.89	0.14	65.2	16.2	1.18	0.18	4.08	0.13	0.02	97.2
K20	32	3.78	0.24	3.77	1.21	0.16	67.6	14.6	1.70	0.15	4.66	0.15	0.02	97.9
K20	33	4.15	0.21	3.54	1.47	0.13	66.6	15.1	1.60	0.12	4.79	0.13	0.01	97.9
K20	34	4.01	0.23	3.85	1.40	0.06	66.1	15.0	1.63	0.13	5.07	0.15	0.00	97.6
K20	36	4.31	0.18	4.06	1.26	0.11	65.7	15.3	1.62	0.20	4.72	0.15	0.05	97.6
K20	37	4.66	0.19	3.63	1.26	0.09	66.1	15.9	1.53	0.16	4.43	0.13	0.03	98.0
K20	38	4.40	0.22	3.69	1.36	0.10	66.3	15.5	1.59	0.17	4.94	0.13	0.00	98.4
K20	39	3.95	0.23	3.93	1.44	0.09	66.0	15.2	1.62	0.15	5.20	0.15	0.00	97.9
	Average	4.24	0.21	3.87	1.25	0.09	66.0	15.4	1.54	0.14	4.60	0.14	0.02	97.5
	SD	0.32	0.02	0.21	0.18	0.03	0.77	0.44	0.14	0.04	0.44	0.01	0.02	
K21	50	4.83	0.20	3.99	1.50	0.18	64.7	16.0	1.43	0.15	5.15	0.13	0.00	98.2
K21	51	4.31	0.19	4.00	1.19	0.08	66.0	15.6	1.62	0.14	4.55	0.13	0.00	97.8
K21	52	4.59	0.23	3.75	1.61	0.16	64.6	15.5	1.56	0.21	5.58	0.15	0.00	97.9
K21	53	4.57	0.24	4.10	1.52	0.12	64.8	15.5	1.56	0.14	5.01	0.14	0.03	97.7
K21	54	4.49	0.24	3.78	1.48	0.15	65.5	16.0	1.53	0.11	4.72	0.13	0.01	98.0
K21	56	4.76	0.24	3.98	1.62	0.15	64.8	15.7	1.52	0.15	5.54	0.16	0.01	98.6
K21	57	4.14	0.21	3.86	1.33	0.12	66.0	15.4	1.58	0.17	4.60	0.15	0.00	97.5
K21	58	4.48	0.23	3.67	1.51	0.14	65.4	15.9	1.65	0.10	5.18	0.12	0.02	98.4
K21	59	4.84	0.23	3.86	1.54	0.14	63.8	15.6	1.47	0.15	5.00	0.15	0.02	96.7
K21	60	4.91	0.26	4.06	1.62	0.17	65.0	15.0	1.48	0.21	5.63	0.16	0.03	98.5
K21	62	3.90	0.23	3.62	1.56	0.13	65.8	15.0	1.69	0.11	5.54	0.16	0.01	97.7
K21	63	4.15	0.17	3.54	1.32	0.11	66.4	15.5	1.58	0.17	4.65	0.14	0.02	97.7
K21	64	4.76	0.22	3.71	1.61	0.14	64.5	15.8	1.58	0.20	5.35	0.14	0.04	98.0
K21	65	4.71	0.24	3.60	1.70	0.12	64.6	15.5	1.55	0.20	4.66	0.14	0.01	96.9
K21	66	3.77	0.20	4.17	1.19	0.15	66.9	15.4	1.73	0.14	4.27	0.14	0.03	98.1
K21	67	4.74	0.23	3.55	1.47	0.18	64.7	16.0	1.60	0.13	5.35	0.13	0.01	98.0
	Average	4.50	0.22	3.83	1.49	0.14	65.2	15.6	1.57	0.15	5.05	0.14	0.02	97.9
	SD	0.35	0.02	0.21	0.15	0.03	0.83	0.30	0.08	0.04	0.43	0.01	0.01	
K23	68	4.25	0.19	3.67	1.38	0.16	65.9	15.3	1.59	0.18	4.97	0.16	0.02	97.7

K23	69	3.98	0.22	3.34	1.26	0.13	64.1	14.9	1.53	0.12	4.40	0.13	0.03	94.2
K23	71	4.37	0.23	3.60	1.37	0.09	66.7	15.7	1.59	0.11	4.93	0.14	0.02	98.8
K23	72	3.87	0.19	3.50	1.16	0.06	67.1	15.3	1.71	0.14	4.59	0.15	0.01	97.7
K23	73	4.20	0.23	3.36	1.37	0.12	65.7	15.4	1.57	0.14	4.91	0.14	0.01	97.1
K23	74	4.57	0.25	3.79	1.54	0.12	65.9	15.2	1.63	0.15	5.09	0.15	0.00	98.4
K23	75	3.50	0.20	3.51	0.92	0.16	67.0	14.9	1.83	0.11	4.73	0.17	0.00	97.0
K23	76	4.08	0.23	3.25	1.36	0.17	64.4	14.9	1.47	0.09	4.82	0.18	0.02	94.9
K23	78	4.68	0.23	3.58	1.54	0.18	65.7	15.5	1.54	0.16	5.32	0.16	0.02	98.6
Average SD		4.17	0.22	3.51	1.32	0.13	65.8	15.3	1.61	0.13	4.86	0.15	0.01	97.2
		0.36	0.02	0.17	0.19	0.04	1.04	0.28	0.11	0.03	0.27	0.02	0.01	
K25	87	3.77	0.17	3.95	1.08	0.08	68.0	15.4	1.58	0.06	4.04	0.13	0.02	98.3
K25	88	3.66	0.19	3.98	1.15	0.07	68.0	15.2	1.73	0.16	4.29	0.13	0.00	98.6
K25	89	3.66	0.23	3.42	1.12	0.12	68.4	15.0	1.61	0.09	4.45	0.14	0.02	98.3
K25	90	3.76	0.19	3.97	1.13	0.05	68.1	15.3	1.66	0.14	4.11	0.13	0.01	98.5
K25	91	4.76	0.17	3.99	1.00	0.03	66.8	16.9	1.40	0.14	3.96	0.12	0.02	99.2
K25	92	3.71	0.22	3.59	1.10	0.03	68.2	15.4	1.62	0.16	4.25	0.14	0.02	98.4
K25	93	3.72	0.20	3.39	1.10	0.05	68.7	15.2	1.66	0.22	4.28	0.16	0.00	98.6
K25	94	3.88	0.19	4.05	1.26	0.17	68.4	15.5	1.66	0.08	4.49	0.12	0.00	99.8
K25	95	4.56	0.24	3.45	1.47	0.16	66.7	15.4	1.58	0.16	4.69	0.14	0.03	98.5
K25	96	3.98	0.24	3.39	1.36	0.12	67.8	15.2	1.61	0.14	5.29	0.16	0.04	99.2
K25	97	4.22	0.22	4.15	1.39	0.17	66.8	15.4	1.54	0.15	4.98	0.12	0.01	99.2
Average SD		3.97	0.21	3.76	1.19	0.09	67.8	15.5	1.60	0.14	4.44	0.14	0.02	98.8
		0.38	0.02	0.30	0.15	0.06	0.72	0.50	0.08	0.05	0.41	0.01	0.01	
K26	99	3.91	0.18	3.64	1.08	0.04	68.4	15.3	1.64	0.14	4.16	0.16	0.01	98.7
K26	100	4.10	0.23	3.28	1.43	0.15	67.1	15.1	1.64	0.16	4.88	0.14	0.02	98.2
K26	105	4.35	0.19	3.32	1.33	0.10	67.7	15.5	1.62	0.13	4.77	0.16	0.00	99.2
K26	107	4.13	0.25	3.60	1.33	0.08	68.0	15.4	1.67	0.14	4.55	0.16	0.00	99.3
K26	109	3.50	0.21	3.56	1.02	0.07	68.6	14.4	1.74	0.09	4.28	0.15	0.00	97.6
K26	110	3.94	0.20	3.95	0.82	0.07	67.2	15.8	1.57	0.05	3.39	0.14	0.02	97.1
K26	112	4.25	0.19	3.83	1.09	0.06	68.3	15.9	1.65	0.17	4.05	0.13	0.01	99.5
K26	113	3.57	0.21	3.75	1.06	0.03	69.1	15.2	1.73	0.16	4.01	0.14	0.00	98.9
K26	114	3.65	0.19	4.04	1.05	0.05	68.6	15.2	1.63	0.13	4.09	0.14	0.03	98.7
Average SD		3.93	0.21	3.66	1.13	0.07	68.1	15.3	1.65	0.13	4.24	0.15	0.01	98.6
		0.30	0.02	0.26	0.19	0.04	0.68	0.43	0.05	0.04	0.45	0.01	0.01	
K28	125	3.60	0.23	3.61	1.10	0.08	69.5	15.2	1.75	0.13	3.55	0.16	0.02	98.8
K28	127	4.25	0.21	3.68	1.35	0.10	67.4	15.6	1.65	0.14	4.92	0.15	0.03	99.4
K28	128	4.43	0.21	3.69	1.50	0.15	67.1	15.8	1.54	0.23	4.78	0.14	0.00	99.5
K28	129	3.51	0.19	3.40	1.14	0.05	67.4	14.9	1.65	0.15	4.15	0.18	0.02	96.7
K28	131	3.58	0.18	3.61	0.91	0.01	69.1	15.4	1.73	0.14	3.75	0.15	0.00	98.5
K28	132	3.55	0.22	3.74	1.13	0.03	69.6	15.5	1.74	0.16	4.36	0.15	0.01	100.2
K28	134	3.53	0.16	3.52	1.07	0.00	68.5	15.0	1.65	0.06	3.88	0.18	0.00	97.6
K28	136	4.51	0.19	4.00	0.97	0.00	67.2	16.5	1.51	0.10	3.66	0.13	0.03	98.8
K28	137	3.79	0.22	3.45	1.09	0.04	69.5	15.3	1.77	0.16	4.30	0.16	0.01	99.7
K28	138	3.65	0.20	3.23	1.08	0.03	68.8	15.1	1.58	0.12	4.14	0.16	0.01	98.1
K28	139	3.61	0.18	3.93	1.10	0.03	68.6	15.1	1.66	0.15	4.14	0.14	0.00	98.6
K28	140	4.29	0.21	3.88	1.42	0.13	66.5	15.4	1.52	0.11	5.12	0.17	0.02	98.7
Average SD		3.86	0.20	3.64	1.16	0.05	68.3	15.4	1.65	0.14	4.23	0.16	0.01	98.7
		0.39	0.02	0.23	0.18	0.05	1.09	0.43	0.09	0.04	0.50	0.02	0.01	

K34	142	4.62	0.22	3.74	1.50	0.10	67.0	15.6	1.51	0.12	5.08	0.16	0.04	99.6
K34	143	3.79	0.18	3.65	1.01	0.03	69.3	15.3	1.78	0.17	3.79	0.18	0.03	99.2
K34	146	3.77	0.19	3.45	1.12	0.02	69.3	15.1	1.76	0.18	4.04	0.16	0.02	99.1
K34	147	3.10	0.22	3.14	1.18	0.07	70.7	14.2	2.00	0.21	4.46	0.17	0.01	99.5
K34	149	3.94	0.23	3.56	1.30	0.11	68.2	15.6	1.71	0.13	4.48	0.13	0.02	99.4
K34	150	4.35	0.21	3.69	1.28	0.10	67.7	15.5	1.57	0.14	4.51	0.16	0.02	99.2
K34	151	4.77	0.21	3.53	1.51	0.08	66.1	16.0	1.55	0.17	5.04	0.15	0.03	99.2
K34	152	3.86	0.19	3.52	1.04	0.00	69.6	15.1	1.66	0.12	3.71	0.16	0.01	98.9
K34	153	3.89	0.18	3.49	1.15	0.03	68.8	15.2	1.69	0.12	4.04	0.15	0.01	98.7
K34	154	4.34	0.22	3.81	0.87	0.10	68.4	15.9	1.58	0.10	4.04	0.15	0.00	99.5
K34	155	3.44	0.21	3.25	1.17	0.07	67.7	14.8	1.79	0.12	4.32	0.18	0.00	97.0
K34	156	3.75	0.19	3.36	1.13	0.05	69.3	15.3	1.76	0.13	4.18	0.15	0.03	99.3
K34	157	3.63	0.22	3.51	1.13	0.00	69.3	15.5	1.75	0.18	4.00	0.14	0.02	99.3
K34	158	4.05	0.19	3.54	1.29	0.07	68.5	15.2	1.71	0.17	4.46	0.17	0.04	99.3
K34	159	3.67	0.20	4.17	1.06	0.04	68.8	15.3	1.75	0.12	4.20	0.15	0.01	99.4
K34	160	3.58	0.22	3.79	1.17	0.05	69.2	15.1	1.75	0.19	4.11	0.15	0.01	99.4
K34	161	3.54	0.21	3.52	1.14	0.06	69.2	15.5	1.75	0.18	4.51	0.16	0.00	99.6
K34	162	3.63	0.23	3.47	1.02	0.03	68.4	15.1	1.74	0.13	3.88	0.14	0.00	97.8
K34	163	2.85	0.23	3.56	0.69	0.10	71.8	14.2	2.04	0.14	3.83	0.16	0.01	99.6
K34	164	3.76	0.17	3.55	1.16	0.01	68.9	15.1	1.64	0.10	4.28	0.15	0.03	98.8
K34	165	3.53	0.19	3.79	1.10	0.03	69.4	15.3	1.79	0.16	4.05	0.15	0.00	99.4
K34	166	3.67	0.20	3.86	1.13	0.01	69.2	15.0	1.71	0.15	4.30	0.15	0.00	99.4
K34	Average	3.80	0.20	3.59	1.14	0.05	68.9	15.2	1.73	0.15	4.24	0.15	0.01	99.1
	SD	0.44	0.02	0.22	0.18	0.03	1.17	0.44	0.13	0.03	0.36	0.01	0.01	
K35	167	3.63	0.24	3.85	1.27	0.00	67.8	15.8	1.76	0.13	5.26	0.15	0.01	99.9
K35	173	4.35	0.22	3.29	1.34	0.00	68.2	15.4	1.75	0.14	4.45	0.15	0.02	99.4
K35	174	4.60	0.21	4.16	1.33	0.00	67.3	15.1	1.73	0.14	5.06	0.13	0.03	99.9
K35	178	4.71	0.23	3.73	1.36	0.00	67.6	15.8	1.58	0.15	5.00	0.15	0.04	100.4
K35	180	4.58	0.22	3.12	1.17	0.00	67.4	16.2	1.67	0.14	5.08	0.12	0.02	99.8
K35	Average	4.37	0.22	3.63	1.29	0.00	67.7	15.6	1.70	0.14	4.97	0.14	0.02	99.9
	SD	0.44	0.01	0.42	0.08	0.00	0.36	0.41	0.07	0.01	0.31	0.01	0.01	
K130	9	3.38	0.13	3.74	0.91	0.01	70.9	15.3	1.60	0.14	2.81	0.16	0.00	99.0
K130	11	3.68	0.14	4.04	0.81	0.02	70.4	15.2	1.57	0.13	2.51	0.10	0.00	98.6
K130	12	3.61	0.16	3.52	0.90	0.00	70.3	15.3	1.44	0.17	2.65	0.14	0.00	98.1
K130	13	3.25	0.14	4.06	0.90	0.00	70.7	15.1	1.50	0.15	3.11	0.15	0.01	99.0
K130	14	3.21	0.17	3.86	0.92	0.02	70.0	15.1	1.62	0.14	2.68	0.13	0.00	97.9
K130	15	3.17	0.12	3.94	0.85	0.00	70.4	15.0	1.62	0.15	2.67	0.13	0.02	98.0
K130	17	2.98	0.16	3.63	0.56	0.02	71.3	15.5	1.64	0.08	2.29	0.13	0.00	98.3
K130	20	3.67	0.15	4.36	0.73	0.00	71.2	15.7	1.37	0.10	2.44	0.12	0.00	99.8
K130	21	3.38	0.17	3.67	0.91	0.00	69.1	15.2	1.61	0.09	2.79	0.15	0.00	97.0
K130	22	3.28	0.18	3.49	0.91	0.00	71.4	15.3	1.66	0.09	2.71	0.13	0.01	99.1
K130	23	3.62	0.11	3.50	0.94	0.01	70.8	15.4	1.55	0.14	2.76	0.14	0.01	98.9
K130	24	3.47	0.14	3.47	0.89	0.00	70.8	15.5	1.58	0.16	2.69	0.16	0.00	98.8
K130	25	3.40	0.16	3.94	0.87	0.00	70.3	15.3	1.61	0.15	2.72	0.13	0.01	98.6
K130	Average	3.39	0.15	3.79	0.85	0.01	70.6	15.3	1.57	0.13	2.68	0.14	0.00	98.5
	SD	0.21	0.02	0.27	0.10	0.01	0.61	0.18	0.08	0.03	0.20	0.02	0.01	
K131	26	3.55	0.14	3.71	0.99	0.00	68.4	15.1	1.57	0.21	2.76	0.18	0.03	96.7
K131	31	3.62	0.17	3.75	0.94	0.00	70.3	15.5	1.52	0.15	2.93	0.17	0.01	99.0

K131	32	3.48	0.17	3.88	0.94	0.02	69.3	15.1	1.58	0.10	2.81	0.17	0.02	97.6
K131	33	3.35	0.15	3.89	0.88	0.00	69.5	15.3	1.66	0.06	2.67	0.14	0.02	97.6
K131	34	3.43	0.14	4.19	0.90	0.00	70.4	15.2	1.56	0.07	2.82	0.17	0.01	98.8
K131	35	3.60	0.14	3.81	0.93	0.00	69.9	15.4	1.57	0.18	2.78	0.16	0.01	98.4
K131	37	3.40	0.16	3.48	0.91	0.00	71.3	15.3	1.68	0.22	2.86	0.15	0.00	99.5
K131	39	3.42	0.15	3.55	0.92	0.00	71.3	15.5	1.60	0.11	2.84	0.16	0.00	99.5
K131	40	3.51	0.14	3.41	0.79	0.00	71.1	15.6	1.68	0.11	2.53	0.15	0.02	99.0
K131	41	4.46	0.14	3.96	1.05	0.00	69.1	16.3	1.20	0.18	2.52	0.10	0.01	99.1
K131	42	3.37	0.15	3.79	0.87	0.00	70.0	15.2	1.60	0.10	2.73	0.15	0.02	97.9
	Average	3.56	0.15	3.77	0.92	0.00	70.1	15.4	1.56	0.14	2.75	0.15	0.01	98.4
	SD	0.31	0.01	0.22	0.07	0.01	0.94	0.34	0.13	0.05	0.13	0.02	0.01	
K132	43	3.23	0.15	3.50	0.95	0.00	69.1	14.6	1.59	0.15	2.95	0.16	0.03	96.4
K132	52	3.42	0.15	4.11	0.93	0.00	70.3	15.4	1.61	0.21	2.81	0.15	0.01	99.1
K132	53	3.43	0.18	3.83	0.94	0.01	69.9	15.3	1.62	0.12	2.91	0.18	0.02	98.3
K132	54	3.31	0.14	3.40	0.96	0.00	71.9	15.4	1.70	0.16	2.79	0.12	0.01	99.9
K132	55	3.39	0.17	3.71	0.90	0.00	71.1	15.4	1.57	0.10	2.82	0.16	0.00	99.4
K132	58	3.43	0.15	4.26	0.91	0.00	70.9	15.5	1.57	0.06	2.84	0.14	0.03	99.7
K132	60	3.51	0.16	3.37	0.90	0.00	70.6	15.2	1.57	0.14	2.68	0.15	0.01	98.2
K132	61	3.28	0.17	3.55	0.96	0.02	71.5	15.3	1.69	0.12	2.85	0.16	0.00	99.6
K132	63	3.57	0.17	3.45	0.98	0.00	71.2	15.6	1.53	0.13	2.94	0.18	0.00	99.7
K132	64	4.07	0.14	4.25	0.80	0.00	70.1	16.2	1.41	0.10	2.32	0.14	0.00	99.5
K132	66	2.43	0.15	3.13	0.68	0.00	72.7	13.6	1.85	0.13	2.62	0.17	0.01	97.4
K132	67	3.52	0.14	4.07	0.96	0.00	69.9	15.2	1.56	0.06	2.81	0.15	0.01	98.3
K132	68	3.42	0.14	3.63	0.88	0.00	70.6	15.6	1.60	0.06	2.65	0.17	0.02	98.8
K132	69	3.40	0.12	3.42	0.92	0.00	70.3	15.3	1.61	0.14	2.72	0.17	0.08	98.1
K132	70	3.25	0.14	3.75	0.87	0.00	70.9	15.2	1.59	0.04	2.76	0.14	0.01	98.6
K132	71	3.80	0.13	4.18	0.61	0.00	70.7	16.4	1.34	0.08	2.06	0.11	0.00	99.4
	Average	3.40	0.15	3.72	0.88	0.00	70.7	15.3	1.59	0.11	2.72	0.15	0.01	98.8
	SD	0.33	0.01	0.35	0.10	0.01	0.85	0.60	0.11	0.05	0.23	0.02	0.02	
K135	72	3.03	0.15	3.93	0.74	0.00	71.8	14.5	1.86	0.12	2.53	0.19	0.00	98.7
K135	84	3.84	0.19	3.59	1.10	0.04	69.4	15.6	1.65	0.10	4.04	0.18	0.01	99.7
K135	85	3.60	0.19	3.68	1.10	0.02	69.2	15.5	1.65	0.09	3.86	0.14	0.03	99.1
K135	86	3.41	0.17	3.62	1.08	0.08	66.7	15.2	1.60	0.13	3.94	0.18	0.00	96.0
K135	87	3.78	0.17	3.59	1.02	0.00	69.1	15.4	1.68	0.21	3.92	0.17	0.01	99.1
K135	92	3.84	0.15	3.40	1.05	0.05	69.4	15.4	1.61	0.06	3.38	0.18	0.00	98.5
K135	93	3.46	0.18	3.61	0.95	0.00	70.1	15.3	1.74	0.13	3.02	0.15	0.02	98.6
K135	94	3.65	0.20	3.89	1.02	0.00	70.2	15.3	1.64	0.10	3.83	0.16	0.00	99.9
K135	95	3.70	0.16	3.72	0.97	0.00	70.1	15.3	1.77	0.10	3.16	0.17	0.01	99.1
K135	96	3.45	0.19	3.57	1.08	0.02	70.5	15.2	1.75	0.19	4.11	0.17	0.00	100.3
	Average	3.58	0.17	3.66	1.01	0.02	69.6	15.3	1.69	0.12	3.58	0.17	0.01	98.9
	SD	0.25	0.02	0.16	0.11	0.03	1.31	0.32	0.08	0.05	0.53	0.01	0.01	
K140	98	4.22	0.23	3.55	1.43	0.12	67.5	15.7	1.65	0.10	4.90	0.15	0.03	99.6
K140	99	4.47	0.22	3.16	1.45	0.12	65.8	15.8	1.54	0.16	4.96	0.14	0.01	97.8
K140	100	4.52	0.23	4.08	1.49	0.15	66.5	15.9	1.67	0.14	4.34	0.15	0.03	99.1
K140	101	4.51	0.23	3.57	1.50	0.16	66.8	15.9	1.55	0.10	4.84	0.15	0.02	99.3
K140	104	4.00	0.20	3.55	1.20	0.01	68.9	15.3	1.64	0.14	4.11	0.17	0.00	99.2
K140	105	3.45	0.22	3.61	1.15	0.04	69.4	15.1	1.59	0.17	4.19	0.14	0.01	99.0
K140	107	5.09	0.24	3.57	1.56	0.13	65.9	16.2	1.50	0.14	5.07	0.15	0.04	99.5

K140	109	4.30	0.23	3.75	1.51	0.14	66.5	15.7	1.60	0.20	5.06	0.13	0.00	99.1
	Average	4.32	0.22	3.60	1.41	0.11	67.2	15.7	1.59	0.14	4.68	0.15	0.02	99.1
	SD	0.47	0.01	0.25	0.15	0.06	1.33	0.34	0.06	0.03	0.40	0.01	0.02	
K142	114	3.63	0.21	3.66	1.16	0.04	68.5	15.2	1.68	0.22	3.96	0.13	0.00	98.3
K142	115	4.11	0.19	4.16	1.26	0.08	67.6	15.8	1.52	0.15	4.43	0.14	0.00	99.4
	Average	3.87	0.20	3.91	1.21	0.06	68.1	15.5	1.60	0.19	4.20	0.13	0.00	98.9
	SD	0.33	0.01	0.35	0.07	0.02	0.64	0.48	0.11	0.05	0.34	0.01	0.00	
K143	124	4.59	0.23	3.68	1.71	0.16	65.8	15.9	1.53	0.18	4.95	0.15	0.03	98.9
K143	125	4.70	0.23	3.70	1.56	0.12	66.4	16.1	1.53	0.14	4.62	0.13	0.02	99.2
K143	126	4.72	0.22	3.57	1.65	0.13	65.9	15.9	1.52	0.14	5.04	0.13	0.00	98.9
K143	127	4.63	0.22	3.72	1.54	0.04	66.1	16.1	1.55	0.17	5.00	0.15	0.03	99.2
K143	129	4.54	0.23	3.76	1.59	0.10	67.0	16.2	1.54	0.22	4.96	0.12	0.01	100.2
K143	130	4.77	0.23	3.46	1.63	0.10	66.3	16.2	1.55	0.15	5.15	0.15	0.03	99.7
K143	131	4.90	0.25	4.01	1.59	0.09	66.6	16.2	1.49	0.14	5.49	0.16	0.00	100.8
K143	132	4.69	0.20	3.57	1.59	0.14	66.6	16.1	1.50	0.20	5.26	0.14	0.00	100.0
K143	133	4.48	0.22	3.83	1.52	0.18	67.0	15.8	1.55	0.15	4.99	0.13	0.02	99.9
K143	134	4.51	0.22	3.63	1.53	0.10	66.6	15.9	1.55	0.17	4.99	0.14	0.03	99.4
K143	135	4.35	0.20	3.61	1.54	0.17	67.0	16.1	1.54	0.15	4.98	0.13	0.00	99.8
K143	136	4.72	0.23	3.85	1.69	0.14	66.4	16.4	1.54	0.14	5.29	0.13	0.02	100.5
K143	137	4.66	0.18	3.98	1.50	0.15	66.7	16.0	1.54	0.19	5.02	0.13	0.00	100.0
	Average	4.63	0.22	3.72	1.59	0.13	66.5	16.1	1.53	0.16	5.06	0.14	0.01	99.7
	SD	0.14	0.02	0.16	0.06	0.04	0.39	0.15	0.02	0.03	0.21	0.01	0.01	
K144	139	3.93	0.21	3.67	1.40	0.08	65.9	15.1	1.58	0.10	4.68	0.14	0.00	96.8
K144	141	4.16	0.23	3.71	1.20	0.16	68.3	15.7	1.41	0.17	4.58	0.15	0.00	99.7
K144	143	4.47	0.22	3.53	1.46	0.08	67.2	15.4	1.47	0.15	5.29	0.13	0.00	99.3
K144	144	4.86	0.18	4.07	1.38	0.10	66.6	16.7	1.35	0.07	4.43	0.13	0.01	99.9
K144	145	4.42	0.20	3.81	1.04	0.10	67.6	16.3	1.45	0.19	4.32	0.14	0.02	99.5
K144	146	3.61	0.25	3.42	1.30	0.16	69.4	14.8	1.76	0.19	4.62	0.15	0.01	99.6
K144	147	4.35	0.19	3.72	1.29	0.09	67.2	16.0	1.52	0.20	4.52	0.15	0.01	99.2
K144	148	4.27	0.23	3.36	1.69	0.14	68.0	15.5	1.59	0.11	5.00	0.14	0.00	100.0
K144	149	4.59	0.22	3.91	0.99	0.12	67.9	16.1	1.44	0.13	4.67	0.14	0.00	100.2
K144	150	4.12	0.25	3.44	1.79	0.14	67.7	15.0	1.66	0.12	5.48	0.15	0.00	99.8
	Average	4.28	0.22	3.66	1.35	0.12	67.6	15.7	1.52	0.14	4.76	0.14	0.00	99.4
	SD	0.35	0.02	0.23	0.25	0.03	0.94	0.62	0.12	0.04	0.38	0.01	0.01	
K146	159	4.77	0.24	3.70	1.51	0.14	67.3	16.2	1.57	0.09	4.95	0.13	0.02	100.5
K146	160	3.94	0.23	4.04	1.23	0.07	67.4	15.3	1.52	0.14	4.84	0.15	0.01	98.8
K146	161	4.34	0.19	3.34	1.46	0.12	66.9	15.6	1.50	0.19	4.94	0.14	0.02	98.8
K146	163	4.35	0.22	3.67	1.53	0.12	66.6	15.6	1.55	0.14	5.17	0.16	0.03	99.1
K146	164	4.63	0.24	3.59	1.55	0.17	66.7	15.6	1.53	0.11	5.33	0.16	0.04	99.6
K146	165	4.26	0.21	3.51	1.46	0.11	66.8	15.9	1.56	0.17	4.90	0.15	0.03	99.0
K146	166	4.18	0.23	4.00	1.33	0.18	67.5	15.6	1.61	0.19	5.21	0.16	0.00	100.2
K146	167	4.06	0.23	4.08	1.42	0.09	66.5	15.2	1.74	0.18	5.16	0.15	0.00	98.8
K146	169	4.10	0.21	3.56	1.34	0.12	67.1	15.6	1.60	0.23	4.79	0.14	0.01	98.8
K146	170	4.38	0.20	3.87	1.18	0.11	63.1	16.2	1.34	0.10	4.23	0.18	0.01	94.9
K146	171	4.53	0.22	2.96	1.50	0.14	63.9	15.5	1.34	0.11	5.56	0.13	0.01	95.8
K146	172	4.30	0.23	3.65	1.46	0.13	66.5	15.7	1.56	0.13	4.86	0.14	0.00	98.6
K146	173	3.81	0.21	3.32	1.11	0.01	69.0	15.6	1.83	0.12	4.00	0.18	0.02	99.1
K146	174	3.61	0.17	1.91	1.06	0.02	69.4	15.5	1.80	0.13	3.94	0.16	0.00	97.7

K146	176	4.47	0.25	3.57	1.54	0.10	66.2	16.0	1.50	0.19	4.93	0.17	0.00	98.9
	Average	4.25	0.22	3.52	1.38	0.11	66.7	15.7	1.57	0.15	4.85	0.15	0.01	98.6
	SD	0.31	0.02	0.53	0.16	0.05	1.58	0.29	0.14	0.04	0.47	0.02	0.01	
K147	9	4.18	0.22	3.58	1.39	0.03	66.2	15.5	1.60	0.15	4.84	0.13	0.02	97.9
K147	10	4.71	0.22	3.47	1.50	0.11	66.3	15.6	1.52	0.10	4.87	0.14	0.02	98.5
K147	14	4.21	0.20	3.82	1.19	0.07	67.7	15.5	1.64	0.17	4.35	0.17	0.01	99.0
K147	16	4.02	0.18	4.11	1.30	0.11	66.5	15.3	1.58	0.14	4.59	0.15	0.02	97.9
K147	17	4.00	0.21	3.77	1.29	0.06	66.5	15.3	1.64	0.13	4.48	0.14	0.03	97.5
K147	18	4.12	0.20	3.75	1.34	0.06	66.5	15.5	1.61	0.10	4.57	0.15	0.04	97.9
K147	20	4.17	0.22	3.79	1.37	0.12	67.4	15.6	1.60	0.19	4.88	0.13	0.02	99.5
K147	21	4.09	0.19	3.57	1.36	0.04	66.7	15.7	1.55	0.14	4.60	0.15	0.00	98.1
K147	24	3.99	0.22	3.35	1.29	0.10	66.7	15.5	1.62	0.11	4.55	0.15	0.01	97.6
K147	25	4.20	0.21	3.54	1.40	0.11	66.3	15.6	1.52	0.16	4.89	0.15	0.01	98.1
K147	27	3.38	0.22	3.27	0.92	0.11	67.3	14.7	1.70	0.16	4.53	0.17	0.00	96.4
K147	28	4.04	0.21	3.78	1.34	0.14	66.8	15.5	1.63	0.18	4.54	0.13	0.00	98.3
K147	29	4.10	0.18	3.44	1.27	0.10	68.0	15.7	1.66	0.22	4.57	0.14	0.03	99.4
K147	30	4.23	0.21	3.40	1.34	0.10	66.6	15.6	1.60	0.19	4.67	0.17	0.00	98.1
K147	31	4.09	0.20	3.54	1.31	0.15	67.1	15.8	1.59	0.24	4.76	0.13	0.05	98.9
	Average	4.10	0.21	3.61	1.31	0.09	66.8	15.5	1.60	0.16	4.65	0.15	0.02	98.2
	SD	0.26	0.01	0.22	0.13	0.04	0.53	0.27	0.05	0.04	0.16	0.01	0.02	
K149	40	4.04	0.19	3.51	1.20	0.11	67.4	15.7	1.60	0.11	4.40	0.15	0.02	98.4
K149	41	4.20	0.20	3.58	1.21	0.07	67.6	15.6	1.64	0.26	4.42	0.15	0.02	98.9
K149	42	3.99	0.19	3.53	1.26	0.09	67.8	15.5	1.58	0.09	4.39	0.15	0.00	98.6
K149	43	3.97	0.23	3.89	1.31	0.12	66.0	14.4	1.65	0.18	4.35	0.14	0.00	96.1
K149	46	4.02	0.19	3.53	1.24	0.10	67.6	15.8	1.60	0.10	4.52	0.13	0.03	98.9
K149	47	4.90	0.23	3.73	1.28	0.11	64.7	16.5	1.49	0.15	5.42	0.14	0.00	98.6
K149	48	4.28	0.22	3.56	1.36	0.14	67.5	15.6	1.62	0.10	4.80	0.15	0.00	99.3
K149	50	4.31	0.22	3.51	1.35	0.11	67.9	15.7	1.59	0.14	4.61	0.16	0.06	99.7
K149	51	3.77	0.21	3.33	1.17	0.12	64.5	14.9	1.49	0.04	3.82	0.27	0.03	93.5
K149	52	5.06	0.27	3.97	1.64	0.16	67.6	16.7	1.56	0.24	6.27	0.14	0.01	103.6
K149	54	3.99	0.20	3.45	1.15	0.01	68.1	15.6	1.63	0.04	4.35	0.16	0.02	98.7
K149	57	4.58	0.19	3.38	1.44	0.09	66.7	15.7	1.51	0.15	4.88	0.15	0.02	98.7
K149	58	4.15	0.25	3.32	1.33	0.05	67.3	15.6	1.58	0.08	3.61	0.14	0.00	97.4
K149	59	4.10	0.22	3.49	1.27	0.03	67.7	15.6	1.58	0.18	4.23	0.14	0.02	98.5
	Average	4.24	0.21	3.56	1.30	0.09	67.0	15.6	1.58	0.13	4.58	0.15	0.02	98.5
	SD	0.37	0.02	0.19	0.13	0.04	1.17	0.56	0.05	0.07	0.65	0.03	0.02	
K150	68	3.83	0.23	3.96	0.71	0.13	67.3	15.2	1.65	0.18	4.67	0.14	0.02	98.0
K150	69	3.84	0.24	4.07	0.75	0.15	68.4	14.9	1.60	0.17	5.37	0.16	0.00	99.6
K150	70	3.49	0.18	3.69	1.08	0.05	68.3	15.2	1.69	0.16	4.08	0.11	0.02	98.1
K150	72	3.69	0.20	3.74	0.90	0.05	67.9	15.2	1.64	0.12	3.98	0.12	0.02	97.5
K150	74	4.18	0.21	3.78	1.18	0.06	68.7	15.6	1.59	0.14	4.26	0.16	0.01	99.8
K150	76	3.92	0.22	3.54	1.26	0.06	68.7	15.7	1.65	0.23	4.39	0.11	0.00	99.8
K150	77	3.93	0.19	3.86	1.33	0.08	67.6	15.6	1.61	0.09	4.38	0.13	0.00	98.7
K150	78	4.01	0.19	3.47	1.25	0.14	67.7	15.6	1.64	0.09	4.09	0.13	0.00	98.2
K150	79	4.51	0.24	3.88	1.39	0.12	66.9	15.8	1.52	0.12	5.09	0.14	0.00	99.7
K150	80	4.40	0.23	3.57	1.28	0.10	68.1	15.6	1.62	0.15	4.58	0.14	0.00	99.8
K150	81	3.90	0.22	3.67	0.41	0.11	69.3	14.3	1.77	0.07	3.26	0.14	0.01	97.1
Average		3.97	0.21	3.75	1.05	0.09	68.1	15.3	1.63	0.14	4.38	0.13	0.01	98.8

	<i>SD</i>		<i>0.30</i>	<i>0.02</i>	<i>0.19</i>	<i>0.31</i>	<i>0.04</i>	<i>0.68</i>	<i>0.46</i>	<i>0.06</i>	<i>0.05</i>	<i>0.57</i>	<i>0.02</i>	<i>0.01</i>	
K152		83	4.22	0.25	3.44	1.30	0.21	67.5	15.3	1.62	0.13	4.93	0.16	0.00	99.0
K152		84	3.55	0.19	3.73	1.09	0.06	69.4	15.1	1.70	0.11	4.19	0.12	0.00	99.2
K152		85	3.52	0.16	3.32	1.07	0.17	69.5	14.9	1.67	0.11	4.43	0.15	0.00	99.0
K152		86	3.28	0.20	3.17	1.12	0.04	69.3	14.7	1.83	0.15	4.29	0.16	0.00	98.2
K152		87	3.71	0.23	3.31	1.40	0.11	67.9	14.9	1.72	0.18	4.46	0.16	0.02	98.0
K152		88	5.31	0.24	3.71	2.02	0.19	63.5	16.0	1.38	0.18	6.25	0.13	0.02	99.0
K152		89	4.31	0.19	3.44	1.26	0.09	65.1	15.1	1.44	0.16	4.55	0.12	0.01	95.8
K152		90	3.60	0.22	3.56	1.11	0.04	69.8	15.0	1.81	0.14	3.97	0.14	0.01	99.4
K152		94	3.50	0.17	3.49	1.05	0.07	69.4	15.3	1.72	0.11	3.94	0.14	0.01	98.8
K152		95	3.76	0.21	3.55	1.13	0.09	69.2	15.5	1.72	0.11	4.10	0.11	0.00	99.5
K152		96	3.66	0.19	3.63	1.06	0.04	68.9	15.3	1.66	0.15	3.91	0.15	0.00	98.6
K152		106	4.45	0.18	3.60	0.71	0.00	67.6	16.4	1.54	0.18	3.35	0.15	0.00	98.2
K152		107	4.98	0.21	3.55	2.13	0.11	63.6	15.9	1.32	0.26	5.13	0.10	0.03	97.3
K152		109	3.32	0.18	3.63	1.05	0.05	69.9	14.7	1.80	0.15	4.46	0.14	0.00	99.4
K152		110	3.58	0.18	3.51	1.06	0.08	69.7	15.1	1.75	0.14	4.13	0.15	0.02	99.4
K152		111	3.54	0.18	3.57	1.03	0.01	70.0	15.2	1.74	0.14	3.97	0.15	0.01	99.4
K152		112	3.68	0.18	3.47	1.15	0.08	69.1	15.1	1.63	0.29	3.66	0.14	0.02	98.5
K152		113	3.59	0.20	3.47	1.06	0.00	69.2	15.3	1.73	0.15	3.98	0.16	0.00	98.8
	<i>Average</i>		<i>3.86</i>	<i>0.20</i>	<i>3.51</i>	<i>1.21</i>	<i>0.08</i>	<i>68.3</i>	<i>15.3</i>	<i>1.65</i>	<i>0.16</i>	<i>4.32</i>	<i>0.14</i>	<i>0.01</i>	<i>98.6</i>
	<i>SD</i>		<i>0.56</i>	<i>0.02</i>	<i>0.14</i>	<i>0.34</i>	<i>0.06</i>	<i>2.07</i>	<i>0.46</i>	<i>0.15</i>	<i>0.05</i>	<i>0.64</i>	<i>0.02</i>	<i>0.01</i>	
K155		114	3.81	0.20	3.55	1.17	0.10	68.2	15.2	1.69	0.18	3.70	0.14	0.03	98.0
K155		117	3.16	0.18	3.09	1.24	0.00	68.5	14.4	1.93	0.15	3.04	0.11	0.00	95.7
K155		122	3.35	0.25	2.86	1.41	0.19	67.2	14.6	2.27	0.11	4.83	0.01	0.00	97.2
K155		124	3.76	0.19	3.45	1.12	0.02	69.1	15.5	1.69	0.15	4.08	0.14	0.03	99.2
K155		125	4.40	0.23	3.82	1.65	0.12	66.3	15.3	1.59	0.17	5.18	0.12	0.00	98.9
K155		127	4.02	0.19	3.58	1.24	0.08	67.6	15.4	1.62	0.13	4.37	0.15	0.03	98.4
K155		128	3.82	0.18	3.34	1.18	0.07	68.9	15.2	1.67	0.13	4.14	0.15	0.01	98.8
K155		129	3.80	0.18	3.35	1.17	0.01	69.0	15.3	1.66	0.10	4.36	0.14	0.01	99.1
	<i>Average</i>		<i>3.76</i>	<i>0.20</i>	<i>3.38</i>	<i>1.27</i>	<i>0.07</i>	<i>68.1</i>	<i>15.1</i>	<i>1.76</i>	<i>0.14</i>	<i>4.21</i>	<i>0.12</i>	<i>0.01</i>	<i>98.1</i>
	<i>SD</i>		<i>0.38</i>	<i>0.03</i>	<i>0.30</i>	<i>0.18</i>	<i>0.06</i>	<i>1.00</i>	<i>0.40</i>	<i>0.23</i>	<i>0.03</i>	<i>0.66</i>	<i>0.05</i>	<i>0.01</i>	
K79		139	4.71	0.21	4.09	1.33	0.06	67.4	15.6	1.56	0.18	4.39	0.13	0.03	99.7
K79		140	4.41	0.18	3.57	1.32	0.10	67.4	15.5	1.56	0.16	4.90	0.14	0.00	99.2
K79		141	5.24	0.23	3.90	1.74	0.14	65.6	15.9	1.52	0.14	5.44	0.14	0.00	100.0
K79		143	5.00	0.22	3.50	1.61	0.15	65.6	15.8	1.49	0.16	5.29	0.16	0.00	99.0
K79		144	4.19	0.23	3.39	1.34	0.10	66.5	15.5	1.53	0.18	4.62	0.18	0.00	97.6
K79		145	4.68	0.19	3.34	1.35	0.10	67.4	15.5	1.54	0.12	4.81	0.15	0.01	99.1
K79		146	4.58	0.20	3.44	1.41	0.05	67.6	15.6	1.48	0.21	4.79	0.15	0.00	99.4
K79		149	4.96	0.21	3.67	1.53	0.12	65.9	15.6	1.57	0.20	5.16	0.15	0.02	99.1
K79		150	4.27	0.19	3.10	1.54	0.08	66.8	15.6	1.54	0.14	4.84	0.16	0.01	98.1
K79		151	4.47	0.19	3.49	1.36	0.07	66.9	15.5	1.56	0.23	5.16	0.14	0.00	99.0
K79		152	4.81	0.23	4.04	1.56	0.15	65.5	15.7	1.55	0.18	4.94	0.16	0.05	98.8
K79		153	4.34	0.20	3.40	1.38	0.10	66.4	15.4	1.56	0.18	4.17	0.17	0.02	97.3
K79		154	4.38	0.23	3.37	1.34	0.11	67.7	15.6	1.61	0.10	4.78	0.16	0.02	99.4
	<i>Average</i>		<i>4.62</i>	<i>0.21</i>	<i>3.56</i>	<i>1.45</i>	<i>0.10</i>	<i>66.7</i>	<i>15.6</i>	<i>1.54</i>	<i>0.17</i>	<i>4.87</i>	<i>0.15</i>	<i>0.01</i>	<i>98.9</i>
	<i>SD</i>		<i>0.32</i>	<i>0.02</i>	<i>0.29</i>	<i>0.13</i>	<i>0.03</i>	<i>0.80</i>	<i>0.13</i>	<i>0.03</i>	<i>0.04</i>	<i>0.35</i>	<i>0.01</i>	<i>0.02</i>	
K81		155	4.97	0.23	3.86	1.90	0.16	63.9	16.1	1.43	0.17	5.95	0.15	0.06	98.8
K81		156	5.29	0.23	3.84	1.87	0.17	63.7	16.0	1.39	0.11	6.34	0.14	0.06	99.1

K81	157	5.46	0.24	3.88	1.84	0.14	63.3	15.9	1.43	0.12	5.96	0.15	0.03	98.4
K81	158	5.29	0.24	3.74	1.90	0.18	63.6	15.9	1.42	0.13	5.92	0.16	0.04	98.5
K81	159	5.51	0.26	4.11	1.72	0.17	64.0	16.0	1.50	0.19	5.61	0.15	0.06	99.3
K81	160	4.78	0.23	3.67	1.62	0.18	65.4	16.5	1.55	0.18	4.59	0.11	0.05	98.9
K81	161	5.10	0.23	3.80	1.91	0.13	63.7	16.1	1.43	0.15	5.94	0.15	0.04	98.6
K81	162	5.60	0.22	3.84	1.75	0.17	64.2	16.0	1.44	0.17	5.52	0.18	0.05	99.1
K81	163	5.07	0.27	3.86	1.87	0.19	63.5	16.3	1.40	0.11	5.65	0.15	0.05	98.4
K81	164	5.69	0.26	3.84	2.00	0.17	63.3	16.1	1.35	0.17	6.25	0.14	0.03	99.2
K81	165	5.15	0.22	3.56	1.74	0.20	64.3	16.1	1.47	0.19	5.54	0.13	0.02	98.6
K81	166	5.18	0.25	3.84	1.87	0.14	64.6	16.2	1.44	0.18	5.48	0.13	0.04	99.3
K81	167	5.27	0.24	3.99	1.84	0.15	64.0	16.0	1.47	0.13	5.43	0.14	0.05	98.7
K81	168	5.32	0.27	3.42	1.88	0.19	64.3	16.0	1.43	0.12	6.23	0.15	0.05	99.2
K81	169	5.50	0.23	3.54	1.91	0.13	63.7	16.0	1.45	0.25	6.01	0.15	0.06	98.9
	Average	5.28	0.24	3.79	1.84	0.16	64.0	16.1	1.44	0.16	5.76	0.14	0.04	98.9
	SD	0.25	0.02	0.18	0.09	0.02	0.55	0.17	0.05	0.04	0.44	0.01	0.01	
K94	9	5.04	0.23	3.51	1.76	0.13	63.9	15.8	1.47	0.17	5.64	0.14	0.00	97.8
K94	10	4.95	0.26	3.62	1.91	0.22	64.1	15.4	1.53	0.21	6.29	0.16	0.03	98.7
K94	11	5.39	0.24	3.76	1.68	0.16	63.9	16.5	1.30	0.12	5.55	0.14	0.02	98.7
K94	12	5.17	0.23	3.55	1.88	0.11	63.7	16.0	1.56	0.15	5.88	0.15	0.01	98.3
K94	13	4.35	0.18	3.48	1.27	0.07	66.9	15.8	1.70	0.17	4.59	0.13	0.02	98.6
K94	14	5.11	0.22	3.13	1.96	0.17	64.3	16.0	1.41	0.19	6.01	0.14	0.00	98.7
K94	15	5.40	0.23	3.72	1.86	0.11	64.0	16.0	1.46	0.19	5.90	0.13	0.00	99.0
K94	16	5.19	0.24	3.68	1.82	0.09	63.9	15.8	1.40	0.10	6.03	0.15	0.00	98.4
K94	17	5.20	0.27	3.81	1.79	0.12	64.0	16.0	1.52	0.15	5.45	0.13	0.00	98.4
K94	18	5.09	0.23	3.70	1.71	0.17	64.2	16.1	1.50	0.14	5.19	0.15	0.02	98.2
K94	19	5.16	0.26	3.81	1.92	0.15	64.0	16.1	1.51	0.20	6.11	0.14	0.00	99.3
K94	20	5.42	0.26	3.59	1.90	0.14	63.6	16.0	1.38	0.22	6.06	0.14	0.00	98.8
K94	22	4.88	0.24	3.51	1.83	0.14	63.9	16.0	1.43	0.11	5.64	0.14	0.03	97.7
K94	23	5.38	0.25	3.68	1.79	0.15	63.9	15.9	1.49	0.21	5.41	0.15	0.00	98.3
	Average	5.12	0.24	3.61	1.79	0.14	64.2	16.0	1.48	0.17	5.70	0.14	0.01	98.5
	SD	0.28	0.02	0.18	0.17	0.04	0.81	0.23	0.10	0.04	0.45	0.01	0.01	
K97	24	4.13	0.20	3.53	1.30	0.08	66.7	15.7	1.68	0.19	4.62	0.16	0.03	98.3
K97	25	4.01	0.20	3.56	1.31	0.07	66.9	15.6	1.61	0.16	4.61	0.18	0.02	98.2
K97	26	4.04	0.21	3.52	1.23	0.04	67.3	15.7	1.66	0.07	4.42	0.16	0.01	98.4
K97	28	4.02	0.21	4.22	1.32	0.06	66.4	15.7	1.64	0.19	4.53	0.16	0.02	98.4
K97	29	4.07	0.20	4.35	1.23	0.12	66.6	15.6	1.62	0.14	4.48	0.16	0.02	98.5
K97	30	4.82	0.24	3.50	1.88	0.13	64.6	16.0	1.51	0.15	5.60	0.14	0.00	98.5
K97	31	4.01	0.21	3.75	1.31	0.06	67.2	15.7	1.67	0.19	4.61	0.17	0.01	98.8
K97	33	4.19	0.20	3.85	1.26	0.10	66.6	15.6	1.67	0.19	4.65	0.16	0.03	98.4
K97	34	4.24	0.20	3.66	1.33	0.11	66.7	15.6	1.66	0.09	4.46	0.16	0.00	98.2
K97	35	4.26	0.19	4.01	1.29	0.08	67.0	15.6	1.67	0.07	4.51	0.14	0.02	98.8
	Average	4.18	0.21	3.79	1.35	0.08	66.6	15.7	1.64	0.14	4.65	0.16	0.02	98.4
	SD	0.24	0.01	0.31	0.19	0.03	0.76	0.13	0.05	0.05	0.34	0.01	0.01	
K102	44	4.71	0.22	3.79	1.24	0.15	62.9	15.5	1.48	0.09	4.23	0.11	0.04	94.5
K102	45	4.71	0.23	3.76	1.82	0.13	65.1	15.6	1.55	0.23	5.76	0.15	0.00	99.0
K102	46	5.04	0.24	3.57	1.89	0.07	64.2	16.2	1.48	0.18	5.62	0.13	0.00	98.6
K102	47	5.32	0.28	3.56	1.87	0.16	64.0	16.2	1.46	0.23	5.92	0.13	0.03	99.1
K102	48	4.96	0.20	3.63	1.70	0.14	64.6	16.4	1.42	0.17	5.25	0.12	0.02	98.5

K102	49	4.78	0.27	3.66	1.85	0.16	64.4	15.8	1.54	0.14	5.88	0.13	0.00	98.6
K102	50	5.12	0.26	3.68	1.82	0.13	64.4	16.1	1.43	0.22	5.69	0.12	0.02	99.0
K102	51	5.49	0.23	3.79	1.61	0.13	64.3	16.6	1.30	0.10	5.19	0.12	0.02	98.8
K102	52	4.90	0.24	3.55	1.87	0.13	64.5	15.9	1.52	0.16	5.78	0.13	0.00	98.6
K102	53	4.54	0.23	3.53	1.77	0.16	65.3	15.9	1.68	0.12	5.30	0.10	0.01	98.6
K102	54	4.74	0.23	3.60	1.80	0.11	65.0	16.3	1.58	0.24	5.03	0.11	0.01	98.7
K102	55	5.02	0.21	3.51	1.78	0.11	64.5	16.3	1.45	0.15	5.40	0.13	0.00	98.5
K102	56	4.98	0.21	3.73	1.92	0.11	64.2	16.1	1.52	0.13	5.78	0.16	0.04	98.9
K102	57	5.36	0.26	3.99	1.83	0.12	63.8	16.4	1.38	0.15	5.69	0.13	0.01	99.0
K102	58	5.15	0.24	3.71	1.78	0.11	64.1	15.9	1.46	0.20	5.97	0.13	0.02	98.7
	Average	4.99	0.24	3.67	1.77	0.13	64.4	16.1	1.48	0.17	5.50	0.13	0.01	98.5
	SD	0.27	0.02	0.13	0.17	0.02	0.58	0.31	0.09	0.05	0.45	0.01	0.01	
K103	59	5.16	0.21	3.69	1.57	0.11	65.5	15.9	1.46	0.12	5.17	0.15	0.02	99.0
K103	60	5.40	0.25	3.37	2.02	0.16	63.7	15.8	1.34	0.17	6.04	0.15	0.02	98.4
K103	62	4.47	0.22	3.67	1.55	0.08	66.9	15.8	1.48	0.13	4.97	0.16	0.02	99.4
K103	64	4.96	0.19	3.52	1.61	0.16	66.1	16.0	1.44	0.23	5.34	0.16	0.02	99.7
K103	65	4.86	0.21	3.40	1.56	0.07	66.2	15.9	1.48	0.14	5.15	0.14	0.00	99.1
K103	66	5.31	0.24	3.50	1.63	0.10	64.9	15.9	1.47	0.20	5.35	0.15	0.04	98.7
K103	67	4.71	0.25	3.67	1.71	0.11	65.2	16.1	1.44	0.20	5.32	0.15	0.01	98.8
K103	68	4.77	0.24	4.21	1.59	0.14	64.8	15.7	1.55	0.15	5.20	0.18	0.00	98.5
K103	69	5.20	0.23	3.62	1.63	0.15	64.9	15.9	1.44	0.08	5.46	0.17	0.04	98.8
K103	72	4.48	0.22	3.78	1.21	0.09	66.2	16.1	1.55	0.13	4.75	0.15	0.00	98.7
K103	73	4.28	0.23	3.22	1.46	0.09	63.5	15.1	1.50	0.17	5.09	0.16	0.01	94.8
	Average	4.87	0.23	3.60	1.60	0.11	65.3	15.8	1.47	0.16	5.26	0.16	0.02	98.5
	SD	0.37	0.02	0.26	0.19	0.03	1.06	0.27	0.06	0.04	0.32	0.01	0.01	

AMPHIBOLE

Eruption	Sample	Point name	SiO ₂	TiO ₂	Al ₂ O ₃	FeO	MnO	MgO	CaO	Na ₂ O	K ₂ O	P ₂ O ₅	Cr ₂ O ₃	NiO	Total
2014 K123		K123_1_amp	44.1	1.90	9.73	14.0	0.39	13.3	11.2	1.78	0.31	0.00	0.00	0.00	96.8
		K123_1_amp	44.6	1.55	9.43	13.9	0.43	13.4	11.2	1.74	0.30	0.00	0.00	0.00	96.6
		K123_1_amp	44.7	1.66	9.45	14.0	0.43	13.2	11.2	1.73	0.29	0.00	0.00	0.00	96.7
		K123_1_amp	44.6	1.93	9.71	14.2	0.39	13.6	11.4	1.80	0.30	0.00	0.00	0.00	98.0
		K123_1_amp	44.5	1.59	9.37	14.1	0.42	13.4	11.4	1.70	0.29	0.00	0.00	0.00	96.7
		SD	0.22	0.18	0.17	0.11	0.02	0.14	0.11	0.04	0.01	0.00	0.00	0.00	

Supplementary Table 1: Petrography description of all thin sections, with crystallisation assemblage, mineral modes, textures, grain size, groundmass type and description, types of textures of phenocrysts present, and description of sample ov

Eruption	Sample	Type of sample	Location		Crystallisation sequence/assemblage	Mineral modes								Texture	Grain Size	Groundmass Type		
			Latitude (°S)	Longitude (°E)		Plag	Cpx	Opx	Timag	Amph	Gmass	Vesicles	Glass/melt inclusions			Type 1	Type 2	Type 3
2014	K35	Tephra fall - pumice	7°56'09.65"	112°16'57.92"	Plag (dominant) + Cpx + Opx + Oxide	30.0	5.0	4.5	1.9	0.0	33.2	24.8	0.6	Vesicular, glassy (devitrified), more glomeroporphyritic than K34 and some other 2014 fall samples. Crystals less fractured than in K34.	Plag: 1600 - 150µm; Cpx: 2500 - 200µm; Opx: 2000 - 250µm; Oxides: 300µm	x		
2014	K62	Tephra fall - pumice	7°56'10.33"	112°16'9.53"	Plag (dominant) + Cpx + Opx + Oxide	25.3	3.3	4.7	1.8	0.0	30.2	34.7	0.1	More coarsely vesiculated than other samples, less glomerocrysts. Glass like that in K35. Dominantly more plag than others.		x		
2014	K75	Tephra fall - pumice	7°55'36.28"	112°14'30.19"	Plag (dominant) + Cpx + Opx + Oxide	17.8	3.6	3.7	1.7	0.0	31.5	41.5	0.2	Most coarsley vesiculated of all the samples. As a result, more finer grained phenocrysts - as less room to occupy space (but some still present), groundmass less microphenocrysts, but mainly plag.			x	
2014	K110	Tephra fall - pumice	7°57'53.10"	112°15'19.32"	Plag (dominant) + Cpx + Opx + Oxide +- amph?									Grain mount thin section - mainly individual grains of pumice, lava and crystal fragments. Dominantly plag and cpx. Some individual phenocrysts are fragmented.		n/a		
2014	K111	Tephra fall - pumice	7°57'53.10"	112°15'19.32"	Several different clasts on section - but dominantly all Plag + Cpx + Opx + Oxide	18.0	4.6	2.8	2.2	0.0	27.9	43.7	0.9	Section made of multiple clasts - mostly pumice clasts, but some lava and tuff clasts (not described here). Juvenile pumice clasts very similar to K112, very finely vesicular, glassy and dominantly plag with some fragmented phenocrysts.	Plag: 900 - 250µm; Cpx: 900 - 250µm; Opx: 800 - 450µm; Oxides: 250µm		x	
2014	K112	Tephra fall - pumice	7°57'53.10"	112°15'19.32"	Plag (dominant) + Cpx + Opx + Oxide	24.3	4.3	3.4	2.4	0.0	24.3	40.6	0.6	Vesicular, and largely finely vesicular - less dominated by glass. Much less glomeroporphyritic (if any). Less phenocryst rich as so vesicular. Phenocrysts fragmented	Plag: 1200 - 150µm; Cpx: 2200 - 200µm; Opx: 850 - 200µm; Oxides: 150µm		x	
2014	K113	PDC - pumice	7°57'12.48"	112°15'58.58"	Several different clasts on section - but dominantly all Plag + Cpx + Opx + Oxide									Porphyritic, vesicular and glassy. Mixture of phenocryst sizes - some fragmented. Mostly plag.		x	x	
2014	K114	PDC - pumice	7°57'12.48"	112°15'58.58"	Several different clasts on section - but dominantly all Plag + Cpx + Opx + Oxide									Dominantly vesicular, porphyritic with some glomerocrysts. Fragmented phenocrysts.		x	x	x (lavas only)

2014	K115	PDC - pumice	7°57'12.48"	112°15'58.58"	Several different clasts on section - but dominantly all Plag + Cpx + Opx + Oxide													Dominantly vesicular, porphyritic with some glomerocrysts. Fragmented phenocrysts.		x	x (lavas only)	
2014	K116	Tephra fall - pumice	7°57'12.48"	112°15'58.58"	Plag (dominant) + Cpx + Opx + Oxide													Dominantly vesicular, porphyritic. Fragmented phenocrysts. With very altered glomerocrysts.			x	
2014	K120	PDC - pumice	7°57'19.21"	112°17'47.81"	Plag (dominant) + Cpx + Opx + Oxide	24.4	9.6	2.5	1.1	0.0	36.5	25.0	0.9					Juvenile pumice clasts vesicular and glassy, some finely vesicular clasts. Fragmented phenocrysts - generally aphanitic to porphyritic and glomerocrystic	Plag: 2200 - 200µm; Cpx: 1200 - 500µm; Opx: 700 - 400µm; Oxides: 200µm	x	x	x (lavas only)
2014	K121	PDC - pumice	7°57'19.21"	112°17'47.81"	Several different clasts on section - but dominantly all Plag + Cpx + Opx + Oxide													Largely and finely vesicular, glassy, porphyritic.		x	x (lavas only)	
2014	K122	PDC - pumice	7°57'19.21"	112°17'47.81"	Several different clasts on section - but dominantly all Plag + Cpx + Opx + Oxide													Largely and finely vesicular, glassy, porphyritic.			x	
2014	K123	PDC - pumice	7°57'19.21"	112°17'47.81"	Plag (dominant) + Cpx + Opx + Oxide + amph??	35.3	8.1	4.1	3.0	0.1	27.4	21.8	0.2					Vesicular, glassy, porphyritic, with few microcrysts.	Plag: 1100 - 150µm; Cpx: 1500 - 300µm; Opx: 1100 - 250µm; Oxides: 200µm	x	x	
2014	K125	PDC - pumice	7°57'19.21"	112°17'47.81"	Plag (dominant) + Cpx + Opx + Oxide													Vesicular, glassy, porphyritic, with few microcrysts.		x		
1990	K34	Tephra fall - pumice	7°56'09.65"	112°16'57.92"	Plag (dominant) + Cpx + Opx + Oxide	33.2	3.9	4.0	2.7	0.0	33.8	21.5	0.8					Vesicular, glassy, glomeroporphyritic. Many phenocrysts are fragmented. Bottom half of section is more quenched/crystalline glassy groundmass	Plag: 2200 - 200µm (micro <100µm); Cpx: 1700 - 350µm; Opx 1500 - 400µm; Oxides: 300 - <100µm	x	x	
1990	K59	Tephra fall - pumice	7°56'10.33"	112°16'9.53"	Plag (dominant) + Cpx + Opx + Oxide	21.4	5.5	2.1	2.1	0.0	40.4	28.4	0.1					Very large vesicles, more than K34. samples and glassy, glomeroporphyritic and porphyritic.		x		

1990	K76	Tephra fall - pumice	7°55'36.28"	112°14'30.19"	Plag (dominant) + Cpx + Opx + Oxide (both)	23.8	2.6	2.7	1.7	0.0	30.2	38.7	0.4	Top clast: more crystalline/glassy, less vesicular groundmass than bottom pumice clast. More porphyritic.	Plag: 2000 - 250µm; Cpx: 800 - 300µm; Opx: 1200 - 350µm; Oxides: 250µm	T: x; B: x
1990	K126	PDC - pumice	7°57'19.21"	112°17'47.81"	Plag (dominant) + Cpx + Opx + Oxide									Very vesicular, and finely vesicular. Less porphyritic as less crystalline groundmass.		x
1990	K158	Tephra fall - pumice	7°57'39.99"	112°20'55.22"	Plag (dominant) + Cpx + Opx + Oxide									Vesicular, glassy, glomeroporphyritic. Many phenocrysts are fragmented. Right half of section is more quenched/crystalline glassy groundmass (darker)		x
2007-2008	KD2	Lava dome	7°56'16.29"	112°18'9.95"	Plag (dominant) + Cpx + Opx + Oxide	38.9	9.0	9.9	3.9	0.0	30.8	7.5	0.0	Porphyritic, some glomerocrysts and small vesicles	Plag: 2300 - 150µm; Cpx: 2000 - 150µm; Opx: 1900 - 200µm; Oxides: 200µm	x
2007-2009	M1	Lava dome	7°56'16.29"	112°18'9.95"	Plag (dominant) + Cpx + Opx + Oxide									More crystalline groundmass, with larger phenocrysts all together. Some large vesicles, but generally much less than pyroclastic samples. Porphyritic.		x

erall.

Description groundmass	Plagioclase					Clinopyroxene				Orthopyroxene				Glomerocryst		
	Type 1		Type 2	Type 3	Type 3	Type 1	Type 2	Type 3	Type 4	Type 1	Type 2	Type 3	Type 4	Type 1	Type 2	Type 3
	a	b	c													
Glassy/vitric - brown glass rich, with large vesicles. Dominantly more type 1 groundmass than K34 (less finely vesicular - dominantly more glassy). Microcrystalline plag (and microlites), cpx and lesser opx in groundmass.	x	x	x	x	x	x	x	x	x	x	x	x	x	x		x
Glassy/vitric, brown glass under ppl, largely more vesicular than K35. Less glass as more vesicles.	x	x	x	x	x	x	x	x	x	x		x	x			
Type 1 groundmass - but very largely vesicular. Some areas where it looks as though it could be type 2 groundmass (bottom left corner) - possibly less devitrified glass here - lighter in colour, associated with being more finely vesicular here.	x	x	x	x	x	x	x		x	x		x	x			
n/a	x	x	x	x	x	x	x	x	x	x	x	x	x	x	x	
Groundmass of pumices very similar to K112 - some other pumices have the banded glass/vesicles like in K34. Less abundance of microcrysts due to high vesicle coverage, less crystalline overall too.	x	x	x	x	x	x	x			x	x	x			x	
Type 2 groundmass but glass in groundmass is quite dark. Some vesicles look 'wipsy' elongated - flow structures? Flow around some phenocrysts. Small vesicles in higher abundance.	x	x	x	x	x	x	x	x	x	x	x	x	x		x	
Two clasts have a darker more glassy groundmass, less finely vesicular but with larger vesicles (type 1). Other clasts are more like K112 - more finely vesicular so less glass in groundmass, with some flow banding and elongated vesicles.	x	x	x	x	x	x	x		x	x		x	x			x
Mixture of type 1 and 2 groundmass'. Both glassy and very vesicular. Some clasts are flow banded (with more devitrified glass in areas - darker) like K34. However dominantly more type 2 groundmass in general.	x	x	x	x	x	x		x	x	x		x	x	x		

Quite microcrystalline rich. Glassy - more devitrified. Less finely vesicular, but still presence of larger vesicles. Plag microlites.	x	x	x	x		x		x	x		x	x		x	
Very finely and largely vesicular, although still remains quite a large or uniformly large phenocryst population. Microcryst poor.	x	x	x	x	x	x	x	x	x		x	x		x	
Some clasts are type 1, some are type 2 groundmass (pumice). Some have darker/more devitrified glass as groundmass, commonly with smaller microphenocrysts and less finely vesicular - dominantly more crystalline in general. Others that are more finely vesicular are dominantly less crystalline, with elongated vesicles. Also have less microcrysts and glass in groundmass. Other lavas have a more phenocryst/microlite rich crystalline groundmass with larger phenos. in general - most crystalline.	x	x	x	x	x	x	x	x	x	x	x	x		x	
Groundmass/vesicle texture is somewhere inbetween 1 and 2 - flow banded possibly - areas of smaller vesicles dominating groundmass, and other areas where it is more glassy (less small vesicles). Microcryst poor.	x	x	x	x		x		x	x		x	x			
Dominantly vesicles type 2 - but around edges of clasts more devitrified glassy and less vesicular (type 1 groundmass). Much less crystalline groundmass and overall.	x	x	x	x		x		x			x	x			
Type 1 and type 2 groundmass - a has type 2, all others have groundmass type 1 - like K35. Glassy with larger vesicles - some possibly smaller. Type 2 very finely vesicular, but still with a glassy groundmass - but less devitrified? Can see flow structures of bubbles. Clast c - some areas where groundmass is more crystalline than others.	x	x	x	x	x	x	x	x		x	x	x			
Type 1 - large vesicles in glassy groundmass, much like K35. Less finely vesicular. Dominantly plag as large phenocrysts and microcrysts with lesser cpx and even lesser opx.	x	x	x	x	x	x	x	x	x	x	x	x		x	
Type 1 - Large vesicles in a glassy groundmass. Some smaller vesicles in groundmass almost like type 2 in areas. Areas where the glass is darker or devitrified, glass is in higher abundance and less finely vesicular. Flow structures seen in some elongated vesicles. Microphenocrysts in groundmass of plag (microlites), cpx, opx and oxide.	x	x	x	x	x	x		x	x	x		x	x	x	
Type 1 - Large vesicles in dark devitrified glassy groundmass. Some areas of lighter glass have more fine vesicles. Groundmass very similar to K34 - just less flow banded or evidence for flow structure (elongated vesicles). Microphenocrysts in groundmass rare - but plag, cpx and lesser opx and oxide.	x	x	x	x	x	x		x	x	x	x		x	x (rare - but plag dom)	

Top half: Type 1/3 groundmass? Devitrified dark brown glassy groundmass with few large phenocrysts, but groundmass appears slightly finely vesicular (compared to pumice samples). Bottom half: Type 1 + 2 groundmass - looks flow banded like K34 - areas of flow structures with elongated vesicles - finely vesicular with some larger vesicles. Type 1 groundmass is more microcrystalline.	x	x	x	x	x	x	x		x	x	x	x		x
Very finely and largely vesicular, meaning less crystalline. Dominantly plag, little microcrysts.	x	x	x	x		x		x	x		x	x	x	
Like K34 - mixture of type 1 and 2 groundmass in bands, very vesicular and glassy.	x	x	x	x	x	x		x	x		x	x		x
Type 3 - more crystalline, still quite glassy but a higher proportion of microcrysts and plag microlites. Some small vesicles present - similar to Jeffery et al., 2013	x	x	x	x	x	x	x	x	x	x	x	x	x	
Type 3 - more crystalline but also has some vesicles. Greater proportion of phenocrysts than others.	x	x	x	x	x	x	x	x		x	x	x		x

Other descriptions/additional	Classification	Analyses
<p>Plag is complexely zoned (even in glomerocrysts), only ever has inclusions of glass and smaller fragments of plag, some cpx. Plag often twinned and zoned. Type 1 plag most common with oscillatory zoning. Plag euhedral mostly. Plag most common microlite/microcryst. Opx is heavily altered as anhedral growths, often has oxide and plag in embayments. Often has cpx rims, where completely rimmed by cpx looks like cpx is replacing opx. Cpx phenocrysts larger than opx, has oxide and plag inclusions, with less opx as inclusions. Cpx is often twinned, large cpx phenocrysts as okiocrysts with opx chadacrysts inside. Glomerocrysts are mostly plag dominated, but some with near equal amounts of cpx and opx. Oxides as single free and as inclusions, but most commonly in growths with cpx and opx. Some phenocrysts are fragmented.</p> <p>Some phenocrysts are fragmented again. Plag more clearly zoned in sieved textures phenocrysts, less common than in other samples. Little samples with just sieved cores. Coarser plag phenos in general. Most commonly oscillatory zoned. Some very large plag phenos with zoning and twinning. Plag more well formed (euhedral). Smaller phenos with lamelle. More opx than cpx in this sample. Less evidence for opx reacting to cpx - seems to have evidence for a further reaction straight to plag? Cpx and opx are both quite altered with inclusions of plag and oxides. oxides occur as singular phenos (rare) and mostly as inclusions.</p> <p>Fragmented phenocrysts common again. Oscillatory zoned plag with sieved textures is the most common. Often phenocrysts are subhedral, but mostly euhedral. Inclusions of glass in some plag, no oxides. Rare to have only heavily sieved cores. Some smaller phenocrysts not zoned - twinned with lamellae. Near equal amounts of cpx and opx. Cpx often completely surrounds opx, or has a partial rim of cpx. Oxide and plag inclusions in both cpx and opx. Some massive cpx phenocrysts with high birefringence (gold, blue, purple), often singular phenocrysts, or occur in growths with plag, opx, with plag and oxide inclusions. Opx appears the most altered. Very commonly embayed. Some opx replaced by cpx then plag (only on rims) - not seen very commonly in other samples (usually in cores too), usually subhedral, but where it is surrounded by cpx it is anhedral. Oxides again most commonly as inclusions in cpx and opx, rare singular phenocrysts. No true glomerocrysts.</p> <p>Individual glomeroporphyritic clasts - very crystalline, mainly plag. Lava/dense lithic clasts are dominantly plag (microlites and phenocrysts) with oxide, and minor microcrysts of opx and cpx. Other lava clasts appear quite altered - have many vesicles. Pumice clasts very similar to K35 - vesicular and glassy with dominantly plag - often zoned (oscillatory) with and without sieve textures. Other clasts are clusters of different minerals - e.g. cpx, plag, opx, oxides all interlocking grains; cpx has inclusions of plag and opx, oxides; opx has inclusions of plag and oxides. Individual mineral grains are plag, opx and cpx, ti-mag. Some glass as inclusions in minerals. Possibly some glass shards with minerals attached to them too. Plag dominantly oscillatory zoned and sieve textured; glass inclusions; microlites/microphenos in the lava/pumice clasts. Varying degrees of embayments due to fluid interaction (glass inclusions) seen. Heavily resorbed/embayed opx (holes). Cpx is also embayed; often twinned. Plag dominated glomerocrysts common. oxides often in opx and cpx (inclusions), never in plag.</p> <p>All zoned plag (any type of zoning) are sieved. Can see flow structures/ elongated vesicles around phenocryst formations. Pumices lack glomerocrysts. Some plag has embayments - around rims and centre rims, with holes and glass infilling sometimes - varying degrees of reaction with melt? Some fragmented plag. Some clasts with very minor cpx and opx, some with plag and very minor opx (near to no cpx). In this sample there is no evidence for a reaction of opx to cpx to plag (apart from small plag inclusions in the opx and cpx's), i.e. no embayed phenos, or opx surrounded by cpx. Although as in all sections, the opx is much more altered. Some opx are slightly zoned. Some cpx and plag has obvious glass inclusions. Some cpx slightly osc zoned too.</p> <p>Very rare for plag to be embayed - if does embayments look as though they are filled with opx. Quite often large phenos with no or little zoning, but with twinning. Commonly have sieve textures but also commonly have no sieve textures at all \pm minor amounts of resorption/replacement than other samples. Possibly some apatite and melt inclusions in plagioclase, plag most commonly sieve textured. Opx core completely replaced and reacted to plagioclase - can sometimes see all the relict crystal edges but in others are anhedral. Alteration of cpx and opx to plag in stages - some completely replaced to plag in cores, others earlier stages (not as replaced). Microphenocrysts rarer than in other samples. Opx's seem more altered in most samples than cpx. Oxide rarely singular, commonly as inclusions in cpx and opx, or growths of both.</p> <p>Lots of fractured/fragmented phenocrysts in all clasts. Mostly all plag is sieve textured and mostly all zoned of some sort (dominantly oscialltory). Oxide in less occurrence as generally less cpx and opx in clasts - less as singular phenocrysts. One opx dominated glomerocryst type growth. Most have near to equal amounts of cpx and opx, and more than the other 3 clasts. Other clasts have mostly plag, with lesser opx and even less cpx (similar to K112). In probe section larger cpx and opx embayed crystals in growths appear slightly zoned - subhedral.</p> <p>All phenocrysts quite fractured in all minerals. Plag most commonly sieved/resorbed, with oscillatory and patchy zoning. Common melt inclusions (usually at cores). Cpx often twinned (type 1) and sometimes has melt inclusions, with oxide and plag inclusions. Can appear faintly osc zoned. Opx often rimmed by cpx. Often completely embayed at the core. Remnant opx in glomerocrysts (which are cpx domianted), with plag and oxides as interstitial growths.</p>	<p>2 px basaltic andesite</p> <p>2 px basaltic andesite</p> <p>2 px basaltic andesite</p> <p>2 px basaltic andesite</p> <p>2 px basaltic andesite</p> <p>2 px basaltic andesite</p> <p>2 px basaltic andesite</p>	<p>Petrographic, XRF, ICP-MS, EMP</p> <p>Petrographic, XRF, ICP-MS</p> <p>Petrographic, XRF, ICP-MS</p> <p>Petrographic</p> <p>Petrographic, XRF, ICP-MS, EMP</p> <p>Petrographic, XRF, ICP-MS, EMP</p> <p>Petrographic, XRF, ICP-MS</p> <p>Petrographic, XRF, ICP-MS</p>

Very similar to K121. Dominantly plag, with lesser cpx and opx. Opx appears the most altered and is often rimmed or replaced by cpx. Cpx and opx have inclusions of plag and/± oxides. Plag is often sieve/seriate textured - moving to embayed if this is to a high degree. Also present as microlites in groundmass.	2 px basaltic andesite	Petrographic, XRF, ICP-MS
More opx than cpx. Plag often is very heavily melt included, complexely zoned and sieved, rarely not sieved/resorbed. Some cpx faintly zoned, replaced ± rims opx. Opx is highly altered - embayed at core. Oxides most commonly as inclusions, but sometimes single free phenocrysts.	2 px basaltic andesite pyroclast (pumice)	Petrographic, XRF, ICP-MS
Majority of clasts type 2 groundmass, some type 1. Some have elements of both - banded like K34. Type A groundmass - fragmented phenocrysts common (all minerals), lots of microlites of plag and microphenocrysts. The plag in these clasts seem slightly more complexley osc zoned. Other type 1 clasts distinctively more phenocryst rich than type 2 - this is quite common. Heavily sieve textured plag and fragmented phenocrysts, with glomerocrysts. Plag generally heavily sieved (rarely not), with glass/melt inclusions. High occurrence of plag microlites in groundmass. Cpx more common than opx, however in some clasts cpx is rare and only occurs as microcrysts. In some cases is completely anhedral and altered, and replaced by plag (?). Oxides single free and as inclusions. Can see some faintly zoned phenocrysts of cpx and opx.	2 px basaltic andesite	Petrographic, XRF, ICP-MS, EMP
Oxide rich as single free and inclusions. Plag dominant, and more opx than cpx. Fragmented phenocrysts. Cpx and opx most common as intergrown phenocrysts. Cpx and opx have inclusions of plag and oxides. Plag also has some melt inclusions if very sieve textured.	2 px basaltic andesite	Petrographic
Mostly all juvenile clasts (not very good section). Very vesicular clasts. Dominantly more opx than cpx, but overall more plag. Cpx only occurs as embayed growths with opx and plag.	2 px basaltic andesite	Petrographic
Plag mostly commonly sieved with high amount of glass inclusions. Some quite embayed where reaction with melt higher and more sieving has occurred. Some fragmented phenocrysts. Some cpxs have oxide inclusions, and are twinned with some glass. Clast c has some anhedral cpx that has reacted with plag at the core. Some cpx phenocrysts appear faintly oscillatory zoned with oxide inclusions. Opx phenocrysts quite heavily altered/embayed in some cases - sieved type 3. Some are intergrown with cpx - both zoned and heavily included (with oxide and plag) - like glomerocrysts. Clear reactions seen with opx to cpx, and cpx to plag. Later stage crystallisation than some other pumice samples? Only sample with some hornblende.	2 px basaltic andesite	Petrographic, XRF, ICP-MS, EMP
Plag commonly completely osc zoned with glass inclusions. Where there has been a higher degree of zoning and sieving/reaction they are heavily embayed. Some medium/smaller phenocrysts discontinuous zoning, with no sieving (but rare). Few fractured phenocrysts compared to fall samples. Cpx commonly found in larger growths, like glomerocrysts? With opx and plag. Commonly larger phenos appear to have some glass inclusions and may be faintly zoned, others twinned and larger. Same as K123 where the cpx has very relict opx (at core only) and replaced by plag - very broken cpx, common around vesicles. Opx sometimes not as altered - but rimmed by cpx, with small inclusions of oxide, with or without plag inclusions. Type 3 partly sieved and zoned sometimes - when replaced heavily by cpx and plag quite common in large clusters - relict glomerocrysts?	2 px basaltic andesite	Petrographic, XRF, ICP-MS
Glomerocrysts dominantly cpx (with opx and plag). Slightly more pyroxenes than K35. Opx in some cases surrounded by a rim of cpx, and has cpx as inclusions. Cpx always has inclusions of oxide and plag (3 types - only each one, plus combination of both). Plag in this sample has no oxide inclusions, just glass, possible apatite inclusions. Rare unsieved/resorbed plag. Fragmented phenocrysts of opx, cpx and plag. Opx is anhedral and replaced by cpx and plag. Oxides commonly accessory minerals in most cases - in growths with opx, cpx. Oxides in glomerocrysts, but most commonly with growths/as inclusions in cpx and opx, or singular phenos (not in plag). Plag mainly euhedral - subhedral. Some smaller cpxs have heavily sieved cores/resorbed centres. Small phenocrysts of plag sometimes surround growths of cpx and opx.	2 px basaltic andesite	Petrographic, XRF, ICP-MS, EMP
Plag less sieve textured in this sample than in others. All types of sieving present with all types of zoning. Osc zoning most common and very clear. Some fragmented plag phenocrysts. Some larger plag sector zoned and osc zoned. Some has glass inclusions (possibly?). Microlites present. Microphenos in groundmass of mainly plag, lesser cpx and opx, oxide. More fragmented phenocrysts as a whole than 2014 samples? Common to all 1990 samples? Cpx phenocrysts often larger - twinned with oxide (some without) and plag inclusions. Some are embayed showing a reaction with plagioclase - where they show varying degrees of alteration. Some anhedral phenocrysts appear to have opx at the very centre (reaction opx - cpx to plag?), with oxide inclusions. Some larger opx phenocrysts but they are quite altered on the surface - have small inclusions of plag and oxides. Most common occurrence in growths with cpx, with plag and oxide inclusions. Other growths with plag too - like glomerocrysts. Reaction opx to cpx to plag?	2 px basaltic andesite	Petrographic, XRF, ICP-MS

Two clasts on section. Both have no glomerocrysts Note: mineral modes only done for the bottom pumice clast. Plags in top lava are mostly sieved. Some heavily resorbed and embayed in the centre - with embayments revealing the groundmass underneath of cpxs - glass inclusions too, sieved around the outside in the osc and convolute zones. Fair few like this - heavily altered at the core, and some all over. Some smaller plag microphenos are not sieved or zoned - just twinned and lamellae. Much less cpx and opx than other samples - they are often growths with plag and have oxide and plag inclusions. Some fragmented phenos. Pumice clast: same minerals apart from the groundmass texture. Less dense phenocrysts to vesicles/groundmass cover. Less cpx and opx than in other samples - dominantly plag. Fragmented phenos more common. Cpx is commonly in growths with plag \pm opx, with oxide inclusions. Often twinned and larger phenos. Opx appears as highly altered - some are very embayed. Growth \pm cpx, with plag - plag replacing opx, and often anhedral in these cases - some have holes.	2 px basaltic andesite	Petrographic, XRF, ICP-MS, EMP
Phenocrysts quite fragmented as very vesicular. Quite dirty sample? Crystals not very well formed or very large. Lesser cpx and opx than plag. Some glomerocrysts or very altered opx/cpx? To plag.	2 px basaltic andesite	Petrographic, XRF, ICP-MS
Glomerocrysts opx dominated completely altered and resorbed by cpx and plag, plag is as inclusions but also larger intergrown laths. Oxide as inclusions in cpx and opx. Anhedral and altered opx common - often rimmed by cpx. Plag often complexly zoned (osc) rarely without resorption/sieve textures. Very similar to other 1990 samples with flow banding/ differences in groundmass glass throughout sample.	2 px basaltic andesite	Petrographic, XRF, ICP-MS
Groundmass much more crystalline than the pumice samples - no smaller vesicles but some larger ones (very few). Dominantly plagioclase, mostly sieved. Where sieving is high phenocrysts are embayed - revealing groundmass below and sometimes cpx. Only plag with oxide inclusions in some phenocrysts. Few more oxides than in the pumice samples. More cpx than opx in sample. Cpx is generally in larger phenocrysts, twinned, and often in clusters of intergrown plag and opx (glomerocrysts?). Opx is the most altered in this sample - some phenocrysts completely unrecognisable - completely reacted to something else - plag or cpx? Glomerocrysts here, or type 3 opx? Reaction of opx to cpx to plag. No fractured phenocrysts. generally more phaneritic than 2014/1990 samples.	2 px basaltic andesite	Petrographic, XRF, ICP-MS, EMP
Plag is commonly lath shaped, it is nearly always zoned (even if faintly) osc zoned. Some discontinuous zoning. Smaller microphenocrysts/microlites are also lath shaped - twinned with lamellae. Plag dominated glomerocrysts common. Plag has no inclusions (cant see glass?). Cpx's often larger phenocrysts, and appear faintly zoned (although heavily included). Opx clearly reacted to cpx which has been replaced by plag - crystallisation sequence? oxides most commonly associated with pyroxenes. No fractured phenocrysts - generally more phaneritic than 2014/1990 samples.	2 px basaltic andesite	Petrographic

AMPHIBOLE

Eruption	Sample	Point name	SiO ₂	TiO ₂	Al ₂ O ₃	FeO	MnO	MgO	CaO	Na ₂ O	K ₂ O	P ₂ O ₅	Cr ₂ O ₃	NiO	Total
2014 K123		K123_1_amp	44.1	1.90	9.73	14.0	0.39	13.3	11.2	1.78	0.31	0.00	0.00	0.00	96.8
		K123_1_amp	44.6	1.55	9.43	13.9	0.43	13.4	11.2	1.74	0.30	0.00	0.00	0.00	96.6
		K123_1_amp	44.7	1.66	9.45	14.0	0.43	13.2	11.2	1.73	0.29	0.00	0.00	0.00	96.7
		K123_1_amp	44.6	1.93	9.71	14.2	0.39	13.6	11.4	1.80	0.30	0.00	0.00	0.00	98.0
		K123_1_amp	44.5	1.59	9.37	14.1	0.42	13.4	11.4	1.70	0.29	0.00	0.00	0.00	96.7
		SD	0.22	0.18	0.17	0.11	0.02	0.14	0.11	0.04	0.01	0.00	0.00	0.00	